

5-17-2013

# The Investigation of Iron(II) Complexes and Their Catalytic Applications

Matthew Joseph Lenze

University of Missouri-St. Louis, [matt.chemguy@gmail.com](mailto:matt.chemguy@gmail.com)

Follow this and additional works at: <https://irl.umsl.edu/dissertation>

 Part of the [Chemistry Commons](#)

---

## Recommended Citation

Lenze, Matthew Joseph, "The Investigation of Iron(II) Complexes and Their Catalytic Applications" (2013). *Dissertations*. 308.  
<https://irl.umsl.edu/dissertation/308>

This Dissertation is brought to you for free and open access by the UMSL Graduate Works at IRL @ UMSL. It has been accepted for inclusion in Dissertations by an authorized administrator of IRL @ UMSL. For more information, please contact [marvinh@umsl.edu](mailto:marvinh@umsl.edu).

# The Investigation of Iron(II) Complexes and Their Catalytic Applications

Matthew J. Lenze

M.S. in Chemistry, University of Missouri-St. Louis, 2010

B.S. in Chemistry, University of Missouri-St. Louis, 2008

A Thesis submitted to the Graduate School at the University of Missouri - St. Louis in  
partial fulfillment of the requirements for the degree

Doctor of Philosophy in Chemistry

May 2013

## Advisory Committee

Eike Bauer, Ph.D.

Chairperson

Christopher Spilling, Ph. D.

Wesley Harris, Ph. D.

Keith Stine, Ph. D.

## Table of Contents

<b>LIST OF ABBREVIATIONS .....</b>	<b>5</b>
<b>ABSTRACT.....</b>	<b>6</b>
<b>CHAPTER 1 Introduction .....</b>	<b>8</b>
<b>1.2 References.....</b>	<b>24</b>
<b>CHAPTER 2 New Indenyl Phosphinooxazoline Complexes of Iron and Their Catalytic Application in the Mukaiyama aldol reaction .....</b>	<b>28</b>
<b>2.1 Aim of the Chapter .....</b>	<b>28</b>
<b>2.2 Introduction.....</b>	<b>28</b>
<b>2.3 Results .....</b>	<b>32</b>
2.3.1 Synthesis of the phosphinooxazolines .....	32
2.3.2 Synthesis of new indenyl phosphinooxazoline complexes of iron .....	36
2.3.3 Catalytic activation of carbonyl compounds.....	43
<b>2.4 Discussion .....</b>	<b>46</b>
2.4.1 Comparison of structurally similar complexes	
<b>2.5 Summary and Prospective .....</b>	<b>48</b>
<b>2.6 Chapter 2 Experimental.....</b>	<b>49</b>
<b>2.7 References.....</b>	<b>61</b>
<b>CHAPTER 3 Investigations of New Iron Phosphinooxazoline Complexes and Iron(II) Triflate and Their Catalytic Activity in the Oxidation of Activated Methylene Groups.....</b>	<b>65</b>
<b>3.1 Aim of the Chapter .....</b>	<b>65</b>
<b>3.2 Introduction.....</b>	<b>65</b>
<b>3.3 Results .....</b>	<b>67</b>

3.3.1	Syntheses of iron complexes of the general formula $[\text{Fe}(\text{PHOX})_2(\text{X})_2]$	
3.3.2	Catalytic oxidation of activated methylene groups.....	74
3.3.3	Additional experiments to better understand the nature of the mechanism of the oxidation reactions .....	77
<b>3.4</b>	<b>Discussion .....</b>	<b>80</b>
3.4.1	Kinetics .....	80
<b>3.5</b>	<b>Summary and Prospective .....</b>	<b>83</b>
<b>3.6</b>	<b>Chapter 3 Experimental.....</b>	<b>83</b>
<b>3.7</b>	<b>References.....</b>	<b>89</b>
	<b>Chapter 4 <math>\alpha</math>-Aminopyridine and N-, O- Coordinating Polydentate Pyridyl Ligands and the Catalytic Activity of Their Respective Iron(II) Complexes in Oxidation Reactions: A Comparative Study of Activity and Ligand Decomposition.....</b>	<b>90</b>
<b>4.1</b>	<b>Aim of the Chapter .....</b>	<b>90</b>
<b>4.2</b>	<b>Introduction.....</b>	<b>90</b>
<b>4.3</b>	<b>Results .....</b>	<b>94</b>
4.3.1	Synthesis of new iron complexes.....	94
4.3.2	Characterization of the new iron complexes.....	99
4.3.3	Catalysis and catalytic efficiency.....	108
4.3.4	Experiments to better understand the course of the oxidation reaction.	118
4.3.5	Ligand decomposition pathways and their impact on catalytic activity	132
<b>4.4</b>	<b>Discussion .....</b>	<b>137</b>
<b>4.5</b>	<b>Summary and Prospective .....</b>	<b>139</b>
<b>4.6</b>	<b>Chapter 4 Experimental.....</b>	<b>140</b>
<b>4.7</b>	<b>References.....</b>	<b>155</b>
	<b>Chapter 5 Chemoselective, Iron(II)-catalyzed Oxidation of Secondary Alcohols over Primary Alcohols Utilizing <math>\text{H}_2\text{O}_2</math> as the Oxidant.....</b>	<b>163</b>
<b>5.1</b>	<b>Aim of the Chapter .....</b>	<b>163</b>

<b>5.2 Introduction.....</b>	<b>163</b>
<b>5.3 Results .....</b>	<b>165</b>
5.3.1 Catalytic efficacy and selectivity screening.....	165
5.3.2 Experiments to better understand the selectivity .....	169
<b>5.4 Summary and Prospective .....</b>	<b>172</b>
<b>5.5 Chapter 5 Experimental.....</b>	<b>172</b>
<b>5.6 References.....</b>	<b>182</b>

## List of Abbreviations

Bn.....	Benzyl
CH <sub>2</sub> Cl <sub>2</sub> .....	Dichloromethane
DMAP.....	4-(Dimethylamino)pyridine
DMF.....	<i>N,N</i> -Dimethylformamide
Et <sub>3</sub> N.....	Triethylamine
Et <sub>2</sub> O.....	Diethyl Ether
FAB.....	Fast Atom Bombardment
IR.....	Infrared
Me.....	Methyl
CH <sub>3</sub> CN.....	Acetonitrile
MS.....	Mass Spectrometry
3-NBA.....	3-Nitrobenzyl Alcohol
NMR.....	Nuclear Magnetic Resonance
OTf.....	Triflate (OSO <sub>2</sub> CF <sub>3</sub> )
Ph.....	Phenyl
PhMe.....	Toluene
ppm.....	Parts Per Million
THF.....	Tetrahydrofuran
TLC.....	Thin Layer Chromatography
TsCl.....	<i>m</i> -Toluenesulfonyl Chloride

## Abstract

Several new  $\eta^5$ -indenyl (Ind) complexes of iron featuring phosphinooxazoline (PHOX) ligands were synthesized and spectroscopically characterized and in a few cases structurally. The complexes were synthesized using phosphinooxazoline ligands **2.1** and the corresponding iron precursor  $[\text{Fe}(\eta^5\text{-Ind})\text{I}(\text{CO})_2]$ , yielding novel piano-stool iron complexes of the general formula  $[\text{Fe}(\eta^5\text{-Ind})(\text{CO})(\text{PHOX})]^+$  in 73% to 81% isolated yields. The complexes were tested for their efficacy in a carbon-carbon bond formation known as the Mukaiyama aldol reaction.

The  $[\text{Fe}(\eta^5\text{-Ind})(\text{CO})(\text{PHOX})]^+$  complexes were capable of activating the carbonyl of aromatic aldehydes towards by attack 1-(*tert*butyldimethylsilyloxy)-1-methoxyethene to form the expected silyl protected  $\beta$ -hydroxyesters. The electronic and steric tuning of the complexes only exerted a minor influence on the catalytic ability of the corresponding complexes. In these complexes, the  $\eta^5$ - $\eta^3$  haptotropic shift, of the indenyl ligand, have shown to undergo this shift 100 times faster than their cyclopentadienyl (Cp) analogues. Accordingly, a noticeable increase in catalytic activity was observed in the Mukaiyama aldol reaction upon exchange of the Cp ligand for the Ind ligand.

Also, new well-defined complexes bearing bi- and tridentate  $\alpha$ -aminopyridine as well as N-, O- coordinating multidentate ligands were synthesized and in some cases structurally characterized. The complexes were synthesized utilizing the respective ligands **4.16**, **4.18**, **4.20**, **4.22**, **4.24** and **4.26** and the iron precursor  $\text{Fe}(\text{OTf})_2$ , generating complexes of the general formula  $[\text{Fe}(\text{L})_n(\text{OTf})_2]$  (where  $n=1,2$ ) depending on the denticity of the ligands. The complexes were monitored for their catalytic ability in the

oxidation of hydrocarbons and alcohols utilizing environmentally benign peroxide oxidants. Investigations to determine their respective mechanistic pathways were performed using the catalytic oxidation of cyclohexane with ROOH (R = H, *t*-Bu) to an alcohol/ketone mixture. The low alcohol/ketone ratio revealed that these oxidations largely follow a radical mechanism, except when  $[\text{Fe}(\mathbf{4.16})_2]\text{OTf}_2$  was employed and  $\text{H}_2\text{O}_2$  was added slowly.

Together with known bi- and tridentate iron complexes, a comparative study showed reactivity differences for the newly prepared complexes. The catalytic activity of the complexes is related, in part, to the increasing number of donor atoms, with complexes  $[\text{Fe}(\mathbf{4.16})_2]\text{OTf}_2$ ,  $[\text{Fe}(\mathbf{4.22})(\text{OTf})]$  and  $[\text{Fe}(\mathbf{4.24})(\text{OTf})]\text{OTf}$  displaying the highest activities. Ligand decomposition pathways for the complexes were also studied and revealed that the  $\text{NCH}_2$  units of the ligand were oxidized to the corresponding amides, and which showed that the oxidative ligand deterioration only had a marginal effect on catalytic activity. Complex  $[\text{Fe}(\mathbf{4.16})_2]\text{OTf}_2$  was also investigated as a mild, iron-based catalyst system that is capable of selectively oxidizing secondary alcohols to the corresponding hydroxyl ketones in the presence of primary alcohols within 15 minutes at room temperature, whilst using  $\text{H}_2\text{O}_2$  as the oxidant.



## Chapter 1. *Introduction*

Organic chemistry is referred to as the chemistry of life and, thus, axiomatic to biology and medicine. The importance of organic chemistry in modern society cannot be overstressed as it is an integral part of many facets of life. It is responsible for the production of food, manufacturing of many clothes (synthetic materials, dyes etc.), treatment of illness, synthesis of agrochemicals and petrochemicals and holds the key to solving many of the world's problems. Ergo, the expansion of such knowledge is imperative for our survival and plays a pivotal role in shaping our future. The introduction of new synthetic methodologies facilitates the evolution of improved synthetic techniques, thus, permitting the synthesis of previously impervious compounds. One way to accomplish transformations that would otherwise be impossible is through the use of transition metal catalysis.

The field of transition metal catalysis has made significant contributions to modern society in the past decade in the form of medicine and technological advancements. New catalysts capable of expanding and improving upon known reaction manifolds can minimize the consumption of energy and production of waste, which is particularly important in these times of increased environmental awareness. Transition metal based organometallic catalysts are of particular interest for many reasons: 1.) Ability to form both  $\sigma$  and  $\pi$  bonds with potential substrates 2.) Their ligands can be sterically and electronically tuned to have a desired influence on the chemical behavior of the metal complex 3.) Transition metals can adopt a multitude of oxidation states and coordination geometries, giving them the ability to change oxidation state and coordination numbers in catalytic cycles.<sup>1</sup>

Another attractive feature of organometallic catalysis is that the employment of an asymmetric catalyst allows for the possibility of asymmetric induction in achiral compounds. An example of a reaction that typically uses transition metal based catalysts is transfer hydrogenation. In 1991, Backvall and co-workers showed that the achiral  $\text{RuCl}_2(\text{PPh}_3)_3$  complex is an effective transfer hydrogenation catalyst at elevated temperatures<sup>2</sup> and in 2000, Noyori demonstrated that his chiral ruthenium based catalyst was capable of successfully accomplishing an asymmetric catalytic hydrogen transfer.<sup>3</sup>

The demand for chiral intermediates has soared with respect to the pharmaceutical and agrochemical industries. The world market for chiral compounds reached US\$ 15 billion in 2009 and has drastically increased annually. Nevertheless, in order for chemical manufacturers to even consider targeting the synthesis of such chiral molecules, they must be able to be acquired in high yield, be optically pure and be available at the lowest cost possible. The formation of enantiopure compounds with high enantioselectivity is one of the most challenging tasks for synthetic chemists, and one of the only practical routes to accomplish the synthesis is through employment of asymmetric catalysis. That being said, a catalytic version of asymmetric reactions is one of the most important and commonly studied fields in modern organic chemistry. There exists a broad range of applications that are encompassed by asymmetric catalysis such as alkylation, conjugate addition, cycloaddition, hydroformylation, hydrogenation and oxidation.<sup>4</sup> All of the aforementioned asymmetric transformations are catalyzed by a complex bearing a precious metal such as Pd, Ru, Rh, Ir, Os or Cr. However, although effective, their scarcity, toxicity and high cost make them extremely unattractive.

An increased state of environmental awareness has caused the chemical industries to shift their concerns and protocols to fall within the principles of Green Chemistry. The fundamentals of Green Chemistry encourage the use of less-toxic substances, reduction of waste, minimizing the consumption of energy and promote atom economy; all of which would reduce the negative impact that performing chemistry has on the environment. Fortunately, transition-metal catalysis is a prime technology that could be used for promoting and advancing the principles of Green Chemistry, more specifically, by eliminating waste generated (fewer synthetic steps=less solvent & substrates) and decreasing amounts of energy required (lower temperatures needed and shorter reaction times). Albeit the utility of transition metal based catalysis is attractive and falls within the guidelines of green chemistry, many of the aforementioned transition metals (Pd, Ru, Rh, Ir, Os etc.) commonly used in such transformations feature drawbacks as previously discussed. Moreover, the potential toxicity of these metals leads to concentration limits in pharmaceutical production to meet health standards (Table 1.1). Accordingly, it is desirable to find a less expensive, non-toxic alternative to the existing catalyst systems.

---

Element	Oral Concentration Limit [ppm]	Parenteral Limit [ppm]	Concentration
Pt, Pd, Ir, Rh, Ru, Os	5 (group)	0.5 (group)	
Mo, V, Ni, Cr	10	1.0	
Cu, Mn	15	1.5	
Zn, Fe	20	2.0	

---

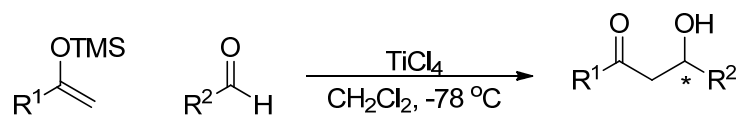
**Table 1.1.** Toxicity of transition metals that are commonly used in catalysis.

Iron seems to be a prime candidate under the aforesaid considerations. Iron is an excellent choice, as it is extremely abundant, resulting in low cost, it is easy to handle, it is relatively non-toxic and classified as environmentally benign. All of which offer advantages, with respect to viable and sustainable chemistry, relative to previously discussed catalyst systems. As a result of the recent economic and environmental race to fall within the tenets of Green Chemistry, iron catalysis has become increasingly more attractive in both academia and industry and iron catalysts have been applied in a number of organic and inorganic transformations such as carbon-carbon bond formations,<sup>5</sup> carbon-heteroatom bond formations,<sup>6</sup> polymerizations,<sup>7</sup> reductions,<sup>8</sup> oxidations<sup>9</sup> and others.<sup>10</sup>

Organoiron chemistry was started in 1891, with both Mond<sup>11</sup> and Bethelot,<sup>12</sup> through their independent discovery of iron pentacarbonyl. An additional milestone was the report of ferrocene in 1951 by Pauson.<sup>13</sup> However, the synthetic utility of iron catalysis really

came into focus with the Reppe synthesis involving acetylenes and iron pentacarbonyl.<sup>14</sup> Additionally, in 1971, Kochi and coworkers reported their results on the iron-catalyzed cross coupling of aryl grignards with organo-halides.<sup>15</sup> Currently, the increase in the number of organic reactions being catalyzed by iron complexes exemplifies a renaissance of this metal in transition metal catalysis. Several examples; in 2003, Jensen reported the use of an Fe(acac)<sub>3</sub> (10 mol%) mediated coupling between an acetylenic grignard and a  $\beta$ -triflate enol ester for the preparation of a key intermediate during the total synthesis of *Latrunculin B*.<sup>16</sup> In 2007, Nakamura reported a FeCl<sub>3</sub>-TMEDA catalyzed Kumada-like coupling reaction between aryl grignards and alkyl halides with yields as high as 99%.<sup>17</sup> Even more recently, in 2009, White and Chen et al. developed a stereoselective oxidation of methine groups<sup>18</sup>, and in 2010 Vallee *et al*<sup>19</sup> reported an iron(II) catalyzed radical-induced aryl-phenyl coupling between an aryl halide and benzene. All of which exhibit the catalytic efficacy and unique versatility associated with applying iron as a catalyst.

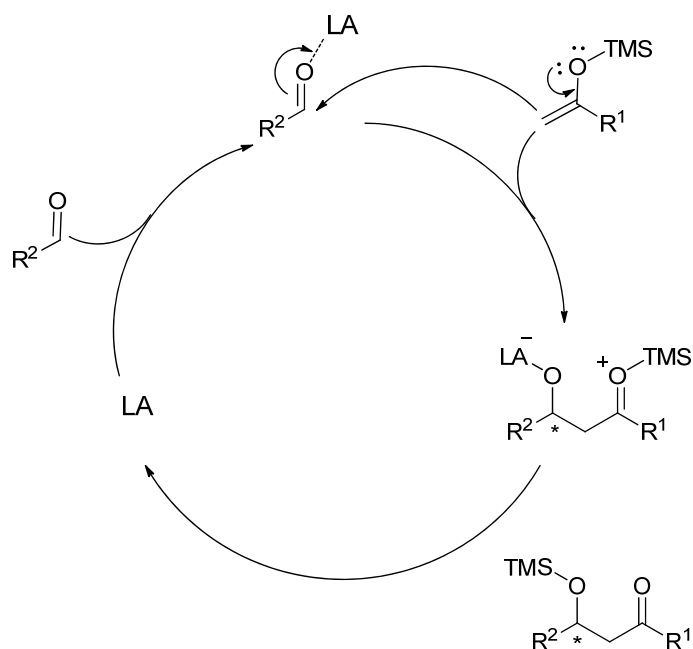
The benefits of utilizing iron complexes as catalysts were clear and demonstrated comparable, if not better, catalytic activity relative to other transition metal based catalysts in a plethora of organic transformations. Consequently, our research group decided to thoroughly explore the advantages and opportunities associated with the up and coming field of iron catalysis. Initial interests of our group entailed the application of iron complexes as catalysts in carbon-carbon bond formation reactions as well as various oxidation reactions. The carbon-carbon bond forming reaction to be studied is referred to as the Mukaiyama aldol reaction. The Mukaiyama aldol reaction is a Lewis acid catalyzed addition of silyl enol ether to carbonyl compounds.<sup>20</sup>



**Scheme 1.1.** Representative example of the Mukaiyama aldol reaction.

Overall, the Mukaiyama aldol reaction involves the addition of a silyl-trapped enol to the carbonyl of an aldehyde, ketone or ester generating a 1,3 ketol. The initial step of the reaction is the coordination of the Lewis acid to the oxygen of the carbonyl group, inducing metal stabilized polarization of the carbonyl bond, thus, increasing electrophilicity of the carbonyl carbon and facilitating attack of the silyl enol ether (Scheme 1.2). The key intermediate of this reaction is the formation of the transition state which determines the stereoselectivity of the final product. Despite the fact that the “open” transition state model was commonly used to explain the outcome of the Mukaiyama aldol addition, the recent enantioselective versions of the reaction are explained using the more sophisticated “closed” transition state model such as the Zimmerman-Traxler model, where the destiny of the reaction is totally dependent on the size of the substituents in addition to the size and electronic nature of the Lewis acid.

Typical Mukaiyama aldol reaction conditions are not practical and require the employment of substoichiometric amounts of toxic metal salts, such as TiCl<sub>4</sub> and AlCl<sub>3</sub>, prolonged reaction times and cryogenic temperatures. Moreover, many of the original commonly used Lewis acids lack chirality, and thus, stereoselectivity was rarely observed. Therefore, the replacement of the currently accepted conditions with an iron based catalyst seems necessary and demonstrates a viable solution not only to our environmental concerns, but would also aid in the progression of synthetic methodologies.

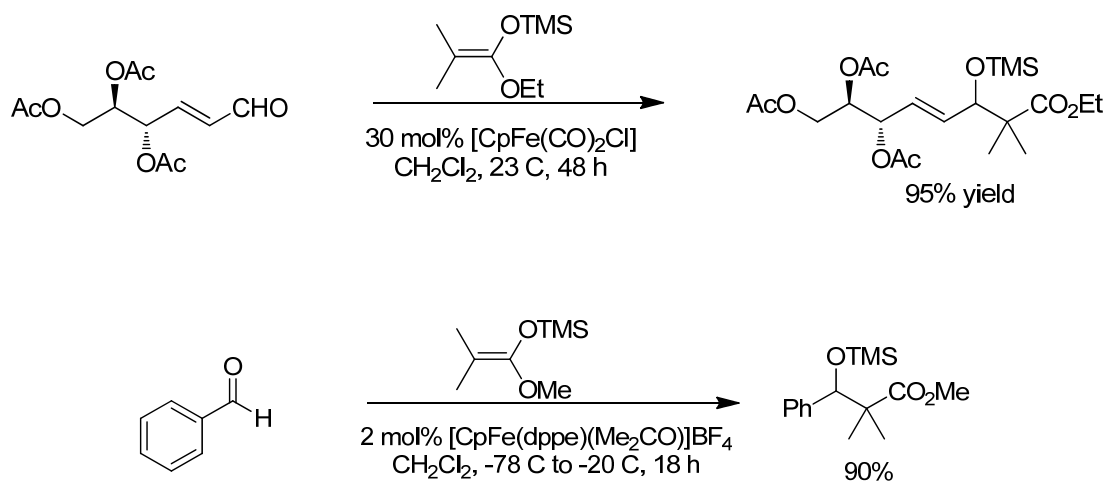


**Scheme 1.2.** Proposed catalytic cycle for the Mukaiyama aldol reaction.

The Mukaiyama aldol reaction was discovered in 1973<sup>21</sup> and has made a noteworthy contribution to synthetic chemistry by expanding the scope of and improving upon the limitations associated with the well established aldol condensation, but the reaction itself had its own limitations. Following the preliminary stages of the Mukaiyama aldol reaction, Mukaiyama reported that moderate yields could only be obtained when extremely electron rich silyl enol ethers were reacted with aromatic aldehydes and accompanied by the addition of substoichiometric and stoichiometric quantities of toxic Lewis acids such as TiCl<sub>4</sub>, SnCl<sub>4</sub>, FeCl<sub>3</sub>, AlCl<sub>3</sub>, Et<sub>2</sub>O-BF<sub>3</sub> and ZnCl<sub>2</sub>. Moreover, under such conditions there was very little chance for chemo- and regioselective control via the Lewis acid.<sup>22</sup>

From the mid-1970s to about the mid 1980s, the selectivity of this reaction could only be controlled by carefully choosing substrates and reaction conditions and not with the Lewis acid applied.<sup>23</sup> In 1986, studies began to be designed to control the stereochemical

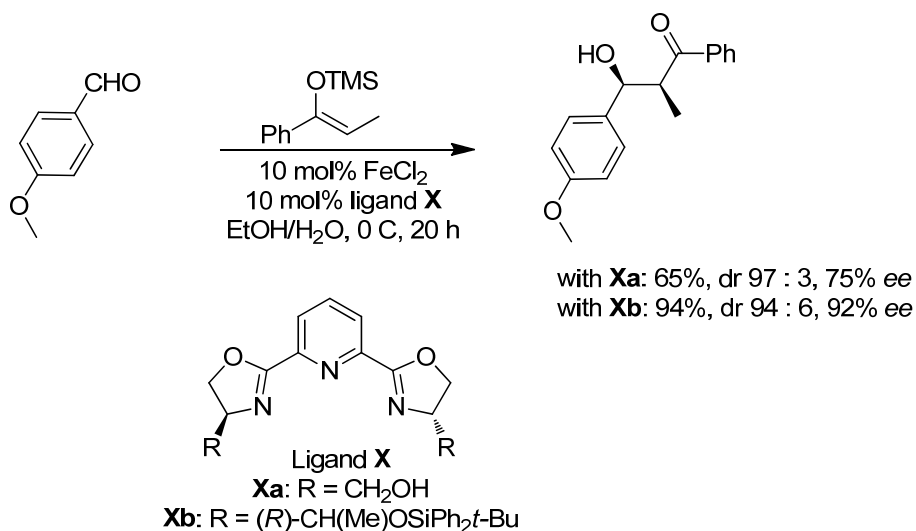
outcome through use of chiral Lewis acids.<sup>24</sup> Although these new chiral Lewis acids were successful, they were needed in stoichiometric amounts, hampering their application and practicality. It wasn't until the end of the 1980s that a catalytic version of chiral Lewis acids was developed.<sup>25</sup> Again, many of the Lewis acids employed in the Mukaiyama aldol reaction used toxic metals. Be that as it may, iron based Lewis acids also proved to be effective.



**Scheme 1.3.** Iron-catalyzed Mukaiyama aldol reactions.

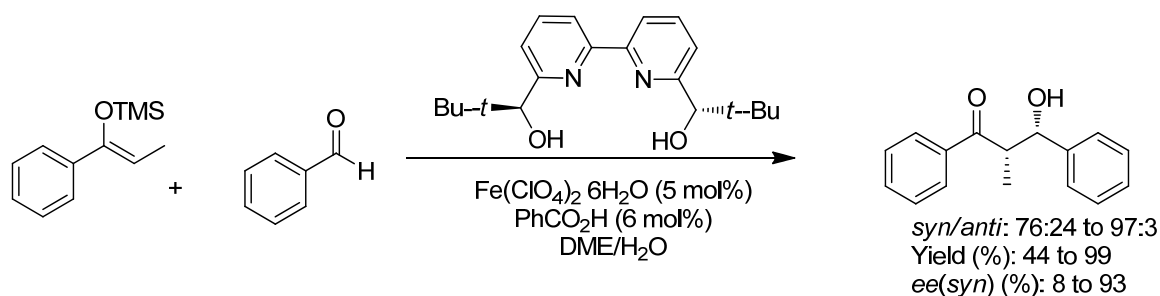
In 1989, Columbo *et al.* reports the use of the complex  $\text{CpFe}(\text{CO})_2\text{Cl}$ <sup>26</sup> as a catalyst (Scheme 1.3, top) and in 1992, Bach *et al.* reported the use of  $[\text{CpFe}(\text{dppe})(\text{acetone})]\text{BF}_4$ <sup>27</sup> as a catalyst (Scheme 1.3, bottom), both for the reaction between silyl ketene acetals and  $\alpha,\beta$ -unsaturated aldehydes.





**Scheme 1.4.** Iron catalyzed asymmetric version of the Mukaiyama aldol reaction.

Encouragingly, in 2006, Jankowska *et al.* established an asymmetric variant of the Mukaiyama aldol reaction that he reported to be catalyzed by FeCl<sub>2</sub> and PYBOX ligands (Scheme 1.4).<sup>28</sup> Another highly enantioselective version of the Mukaiyama aldol reaction was reported by Ollevier Plancq in 2012, in which they demonstrated that a chiral iron(II) bipyridine complex could be employed under aqueous conditions and still result in good enantioselective control as shown in Scheme 1.5.<sup>29</sup> However, although good to high ee's were obtained with the use of the previously mentioned chiral iron catalysts, their systems involved the *in-situ* formation of the catalyst by combining the iron precursor and chiral ligands, making these systems, at best, poorly defined.



**Scheme 1.5.** Ollevier's chiral iron catalyst and its activity in the Mukaiyama aldol reaction.

Overall, several Lewis acid catalysts have been investigated for use in the Mukaiyama aldol reaction, and studies reveal that iron is one of the least commonly used metals, outlining the fact that the application of iron as a catalyst in the Mukaiyama aldol reaction is underexplored and offers the advantage for the development of a well-defined, environmentally friendly iron catalysts.

Over the years, the Mukaiyama aldol reaction has been fine-tuned and is currently classified as being one of the most powerful routes for the formation of a carbon-carbon bond due to the formation of a stereocenter throughout the course of the reaction. As a result, it is commonly employed in the synthesis of natural products where the stereochemical outcome can be controlled through the use of asymmetric catalysis. Namely, it was utilized in the synthesis of natural products such as Spirocurasone,<sup>30</sup> (+)-Ansamacrolactam<sup>31</sup> and (+)-Cryptocaryanone.<sup>32</sup> Sugimura *et al.* report a Lewis acid promoted reaction of  $\beta$ ,  $\lambda$ -unsaturated  $\alpha$ ,  $\alpha$ -dimethoxy esters with silyl nucleophiles using  $\text{TiCl}_4$  and  $\text{BF}_3 \cdot \text{Et}_2\text{O}$ .<sup>33</sup> In some cases racemic mixtures are obtained,<sup>15</sup> and in other cases, where one or more stereocenters already exist, a mixture of diastereomers becomes a possibility. The ability to strategically gain a stereoselective control during the formation of any given stereocenter is one of the most coveted operations in the modern world of or-

ganic chemistry and imperative throughout any natural product synthesis. Nevertheless, selectivity is not always observed, and in these cases, poor to no enantiomeric excess (ee's) or diastereomeric excess/ratio (de's/dr's) are the result. To this end, the application of asymmetric catalysis is clearly advantageous because inducing the formation of a specified stereocenter in the final product can be as simple as selecting a given enantiomer of the chiral catalyst to be used. The product of the Mukaiyama aldol reaction, the  $\beta$ -hydroxycarbonyl compound, plays an important role in the preparation of both medicinal and agricultural chemicals. Thus, development of an asymmetric catalytic system capable of mediating a facile and expedited synthesis of such synthetically useful molecules seems lucrative.

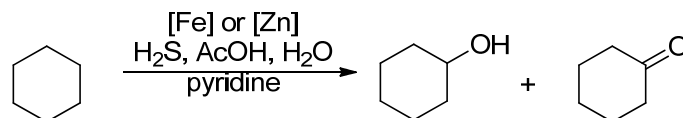
Our group was also interested in exploring possible catalyst systems that were capable of expanding the scope of oxidation reactions catalyzed by iron complexes. Iron catalyzed oxidation reactions have been investigated extensively in recent years, especially in light of our heightened ecological cognizance, because there is a lack of efficient and benign catalysts capable of expediting the selective oxidation of organic substrates, under mild conditions. This quandary is being addressed through the development and optimization of biomimetic or bioinspired catalysts, which is based on our detailed knowledge of enzymatic systems that have been used by living organisms for selective oxidations throughout the evolution of life. These pervasive enzymes have attracted the interests of chemists for many reasons, two of which are: 1) they catalyze the selective oxidation of almost any organic substrate, using  $O_2$ , including alkanes. 2) they play a vital role in xenobiotic and drug metabolism, which is a compelling step in the adaptation of living organisms and their ever-evolving chemical habitats. Fortunately, for our sake there has

been a considerable amount of research done throughout the past 30 years on the heme based class of xenobiotic metabolizing enzymes, cytochrome P450. This has resulted in a comprehensive understanding of oxidation reactions catalyzed by P450s, a thorough understanding of the mechanisms associated with nonheme iron-containing catalysts and it led to the strategic design of an improved class of bioinspired oxidation catalysts.

Before the demand, by various chemical industries, of such a large hydrocarbon feedstock as raw materials arose, the organic building blocks were simply oxidized using inorganic oxidizing reagents such as chromium, titanium and manganese oxides, halogens and nitric acids. Only very seldomly, when the targets were active pharmaceutical ingredients, did the industries attempt to employ molecular oxygen or aqueous peroxides. However, now that more than 90% of organic chemicals sold on the market today stem from the saturated hydrocarbons in petroleum and oxidation products thereof, a call for change seems absolutely essential in terms of tolerability, as current conditions for oxidation reactions are not sustainable. Not only are the current methods for oxidation reactions hazardous, most are unselective and usually involve oxidative cleavage or the concomitant combustion of alkanes. Very few efforts oriented towards development of a nontoxic, selective catalyst that uses less harmful oxidants such as molecular oxygen and aqueous peroxides as terminal oxidants have been made until recently.

Tabushi and coworkers have reported the oxidation of adamantane to 1- and 2-adamantols by the Mn(III)porphyrin/Pt/H<sub>2</sub> system under dioxygen atmosphere at room temperature.<sup>34</sup> The most memorable of which was discovered by Barton who developed a family of systems, the so-called Gif and GoAgg systems, for aerobic oxidation and oxida-

tive functionalization of alkanes under mild conditions using iron and zinc salts in pyridine and acetic acid (Scheme 1.6).<sup>35</sup>



**Scheme 1.6.** Oxidation of cyclohexane using Gif and GoAgg systems.

Barton *et al.* described these conditions as a new procedure for the oxidation of saturated hydrocarbons, but the conditions were not selective and led to product mixtures of the corresponding alcohol(s) and ketone(s).<sup>35</sup> Other systems perform alkane oxidations using aldehydes as reducing agents and were reported by Murahashi and coworkers, who attempted the aerobic oxidation of cyclohexane and adamantane by ruthenium or iron catalysts in the presence of acetaldehyde.<sup>36</sup> A Ru(III)-EDTA system,<sup>37</sup> Ru substituted polyoxometalate<sup>38</sup> and [Co(NCMe)<sub>4</sub>(PF<sub>6</sub>)<sub>2</sub>]<sup>39</sup> have also been reported to catalyze the aerobic oxidation of many alkanes. Unfortunately, although all previously discussed systems are effective and use oxygen, most of them require additional steps to remove the toxic metals from the final oxidation product, and most are unselective or use “undesirable” conditions per suggested by the principles of “Green Chemistry”.

The oxidation of hydrocarbons is not difficult, but oxidizing them selectively, *i. e.* stopping the reaction at a useful stage rather than allowing them to form the thermodynamically favored total oxidation, while employing environmentally benign oxidants such as molecular O<sub>2</sub> and aqueous peroxides, is where the issue lies. Consequently, our group has devoted substantial efforts towards the development of such a system.

As mentioned before, heme and nonheme iron enzymes, such as methane monooxygenase<sup>40</sup> and Rieske dioxygenase,<sup>41</sup> catalyze such reactions and have inspired the development of various models of oxidation catalysts.<sup>42</sup> Every system has its advantages and disadvantages. While heme systems have their advantages with respect to selectivity, the tuning efforts of the surrounding porphyrin ligand are virtually nonexistent, rendering optimization efforts difficult. The nonheme based systems offer the advantage of performing seemingly endless steric and electronic tuning on the ligands backbone. Moreover, you may also selectively modify the number of donor atoms or the identity of the donor atom itself. Accordingly, a tremendous amount of research has taken place to develop a nonheme iron based catalyst system that uses nontoxic and more “desirable” conditions.

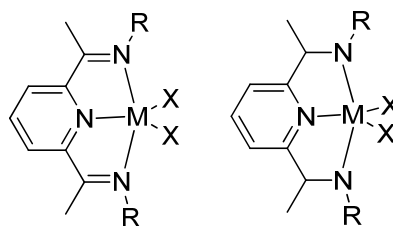


**Figure 1.1.** Britovsek’s metal complexes bearing tridentate imine (left) and amine (right) ligands.

In 2005, England *et al.* reported the synthesis of iron(II), manganese(II), cobalt(II) and ruthenium(II) complexes featuring tridentate nitrogen ligands (Figure 1.1) and their subsequent application in the catalytic oxidation of alkanes.<sup>43</sup> However, the application of the complexes as catalysts in oxidation reactions leads predominantly to the unselective Barton type reactivity.

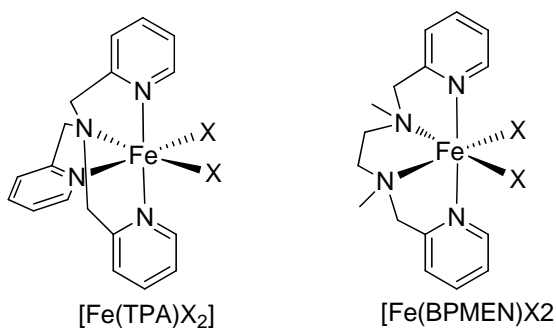
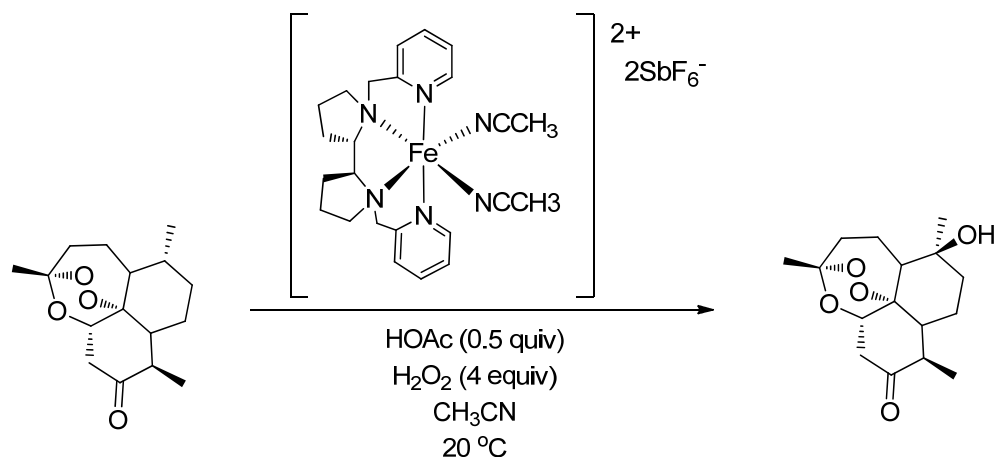


**Figure 1.2.** Iron complexes featuring the TPA (left) and BPMEN (right) that are capable of stereospecific alkane hydroxylation using H<sub>2</sub>O<sub>2</sub>.

Based on the enhanced reactivity associated with complexes bearing tetradentate ligands, Britovsek and coworkers decided to investigate such complexes further and probe for their selectivities and activity in alkane oxidation catalysis.<sup>44</sup> An increasing number of publications describing such systems have been documented and report that the effective nonheme catalysts are those featuring tetradentate N<sub>4</sub> ligands, belonging to the tripodal TPA and linear BPMEN family (Figure 1.2), that can perform stereospecific alkane hydroxylation using H<sub>2</sub>O<sub>2</sub>.<sup>42</sup>



**Scheme 1.7.** Iron catalyst, discovered by White and Chen, and its selective oxidation of the methine group in the natural product, artemisinin

In 2009, Chen and White introduced the versatility of their chiral iron(II) complexes and their high selectivity and activity in the non-directed oxidation of methine carbons.<sup>45</sup> Ergo, it appears obvious that most current catalyst systems, applied towards the oxidation of organic substrates, are either limited with respect to their effectiveness, *i.e.* Gif and GoAgg systems, or limited with respect to their selectivity, *i.e.* White and Chen's selective oxidation of methine units. Whereas very few examples of oxidation catalysts exist that can effectively AND selectively oxidize C-H bonds. Hence, discovery of catalyst systems that can follow this desirable trend in reactivity would be particularly useful, because they would nicely benefit existing synthetic strategies and give rise to innovative pathways.

The objectives of this research are two-fold: (1) to pioneer well defined iron complexes that exhibit high Lewis acidity capable of activating a number of carbonyl containing compounds towards attack by a silyl enol ether. Iron indenyl complexes featuring phosphinooxazoline ligands were targeted because the corresponding cyclopentadienyl analogues exhibited moderate activity and prolonged reaction times. Once a platform, for the general reaction to be catalyzed is established, substitutions on the oxazoline ring of the phosphinooxazoline ligand were made in an attempt to tune reactivity and potentially induce enantioselectivity. After a lead complex with respect to exhibiting superior catalytic activity was identified, its ability to activate a plethora of aldehydes towards addition in the Mukaiyama aldol reaction was monitored. (2) to develop novel and well defined iron complexes capable of accomplishing efficient oxidations of substrates such as activated methylene groups, alkanes and alcohols. Iron complexes bearing bi- and tridentate aminopyridine ligands as well as *N*- and *O*- multidentate based ligands were designed



because many corresponding complexes having bidentate iminopyridine ligands displayed only moderate activity and required “undesirable” reaction conditions. Reactions using these iron complexes to efficiently and selectively oxidize many organic substrates whilst using environmentally benign oxidation conditions, will be performed. Once an iron complex capable of efficiently and selectively oxidizing organic substrates is discovered, the effects of changing the number and type of donor atoms will be studied. Kinetic studies of all isolated catalysts will also be performed. If selectivity is observed, factors that contribute to selectivity enhancement and factors that hamper selectivity will be investigated for all complexes exhibiting selectivity

## 1.2 References

- <sup>1</sup> Masters, C.; Homogeneous Transition-metal Catalysis: a Gentle Art, Chapman and Hall: New York, 1981.
- <sup>2</sup> J. E. Backvall et al., *Chem. Comm.* **1991**, 337, 1063.
- <sup>3</sup> M. Yamakawa, I. Yamada, R. Noyori, *Angew. Chem. Int. Ed.* **2000**, *40*, 2818.
- <sup>4</sup> S. Gaillard, J. Luc Renaud, *Chem. Sus. Chem.* **2008**, *1*, 505.
- <sup>5</sup> Czaplík, W.M; Mayer, M.; Jacobi von Wangelin, A. *Angew. Chem. Int. Ed.* **2009**, *48*, 607.
- <sup>6</sup> a) Wallenhorst, C.; Kehr, K.; Luftmann, H.; Fröhlich, R.; Erker, G. *Organometallics* **2008**, *27*, 6547; b) McTavish, S.; Britovsek, G. J. P.; Smith, T. M.; Gibson, V. C.; White, A. J. P.; Williams, D. J. *J. Mol. Catal. A: Chem.* **2007**, *261*, 293.
- <sup>7</sup> Casey, C. P.; Guan, H. *J. Am. Chem. Soc.* **2009**, *131*, 2499.

- <sup>8</sup> a) Feng, Y.; Ke, C.; Xue, G.; Que, L. Jr., *Chem. Commun.* **2009**, 50; b) Chen, V.M.; White, C. *Science* **2007**, 318, 783.
- <sup>9</sup> S. Prateptongkum, I. Jovel, R. Jackstell, N. Vogl, C. Weckbecker, M. Beller, *Chem. Commun.* **2009**, 1990.
- <sup>10</sup> S. Prateptongkum, I. Jovel, R. Jackstell, N. Vogl, C. Weckbecker, M. Beller, *Chem. Commun.* **2009**, 1990.
- <sup>11</sup> L. Mond, F. Quinke, *J. Chem. Soc.* **1891**, 59, 604.
- <sup>12</sup> M. Berthelot, C. Hebd. *Seances Acad. Sci.* , **1891**, 112, 1343.
- <sup>13</sup> T. Kealy, P. Pauson, *Nature*, **1951**, 168, 1039.
- <sup>14</sup> W. Reppe, H. Vetter, *Justus Liebigs Ann. Chem.* **1953**, 582, 133.
- <sup>15</sup> a) M. Tamura, J. Kochi, *Synthesis*, **1971**, 303; b) M. Tamura, J. Kochi, *J. AM. Chem. Soc.* **1971**, 93, 1487.
- <sup>16</sup> A. Furstner, D. DeSouza, L. Parra-Rapado, J. Jensen, *Angew. Chem. Int. Ed.* **2003**, 42, 5358.
- <sup>17</sup> M. Nakamura, K. Matsuo, S. Ito, E. Nakamura, *J. Am. Chem. Soc.* **2004**, 126, 3686.
- <sup>18</sup> a) M. Chen, C. White, *Science*, **2007**, 318, 783.; b) N. Vermeulen, M. Chen, C. White, *Tetrahedron*, **2009**, 65, 3078.
- <sup>19</sup> F. Vallee, J. Mousseau, A. Charette, *J. Am. Chem. Soc.* **2010**, 132, 1514.
- <sup>20</sup> (a) Mukaiyama, T.; Narasaka, K.; Banno, K. *Chem Lett.* **1973**, 1011; (b) Mukaiyama, T.; Banno, K.; Narasaka, K. *J. Am. Chem. Soc.* **1974**, 96, 7504.
- <sup>21</sup> a) T. Mukaiyama, *Chem. Lett.* **1973**, 1011.; b) T. Mukaiyama, *J. Am. Chem. Soc.* **1974**, 96, 7503.; c) T. Mukaiyama, *Chem. Lett.* **1975**, 741.
- <sup>22</sup> K. Banno, K. Narasaka, T. Mukaiyama, *J. Am. Chem. Soc.* **1974**, 96, 7503.

- <sup>23</sup> T. Mukaiyama, *Angew. Chem. Int. Ed. Engl.* **1977**, *16*, 817.
- <sup>24</sup> C. Gennari, *Comprehensive Organic Synthesis*; B. Trost., Ed.; Pergamon: Oxford, 1993; Vol. 2, Chapter 2.4, p 629.
- <sup>25</sup> T. Mukaiyama, *Aldrichimica Acta*, **1996**, *29*, 59.
- <sup>26</sup> L. Columbo, F. Ulgheri, L. Prati, *Tetrahedron Lett.* **1989**, *30*, 6435.
- <sup>27</sup> T. Bach, D. Fox, T. Reetz, *J. Chem. Soc., Chem. Comm.* **1992**, 1634.
- <sup>28</sup> J. Jankowska, J. Paradowska, J. Mlynarshi, *Tetrahedron Lett.* **2006**, *47*, 5281.
- <sup>29</sup> T. Ollevier, B. Plancq., *J. Chem. Soc.: Chem. Comm.*, **2012**, *48*, 2289.
- <sup>30</sup> H. Abe, A. Sato, T. Kobayashi and H. Ito, *Org. Lett.* **2013**, *15*, 1298.
- <sup>31</sup> S. Yang, Y. Xi, R. Zhu, L. Wang, J. Chen and Z. Yang, *Org. Lett.* **2012**, *15*, 812.
- <sup>32</sup> B. Zhang, Z. Yhang, J. Yang, G. Zhao, B. Ma, X. Xie and X. She, *Syn. Lett.* **2012**, *23*, 2129.
- <sup>33</sup> H. Sugimura, H. Miyazaki and Y. Makita, *Tet. Lett.*, **2012**, *53*, 4584.
- <sup>34</sup> I. Tabushi, A. Yazaki, *J. Am. Chem. Soc.* **1979**, *101*, 6456; b) I. Tabushi, A. Yazaki, *J. Am. Soc.* **1981**, *103*, 7371; c) I. Tabushi, *Coord. Chem. Rev.* **1988**, *86*, 1.
- <sup>35</sup> D. Barton, J. Boivin, M. Gastiger, K. Morzycki, R. S. Hay-Motherwell, W. Motherwell, N. Ozbalik, K. Schwartzentruber, *J. Chem. Soc., Perkin Trans*, **1986**, *1*, 947; b) N. Komiyama, T. Naoto, S. Murahashi, *Tetrahedron Lett.* **1996**, *37*, 1633.
- <sup>36</sup> S. Murahashi, Y. Oda, T. Naoto, *J. Am. Chem. Soc.* **1992**, *114*, 7915; b) N. Komiyama, T. Naoto, S. Murahashi, *Tetrahedron Lett.* **1996**, *37*, 1633; N. Komiyama, T. Naoto, Y. Oda, S. Murahashi, *J. Mol. Catal. A: Chemical*, **1997**, *117*, 21.
- <sup>37</sup> a) M. M. T. Khan, R. S. Shukla, *J. Mol. Catal.* **1988**, *44*, 85; b) M. M. T. Khan, H. C. Bajaj, R. S. Shukla, S. A. Mirza, R. S. Shukla, *J. Mol. Catal.* **1988**, *44*, 51.

<sup>38</sup> R. Neumann, A. M. Khenkin, M. Dahan, *Angew. Chem. Int. Ed.* **1995**, *34*, 1587.

<sup>39</sup> A. S. Goldstein, R. S. Drago, *Inorg. Chem.* **1991**, *30*, 4506.

<sup>40</sup> M. Merckx, D. Kopp, H. Sazinsky, J. Blazyk, J. Muller, S. Lippard, *Angew Chem. Int. Ed.* **2001** *40*, 2782.

<sup>41</sup> M. Costas, M. Mehn, M. Jensen, L. Que, *Chem. Rev.* **2004**, *104*, 939. B) M. Abu-Omar, A. Loaiza, N. Hontzeas, *Chem. Rev.* **2005**, *105*, 2227.

<sup>42</sup> M. Costas, M. Chen, L. Que, *Coord. Chem. Rev.*, **2000**, *202*, 517.; b) K. Chen, L. Que, *J. Am. Chem. Soc.* **2001**, *123*, 6327.; c) G. Britovsek, J. England, A. White, *Inorg. Chem.* **2005**, *44*, 8125.; d) Y. Mekmouche, S. Menage, C. Toia-Duboc, M. Fontecave, J. Galey, C. Lebrum, J. Pecaut, *Angew. Chem. Int. Ed.* , **2001**, *40*, 949.

<sup>43</sup> J. England, S. Spitzmesser, A. White, D. Williams, G. Britovsek., *Dalton Transactions*, **2005**, 945.

<sup>44</sup> J. England, A. White, G. Britovsek., *Dalton Transactions*, **2006**, 1399.

<sup>45</sup> M. Chen, C. White, *Science*, **2007**, *318*, 783.; b) N. Vermeulen, M. Chen, C. White, *Tetrahedron*, **2009**, *65*, 3078.

## **Chapter 2.** *New indenyl phosphinooxazoline complexes of iron and their catalytic activity in the Mukaiyama aldol reaction*

### **2.1 Aim of the Chapter:**

It is known that piano-stool iron complexes bearing an indenyl ligand are known to be far more reactive in ligand exchange reactions than their cyclopentadienyl counterparts and this difference in reactivity is referred to as the “indenyl effect”.<sup>1</sup> Thus, I was interested in determining whether or not changing the cyclopentadienyl ligand to an indenyl ligand would increase the activity of an iron based catalyst. Ergo, I set out to synthesize complexes of the general formula  $[\text{Fe}(\eta^5\text{-C}_9\text{H}_7)(\text{CO})(\text{PHOX})]^+$  (Phosphinooxazoline = PHOX). The main objective of this project was to establish fundamentals pertaining to the synthesis of these new indenyl phosphinooxazoline complexes of iron and employ these complexes as Lewis acid catalysts in the Mukaiyama aldol reaction.

### **2.2 Introduction**

Half sandwich or piano-stool complexes of iron have been known to exist as either  $\eta^5$ -cyclopentadienyl complexes or  $\eta^5$ -indenyl complexes, and complexes of this type have become increasingly more prevalent and have already been applied as catalysts in a number of organic reactions, such as reductions<sup>2</sup>, carbon-carbon bond forming reactions<sup>3</sup>, polymerizations<sup>4</sup>, carbon-heteroatom forming reactions etc.<sup>5</sup> It is well understood that in order for any iron complex to be catalytically active, there must be an open coordination site.<sup>6</sup> These sites may be generated in numerous ways; (1) on complexes prepared in situ by addition of a substoichiometric amount of

ligand with a metal salt or (2) preformed well-defined complexes, in which coordination sites are only weakly occupied by non-coordinating solvents or donor atoms of multidentate ligands. (3) Where an open coordination site is formed through abstraction of a ligand.<sup>7</sup> Although alternative (1) appears to be more practical, preformed and well-defined complexes offer an advantage as they are more conducive to studying catalytically active species and performing mechanistic probing.<sup>8</sup> To such a degree, I became interested in surrogate pathways for the creation of open coordination sites on such preformed complexes. Preformed complexes of the type  $[\text{Fe}(\eta^5\text{-C}_9\text{H}_7)(\text{CO})(\text{PHOX})]^+$  are excellent candidates as they allow unique access to an open coordination site and offer the ability to fine tune these complexes via the PHOX ligand.

The previously mentioned phosphinoxazolines (PHOX) are a class of P-N bidentate ligands,<sup>9</sup> which have been widely used in a plethora of transition metal catalyzed organic reactions.<sup>10</sup> The synthetic utility of these ligands is enhanced by the ease by which they may be structurally and chemically modified. It was hypothesized that steric and electronic tuning of these ligands should have a considerable impact on the properties of their metal complexes and consequently, their catalytic activity. Therefore, I aspired to electronically tune multiple PHOX ligands through various substitution patterns of electron withdrawing and electron donating abilities. These electronic substitutions were to take place at the *para* (X) position of the aromatic backbone of PHOX. Next, preparation for the synthesis of multiple PHOX ligands having steric variances incorporated into the oxazoline ring ( $\text{R}^1$  and  $\text{R}^2$ ) were targeted (**2.1**, Figure 2.1). I targeted the synthesis of a number of PHOX ligands that were easiest to prepare and applied them in complex synthesis to investigate their role in complex formation and catalytic ability.

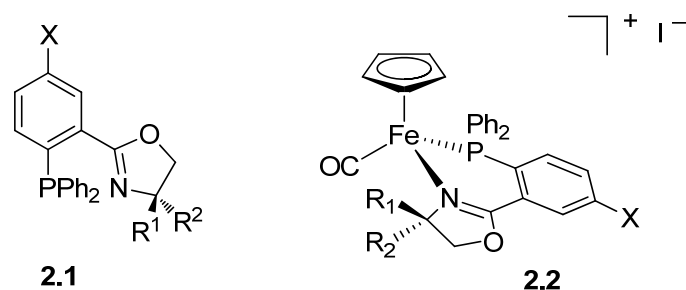
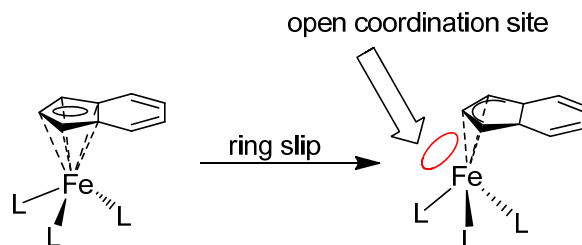


**Figure 2.1.** Phosphinooxazoline ligand (left) and iron Cp complexes thereof (right).

Previously, our group had successfully prepared and structurally characterized the first chelating iron PHOX complexes (**2.2**, Fig 2.1) that are stereogenic at the metal center.<sup>11</sup> The unique characteristic of a chirally enriched metal complex reaches into the realm of enantioselective catalysis. These chiral complexes offer tremendous advantages over traditional racemic complexes with respect to their application in enantioselective catalysis. It has become widely accepted that optically active metal complexes are highly instrumental in affecting the stereoselectivity of many catalytic reactions.<sup>12</sup> The preliminary screening of these Cp complexes **2.2** involved their employment as potential catalysts in oxidation reactions of activated methylene groups. The initial results suggested that these Cp complexes demonstrated significantly less catalytic activity when compared to complexes of the formula  $[\text{Fe}(\text{PHOX})_2]^+\text{OTf}^-$  ( $\text{OTf}^- = \text{CF}_3\text{SO}_3^-$ ). This difference in activity was believed to be the result of  $[\text{Fe}(\text{PHOX})_2]^+\text{OTf}^-$  already bearing an open site in the coordination sphere, a key requirement for activity.<sup>13</sup> The issue surrounding a lack of open coordination sites, observed for Cp complexes **2.2**, was addressed by exchange of the six electron donor cyclopentadienyl ligand for the indenyl ligand to yield complexes of the type  $[\text{Fe}(\eta^5\text{-C}_9\text{H}_7)(\text{CO})(\text{PHOX})]^+$ .

Literature reports have shown that just like the cyclopentadienyl ligand, the anionic indenyl ligand  $\text{C}_9\text{H}_7^-$  (Ind) is known to endure a  $\eta^5$  to  $\eta^3$  haptotropic shift in metal complexes

(Scheme 2.1).<sup>14</sup> This haptotropic shift, observed for the indenyl ligand, is far more facile and rapid than for its cyclopentadienyl  $C_5H_5^-$  (Cp) counterpart and is referred to as the “indenyl effect”.<sup>15</sup>



**Scheme 2.1.**  $\eta^5$  (left) to  $\eta^3$  (right) hapticity change observed for indenyl ligand.

The observed rate enhancement for indenyl derivatives was first described by Mawby and co-workers in studies on the kinetics and mechanisms of methyl migration in  $[Mo(\eta^5-C_9H_7)(Me)(CO)_3]$  as well as CO substitution by phosphines in structurally similar complexes.<sup>16</sup> More convincingly, Basolo and coworkers observed astonishing rate increasing effects of ca.  $10^8$  times for ligand substitution reactions compared with analogous cyclopentadienyl complexes. Henceforth, in my work, all subsequent complex synthesis incorporated the ubiquitous indenyl ligand into the structural framework through use of an iron indenyl precursor,  $[Fe(\eta^5-C_9H_7)I(CO)_2]$ .

The resulting cationic nature of the complexes  $[Fe(\eta^5-C_9H_7)(CO)(PHOX)]^+$  are ideal candidates to be tested for their efficacy as Lewis acid catalysts. Lewis acid catalysts are becoming increasingly more prevalent and well-known for their use in organic synthesis.<sup>17</sup> Moreover, they are considered to be a versatile class of compounds for being accepted as multi-functional activators, ranging from carbonyl activation<sup>18</sup> to ether linkage activation.<sup>19</sup> To this end, I wanted to address the question to what extent such cationic complexes would serve as carbonyl activators in a carbon-carbon bond forming reaction. A powerful route to this transformation is the Lewis acid



facilitated addition of an activated silane to a carbonyl compound and referred to as the Mukaiyama aldol reaction.<sup>20</sup> Although this reaction is considered to be amongst the most important of C-C forming reactions, its application is limited because conventional methods require that a stoichiometric amount of the Lewis acid be used. Additionally, the fastest growing area in the Mukaiyama aldol methodology is the development of asymmetric catalytic processes, utilizing chiral Lewis acid complexes.<sup>21</sup> This asymmetric application has great potential and was substantiated by Kobayashi with his catalytic approach during the total synthesis of *sphingofungins B* and *F*. On that account, it seemed highly desirable to investigate a catalytic approach as an improvement to existing conditions.

## 2.3 Results

### 2.3.1 Synthesis of phosphinooxazoline ligands.

We have already established a general synthetic strategy for the synthesis of PHOX ligands.<sup>22</sup> The overall driving force for choosing this class was motivated by several factors; (1) They could be easily prepared through the use of commercially available amino acids as starting materials, (2) They allowed for easy steric and electronic tuning, (3) Chirality may be employed on the oxazoline ring R<sup>1</sup> and R<sup>2</sup> offering up the unique possibility for asymmetric catalysis and (4) They consistently gave high yields with respect to overall synthesis. Previously in our laboratory, a basic methodology was developed and I just resynthesized them using a slight modification to literature procedures that began with acid chlorides and amino alcohols.<sup>23</sup>

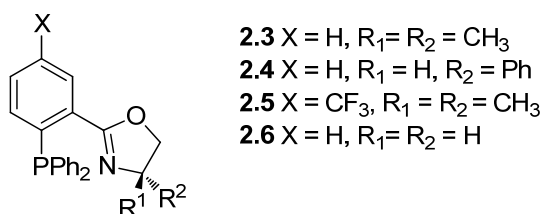
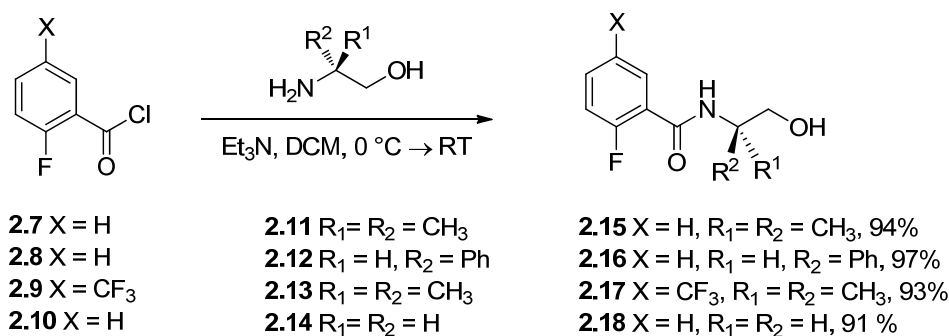


**Figure 2.2.** Sterically and electronically tuned PHOX ligands.

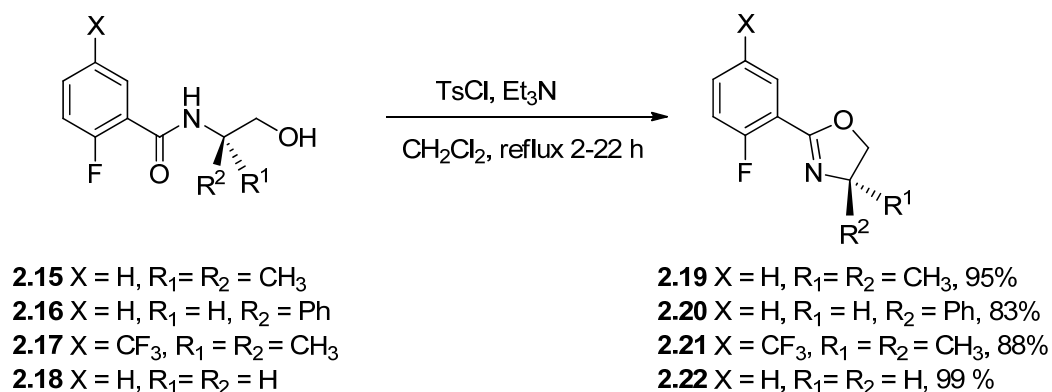
Multiple PHOX ligands were synthesized and characterized, each of which contained different substituents placed on either the aromatic backbone X or alpha to the nitrogen of the oxazoline ring R<sup>1</sup> and R<sup>2</sup> (Figure 2.2). The synthetic pathway started with 2-fluorobenzoic acid chlorides **2.7-2.10** and the starting amino alcohols **2.11-2.14**, both of which are commercially available. This strategy entailed a three step procedure, which was initiated through synthesis of the amide from the acid chloride and amino alcohol (Scheme 2.2). The reaction proceeded neatly to completion in high yield with no evidence of O-acylation. The reaction must be done at low temperatures (0 °C) and under very dilute conditions. As a result, the acid chloride (3 mL of CH<sub>2</sub>Cl<sub>2</sub> per mmol) must be added to a solution of the amino alcohol (4 mL of CH<sub>2</sub>Cl<sub>2</sub> per mmol) all while being vigorously stirred. Following complete addition, the reaction mixture was allowed to stir for an additional hour at room temperature. The progress of the reaction was monitored via TLC. After the additional hour, all of the amino alcohol had reacted. Then, the reaction mixture was washed in order to remove the Et<sub>3</sub>N·HCl salt formed in addition to desired product. The expected amides were spectroscopically pure, according to <sup>1</sup>H and <sup>19</sup>F NMR, and isolated as fluffy white solids in high yields, 91 to 97 % (Scheme 2.2).



**Scheme 2.2.** Synthesis of the amides.

Next, the resulting amides **2.15-2.18** were cyclized under basic conditions (Et<sub>3</sub>N) using an activating group (TsCl) to assist in departure of the hydroxyl group. The intramolecular cyclization was performed under elevated temperatures using CH<sub>2</sub>Cl<sub>2</sub> as solvent. The reactions took from 2.5 hours to as long as 24 hours depending on the sterics. The discrepancy associated with reaction times was most likely due to the difference in size of R<sup>1</sup> and R<sup>2</sup> on the oxazoline ring, as trends in substituent size and reaction times were observed. Amide **2.18**, which did not have any substituents at R<sup>1</sup> and R<sup>2</sup>, proceeded to completion after just 2.5 hours at reflux. The amide **2.16**, which had one phenyl substituent, did not proceed to completion until 15 hours. Amide **2.15**, which had two methyl substituents, appeared to not react completely until 22 hours had passed. And amide **2.17**, which had two methyls at R<sup>1</sup> and R<sup>2</sup> and CF<sub>3</sub> at X, required 36 hours for reaction. Interestingly, any additional time at reflux, for the preceding cyclizations, only caused decomposition of the already cyclized materials. After all of the cyclizations were pushed to completion, H<sub>2</sub>O (1.0-3.0 mL) was added to facilitate the decomposition of excess TsCl. After allowing the reaction to cool to room temperature, the reaction slurry was washed with H<sub>2</sub>O, 2 M aqueous NaHSO<sub>4</sub> and saturated NaHCO<sub>3</sub> to remove Et<sub>3</sub>N·HCl salt and any other water soluble side products. After removal of solvent, the resulting yellow and brown oils were purified via

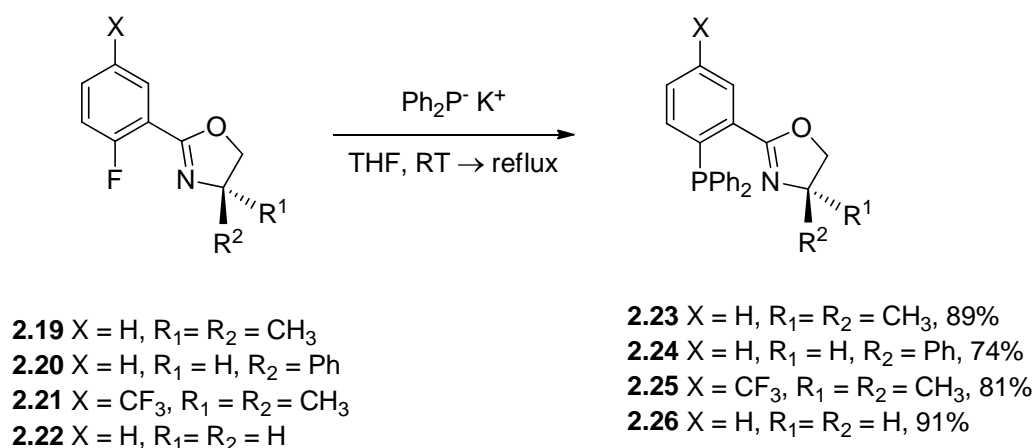
column chromatography which resulted in the targeted products in 83 to 99 % yield as colorless oils (Scheme 2.3).



**Scheme 2.3.** Cyclization of the amides.

These products **2.19-2.22** were then used as starting material for the next step, the diphenylphosphino moiety introduction (Scheme 2.4). This introduction proceeded through a basic electrophilic aromatic substitution of the fluorine atom on the aromatic skeleton. The reaction was performed by adding a 0.5 M solution of potassium diphenylphosphinide in THF dropwise to a solution of the fluorophenylloxazolines **2.19-2.22** in THF. After the addition was complete, the resulting mixture was refluxed, and its progression was monitored using TLC. All of the reactions seemed to be complete after three hours at reflux. Although there differences in reaction times were expected for the diphenylphosphino introduction for oxazolines **2.19-2.22**, as seen in cyclization steps, only minor discrepancies were noticed. This suggests that there is no major influence exerted by the sterics of the oxazoline ring on the rate of substitution. The minor differences in rate of substitution may also be attributed to the fact that the electronics on oxazolines **2.15-2.16**, **2.18** on the aromatic skeleton were similar. This rate similarity held true for all but one of the oxazolines, **2.17**. Oxazoline **2.17** had an extremely electron withdrawing group (CF<sub>3</sub>) located on the phenyl ring. The diphenylphosphino substitution generated the ex-

pected product after forty-five minutes, seemingly due to the electron withdrawing ability of the  $\text{CF}_3$  group. The progress of the reaction could be estimated through dissipation of the red color of the  $\text{KPPH}_2$  solution. Again, the products were purified via column chromatography and isolated as white solids in 74 to 91 % yields (Scheme 2.4). The degree of success for the introduction of the  $\text{PPh}_2$  group could be verified through  $^{31}\text{P}$  and  $^{19}\text{F}$  NMR spectra.



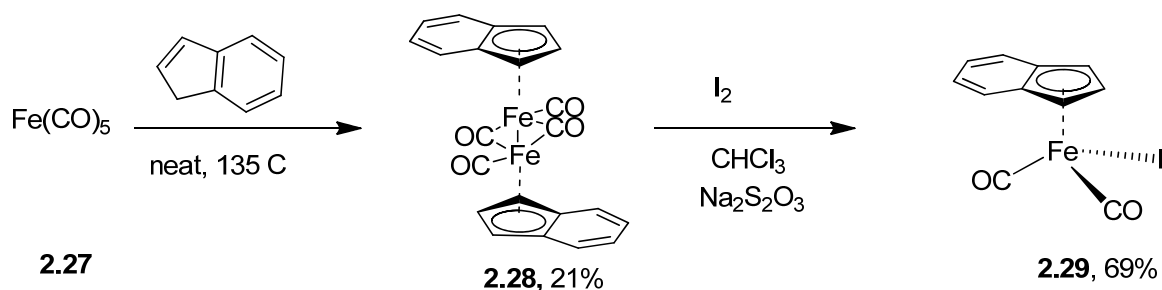
**Scheme 2.4.** Introduction of the diphenylphosphino moiety.

Each one of the four PHOX ligands varied from the other in their steric and electronic properties. Next, the influence that these properties exerted on complex formation and catalytic activity was studied.

### 2.3.2 Synthesis of new indenyl phosphinooxazoline complexes of iron.

Synthesis of the new piano-stool indenyl PHOX complexes of iron was targeted next. The initial stages of complex synthesis involved preparation of the iron indenyl precursor  $[\text{Fe}(\eta^5\text{-Ind})\text{I}(\text{CO})_2]$  following literature procedures (Scheme 2.5).<sup>24</sup> The first step to preparation of the indenyl precursor was formation of a carbonyl-bridged sandwich complex **2.28**. The dimer was

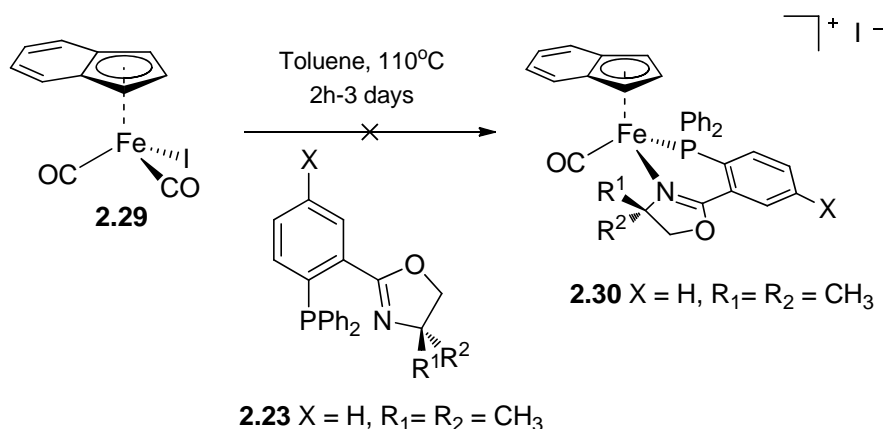
then suspended in chloroform to be oxidized, using iodine under ambient conditions, yielding the expected starting material **2.29** in 69% yield.



**Scheme 2.5.** Preparation of iron indenyl precursor,  $[\text{Fe}(\eta^5\text{-Ind})\text{I}(\text{CO})_2]$  **2.29**.

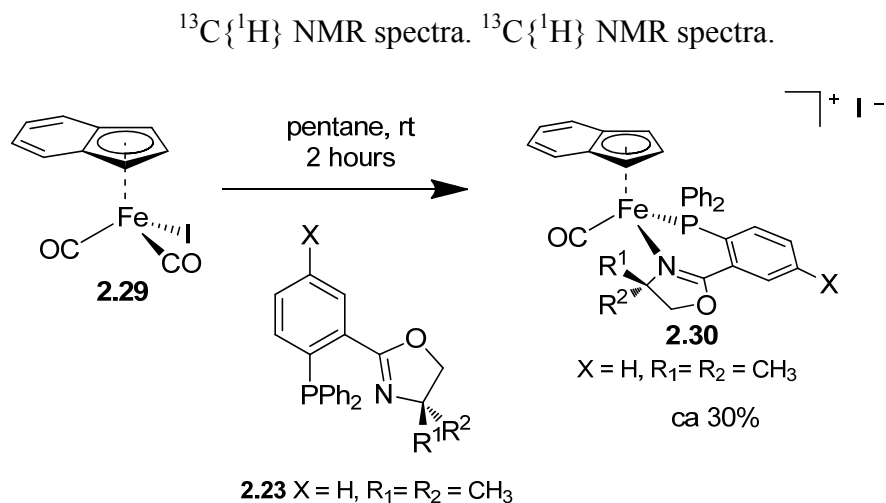
The synthesis of complex **2.2** (Figure 2.1) involved the employment of a similar cyclopentadienyl precursor, which was followed by their reaction with PHOX ligands in refluxing toluene.<sup>7</sup> Spectroscopic studies revealed that the Cp complexes were extremely robust and displayed very little evidence for decomposition in solution. Accordingly, it was believed that using identical reaction conditions for the preparation of structurally related indenyl complexes should result in structurally related complexes of similar stability. The first attempt involved the reaction between ligand **2.23** and precursor **2.29** in refluxing toluene, giving rise to only low conversion (<10%) to the expected iron complex **2.30**. Such a low yield could be explained by PHOX coordination followed by displacement of the indenyl ligand by the  $\pi$  system of the toluene ring. This was believed to be the case as free indene was observed in  $^1\text{H}$  NMR spectrum while a down field shift of the  $\text{CH}_3$  in toluene was observed which may suggest  $\pi$  interaction of the toluene with the empty d orbitals of the iron center. Dissociation of the indenyl ligand was supported by consistent  $^1\text{H}$ ,  $^{13}\text{C}\{^1\text{H}\}$  and  $^{31}\text{P}\{^1\text{H}\}$  spectra. Therefore, slightly modified reaction conditions (toluene, rt) were employed to try and evade the indenyl displacement by toluene. This attempt revealed that no complex was formed and only a multitude of side products and un-

reacted starting material was recovered as shown by the characteristic  $^{31}\text{P}\{^1\text{H}\}$  (-4.5 ppm) shift for the free PHOX ligand and the distinct  $^{13}\text{C}\{^1\text{H}\}$  set of signals for the indenyl precursor. Even after extended reaction times, no product was formed which may be attributed to the poor solubility of **2.29** in the reaction medium at room temperature, but no conclusive evidence for this theory was obtained (Scheme 2.6)



**Scheme 2.6.** Attempted complex iron indenyl PHOX complex synthesis.

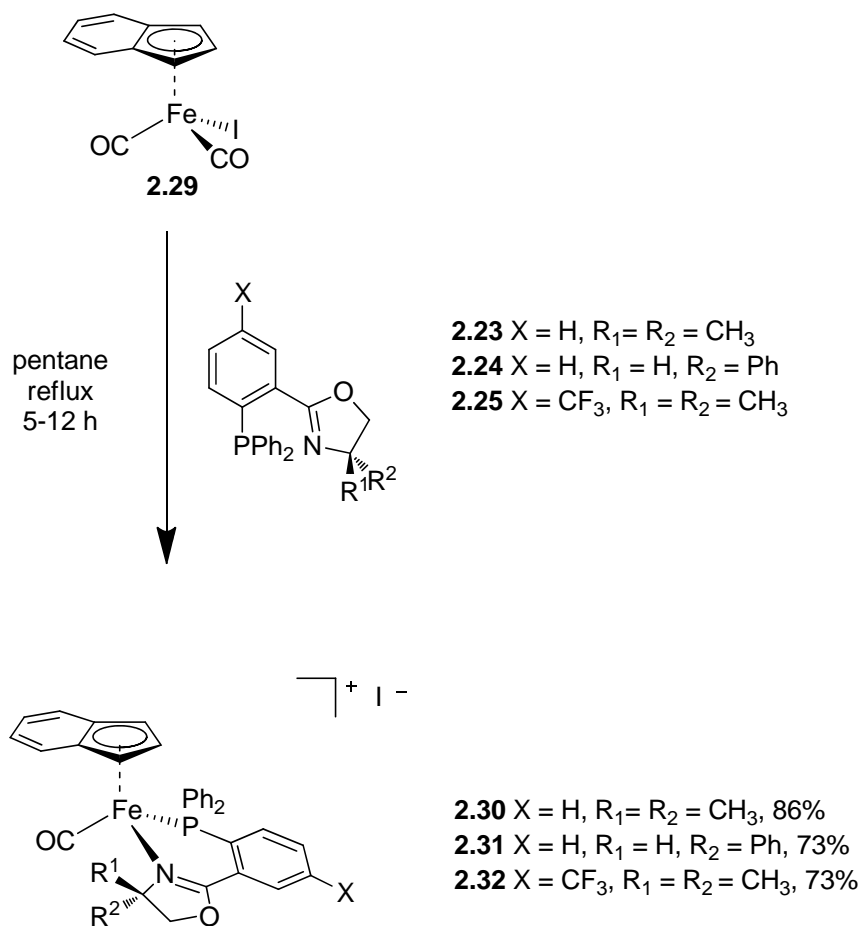
Indenyl complex synthesis still seemed attainable as long as less harsh or milder conditions were employed with a reaction media that did not contain an aromatic or  $\pi$  conjugated system. Appropriately, it was believed that using a nonpolar solvent with a lower boiling point would be more suitable for complex formation. Interestingly, when mild conditions were employed (pentane, rt), reaction results seemed to improve slightly, as new  $\text{H}_1$ ,  $\text{H}_2$ ,  $\text{H}_3$  of the cyclopentadiene portion of the indenyl ligand gave rise to 3 new singlets (5.70, 5.20 and 4.88 ppm) in the  $^1\text{H}$  NMR spectrum in addition to the appearance of a new singlet (64 ppm) in the  $^{31}\text{P}\{^1\text{H}\}$  NMR spectrum (Scheme 2.7) that was significantly different from the free ligand. Albeit, recognizable shifts indicating large amounts of starting materials were also present in the  $^1\text{H}$ ,  $^{31}\text{P}\{^1\text{H}\}$  and



**Scheme 2.7** Additional attempt of complex synthesis under milder conditions.

Again, the ‘sluggishness’ of the reaction may be due to lack of solubility of **2.29** and **2.23** in pentane at room temperature. Therefore, in an effort to rectify any solubility issue, it seemed logical to first apply higher reaction temperatures. Consequently, when the known complex **2.29** was refluxed in pentane with one equivalent of prepared ligand **2.23** for 2 h, the iodide salt of complex  $[\text{Fe}(\eta^5\text{-Ind})(\text{CO})(\mathbf{2.23})]^+$  was isolated as a light red solid after washing with diethyl ether in 86 % yield (Scheme 2.8). Thereupon, similar conditions with ligands **2.24** and **2.25** also gave the iodide salts of the complexes  $[\text{Fe}(\eta^5\text{-Ind})(\text{CO})(\mathbf{2.24})]^+$  and  $[\text{Fe}(\eta^5\text{-Ind})(\text{CO})(\mathbf{2.25})]^+$  as orange-red solids, both isolated in 73 % yield (Scheme 2.8).





**Scheme 2.8.** Synthesis of iron indenyl PHOX complexes.

However, when ligand **2.26** was employed in complex synthesis, no complex was isolated. After analysis of the complex mixture by IR and mass spectrometry, it revealed a mass consistent with coordination of the iodide counterion to the iron center. The IR indicated the presence of a C=O stretching frequency at  $1911\text{ cm}^{-1}$ , but it had a much lower frequency when compared to the other structurally characterized complexes typically around  $1950\text{ cm}^{-1}$ . This deviation in frequency is also compatible with counterion coordination. The unpredicted reactivity of **2.26** stimulated the plausibility of a steric influence, exerted by the ligands, during complex formation. No further studies to investigate the influence were performed.

The new indenyl PHOX complexes of iron were all characterized by NMR ( $^1\text{H}$ ,  $^{13}\text{C}\{^1\text{H}\}$ ,  $^{31}\text{P}\{^1\text{H}\}$ ), MS (including HRMS) and IR. Conveniently, coordination of the PHOX ligands was best seen by a large downfield shift in the  $^{31}\text{P}$  NMR spectra. The free ligands exhibited signals around -4.0 ppm, while the iron complexes thereof exhibited signals between 61.3 and 67.0 ppm. The cyclopentadienyl portion of the indenyl ligand, consistently showed a set of distinct signals in the  $^1\text{H}$  and  $^{13}\text{C}\{^1\text{H}\}$  NMR spectra.<sup>25</sup> The three protons showed characteristic signals between 5.70 and 4.88 ppm and the five carbon atoms displayed signals between 110.0 and 64.5 ppm. Another supplementary piece of evidence supporting PHOX coordination were the IR spectra. The IR spectra support PHOX coordination through a difference in stretching frequencies when comparing the frequency of the free ligand to the frequency observed after complex formation. The free ligands **2.23-2.26** each displayed a distinct  $\nu_{\text{C}=\text{N}}$  stretching frequency between 1630 and 1655  $\text{cm}^{-1}$ , respectively,<sup>7</sup> which undergo a sizable shift to lower wavenumbers (1607 to 1617  $\text{cm}^{-1}$ ) upon coordination to the iron center. As expected for complexes containing one carbonyl ligand, the IR spectra of all complexes showed only a single  $\nu_{\text{C}=\text{O}}$  stretch between 1941 and 1959  $\text{cm}^{-1}$ , whereas the precursor  $[\text{Fe}(\eta^5\text{-Ind})\text{I}(\text{CO})_2]$  displayed two stretches at 2023 and 1967  $\text{cm}^{-1}$ . Evidence of this single carbonyl ligand was also seen in the  $^{13}\text{C}\{^1\text{H}\}$  NMR as a distinct doublet between 217.6 and 221.2 ppm ( $^2J_{\text{CP}} = 29.4$  to 28.0 Hz) as previously seen in structurally similar complexes of iron.<sup>7</sup> The FAB MS displayed molecular ion peaks for all three complexes in addition to a loss of CO.

All three of the prepared iron PHOX complexes have a new chiral metal center, thus when ligands **2.23** and **2.24** were used in complex synthesis a racemic mixture was expected after isolated. However, when chiral ligand **2.25** was used for complex synthesis, diastereoselectivity became an issue, as there were two stereocenters present, one at the metal center and the other on

the ligand. Analysis of the  $^1\text{H}$ , and  $^{31}\text{P}\{^1\text{H}\}$  NMR spectra supported a 94:6 diastereomeric ratio of the isolated material.

In order to unambiguously unveil the molecular structure of **2.30**, X-ray quality crystals were grown, and structural determination was performed using single-crystal X-ray crystallography. The molecular framework is shown in Figure 2.3 where selected bond lengths and angles are given. Upon comparison of key structural data acquired from complex **2.2** to that of complex **2.30** it appears that both complexes are structurally related. The molecular composition of **2.30** confirms the piano stool type coordination around the iron center. The bond angles about the iron range from  $83.76(11)^\circ$  for the N(1)-Fe-P(1) angle to  $99.61(18)^\circ$  for the C(10)-Fe-N(1) angle. Hence, the coordination geometry of the complexes may be best described as slightly distorted octahedral. The elucidated X-ray structure also corroborated the fact that only one of the carbonyl ligands and the iodide was replaced by the PHOX ligand during complex synthesis.

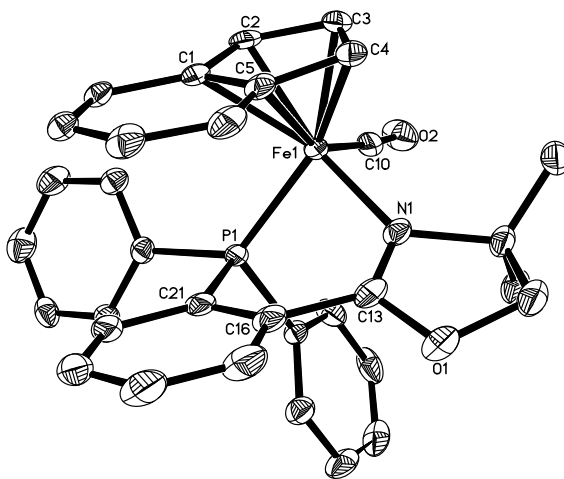
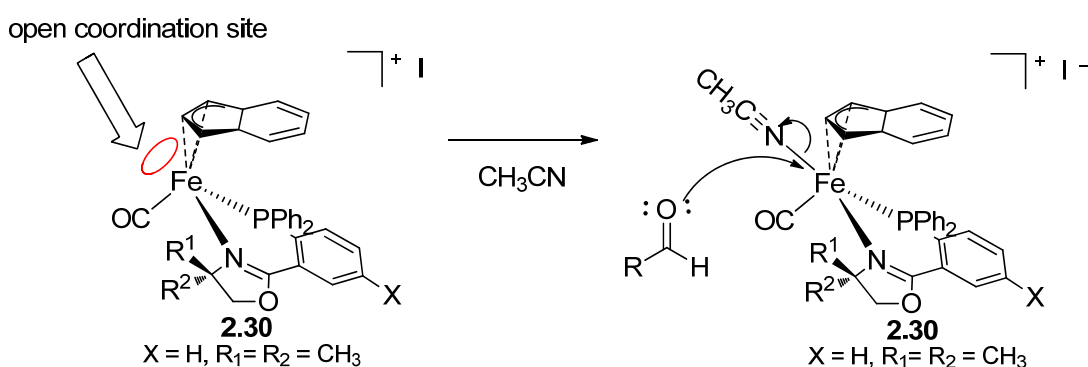


**Figure 2.3.** Molecular structure of **2.30** (depicted with 65 % probability ellipsoids; H atoms and the acetone solvate are omitted for clarity). Key bond lengths (Å) and bond angles ( $^\circ$ ):

Fe-C10, 1.746(5); Fe-N1, 1.999(4); Fe-P1, 2.2091(12); N1-C13, 1.285(6); Fe-C2, 2.100(4); Fe-C4, 2.100(4); Fe-C1, 2.241(4); Fe-C5, 2.228(4); C10-O2, 1.148(6); C10-Fe-N1, 99.61(18); N1-Fe-P1, 83.76(11); C10-Fe-P1, 95.18(14); O2-C10-Fe, 174.1(14). The P-Fe-N “bite angle” was less than  $90^\circ$  and as a consequence the other bond angles were larger.

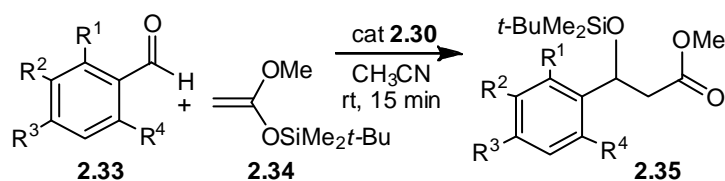
### 2.3.3 Catalytic activation of carbonyl compounds

The initial stages of catalytic screening involved testing complex **2.30** as a gentle Lewis acid catalyst, in the Mukaiyama Aldol reaction of aldehydes **2.33** and 1-(*tert*-butyldimethylsilyloxy)-1-methoxyethene **2.34** to obtain the desired aldol adduct **2.35** (Table 2.1) In order to ensure the highest possible yields for any given catalyzed reaction, one must understand the nature of the reaction mechanism. Familiarity with iron based metal complexes and the prerequisite for their catalytic ability persuaded me to explore reactions conditions conducive to stabilization of their reactive intermediates. I postulated that  $\text{CH}_3\text{CN}$  was an excellent choice of solvent due to its coordinating abilities. It most likely provides an excellent source of stabilization for the reactive intermediate through temporary occupation of the open coordination site at the iron center, which should then be replaced by the aldehyde or ketone (Scheme 2.9).



**Scheme 2.9.** Potential intermediate in presence of  $\text{CH}_3\text{CN}$ .

The presence of open coordination sites are believed to be created by either a ‘ring slippage’ or complete dissociation of the indenyl ligand. However, no dissociation of the indenyl ligand was ever observed, in  $^1\text{H}$  and  $^{13}\text{C}\{^1\text{H}\}$  NMR spectra, under the established reaction conditions (Table 2.1). The utility of  $\text{CH}_3\text{CN}$  as a solvent proved to be effective, as moderate to good yields were obtained when utilized. As a result, I hypothesized that other coordinating solvents should have similar effects on reactivity. Nevertheless, even after exchange of reaction media by both coordinating and non-coordinating solvents, only residual amounts of products were observed when THF, diethyl ether,  $\text{CH}_2\text{Cl}_2$ , MeOH and toluene were used. Other coordinating solvents dissipated product formation and prolonged reaction times. Despite the discouraging results, the idea that the coordinating solvents aid in stabilization of the reactive species was not yet discredited. Analysis of the  $^1\text{H}$  NMR spectrum strongly suggested solvent coordination via an upfield shift of the methyl protons (2.0 – 1.0 ppm). This evidence suggests that other coordinating solvents like MeOH and THF may be too strongly coordinating and therefore hamper the ability of the active species to coordinate to the carbonyl compound resulting in an inability to become activated towards substitution. It was hypothesized that optimal results would be obtained by treating preactivated carbonyl compounds with vinyl silyl ethers in  $\text{CH}_3\text{CN}$  at room temperature. These reaction conditions laid the groundwork for this application and were used in all future studies. An array of electronically and sterically different aromatic aldehydes seemed to show good compatibility in the title reaction, but when several aliphatic aldehydes were employed, only complex mixtures of unidentifiable side products were noticed. Unfortunately, the only aliphatic aldehyde that generated a product capable of being isolated and spectroscopically identified was butyraldehyde. When aromatic ketones, such as acetophenone, were tested, the reaction rates seemed to drastically decrease, which resulted only in an inseparable plethora of products.

**Table 2.1.** Iron catalyzed mukaiyama aldol reaction.

Entry	Aldehyde	Yield <sup>b</sup>	TOF / h <sup>-1</sup> <sup>c</sup>
1	R <sup>1</sup> = R <sup>2</sup> = R <sup>3</sup> = R <sup>4</sup> = H, <b>a</b>	74% <sup>d</sup>	98
2	R <sup>1</sup> = R <sup>2</sup> = R <sup>4</sup> = H, R <sup>3</sup> = NO <sub>2</sub> , <b>b</b>	59%	78
3	R <sup>1</sup> = OMe, R <sup>2</sup> = R <sup>3</sup> = R <sup>4</sup> = H, <b>c</b>	62%	80
4	R <sup>2</sup> = OMe, R <sup>1</sup> = R <sup>3</sup> = R <sup>4</sup> = H, <b>d</b>	78%	101
5	R <sup>3</sup> = OMe, R <sup>1</sup> = R <sup>2</sup> = R <sup>4</sup> = H, <b>e</b>	70%	91
6	R <sup>1</sup> = Cl, R <sup>2</sup> = R <sup>3</sup> = R <sup>4</sup> = H, <b>f</b>	83%	104
7	R <sup>3</sup> = CH <sub>3</sub> , R <sup>1</sup> = R <sup>2</sup> = R <sup>4</sup> = H, <b>g</b>	76%	101
8	R <sup>1</sup> = R <sup>3</sup> = R <sup>4</sup> = CH <sub>3</sub> , R <sup>2</sup> = H, <b>h</b>	64%	86
9	R <sup>1</sup> = CH <sub>3</sub> , R <sup>2</sup> = R <sup>3</sup> = R <sup>4</sup> = H, <b>i</b>	70%	93
10	R <sup>2</sup> = CH <sub>3</sub> , R <sup>1</sup> = R <sup>3</sup> = R <sup>4</sup> = H, <b>k</b>	79%	106
11	R <sup>1</sup> = R <sup>2</sup> = R <sup>4</sup> = H, R <sup>3</sup> = Et, <b>l</b>	48%	64
12	butyraldehyde, <b>m</b>	54%	71

<sup>a</sup> Conditions: The aldehyde **2.33** (0.377 mmol) was dissolved in CH<sub>3</sub>CN (1.0 mL). The catalyst **2.30** (0.011 mmol) was added, followed by 1-(*tert*-butyldimethylsilyloxy)-1-methoxyethene **2.34** (0.377 mmol). After 15 min at rt, the solvent was removed and the products were isolated by column chromatography.

<sup>b</sup> Isolated yields after column chromatography.

<sup>c</sup> Turnover frequency determined from isolated yields: number of moles (product) over (number of moles (catalyst) times reaction time).

<sup>d</sup> Employment of the chiral catalyst **2.31** resulted in essentially no enantiomeric excess for this reaction, as determined by chiral GC.

Therefore, only aromatic aldehydes could be utilized for the title reaction. Accordingly, complex **2.30** was used as a catalyst, in a multitude of reactions, involving the reaction between aromatic aldehydes **2.33** and 1-(*tert*-butyldimethylsilyloxy)-1-methoxyethene **2.34**. Under optimized conditions (3.0 mol% catalyst, CH<sub>3</sub>CN, 15 minutes, room temperature) the corresponding aldol adducts were isolated in 48 to 83% yields as colorless oils (Table 2.1).

Following the successful isolation of a diastereopure complex **2.31**, the idea of its employment as a potential chiral catalyst was instigated. Initial studies of complex **2.31** and its ability to produce enantioselective induction gave discouraging results, as no ee's were observed according to chiral GC (FID). This immediately prompted me to investigate the effect of a lower temperature (-40 °C) on the ee's. The rationale was very clear for the choice of lower temperatures, as it was believed that one could significantly slow the reaction rate, thereby gradually initiating a more ordered transition state between the complexed aldehyde and the incoming vinyl silyl ether. Such a cold temperature impeded the reaction rate tremendously and resulted in longer reaction times of 16 to 24 h with no increase in ee's. As a result, warmer temperatures were investigated (-20 - 15 °C), which also appeared to yield only slightly improved ee's and were accompanied by longer reaction times, (6 to 10 h). It was unclear as to why no ee's had resulted during the employment of catalyst **2.31** in the title reaction. The remaining attempts to attain respectable ee's were then focused on basic temperature variations and the use of methyl ketones in hopes that a stronger steric influence may be exerted to result in higher ee's. This, too, resulted in the retardation of reaction rates, non-existent ee's and the formation of a plethora of side products, as evidenced by chiral GC, GCMS and <sup>1</sup>H NMR. All future attempts to enhance ee's were, thus, placed on hold.

#### **2.4 Discussion - Comparison of structurally similar complexes**

A comparison of the catalytic efficiency for the indenyl PHOX iron complexes **2.30-2.32** revealed that all three gave similar results (Table 2.1, entry 1). No major differences in reaction rates were observed for complexes bearing PHOX ligands with different substitutions. I was troubled by the fact that complexes bearing electronically and sterically unique PHOX ligands displayed such a negligible difference in catalytic ability. Consequently, I compared these novel iron

indenyl complexes to their cyclopentadienyl predecessor **2.2**. Interestingly, the Cp analogue appeared to be an order of magnitude less reactive than its indenyl counterpart for the reaction between benzaldehyde and **2.34** (Table 2.1, entry 1).

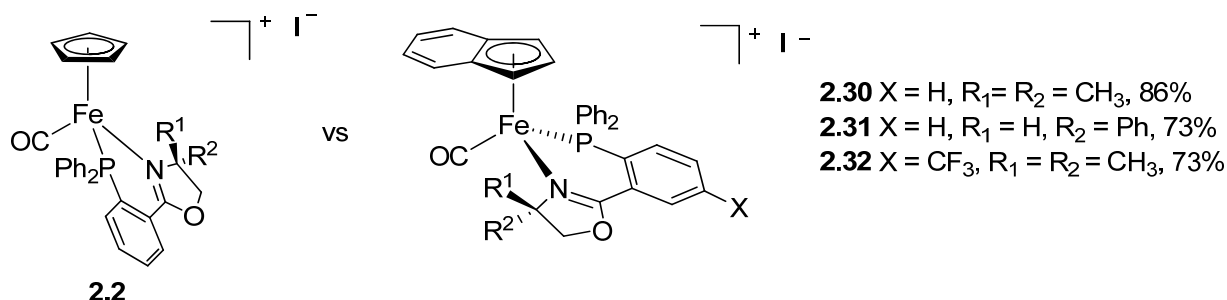


**Figure 2.4.** Comparison of iron indenyl PHOX complex and its cyclopentadienyl analogue.

Overall, the complexes described herein are, at the very least, comparable, if not more reactive, than other transition metal complexes also capable of catalyzing the Mukaiyama aldol reaction. Recently, Nishiyama reported that 8 mol% of the rhenium complex  $Re(CO)_5Br$  is catalytically active in the reaction between vinyl silyl ether **2.34** and aromatic aldehydes to the corresponding adducts (1 h, 80 °C, 50 to 80% isolated yields).<sup>26</sup> Mukaiyama reported that 10 mol% of an  $InCl_3 \cdot AgClO_4$  mixture is catalytically active in the reaction between **2.34** and benzaldehyde (2 h, -78 °C, 96% isolated yield).<sup>27</sup> Reetz describes a similar complex,  $[Fe(Cp)(dppe)(CO)]^+$ , as catalytically active in the reaction between **2.34** and benzaldehyde after photolytic activation (2.5 mol% catalyst, 20 h, -20 °C, 77%, dppe = diphenylphosphinoethane).<sup>28</sup> Although the preceding complexes display catalytic activity, there are several drawbacks, as they all require energy to be put into or taken from the system, they all experience prolonged reaction times and none of them exhibit a stereogenic metal center making the chance for any stereoselective control impossible.



The catalytic activity of the complexes **2.30-2.32** is not quite yet understood, but they are likely to act as gentle Lewis acids in solution. With a better mechanistic understanding, it should be possible to strategically enhance catalytic activity through various tuning efforts. Trivial electronic manipulations, as seen in complex **2.32**, could easily result in a decrease of electron density at the metal center, thus making it more likely to form the proposed catalytically active species. It appears that the only substitution that made a difference in activity was the substitution of Cp for Ind. This difference was attributed to the well known “indenyl effect”.

## 2.5 Summary and Prospective

A number of new, structurally modified iron indenyl PHOX complexes of the general formulation  $[\text{Fe}(\eta^5\text{-Ind})(\text{CO})(\text{PHOX})]^+$  have been prepared and spectroscopically characterized and in one case structurally characterized. The complexes are easily obtained through a reaction between the iron indenyl precursor  $[\text{Fe}(\eta^5\text{-Ind})(\text{CO})_2(\text{I})]$  and one equivalent of each of the three PHOX ligands, in refluxing pentane, in 73 to 86% isolated yield. The reported investigation is, to the best of my knowledge, the first time these new iron indenyl PHOX complexes have been applied as catalysts in the Mukaiyama aldol reaction between various aromatic aldehydes and 1-(*tert*-butyldimethylsilyloxy)-1-methoxyethene generating the expected aldol adducts in 48-83% yields. The novel complexes show significantly enhanced reactivity in comparison to their analogous Cp complexes. The reaction proceeds very quickly with turnover frequencies ranging from 64 to 106  $\text{h}^{-1}$ . Additional modifications to molecular architecture and their influence on catalytic activity would be of interest.

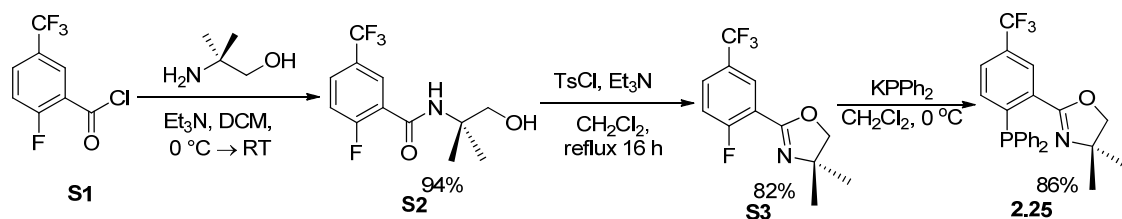
## 2.6 Experimental

**General.** Chemicals were treated as follows: Acetonitrile and pentane were distilled from CaH<sub>2</sub>. The substrates for the catalytic experiments are all commercially available (Aldrich). [Fe( $\eta^5$ -Ind)(CO)<sub>2</sub>I] iron complex **2.2** and the phosphinooxazoline (PHOX) ligands **2.23-2.24**, **2.26** were synthesized according to the literature.<sup>7</sup> PHOX ligand **2.25** was synthesized as outlined below. Metal complex syntheses were carried out under nitrogen employing standard Schlenk techniques and workups were performed under ambient conditions. The catalytic experiments were performed under ambient conditions.

The NMR spectra were obtained at room temperature on a Bruker Avance 300MHz or a Varian Unity Plus 300MHz instrument and referenced to a residual solvent signal or to an internal TMS standard. All coupling constants are given in Hz. Couplings were identified based on peak intensities; all assignments are tentative, and based on structurally related iron<sup>7</sup> and indenyl complexes.<sup>29</sup> GC/MS spectra were recorded on a Hewlett Packard GC/MS system model 5988A. Exact masses were acquired on a of JEOL MStation [JMS-700] mass spectrometer. IR spectra were recorded on a Thermo Nicolet 6700 FT-IR spectrometer. Elemental analyses was obtained via Atlanta Microlabs.

### *Synthesis of the PHOX ligand 2.25.*

The ligand was synthesized following an identical synthetic pathway as previously described for other structurally related PHOX complexes (Scheme S1)



**Scheme 2.10.** Synthetic pathway to the PHOX ligand **2.25**.

### 2-Fluoro-*N*-(2-hydroxy-1,1-dimethylethyl)-5-(trifluoromethyl)benzamide

(**S2**). To a stirred solution of 2-amino-2-methyl-1-propanol (0.648 g, 0.694 mL, 7.28 mmol) in CH<sub>2</sub>Cl<sub>2</sub> (30 mL), Et<sub>3</sub>N (1.40 g, 1.93 mL, 13.9 mmol) was added. The resulting solution was cooled to 0 °C (ice bath) and a solution of the acid chloride **S1** (1.05 mL, 1.57 g, 6.93 mmol) in CH<sub>2</sub>Cl<sub>2</sub> (25 mL) was added dropwisely. The reaction mixture was stirred at 25 °C for 2 hours and then diluted with CH<sub>2</sub>Cl<sub>2</sub> (50 mL). The organic layer was washed with H<sub>2</sub>O (50 mL), 0.2 M solution of aqueous NaHSO<sub>4</sub>, H<sub>2</sub>O, with a saturated aqueous solution of NaHCO<sub>3</sub> and H<sub>2</sub>O. The combined organic layers were dried over MgSO<sub>4</sub> and concentrated *in vacuo*. The crude product was purified by flash column chromatography on SiO<sub>2</sub> (2 x 20 cm column; eluted with 1:0 v/v toluene/EtOAc 7:3 v/v toluene/EtOAc) to obtain the product **S2** (1.81 g, 6.48 mmol, 94%) as white powder.

NMR ( $\delta$ , CDCl<sub>3</sub>) <sup>1</sup>H 8.15 (m, 1H, aromatic), 7.53 (m, 1H, aromatic), 7.39 (m, 1H, aromatic), 6.86 (d, <sup>5</sup>J<sub>HF</sub> = 3.3, 1H, NH), 4.25 (t, <sup>3</sup>J<sub>HH</sub> = 5.7, 1H, OH), 3.70 (d, <sup>3</sup>J<sub>HH</sub> = 5.7, 2H, CH<sub>2</sub>), 1.43 (s, 6H, 2CH<sub>3</sub>); <sup>13</sup>C{<sup>1</sup>H} 162.3 (d, <sup>3</sup>J<sub>CF</sub> = 3.3, C=O), 159.8 (d, <sup>1</sup>J<sub>CF</sub> = 249.2, CF), 135.5 - 134.8 (m), 132.9 (d, J<sub>CF</sub> = 2.2), 125.0 (d, J<sub>CF</sub> = 11.0), 121.9 - 121.4 (m, J = 3.7, J<sub>CF</sub> = 3.7, J<sub>CF</sub> = 3.6, J<sub>CF</sub> = 3.3, aromatic), 122.7 (qd, J<sub>CF</sub> = 272.3, J<sub>CF</sub> = 2.7, CF<sub>3</sub>), 114.2 - 113.4 (m, aromatic), 70.1 (s, CH<sub>2</sub>O), 56.8 (s, C(CH<sub>3</sub>)<sub>2</sub>), 24.5 (s, 2CH<sub>3</sub>); <sup>19</sup>F{<sup>1</sup>H} -63.6 (s, 3F, CF<sub>3</sub>), -

111.9 (s, 1F, *F*). MS (EI, *m/z*): 248 ( $[(\mathbf{S2})-\text{OH}]^+$ , 20%), 191 ( $[(\mathbf{S2})-\text{NHC}(\text{CH}_3)_2\text{OH}]^+$ , 100%), 163 ( $\text{C}_6\text{H}_4\text{F}(\text{CF}_3)$ , 20%).

**2-[2-Fluoro-5-(trifluoromethyl)phenyl]-4,4-dimethyl-4,5-dihydro-1,3-oxazole.** To a stirred solution of **S2** (0.940 g, 3.37 mmol) in  $\text{CH}_2\text{Cl}_2$  (50 mL),  $\text{Et}_3\text{N}$  (1.02 g, 1.41 mL, 10.1 mmol),  $\text{TsCl}$  (1.28 g, 6.73 mmol) and DMAP (0.041 g, 0.337 mmol) were added. The resulting solution was stirred at reflux for 16 hours.  $\text{H}_2\text{O}$  (0.5 mL) was added to the reaction mixture and it was refluxed for additional 1 hour. After the reaction mixture was cooled down to 25 °C, it was diluted with  $\text{CH}_2\text{Cl}_2$  (30 mL) and washed with  $\text{H}_2\text{O}$ , 0.2 M solution of aqueous  $\text{NaHSO}_4$ ,  $\text{H}_2\text{O}$ , saturated solution of  $\text{NaHCO}_3$  and  $\text{H}_2\text{O}$ . The combined organic layers were dried over  $\text{MgSO}_4$  and concentrated *in vacuo*. The crude product was purified by flash column chromatography on  $\text{SiO}_2$  (1 x 15 cm column; eluted with 9:1 v/v toluene/ $\text{EtOAc}$ ) to obtain the product **S3** (0.723 g, 2.77 mmol, 82%) as a white solid.

NMR ( $\delta$ ,  $\text{CDCl}_3$ )  $^1\text{H}$  8.02 (m, 1H, aromatic), 7.50-7.35 (m, 2H, aromatic), 4.14 (s, 2H,  $\text{CH}_2$ ), 1.42 (s, 6H,  $2\text{CH}_3$ );  $^{13}\text{C}\{^1\text{H}\}$  [4] 162.8 (d,  $^1J_{\text{CF}} = 264.6$ , CF), 157.7 (d,  $^3J_{\text{CF}} = 5.5$ , C=N), 129.9 - 129.6 (m), 129.0 (quin,  $J_{\text{CF}} = 3.6$ ), 127.1 - 126.5 (m, aromatic), 123.4 (q,  $^1J_{\text{CF}} = 272.2$ ,  $\text{CF}_3$ ), 117.5 (d,  $J_{\text{CF}} = 23.6$ ), 117.3 (d,  $J_{\text{CF}} = 11.5$ , aromatic), 79.1 (s,  $\text{CH}_2\text{O}$ ), 68.2 (s,  $\text{C}(\text{CH}_3)_2$ ), 28.3 (s,  $2\text{CH}_3$ );  $^{19}\text{F}\{^1\text{H}\}$  -63.9 (s, 3F,  $\text{CF}_3$ ), -107.3 (s, 1F, *F*). MS (EI, *m/z*) 261 ( $[(\mathbf{S3})]^+$ , 5%), 246 ( $[(\mathbf{S3})-\text{CH}_3]^+$ , 70%), 191 ( $[(\mathbf{S3})-\text{NC}(\text{CH}_3)_2\text{CH}_2]^+$ , 100%).

**2-[5-Trifluoromethyl-2-(diphenylphosphino)phenyl]-4,4-dimethyl-4,5-dihydro-1,3-oxazole (2.25).** A Schlenk flask was charged with the aryl fluoride (**S3**, 0.467 g, 1.79 mmol) and  $\text{KPPH}_2$  (0.5 M in THF, 3.90 mL, 1.97 mmol) was added dropwisely with stirring. The resulting

reddish solution was refluxed for 1 h. The reaction mixture was diluted with  $\text{CH}_2\text{Cl}_2$  (50 mL) and poured into a saturated aqueous solution of  $\text{NaHCO}_3$  (25 mL). The organic layer was separated, washed with  $\text{H}_2\text{O}$  and dried over  $\text{MgSO}_4$ . The solution was concentrated *in vacuo* and the crude product purified by flash column chromatography on silica (1 x 15 cm column; eluted with 1:0 v/v toluene/EtOAc  $\rightarrow$  7:3 v/v toluene/EtOAc) to obtain the product **1c** (0.659 g, 1.54 mmol, 86%) as a white solid.

NMR ( $\delta$ ,  $\text{CDCl}_3$ )  $^1\text{H}$  8.19-8.09 (m, 1H, aromatic), 7.49 (d,  $^3J_{\text{HH}} = 7.9$ , 1H, aromatic), 7.41-7.25 (m, 10H, aromatic), 6.95 (dd,  $^3J_{\text{HH}} = 8.0$ ,  $J_{\text{PH}} = 3.7$ , 1H, aromatic), 3.75 (s, 2H,  $\text{CH}_2$ ), 1.05 (s, 6H,  $2\text{CH}_3$ );  $^{13}\text{C}\{^1\text{H}\}$  161.1 (d,  $^3J_{\text{CP}} = 3.3$ ,  $\text{C}=\text{N}$ ), 144.2 (d,  $J = 30.2$ , aromatic), 136.9 (d,  $J = 11.0$ , aromatic), 134.2 (d,  $J = 22.0$ , aromatic), 133.8 (d,  $J = 3.8$ , aromatic), 132.3 (d,  $J = 17.0$ , aromatic), 130.0 (d,  $J = 32.4$ , aromatic), 129.1 (s, aromatic), 128.7 (d,  $J = 7.7$ , aromatic), 126.9-126.4 (m, aromatic), 123.8 (q,  $^1J_{\text{CF}} = 272.2$ ,  $\text{CF}_3$ ), 79.0 (s,  $\text{CH}_2\text{O}$ ), 67.9 (s,  $\text{C}(\text{CH}_3)_2$ ), 27.9 (s,  $\text{CH}_3$ );  $^{19}\text{F}\{^1\text{H}\}$  -63.5 (d,  $^6J_{\text{FP}} = 2.1$ ,  $\text{CF}_3$ );  $^{31}\text{P}\{^1\text{H}\}$  -3.1 (s). HRMS calcd for  $\text{C}_{24}\text{H}_{22}\text{F}_3\text{NOP}$  428.1391, found 428.1375; IR ( $\text{cm}^{-1}$ , neat solid)  $\nu_{\text{C}=\text{N}}$  1655 (m).

#### *Synthesis of the iron complexes.*

$[\text{Fe}(\eta^5\text{-Ind})(\text{CO})(\mathbf{2.23})]^+ \Gamma^- (\mathbf{2.30})$ . To a Schlenk flask containing pentane (5 mL) and  $[\text{Fe}(\eta^5\text{-Ind})\text{I}(\text{CO})_2] \mathbf{2.29}$  (0.112 g, 0.316 mmol), the phosphinoxazoline **2.23** (0.136 g, 0.379 mmol) was added and the solids dissolved. The resulting deep brown solution was refluxed for five hours. The light brown-red slurry was then removed from the oil bath and placed at room temperature for ten minutes. The brown supernatant was removed via pipette and the remaining light tan-red solid was washed thoroughly with cold diethyl ether (0 °C,  $2 \times 5$  mL). The solvent was then removed under high vacuum, yielding a light red solid (0.186 g, 0.272 mmol, 86 %).

NMR ( $\delta$ , CD<sub>3</sub>CN) <sup>1</sup>H 7.89–7.84 (m, 1H, aromatic), 7.72–7.59 (m, 8H, aromatic), 7.39–7.23 (m, 5H, aromatic), 7.05–6.94 (m, 4H, aromatic), 6.77–6.71 (m, 1H, aromatic), 5.70 (s, br, 1H, indenyl), 5.21–5.18 (t, <sup>3</sup>J<sub>HH</sub> = 2.8, 1H, indenyl), 4.88 (s, br, 1H, indenyl), 4.20–4.18 (d, <sup>3</sup>J<sub>HH</sub> = 4.4, 1H, CHH), 4.05–4.02 (d, <sup>3</sup>J<sub>HH</sub> = 8.8, 1H, CHH), 1.36 (s, 3H, CH<sub>3</sub>), –0.12 (s, 3H, CH<sub>3</sub>’); <sup>13</sup>C{<sup>1</sup>H} 221.2 (d, <sup>2</sup>J<sub>CP</sub> = 29.4, CO), 167.0 (d, J<sub>CP</sub> = 6.3, C=N), 135.6 (d, J<sub>CP</sub> = 11.7), 134.2 (s), 133.5 (s), 132.8 (d, J<sub>CP</sub> = 2.6), 132.6 (d, J<sub>CP</sub> = 3.6), 132.5 (d, J<sub>CP</sub> = 3.0), 131.9 (s), 131.8 (d, J<sub>CP</sub> = 2.0), 131.79 (s), 131.6 (s), 131.2 (s), 131.1 (d, J<sub>CP</sub> = 2.4), 129.9 (s), 129.7 (s), 129.4 (s), 129.3 (s), 128.4 (s), 128.1(s), 127.7 (d, J<sub>CP</sub> = 4.0), 125.4 (s), 125.3 (s, aromatic), 109.6 (s, indenyl), 107.0 (d, J<sub>CP</sub> = 1.4, indenyl), 85.7 (s, indenyl), 79.5, 72.7 (2s, CH<sub>2</sub> and C(CH<sub>3</sub>)<sub>2</sub>), 72.4 (d, J<sub>CP</sub> = 3.9, indenyl), 65.7 (s, indenyl), 25.6 (s, CH<sub>3</sub>), 23.6 (s, CH<sub>3</sub>’); <sup>31</sup>P{<sup>1</sup>H} 62.9. HRMS calcd for C<sub>33</sub>H<sub>29</sub>FeNO<sub>2</sub>P 558.12848; found 558.1285. MS (FAB, 3-NBA, *m/z*): 558 ([**2.30**]<sup>+</sup>, 20%), 530 ([**2.30**–CO]<sup>+</sup>, 100%). IR (cm<sup>–1</sup>, neat solid)  $\nu_{\text{C=O}}$  1941(m)  $\nu_{\text{C=N}}$  1607 (w).

[Fe( $\eta^5$ -Ind)(CO)(**2.24**)]<sup>+</sup> I<sup>–</sup> (**2.31**). To a Schlenk flask containing pentane (6 mL) and [Fe( $\eta^5$ -Ind)I(CO)<sub>2</sub>] **2.29** (0.103 g, 0.291 mmol), the phosphinooxazoline (**2.24**, 0.142 g, 0.349 mmol) was added and the solids dissolved. The resulting deep brown solution was refluxed overnight. The light tan slurry was removed from the oil bath. The brown supernatant was removed via pipette and the resulting tan-orange solid was washed thoroughly with toluene (2 × 5 mL). The solvent was then removed under high vacuum, yielding a orange-tan solid (0.129 g, 0.212 mmol, 73 %).

NMR ( $\delta$ , CD<sub>3</sub>CN) <sup>1</sup>H 8.09 (m, 1H, aromatic), 7.65–6.83 (m, 23H, aromatic), 6.25 (d, <sup>3</sup>J<sub>HH</sub> = 7.7, 2H, aromatic), 5.33 (s, 1H, indenyl), 4.92–4.83 (m, 2H, indenyl), 4.49–4.43 (m, 1H, CHH), 4.26–4.20 (m, 1H, CHH); <sup>13</sup>C{<sup>1</sup>H} 217.6 (d, <sup>2</sup>J<sub>CP</sub> = 28.0, CO), 168.6 (d, J<sub>CP</sub> = 5.8, C=N), 138.5

(s), 135.0 (d,  $J_{CP} = 11.3$ ), 133.7 (d,  $J_{CP} = 6.0$ ), 28.5 (d,  $J_{CP} = 2.7$ ), 128.3 (s), 128.0 (s), 125.8 (s) 125.7 (s, aromatic), 107.3 (s, indenyl), 107.0 (d,  $J_{CP} = 1.4$ , indenyl), 87.3 (s, indenyl), 76.1, 74.6 (2s,  $CH_2$  and  $CHPh$ ), 70.2 (s, indenyl), 67.4 (d,  $J_{CP} = 2.3$ , indenyl).  $^{31}P\{^1H\}$  65.9 (s, minor diastereomer, 6%), 64.4 (s, major diastereomer, 94%). HRMS calcd for  $C_{37}H_{29}FeNO_2P$  606.12842; found 606.1288. MS (FAB, 3-NBA,  $m/z$ ): 606 ( $[2.31]^+$ , 35%), 578 ( $[2.31-CO]^+$ , 100%). IR ( $cm^{-1}$ , neat solid)  $\nu_{C=O}$  1959 (m),  $\nu_{C=N}$  1612 (w).

$[Fe(\eta^5-Ind)(CO)(2.25)]^+ \Gamma^-$  (**2.32**). To a Schlenk flask containing pentane (5 mL) and  $[Fe(\eta^5-Ind)I(CO)_2]$  **2.29**, (0.028 g, 0.079 mmol), the phosphinoxazoline (**2.25**, 0.041 g, 0.094 mmol) was added and the solids dissolved. The resulting deep brown solution was refluxed for six hours. The light brown-red slurry was removed from the oil bath and allowed to cool to room temperature for ten minutes. The brown supernatant was removed via pipette and the resulting brownish-reddish solid was washed thoroughly with cold diethyl ether (0 °C,  $2 \times 5$  mL). The solvent was then removed under high vacuum, yielding an orange-red solid (0.043 g, 0.057 mmol, 73 %).

NMR ( $\delta$ ,  $CD_3CN$ )  $^1H$  8.1–6.7 (m, 22H, aromatic), 5.8 (s, 1H, indenyl), 5.3 (s, 1H, indenyl), 4.9 (s, 1H, indenyl), 4.2 (d,  $^1J_{HH} = 7.9$ , 1H,  $CHH$ ), 4.1 (d,  $^1J_{HH} = 7.2$ , 1H,  $CHH$ ), 1.45 (s, 3H,  $CH_3$ ),  $-0.08$  (s, 3H,  $CH_3$ );  $^{13}C\{^1H\}$  220.8 (d,  $J_{CP} = 28.4$ , CO), 166.0 (d,  $J_{CP} = 6.7$ ,  $C=N$ ), 135.7 (d,  $J_{CP} = 11.8$ ), 132.5 (s), 132.2 (s), 133.2 (s), 132.9 (s), 132.0 (s), 131.9 (s), 131.7 (s), 131.5 (s), 131.2 (s), 130.6 (s), 130.4 (s), 130.2 (s), 130.0 (s), 129.7 (s), 129.2 (s), 127.2 (s), 126.0 (s), 125.8 (s), 125.6 (s), 110 (s, indenyl), 106.9 (s, indenyl), 86.2 (s, indenyl) 80.1, 73.5, 73.2 64.5 (4s, indenyl  $CH_2$  and  $C(CH_3)_2$ ), 26.0 (s,  $CH_3$ ), 23.7 (s,  $CH_3$ );  $^{31}P\{^1H\}$  62.6. HRMS calcd for

$C_{34}H_{28}F_3FeNO_2P$  626.1159; found 626.1155. MS (FAB, 3-NBA,  $m/z$ ): 626 ( $[\mathbf{2.32}]^+$ , 30%), 598 ( $[\mathbf{2.32-CO}]^+$ , 100%). IR ( $cm^{-1}$ , neat solid)  $\nu_{C=O}$  1949 (s),  $\nu_{C=N}$  1617 (m).

*General procedure for the catalytic experiments.*

The substrate benzaldehyde (**2.33**, 0.040 g, 0.377 mmol) was dissolved in  $CH_3CN$  (1. mL) and the catalyst **2.30**, (0.006 g, 0.011 mmol) was added. The 1-(*tert*-butyldimethylsilyloxy)-1-methoxyethene (**2.34**, 0.377 mmol, 0.082 mL) was added and the red-tan solution was shaken at room temperature for 15 minutes. The product was isolated as a colorless oil (0.082 g, 0.278 mmol, 74%) by column chromatography (silica gel, eluent  $CH_2Cl_2$ /cyclohexane, 2:1).

*Isolated yields and characterization data for the products in Table 2:*

Aldol adduct **2.35a** (Table 2.1, entry 1) from benzaldehyde (**2.33a**, 0.040 g, 0.377 mmol) was isolated as a colorless oil (0.082 g, 0.278 mmol, 74 %). NMR ( $\delta$ ,  $CDCl_3$ )  $^1H$  7.29–7.17 (m, 5H, aromatic), 5.08 (dd,  $^2J_{HH} = 4$ ,  $^2J_{HH} = 4$ , 1H, OCH), 3.68 (s, 3H, OCH<sub>3</sub>), 2.67 (m, CHH), 2.49 (m, 1H, CHH), 0.78 (s, 9H, *t*Bu), –0.49 (s, 3H, SiCH<sub>3</sub>), –0.24 (s, 3H, SiCH<sub>3</sub>);  $^{13}C\{^1H\}$  172.0 (s, C=O), 144.5 (s), 128.7 (s), 127.9 (s), 126.2 (s, aromatic), 72.7 (s, OCH), 52.0 (s, OCH<sub>3</sub>), 46.7 (s, CH<sub>2</sub>), 26.1 (s, C(CH<sub>3</sub>)<sub>3</sub>), 18.5 (s, C(CH<sub>3</sub>)<sub>3</sub>), –4.3 (s, SiCH<sub>3</sub>), –4.9 (s, SiCH<sub>3</sub>). MS (EI,  $m/z$ ) : 237 ( $[(\mathbf{2.35a})-C(CH_3)_3]^+$ ).

Aldol adduct **2.35b** (Table 2.1, entry 2) from 4-nitrobenzaldehyde (**2.33b**, 0.040 g, 0.264 mmol) was isolated as a colorless oil (0.053 g, 0.156 mmol, 59 %). NMR ( $\delta$ ,  $CDCl_3$ )  $^1H$  8.20–8.16 (m, 2H, aromatic) 7.55–7.50 (m, 2H, aromatic), 5.24 (dd,  $^1J_{HH} = 4.6$ ,  $^1J_{HH} = 4.6$ , 1H, OCH), 3.66 (s, 3H, OCH<sub>3</sub>), 2.72 (m, 1H, CHH), 2.56 (m, 1H, CHH), 0.85 (s, 9H, *t*-Bu), 0.03 (s, 3H, SiCH<sub>3</sub>), –0.15 (s, 3H, SiCH<sub>3</sub>);  $^{13}C\{^1H\}$  171.9 (s, C=O), 151.8 (s), 147.8 (s), 127.0 (s), 124.1 (s),



71.7 (s, OCH), 52.1 (s, OCH<sub>3</sub>), 46.2 (s, CH<sub>2</sub>), 26.0 (s, C(CH<sub>3</sub>)<sub>3</sub>), 18.4 (s, C(CH<sub>3</sub>)<sub>3</sub>), -4.4 (s, SiCH<sub>3</sub>), -5.0 (s, SiCH<sub>3</sub>'). IR (cm<sup>-1</sup>, neat solid)  $\nu_{\text{C=O}}$  1738. MS (EI,  $m/z$ ) : 282 ([**(2.35b)**-C(CH<sub>3</sub>)<sub>3</sub>]<sup>+</sup>).

Aldol adduct **2.35c** (Table 2.1, entry 3) from *o*-anisaldehyde (**2.33c**, 0.040 g, 0.293 mmol) was isolated as a colorless oil (0.059 g, 0.181 mmol, 62 %). NMR ( $\delta$ , CDCl<sub>3</sub>) <sup>1</sup>H 7.54 (dd,  $J_{\text{HH}} = 1.5$ ,  $J_{\text{HH}} = 1.5$ , 1H, aromatic), 7.00 (t,  $J_{\text{HH}} = 7.4$ , aromatic), 6.87 (d,  $J_{\text{HH}} = 8.2$ , aromatic), 5.60 (dd,  $^2J_{\text{HH}} = 3.2$ ,  $^2J_{\text{HH}} = 3.2$ , 1H, OCH), 3.88 (s, 3H, PhOCH<sub>3</sub>), 3.74 (s, 3H, OCH<sub>3</sub>), 2.71 (m, 1H, CHH), 2.59 (m, 1H, CHH), 0.92 (s, 9H, *t*-Bu), 0.06 (s, 3H, SiCH<sub>3</sub>), -0.09 (s, 3H, SiCH<sub>3</sub>'); <sup>13</sup>C{<sup>1</sup>H} 173.4 (s, C=O), 156.6 (s), 133.8 (s), 129.6 (s), 128.2 (s), 121.9 (s), 111.3 (s, aromatic), 67.5 (s, OCH), 56.6 (s, OCH<sub>3</sub>), 52.8 (s, OCH<sub>3</sub>), 45.8 (s, CH<sub>2</sub>), 28.3 (s, C(CH<sub>3</sub>)<sub>3</sub>), 27.2 (s, C(CH<sub>3</sub>)<sub>3</sub>), 19.5 (s, C(CH<sub>3</sub>)<sub>3</sub>), -3.4 (s, SiCH<sub>3</sub>), -4.0 (s, SiCH<sub>3</sub>'). IR (cm<sup>-1</sup>, neat solid)  $\nu_{\text{C=O}}$  1739. MS (EI,  $m/z$ ): 267 ([**2.35c**-C(CH<sub>3</sub>)<sub>3</sub>]<sup>+</sup>).

Aldol adduct **2.35d** (Table 2.1, entry 4) from *m*-anisaldehyde (**2.33d**, 0.040 g, 0.293 mmol) was isolated as a colorless oil (0.074 g, 0.228 mmol, 78 %). NMR ( $\delta$ , CDCl<sub>3</sub>) <sup>1</sup>H 7.33–7.26 (m, 1H, aromatic), 6.98–6.96 (m, 2H, aromatic), 5.20 (dd,  $^2J_{\text{HH}} = 3.9$ ,  $^2J_{\text{HH}} = 3.9$ , 1H, OCH), 3.87 (s, 3H, OCH<sub>3</sub>), 3.75 (s, 3H, PhOCH<sub>3</sub>), 2.78 (m, 1H, CHH), 2.62 (m, 1H, CHH), 0.93 (s, 9H, *t*Bu), 0.09 (s, 3H, SiCH<sub>3</sub>), -0.07 (s, 3H, SiCH<sub>3</sub>); <sup>13</sup>C{<sup>1</sup>H} 172.0 (s, C=O), 160.0 (s), 146.2 (s), 130.0 (s), 118.5 (s), 113.6 (s), 111.4 (s, aromatic), 72.5 (s, OCH), 55.6 (s, OCH<sub>3</sub>), 51.9 (s, OCH<sub>3</sub>), 46.7 (s, CH<sub>2</sub>), 26.1 (s, C(CH<sub>3</sub>)<sub>3</sub>), 18.5 (s, C(CH<sub>3</sub>)<sub>3</sub>), -4.3 (s, SiCH<sub>3</sub>), -5.0 (s, SiCH<sub>3</sub>'). IR (cm<sup>-1</sup>, neat solid)  $\nu_{\text{C=O}}$  1740. MS (EI,  $m/z$ ) [9]: 267 ([**2.35d**-C(CH<sub>3</sub>)<sub>3</sub>]<sup>+</sup>).

Aldol adduct **2.35e** (Table 2.1, entry 5) from *p*-anisaldehyde (**2.33e**, 0.040 g, 0.293 mmol) was isolated as a colorless oil (0.067 g, 0.206 mmol, 70 %). NMR ( $\delta$ , CDCl<sub>3</sub>) <sup>1</sup>H 7.31–7.26 (m,

2H, aromatic), 6.90–6.85 (m, 2H, aromatic), 5.13 (dd,  $^2J_{\text{HH}} = 4.2$ ,  $^2J_{\text{HH}} = 4.2$ , 1H, OCH), 3.82 (s, OCH<sub>3</sub>), 3.72 (s, PhOCH<sub>3</sub>), 2.74 (m, 1H, CHH), 2.55 (m, 1H, CHH), 0.87 (s, 9H, *t*Bu), 0.04 (s, 3H, SiCH<sub>3</sub>), –0.15 (s, 3H, SiCH<sub>3</sub>’);  $^{13}\text{C}\{^1\text{H}\}$  172.9 (s, C=O), 160.2 (s, aromatic), 137.5 (s, aromatic), 128.2 (s, aromatic), 114.9 (s, aromatic), 73.1 (s, OCH), 56.4 (s, OCH<sub>3</sub>), 52.7 (s, OCH<sub>3</sub>), 47.6 (s, CH<sub>2</sub>), 26.9 (s, C(CH<sub>3</sub>)<sub>3</sub>), 19.3 (s, C(CH<sub>3</sub>)<sub>3</sub>), –3.4 (s, SiCH<sub>3</sub>), –4.1 (s, SiCH<sub>3</sub>’). MS (EI, *m/z*): 267 ([**2.35e**-C(CH<sub>3</sub>)<sub>3</sub>]<sup>+</sup>).

Aldol adduct **2.35f** (Table 2.1, entry 6) from *o*-chlorobenzaldehyde (**2.33f**, 0.040 g, 0.284 mmol) was isolated as a colorless oil (0.077 g, 0.234 mmol, 83 %). NMR ( $\delta$ , CDCl<sub>3</sub>)  $^1\text{H}$  7.58–7.55 (m, 1H, aromatic), 7.30–7.16 (m, 3H, aromatic), 5.56 (dd,  $^2J_{\text{HH}} = 3.2$ ,  $^2J_{\text{HH}} = 3.2$ , 1H, OCH), 3.69 (s, 3H, OCH<sub>3</sub>), 2.66 (m, 1H, CHH), 2.54 (m, 1H, CHH), 0.85 (s, 9H, *t*Bu), 0.04 (s, 3H, SiCH<sub>3</sub>), –0.16 (s, 3H, SiCH<sub>3</sub>’);  $^{13}\text{C}\{^1\text{H}\}$  171.6 (s, C=O), 141.8 (s), 131.3 (s), 129.6 (s), 129.0 (s), 128.2 (s), 127.3 (s, aromatic), 68.9 (s, OCH), 51.9 (s, OCH<sub>3</sub>), 44.7 (s, CH<sub>2</sub>) 26.1 (s, C(CH<sub>3</sub>)<sub>3</sub>), 18.4 (s, C(CH<sub>3</sub>)<sub>3</sub>), –4.4 (s, SiCH<sub>3</sub>), –5.0 (s, SiCH<sub>3</sub>’). IR (cm<sup>-1</sup>, neat solid)  $\nu_{\text{C=O}}$  1739. MS (EI, *m/z*): 271 ([**2.35f**-C(CH<sub>3</sub>)<sub>3</sub>]<sup>+</sup>).

Aldol adduct **2.35g** (Table 2.1, entry 7) from *p*-toluolbenzaldehyde (**2.33g**, 0.040 g, 0.332 mmol) was isolated as a colorless oil (0.078 g, 0.252 mmol, 76 %). NMR ( $\delta$ , CDCl<sub>3</sub>)  $^1\text{H}$  7.38–7.23 (m, 2H, aromatic), 7.18 (d,  $^2J_{\text{HH}} = 8.01$ , aromatic), 5.17 (dd,  $^2J_{\text{HH}} = 4$ ,  $^2J_{\text{HH}} = 4$ , 1H, OCH), 3.76 (s, 3H, OCH<sub>3</sub>), 2.78 (m, 1H, CHH), 2.59 (m, 1H, CHH), 0.90 (s, 9H, *t*Bu), 0.07 (s, 3H, SiCH<sub>3</sub>), –0.11 (s, 3H, SiCH<sub>3</sub>’);  $^{13}\text{C}\{^1\text{H}\}$  171.9 (s, C=O), 141.3 (s), 129.2 (s), 125.9 (s, aromatic), 70.0 (s, OCH), 51.7 (s, OCH<sub>3</sub>), 44.3 (CH<sub>2</sub>), 25.9 (s, C(CH<sub>3</sub>)<sub>3</sub>), 21.4 (s, C(CH<sub>3</sub>)<sub>3</sub>), 18.3 (s, CH<sub>3</sub>), –

4.4 (s, SiCH<sub>3</sub>), -5.1 (s, SiCH<sub>3</sub>'). IR (cm<sup>-1</sup>, neat solid)  $\nu_{\text{C=O}}$  1736. MS (EI,  $m/z$ ): 251 ([**2.35g**-C(CH<sub>3</sub>)<sub>3</sub>]<sup>+</sup>).

Aldol adduct **2.35h** (Table 2.2, entry 8) from mesitaldehyde (**2.33h**, 0.040 g, 0.269 mmol) was isolated as a colorless oil (0.058 g, 0.172 mmol, 64 %). NMR ( $\delta$ , CDCl<sub>3</sub>) <sup>1</sup>H 6.81–6.77 (m, 2H, aromatic), 5.59 (dd, <sup>2</sup> $J_{\text{HH}} = 3.6$ , <sup>2</sup> $J_{\text{HH}} = 3.6$ , 1H, OCH), 3.70 (s, 3H, OCH<sub>3</sub>), 3.02 (m, 1H, CHH), 2.52–2.46 (m, 4H, CHH and CH<sub>3</sub>), 2.34 (s, 3H, PhCH<sub>3</sub>), 2.29 (s, 3H, CH<sub>3</sub>), 0.84 (s, 9H, *t*Bu), 0.04 (s, 3H, SiCH<sub>3</sub>), -0.23 (s, 3H, SiCH<sub>3</sub>'); <sup>13</sup>C{<sup>1</sup>H} 172.3 (s, C=O), 137.1 (s, aromatic), 136.3 (s, aromatic), 69.3 (s, OCH), 52.0 (s, OCH<sub>3</sub>), 42.5 (s, CH<sub>2</sub>), 26.1 (s, PhCH<sub>3</sub>), 21.2 (s, CH<sub>3</sub>), 20.8 (s, C(CH<sub>3</sub>)<sub>3</sub>), 18.4 (s, C(CH<sub>3</sub>)<sub>3</sub>), -4.6 (s, SiCH<sub>3</sub>), -5.1 (s, SiCH<sub>3</sub>'). IR (cm<sup>-1</sup>, neat solid)  $\nu_{\text{C=O}}$  1737. MS (EI,  $m/z$ ): 279 ([**2.35h**-C(CH<sub>3</sub>)<sub>3</sub>]<sup>+</sup>).

Aldol adduct **2.35i** (Table 2.1, entry 9) from *o*-toluolbenzaldehyde (**2.33i**, 0.040 g, 0.332 mmol) was isolated as a colorless oil (0.072 g, 0.233 mmol, 70 %). NMR ( $\delta$ , CDCl<sub>3</sub>) <sup>1</sup>H 7.59–7.56 (m, 1H, aromatic), 7.39–7.20 (m, 3H, aromatic), 5.47 (dd, <sup>2</sup> $J_{\text{HH}} = 3.1$ , <sup>2</sup> $J_{\text{HH}} = 3.1$ , 1H, OCH), 3.87 (s, 3H, OCH<sub>3</sub>), 2.76 (m, 1H, CHH), 2.60 (m, 1H, CHH), 2.46 (s, 3H, PhCH<sub>3</sub>), 0.95 (s, 9H, *t*Bu), 0.10 (s, 3H, SiCH<sub>3</sub>), -0.08 (s, 3H, SiCH<sub>3</sub>'); <sup>13</sup>C{<sup>1</sup>H} 172.1 (s, C=O), 142.5 (s), 133.7 (s), 130.6 (s), 127.6 (s), 126.6 (s, aromatic), 69.5 (s, OCH), 52.0 (s, OCH<sub>3</sub>), 45.3 (s, CH<sub>2</sub>), 26.0 (s, C(CH<sub>3</sub>)<sub>3</sub>), 19.3, 18.5 (2s, C(CH<sub>3</sub>)<sub>3</sub> and PhCH<sub>3</sub>), -4.4 (s, SiCH<sub>3</sub>), -5.03 (s, SiCH<sub>3</sub>'). MS (EI,  $m/z$ ) [9]: 251 ([**2.35i**-C(CH<sub>3</sub>)<sub>3</sub>]<sup>+</sup>).

Aldol adduct **2.35k** (Table 2.1, entry 10) from *m*-toluolbenzaldehyde (**2.33k**, 0.040 g, 0.332 mmol) was isolated as a colorless oil (0.082 g, 0.265 mmol, 79%). NMR ( $\delta$ , CDCl<sub>3</sub>) <sup>1</sup>H 7.47–7.17 (m, 4H, aromatic), 5.24 (dd, <sup>2</sup> $J_{\text{HH}} = 3.9$ , <sup>2</sup> $J_{\text{HH}} = 3.9$ , 1H, OCH), 3.81 (s, 3H, OCH<sub>3</sub>), 2.84 (m, 1H, CHH), 2.66 (m, 1H, CHH), 1.81 (s, 3H, PhCH<sub>3</sub>), 0.97 (s, 9H, *t*Bu), 0.14 (s, 3H, SiCH<sub>3</sub>), -

0.05 (s, 3H, SiCH<sub>3</sub>' ); <sup>13</sup>C{<sup>1</sup>H} 170.1 (s, C=O), 142.4 (s), 136.4 (s), 126.7 (s), 124.8 (s), 121.2 (s, aromatic), 70.6 (s, OCH), 50.0 (s, OCH<sub>3</sub>), 44.7 (s, CH<sub>2</sub>), 24.0 (s, C(CH<sub>3</sub>)<sub>3</sub>), 19.9 (s, C(CH<sub>3</sub>)<sub>3</sub>), 16.5 (s, PhCH<sub>3</sub>), -6.3 (s, SiCH<sub>3</sub>), -6.9 (s, SiCH<sub>3</sub>'). MS (EI, *m/z*): 251 ([**2.35k**-C(CH<sub>3</sub>)<sub>3</sub>]<sup>+</sup>).

Aldol adduct **2.35l** (Table 2.1, entry 11) from *p*-ethylbenzaldehyde (**2.33l**, 0.040 g, 0.298 mmol) was isolated as a colorless oil (0.046 g, 0.142 mmol, 48%). NMR (δ, CDCl<sub>3</sub>) <sup>1</sup>H 7.25 (d, <sup>2</sup>J<sub>HH</sub> = 9.2, 2H, aromatic), 7.15 (d, <sup>2</sup>J<sub>HH</sub> = 7.9, 2H, aromatic), 5.13 (dd, <sup>2</sup>J<sub>HH</sub> = 4.2, <sup>2</sup>J<sub>HH</sub> = 4.2, 1H, OCH), 3.68 (s, 3H, OCH<sub>3</sub>), 2.77–2.52 (m, 4H, aliphatic), 1.24 (t, <sup>2</sup>J<sub>HH</sub> = 7.7, 3H, CH<sub>3</sub>CH<sub>2</sub>Ph), 0.85 (s, 9H, *t*Bu), 0.016 (s, 3H, SiCH<sub>3</sub>), -0.16 (s, 3H, SiCH<sub>3</sub>); <sup>13</sup>C{<sup>1</sup>H} 170.7 (s, C=O), 142.4 (s, aromatic), 140.3 (s, aromatic), 126.7 (s, aromatic), 124.7 (s, aromatic), 71.1 (s, OCH), 50.5 (s, OCH<sub>3</sub>), 45.3 (s, CH<sub>2</sub>), 27.5 (s, C(CH<sub>3</sub>)<sub>3</sub>), 24.6 (s, C(CH<sub>3</sub>)<sub>3</sub>), 17.0 (PhCH<sub>2</sub>CH<sub>3</sub>), 14.4 (PhCH<sub>2</sub>CH<sub>3</sub>), -5.7 (s, SiCH<sub>3</sub>), -6.4 (s, SiCH<sub>3</sub>'). MS (EI, *m/z*) [9]: ([**2.35l**-C(CH<sub>3</sub>)<sub>3</sub>]<sup>+</sup>).

Aldol adduct **2.35m** (Table 2.1, entry 12) from butyraldehyde (**2.33m**, 0.040 g, 0.277 mmol) was isolated as a colorless oil (0.039 g, 0.149 mmol, 54%). NMR (δ, CDCl<sub>3</sub>) <sup>1</sup>H 4.20 (br, 1H, OCH), 3.67 (s, OCH<sub>3</sub>), 2.46–2.22 (m, 2H, CH<sub>2</sub>), 1.47–1.37 (m, 4H, 2CH<sub>2</sub>), 0.88 (br s, 12H, 4CH<sub>3</sub>), 0.07–0.05 (m, 6H, 2SiCH<sub>3</sub>); <sup>13</sup>C{<sup>1</sup>H} 172.4 (s, C=O), 69.5 (s, OCH), 51.5 (s, OCH<sub>3</sub>), 42.7 (s, CH<sub>2</sub>), 40.1 (s, CH<sub>2</sub>), 25.9 (s, C(CH<sub>3</sub>)<sub>3</sub>), 24.6 (s, C(CH<sub>3</sub>)<sub>3</sub>), 18.4 (s, CH<sub>2</sub>), 18.2 (s, C(CH<sub>3</sub>)<sub>3</sub>), 14.3 (CH<sub>3</sub>), -4.3 (s, SiCH<sub>3</sub>), -4.6 (s, SiCH<sub>3</sub>'). IR (cm<sup>-1</sup>, neat solid) ν<sub>C=O</sub> 1742. MS (EI, *m/z*): 245 ([**2.35m**-CH<sub>3</sub>]<sup>+</sup>, 5%), 203 ([**7m**-C(CH<sub>3</sub>)<sub>3</sub>]<sup>+</sup>, 100%).

#### X-Ray determination for complex **2.30**

X-ray quality crystals of **2.30** were obtained by layering an acetonitrile solution with diethyl ether, which was stored at -18 °C for 15 days. A crystal was mounted from Paratone oil to a

Bruker Kappa Apex II single crystal X-Ray diffractometer equipped with an Oxford Cryostream LT device. Intensity data were collected by a combination of  $\omega$  and  $\phi$  scans. Apex II, SAINT and SADABS software packages were used for data collection, integration and correction of systematic errors, respectively. Crystal data and intensity data collection parameters are listed in Table S1. Structure solution and refinement were carried out using the SHELXTL- PLUS software package. The structure was solved by direct methods and refined successfully in the space group  $P_{21/n}$ . The non-hydrogen atoms were refined anisotropically to convergence. All hydrogen atoms were treated using appropriate riding model (AFIX m3). A disordered solvent motif was located in the lattice which was best modeled as a molecule of acetone, though, it can also be half a molecule of diethyl ether ( $\text{Et}_2\text{O}$ ), which was one of the solvents used for crystallization. However, from two different data sets the best model seems to suggest acetone, which may have been incorporated into the crystallization e.g. as a result of rinsing glassware with acetone.

Complete listings of positional parameters and isotropic displacement coefficients for hydrogen atoms, anisotropic displacement coefficients for the non-hydrogen atoms and tables of calculated and observed structure factors are available in electronic format.

**Table 2.2.** Crystal data and structure refinement for **2.30**.

---

Empirical formula	(C <sub>33</sub> H <sub>29</sub> FeINO <sub>2</sub> P) <sub>2</sub> ·(C <sub>3</sub> H <sub>6</sub> O)
Formula weight	1428.66
Temperature, Wavelength	100(2) K, 0.71073 Å
Crystal system, Space group	Monoclinic, P2 <sub>1/n</sub>
Unit cell dimensions	a = 10.1851(10) Å b = 16.1312(16) Å c = 18.6639(17) Å alpha = gamma = 90°, beta = 96.338(4)°
Volume, Z	3047.7(5) Å <sup>3</sup> , 2
Density (calculated)	1.557 Mg/m <sup>3</sup>
Absorption coefficient	1.594 mm <sup>-1</sup>
Crystal size	0.21 x 0.21 x 0.18 mm <sup>3</sup>
Theta range for data collection	1.67 to 28.85°
Reflections collected	69837
Independent reflections	7802 [R(int) = 0.0371]
Absorption correction	Semi-empirical from equivalents
Max. and min. transmission	0.7645 and 0.7266
Data/ restraints/ parameters	7802 / 0/ 399
Goodness-of-fit on F <sub>2</sub>	1.139
Final R indices [I > 2σ(I)]	R1 = 0.0450, wR2 = 0.1161
R indices (all data)	R1 = 0.0584, wR2 = 0.1238
Largest diff. peak and hole	1.714 and -0.698 e Å <sup>-3</sup>

---

## 2.7. References

<sup>1</sup> O'Connor, J. M.; Casey, C. P. *Chem. Rev.* **1987**, *87*, 307. (a) Rerek, M. E.; Ji, L.-N.; Basolo, F. J. *Chem. Soc., Chem. Commun.* **1983**, 1208; (b) Calhorda, M. J.; Romão, C. C.; Veiros, L. F. *Chem. Eur. J.* **2002**, *8*, 86.

<sup>2</sup> Casey, C. P.; Guan, H. *J. Am. Chem. Soc.* **2009**, *131*, 2499

<sup>3</sup> Cahiez, G.; Foulgoc, L.; Moyeux, A. *Angew. Chem. Int. Ed.* **2009**, *48*, 2969-2972; Loska, R.; Rao Volla, C. M.; Vogel, P. *Adv. Synth. Catal.* **2008**, *350*, 2859

<sup>4</sup> Tomov, A. K.; Gibson, V. C.; Britovsek, G. J. P.; Long, R. L.; van Meurs, M.; Jones, D. J.; Tellmann, K. P.; Chirinos, J. J. *Organometallics* **2009**, *28*, 7033.

<sup>5</sup> Correa, A.; Carril, M.; Bolm, C. *Angew. Chem. Int. Ed.* **2008**, *47*, 2880; (b) Wu, J.-R.; Lin, C.-H.; Lee, C.-F. *Chem. Commun.* **2009**, 4450.

<sup>6</sup> D. Darensbourg, M. Holtcamp, *Macromolecules*, **1995**, *28*, 7577.

<sup>7</sup> S. Costin, N. Rath, E. Bauer, *Inorganica Chimica Acta*, **2009**, *362*, 1935.

<sup>8</sup> Tomov, A. K.; Gibson, V. C.; Britovsek, G. J. P.; Long, R. L.; van Meurs, M.; Jones, D. J.; Tellmann, K. P.; Chirinos, J. J. *Organometallics* **2009**, *28*, 7033.

<sup>9</sup> (a) von Matt, P.; Pfaltz, A. *Angew Chem., Int. Ed. Engl.* **1993**, *32*, 566; (b) Sprinz, J.; Helmchen, G. *Tetrahedron Lett.* **1993**, *34*, 1769; (c) Dawson, G. J.; Frost, C.G.; Williams, J. M.; Coote, S. J. *Tetrahedron Lett.* **1993**, *34*, 3149.

<sup>10</sup> (a) Bélanger, E.; Pouliot, M.-F.; Paquin, J.-F. *Org. Lett.* **2009**, *11*, 2201; (b) Popa, D.; Marcos, R.; Sayalero, S.; Vidal-Ferran, A.; Pericás, M. A. *Adv. Synth. Catal.* **2009**, *351*, 1539. (c) V, Stepanova, I. Smoliakova, *Current Organic Chemistry*, **2012**, *24*, 2893. (d) D. Behenna, J. Mohr, N. Sherden, S. Marinescu, A. Harned, K. Tani, M. Seto, S. Ma, Z. Novak, M. Krout, *Chemistry: A European Journal*, **2011**, *50*, 14199.

<sup>11</sup> Sedinkin, S. L.; Rath, N. P.; Bauer, E. B. *J. Organomet. Chem.* **2008**, *693*, 3081.

<sup>12</sup> Pfister, B; Stauber, S.; Albrecht, S. *J. Organomet. Chem.* **1997**, *533*, 131.

<sup>13</sup> Lenze, M.; Bauer, E. B. *J. Mol. Catal. A: Chem.* **2009**, *309*, 117.

- <sup>14</sup> O'Connor, J. M.; Casey, C. P. *Chem. Rev.* **1987**, *87*, 307.
- <sup>15</sup> (a) Rerek, M. E.; Ji, L.-N.; Basolo, F. J. *Chem. Soc., Chem. Commun.* **1983**, 1208; (b) Calhorda, M. J.; Romão, C. C.; Veiros, L. F. *Chem. Eur. J.* **2002**, *8*, 868.
- <sup>16</sup> A.J. Hart-Davis, R.J. Mawby, *J. Chem. Soc.* **1969** 2403. (b) A.J. Hart-Davis, C. White, R.J. Mawby, *Inorg. Chim. Acta* **1970**, 441.
- <sup>17</sup> "Selectivities in Lewis Acid Promoted Reactions," D. Schinzer Ed., Kluwer Academic Publishers, Dordrecht (1989).
- <sup>18</sup> Maeta, H.; Hashimoto, T.; Hasegawa, T. *Tetrahedron Lett.* **1992**, *33*, 5965.
- <sup>19</sup> Matsumoto, T.; Katsuki, M.; Suzuki, K. *Tetrahedron Lett.* **1988**, *29*, 6935. Matsumoto, T.; Hosoya, T.; Suzuki, K. *Synlett.* **1991**, 709. Matsumoto, T.; Hosoya, T.; Suzuki, K. *Tetrahedron Lett.* **1990**, *31*, 4629.
- <sup>20</sup> (a) Mukaiyama, T.; Narasaka, K.; Banno, K. *Chem Lett.* **1973**, 1011; (b) Mukaiyama, T.; Banno, K.; Narasaka, K. *J. Am. Chem. Soc.* **1974**, *96*, 7504.
- <sup>21</sup> Carreira, E. M. Mukaiyama aldol reaction. *Comprehensive Asymmetric Catalysis.* **1999**, *3*, 997. (b) J. Jankowska, J. Paradowska, J. Mlynarshi, *Tetrahedron Lett.* **2006**, *47*, 5281. (c) T. Ollevier, B. Plancq., *J. Chem. Soc.: Chem. Comm.*, **2012**, *48*, 2289.
- <sup>22</sup> S. Sedinkin, N. Rath, E. Bauer, *J. Organometallic Chem.* , **2008**, *18*, 3081.
- <sup>23</sup> Peer, M.; Jong, J. C.; Kiefer, M.; Langer, T.; Rieck, H.; Schell, H.; Sennhenn, P.; Sprinz, J.; Steinhagen, H.; Wiese, B.; Helmchen, G. *Tetrahedron* **1996**, *52*, 7547.
- <sup>24</sup> (a) Jones, D. J.; Mawby, R. J. *Inorg. Chim. Acta* **1972**, *6*, 157; (b) Belmont, J. A.; Wrighton, M. S. *Organometallics* **1986**, *5*, 1421 and literature cited therein.



<sup>25</sup> (a) Derrah, E. J.; Marlinga, J. C.; Mitra, D.; Friesen, D. M.; Hall, S. A.; McDonald, R.; Rosenberg, L. *Organometallics* **2005**, *24*, 5817; (b) Garcia, M. H.

<sup>26</sup> Nishiyama, Y.; Kaiba, K.; Umeda, R. *Tetrahedron Lett.* **2010**, *51*, 793.

<sup>27</sup> Han, J. S.; Kim, S. B.; Mukaiyama, T. *Bull. Korean. Chem. Soc.* **1994**, *15*.

<sup>28</sup> Bach, T.; Fox, D. N. A.; Reetz, M. T. *J. Chem. Soc., Chem. Commun.* **1992**, 1634.

<sup>29</sup> Lenze, M.; Sedinkin, S.; Rath, N.; Bauer, E. *Tetrahedron Letters*. **2010**. *51*, 2855.

**Chapter 3.** *Investigation of new iron phosphinoxazoline complexes and iron (II) triflate and their catalytic activity in the oxidation of activated methylene groups*

### 3.1 Aim of the Chapter

An interest in alternate uses for the previously described PHOX (PHOX = phosphinoxazoline) ligand class and a more facile route to access an open coordination site led us to investigate a new series of iron phosphinoxazoline complexes. It is well known that the presence of a weakly coordinating atom in a ligand or a counterion is likely to result in a more prevalent open coordination site, a key requirement for catalytic activity. After careful consideration, complexes of the general formula  $[\text{Fe}(\text{PHOX})_2(\text{X})_2]$  appeared to be the best candidate. In this context,  $\text{X}^-$  will be a weakly coordinating counterion, and these complexes will then feature two open coordination sites. Synthesis of such complexes was targeted and the resulting complexes were tested in homogenous catalytic oxidations of activated methylene groups using peroxides as the oxidants.

### 3.2 Introduction

A large number of publications have recently described the application of iron based catalysts in a variety of transformations such as carbon-carbon bond forming reactions,<sup>1</sup> polymerizations,<sup>2</sup> reductions<sup>3</sup> and oxidation reactions.<sup>4</sup> Iron complexes have become prime candidates for catalysts due to their overall abundance (it is the 4<sup>th</sup> most abundant metal in earth's crust), low cost and non-toxicity. My colleagues have recently synthesized and structurally characterized the first phosphinoxazoline PHOX (**3.1**, Figure 3.1) complexes of iron (**3.2**, Figure 3.1).<sup>5</sup> As described previously, PHOX ligands are a bidentate class<sup>6</sup> of ligands and have been successfully

applied as ligands in several transition-metal catalyzed asymmetric reactions.<sup>7</sup> Complex **3.2** is the first report of a chelating PHOX ligand in a mononuclear iron complex. In 2003, Braunstein *et al.* reported cyclopropanation and Diels-Alder reactions to be catalyzed by heterobimetallic iron copper complexes with bridging phosphinooxazoline ligands, in which only the phosphorous atom is coordinated to the iron center.<sup>8</sup>

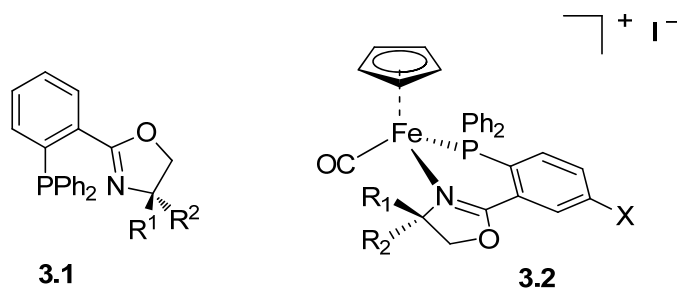


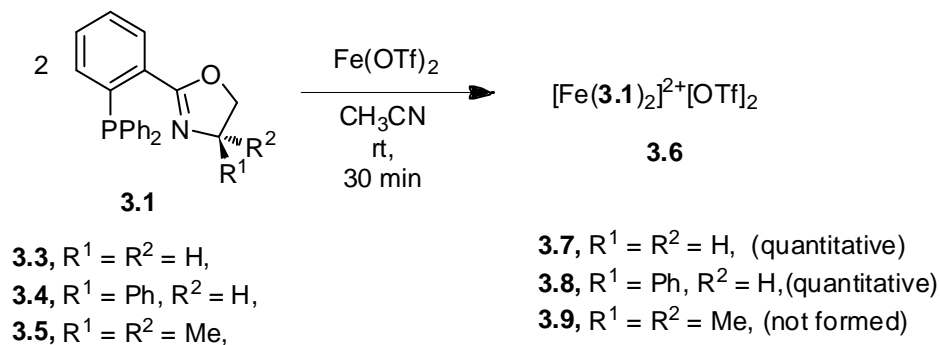
**Figure 3.1.** Phosphinooxazoline PHOX (left) and iron complexes thereof (right).

Oxidation is a powerful, versatile and convenient route for the strategic functionalization of a large number of substrates. Oxidations are also useful because they rapidly increase structural complexity, allowing for further functional group interconversions. However, the use of oxidation reactions in industry is limited on large scales, due to the use of hazardous oxidants and rigorous precautions needed to properly handle the oxidants and their subsequent disposal. Another limiting feature of oxidations in industry, namely the pharmaceutical industry, is the stoichiometric use of highly toxic metals such as chromium, osmium, and ruthenium, which need to be removed from the final product to meet food and health standards. Accordingly, efforts were made towards the development of an environmentally friendly iron catalyst system that was capable of efficiently oxidizing organic substrates in combination with peroxide oxidants.

### 3.3 Results

#### 3.3.1 Syntheses of iron complexes of the general formula $[Fe(PHOX)_2(X)_2]$

The targeted iron PHOX complexes with the general formula  $[Fe(PHOX)_2(X)_2]$  could be easily prepared by reaction of different PHOX ligands with commercially available anhydrous salts. PHOX ligands **3.3-3.5** were easily prepared following a slightly modified literature procedure.<sup>9</sup> Respectively, when two equivalents of ligands **3.3**, **3.4** and **3.5** were reacted with anhydrous  $Fe(OTf)_2$  ( $OTf = CF_3SO_3^-$ )<sup>10</sup> in  $CH_3CN$  at room temperature for 10 min, the iron complexes  $[Fe(\mathbf{3.3})_2]^{2+} [OTf]_2$  ( $[\mathbf{3.7}]^{2+}$ ) and  $[Fe(\mathbf{3.4})_2]^{2+} [OTf]_2$  ( $[\mathbf{3.8}]^{2+}$ ) were generated in nearly quantitative yield (Scheme 3.1).



**Scheme 3.1.** Synthesis of iron complexes **3.7** and **3.8**.

Immediately upon addition of the ligands **3.3-3.5** to the  $Fe(OTf)_2$ , the solution turned into a deep red-orange color, suggesting coordination of the ligands to the iron center. Astonishingly, the reaction between ligand **3.5** and  $Fe(OTf)_2$  was the only unsuccessful attempt in complex synthesis. Analysis of the reaction mixture via infrared spectroscopy suggested that ligand **3.5** did not show any sign of coordination as no shift for the imine stretch ( $\nu_{C=N}$ ) was observed relative

to the free ligand as observed in **3.7** and **3.8**. The lack of complex formation with ligand **3.5** could be explained by the fact the nitrogen of the oxazoline ring was too sterically congested and therefore could not form an effective overlapping of iron and ligand orbitals to form the anticipated Fe-N coordination bond. Conveniently, the formation of complexes **3.7** and **3.8** could be corroborated using evidence from IR and MS suggesting that ligands **3.3** and **3.4** were no longer ‘free’ and they did in fact coordinate to the metal center. The free ligands **3.3** and **3.4** gave characteristic  $\nu_{\text{C=N}}$  stretching frequencies of 1644 and 1630  $\text{cm}^{-1}$ , which show a substantial shift to lower wavenumbers (1626 and 1604  $\text{cm}^{-1}$ ) upon coordination to the iron center. This is clearly outlined for complex **3.7** in Figure 3.2 which shows spectra of the free ligand **3.3** (top trace) and the solvent free complex **3.7** (middle trace). The work of Gosiewska *et al.* established that coordination of one of the oxygen atom to the iron center should desymmetrize the OTf ion, resulting in several S-O stretches, with one being shifted to 1310  $\text{cm}^{-1}$ .<sup>11</sup> Keeping this in mind, the IR spectra should give information about the position of the OTf ion in the neat complex **3.7**, but such an effect was not recognized. However, it was noted in Figure 3.2 (middle trace, neat complex) that the stretch at 1259  $\text{cm}^{-1}$  did contain slight shoulders, which may be due to a loosely coordinated and ‘desymmetrized’ OTf ion. If the assumption that these small shoulders represent a weakly coordinated OTf ion is correct, utilization of  $\text{Fe}(\text{OTf})_2$  as an iron source would clearly be advantageous when catalytic applications are being considered and where open coordination sites are required. Additional IR evidence (bottom trace) supported the idea that the position of the OTf ion could be determined. This was done by recording an IR spectrum of complex **3.7** in acetonitrile, a coordinating solvent. A new band at 2293  $\text{cm}^{-1}$  (not shown) appeared representing the coordination of the acetonitrile to the metal center; the S-O stretch is shifted to 1265  $\text{cm}^{-1}$  and the disappearance of the shoulders on the band at 1259  $\text{cm}^{-1}$  all suggesting a free OTf ion.

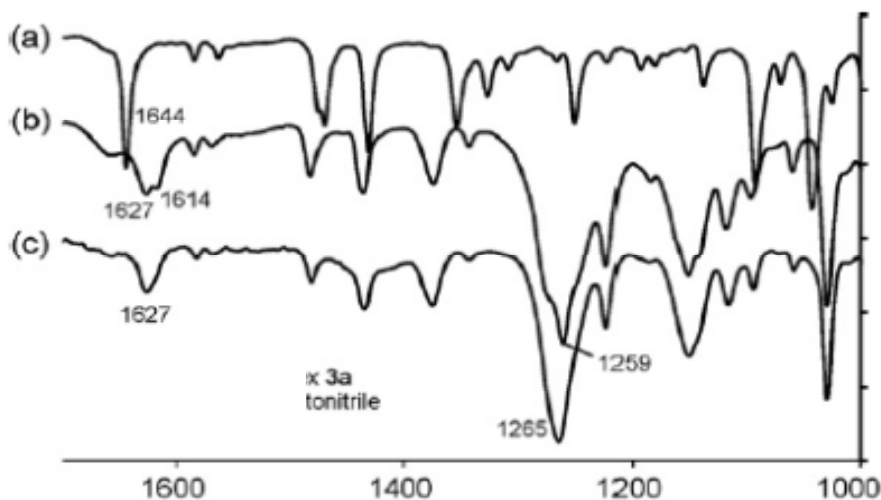


**Figure 3.2.** IR spectra of PHOX ligand **3.3** (top) its respective iron complex **3.7** (middle) and the complex **3.7** in CH<sub>3</sub>CN (bottom) .

The MS (FAB) spectra of **3.7** and **3.8** both support the general formula [Fe(**3.3**)<sub>2</sub>(OTf)<sub>2</sub>] (**3.7**) and [Fe(**3.4**)<sub>2</sub>(OTf)<sub>2</sub>] (**3.8**) as expected. The molecular ion for complex **3.7** corresponds to a species of the formula [Fe(**3.3**)<sub>2</sub>(OTf)]<sup>+</sup> and a fragment thereof, [Fe(**3.3**)(OTf)]<sup>+</sup>. Interestingly, the MS (FAB) for complex **3.7** also showed a peak consistent with [Fe(**3.3**)(OTf)(H<sub>2</sub>O)]<sup>+</sup>. Although this peak was consistent with coordination of a water molecule to the iron center, no OH stretches were seen in the IR of the solid state material. As a result, the water most likely came from the FAB matrix or atmosphere. On the contrary, the MS (FAB) for complex **3.8**, only a molecular ion matching a compound with the formula [Fe(**3.4**)<sub>2</sub>(O)(OTf)]<sup>+</sup> could be observed. After review of the spectroscopic data available to us, it could not be established where the oxygen originated. Again, it could be the case that the complex absorbs water from the FAB matrix and the observed peak in the MS is just the deprotonated species of [Fe(**3.4**)<sub>2</sub>(H<sub>2</sub>O)(OTf)]<sup>+</sup>. The elemental analysis for complex **3.8** is low on carbon, which further sustained the possibility of water absorption.

In order to acquire information regarding the electronic nature of complexes **3.7** and **3.8**, I determined the effective magnetic moment of each complex. The values of the magnetic moments revealed the fact that both complexes were paramagnetic. This effective magnetic moment ( $\mu_{\text{eff}}$ ) was determined via Evans NMR method.<sup>12</sup> The magnetic moments of  $\mu_{\text{eff}} = 2.26$  and  $3.63$  were determined for complexes **3.7** and **3.8**, respectively. A magnetic moment of  $\mu_{\text{eff}} = 2.26$  for complex **3.7** is lower than what is expected from the spin only formula (4.9 BM) for an octahedral Fe(II) complex with high spin configuration. Hypothetically, this could be related to the fact that complex **3.7** does not have an ideal octahedral geometry or due to the presence of spin crossover behavior.<sup>13</sup> The magnetic moment for complex **3.8** ( $\mu_{\text{eff}} = 3.63$  BM) was higher than that of complex **3.7**. As expected, no interpretable  $^1\text{H}$  and  $^{31}\text{P}\{^1\text{H}\}$  NMR spectra could be recorded due to paramagnetism of complex **3.8**, only extremely broad resonances were observed. The broad signals present in the  $^1\text{H}$  NMR for complex **3.8** could also be the result of dynamic processes occurring on the NMR time scale. In fact, no signals were present, for either complex, in the  $^{31}\text{P}\{^1\text{H}\}$  NMR spectra.

On the other hand, complex **3.7** provided reasonable  $^1\text{H}$  and  $^{13}\text{C}\{^1\text{H}\}$  NMR spectra with only slight line broadening. The  $^1\text{H}$  NMR spectrum showed that, for the eight diastereotopic  $\text{CH}_2$  protons of the oxazoline rings, six broad signals were observed. Even though the aromatic region of the  $^{13}\text{C}\{^1\text{H}\}$  NMR spectrum showed poor resolution, carbon atoms of the two oxazoline rings were identified as a double set of signals. The double set of signals strongly suggests that the two oxazoline rings are not equivalent. Furthermore, careful review of the IR spectrum of complex **3.7** (Figure 3.2, middle trace) displays two  $\nu_{\text{C}=\text{N}}$  signals, also supporting two non-equivalent nitrogen donor atoms. As a result, my curiosity led me to investigate whether or not the non-equivalency meant the presence of the cis isomer (Figure 3.3). Accordingly, attempts were made

to structurally elucidate complexes **3.7** and **3.8** utilizing X-ray diffraction, but all attempts were unsuccessful. Hence, an accurate molecular structure for complexes **3.7** and **3.8** could not be determined at this time. After a close investigation of the IR spectrum for **3.8**, the presence of only one  $\nu_{\text{C=N}}$  stretch suggested the oxazoline rings are equivalent. Overall, complex **3.8** provided NMR spectra of very poor quality and provided major discrepancies between expected and experimental values of the elemental analysis. Thus, future studies focused on complex **3.7**.

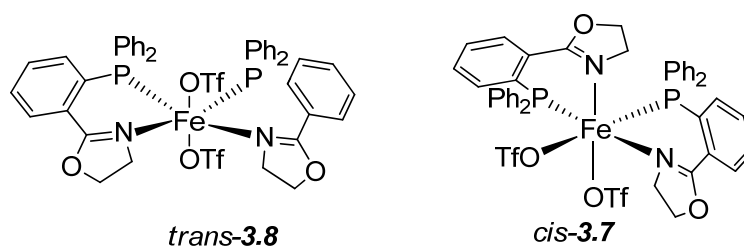
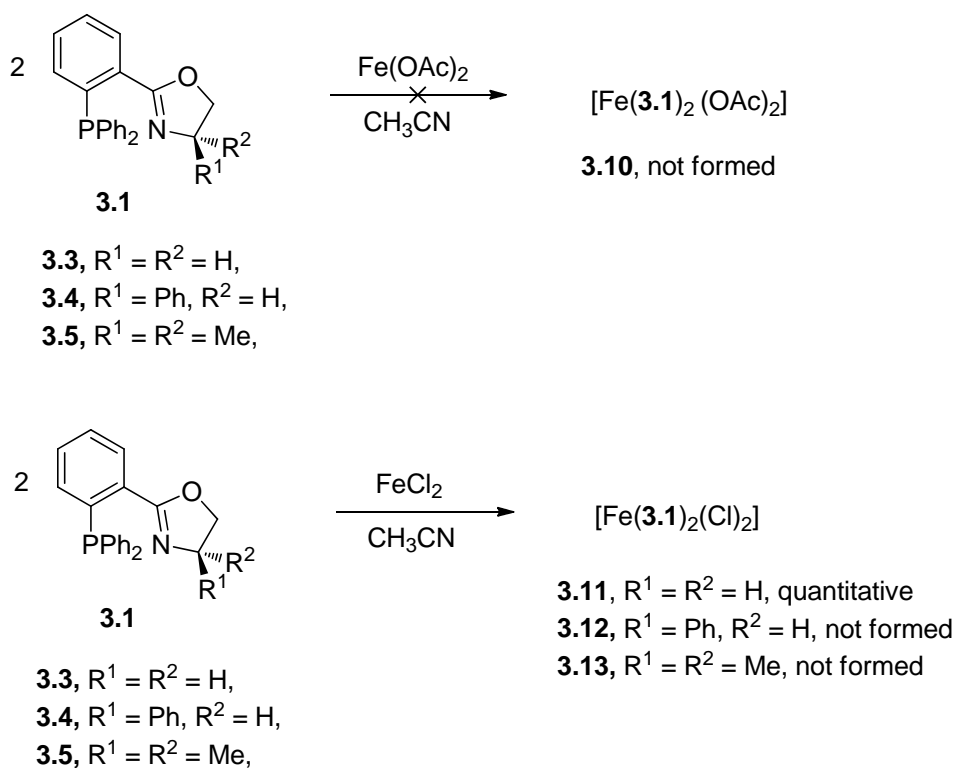


**Figure 3.3.** Possible isomers for complex **3.8** (left) and complex **3.7** (right).

For comparison, I determined what effect changing the iron source would have on complex formation and subsequent catalytic activity. I reacted two equivalents of ligands **3.3-3.5** with  $\text{Fe}(\text{OAc})_2$  in acetonitrile at room temperature. Following a thorough review of IR, MS,  $^1\text{H}$  and  $^{13}\text{C}\{^1\text{H}\}$  NMR spectra, it became evident that no ligand coordination took place in any of three cases. The unsuccessful attempts at complex synthesis using standard conditions led me to explore the efficacy of solvents such as  $\text{CH}_2\text{Cl}_2$ , MeOH, toluene and cyclohexane. In every instance the results were similar, and no evidence of complex formation was observed. The lack of complex formation was contributed to the poor solubility of  $\text{Fe}(\text{OAc})_2$  in the reaction media. When methanol was used, a sudden color change was observed upon addition of PHOX ligand **3.3** to the methanol/ $\text{Fe}(\text{OAc})_2$  solution. I hypothesized that attack of the methanol on the metal

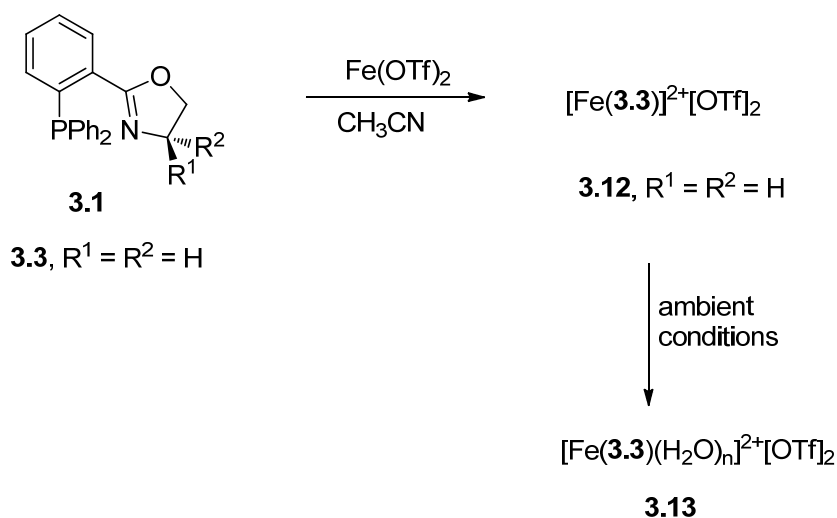


center of the iron PHOX complex, caused the sudden change in color. To this end, through examining the reaction mixture via IR and MS, further corroboration of this hypothesis was obtained. Coordination of a molecule of MeOH to the iron center was easily seen through a characteristic  $\nu_{\text{Fe-O}}$  stretch in the IR as well as a peak, detected in the MS, consistent with a compound of the formula  $[\text{Fe}(\text{OAc})(\text{MeOH})_2]^+\text{OAc}$ . The fact that  $\text{Fe}(\text{OAc})_2$  seemed not to be a good iron source for iron PHOX complex synthesis, I investigated different iron salts for future attempts. Therefore, I reacted ligands **3.3-3.5** with  $\text{FeCl}_2$  under conditions similar to Scheme 3.1. Again, multiple solvents were tested, of which only  $\text{CH}_3\text{CN}$  showed promising results. Surprisingly, even when using  $\text{CH}_3\text{CN}$ , employment of anhydrous  $\text{FeCl}_2$  only yielded one of the desired complexes, that being complex **3.11** (Scheme 3.2).



**Scheme 3.2.** Attempted synthesis of **3.10** using  $\text{Fe}(\text{OAc})_2$  (top) and synthesis of **3.11** using  $\text{FeCl}_2$  (bottom).

Next, an inherent interest in complex comparison led me to synthesize an additional complex, which will subsequently be referred to as the “mono PHOX” iron complex  $[\text{Fe}(\mathbf{3.3})]^{2+}[\text{OTf}]_2$ , bearing only one PHOX within the coordination sphere. The employment of the “mono PHOX” iron complex would have obvious advantages over other complexes of similar type, as it would have an additional two open sites available for substrate coordination. The synthesis was easily accomplished by reacting only one equivalent of ligand **3.3** with the corresponding anhydrous  $\text{Fe}(\text{OTf})_2$  under standard conditions (Scheme 3.3).



**Scheme 3.3.** Synthesis of the “mono PHOX” iron complex **3.13**.

Examination of IR spectra suggested that ligand **3.3** does in fact coordinate to the metal center. There was also a strong and broad stretch resembling  $\nu_{\text{O-H}}$  at  $3300\text{ cm}^{-1}$  which was not observed in the IR spectra for complexes **3.7** and **3.8** (Figure 3.2). As expected, this data was consistent with the assumption that when  $\text{Fe}(\text{OTf})_2$  is treated with only one equivalent of PHOX ligand, the remaining open coordination sites quickly pick up water from the atmosphere. Furthermore, analysis of the MS (FAB) showed the presence of  $[\text{Fe}(\mathbf{3.3})_2(\text{OTf})]^{2+}$  supporting the idea

that the synthesis described in Scheme 3.3 did not just yield the “mono PHOX” complex, but also several side products.

### 3.3.2 Catalytic oxidation of activated methylene groups

Preliminary screening stages were oriented towards applying complex **3.2** (Figure 3.1) and complex **3.7** in an effort to monitor their efficacy towards the catalytic oxidation of various hydrocarbons in combination with different oxidants, and their results are summarized in Table 3.1.

$\text{R}^1-\overset{\text{H}_2}{\text{C}}-\text{R}^2 \xrightarrow[\text{pyridine}]{\text{t-BuOOH, 2-5 mol\% [Fe]}} \text{R}^1-\overset{\text{O}}{\text{C}}-\text{R}^2$					
Entry	Substrate	Product	Catalyst	Yield <sup>a</sup>	TOF (h <sup>-1</sup> ) <sup>b</sup>
1 <sup>c</sup>	Diphenylmethane	Benzophenone	3.2	68%	0.76
2 <sup>c</sup>	Dihydroanthracene	Anthraquinone	3.2	49%	1.1
3 <sup>d</sup>	Fluorene	Fluorenone	3.7	91%	3.8
4 <sup>e</sup>	Fluorene	Fluorenone	3.7	93%	3.9
5 <sup>d</sup>	Dihydroanthracene	Anthraquinone	3.7	38%	1.4
6 <sup>d</sup>	Diphenylmethane	Benzophenone	3.7	43%	1.6
7 <sup>f</sup>	Fluorene	Fluorenone	Fe(OTf) <sub>2</sub>	80%	1.7

<sup>a</sup> Isolated yields after column chromatography or extraction.  
<sup>b</sup> Determined from isolated yield: Number of moles (product) over number of moles (catalyst) times reaction time.  
<sup>c</sup> Conditions: substrate (0.30 mmol), catalyst 3.2 (5mol%), t-BuOOH (3.5 equiv.), 18 hn(9 h for dihydroanthracene) in pyridine (1 mL) at 90 °C.  
<sup>d</sup> Conditions: substrate (0.60 mmol), catalyst 3.7 (2 mol%), t-BuOOH (1.8-2.0 equiv.), 12 h in pyridine (2 mL) at room temperature.  
<sup>e</sup> Conditions identical to those in b but under an atmosphere of nitrogen.  
<sup>f</sup> Conditions: substrate (0.30 mmol), catalyst Fe(OTf)<sub>2</sub> (2.8 mol%), t-BuOOH (2.0 equiv.), 18 h in pyridine (1 mL) at room temperature.

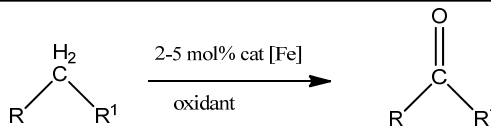
**Table 3.1.** Preliminary screening of iron catalyzed oxidation reactions.

The initial stages established that complexes **3.2** and **3.7** were indeed catalytically active in the oxidation of activated methylene groups. On the other hand, when hydrocarbons, such as cyclohexane and cyclooctene, and the methine group in triphenylmethane and adamantane were used, very low quantities of the expected oxidation products were detected (Table 3.2). Next, different oxidants were tested towards their efficiency in the oxidations. The screening revealed *t*-BuOOH (70 wt% in H<sub>2</sub>O) provided the best results when applied using a 2-3:1 molar ratio of the oxidant to the substrate. Comparison of complexes **3.2** and **3.7** revealed that in order for complex **3.2** (5 mol%) to be catalytically active, prolonged reaction times (16-36 h) and elevated temperatures (90 °C) were required, while complex **3.7** (2 mol%) was catalytically active at room temperature and typically gave better conversion to the oxidized products. Both complexes gave best results when using pyridine as the solvent. It was also discovered that Fe(OTf)<sub>2</sub> was also catalytically active in the oxidation of fluorene to fluorenone (Table 3.1, entry 7). However, it was determined that a catalyst of some sort is required for the other oxidation reactions in Table 3.1 to proceed at a reasonable rate, as no oxidized products were detected when reactions were performed in the absence of catalyst.

Optimized conditions, derived as a result of the preceding investigations, were then applied in combination with complexes **3.2** and **3.7** in the oxidation of multiple substrates and the results are compiled in Table 3.1. The oxidation of dihydroanthracene, diphenylmethane and fluorene to the corresponding ketones was accomplished in 93-38% after isolated yields. These isolations required a 2-3:1 molar ratio of the oxidant to the substrate using pyridine as the solvent at room temperature. Nakanishi and Bolm demonstrated that FeCl<sub>3</sub> was catalytically active in benzylic oxidation using aqueous *t*-BuOOH with yields ranging from 47 to 69%.<sup>14</sup> Britovsek *et al.* showed that Fe(OTf)<sub>2</sub> was catalytically active in the oxidation of cyclohexane using H<sub>2</sub>O<sub>2</sub> to give an al-

cohol/ketone combination from which they determined an alcohol/ketone ratio, but isolated yields were not determined.<sup>15</sup> As previously established, employment of complex **3.2** as a catalyst required prolonged reaction times and elevated temperature, and still the observed oxidation products were detected in smaller amounts. In order to account for its sluggish behavior, it was hypothesized that a coordination site must first be generated in order for it to become catalytically active. Complex **3.7** was active even at room temperature and lower catalyst loading, possibly due to the presence of two open coordination sites, which were only weakly or partially occupied by the OTf ions. Moreover, it was also already established that non-activated hydrocarbons and allylic alcohols could not be oxidized under the optimized reaction conditions (Table 3.2).

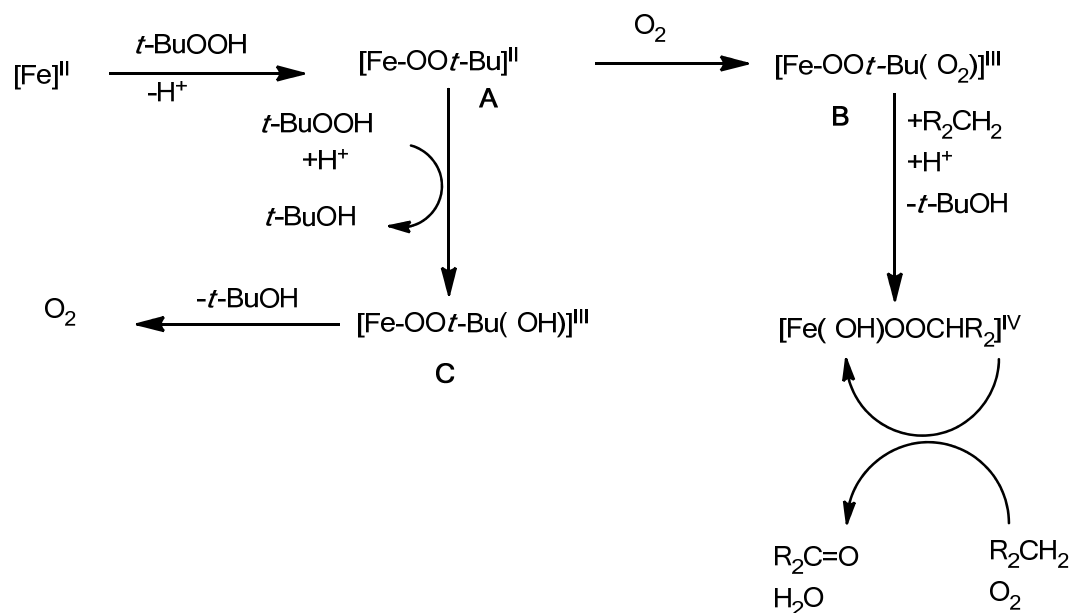
**Table 3.2.** Screening of catalytic activity for complexes **3.2** and **3.7**.

						
Entry	Substrate	Oxidant <sup>a</sup>	Time /temperature	Catalyst <sup>b</sup>	Product	Conversion(%) <sup>c</sup> TOF(h <sup>-1</sup> ) <sup>d</sup>
1	Cinnamyl alcohol	Me <sub>3</sub> NO	44 h/rt	<b>3.2</b>	Cinnamyl aldehyde	39 0.18
2	Diphenylmethane	<i>t</i> -BuOOH	18 h/90°C	<b>3.2</b>	Benzophenone	71 0.79
3	Dihydroanthracene	<i>t</i> -BuOOH	9 h/90°C	<b>3.2</b>	Anthraquinone	56 1.24
4	Fluorene	<i>t</i> -BuOOH	18 h/90°C	<b>3.2</b>	Fluorenone	5 0.06
5	Cyclohexane	Me <sub>3</sub> NO or H <sub>2</sub> O <sub>2</sub>	72 h/rt	<b>3.7</b>	NR	
6	Toluene	H <sub>2</sub> O <sub>2</sub>	30 h/rt	<b>3.7</b>	NR	
7	Toluene	<i>t</i> -BuOOH	30 h/rt	<b>3.7</b>	Benzaldehyde	Traces
8	Cyclooctadiene	<i>t</i> -BuOOH	24 h/80°C	<b>3.7</b>	NR	
9	<i>p</i> -Cymene	H <sub>2</sub> O <sub>2</sub>	32 h/80°C	<b>3.7</b>	NR	
10	Dimethoxytoluene	<i>t</i> -BuOOH	20 h/80°C	<b>3.7</b>	NR	
11	Cinnamyl alcohol	<i>t</i> -BuOOH	24 h/°C	<b>3.7</b>	NR	
12	Tetrahydronaphthalene	<i>t</i> -BuOOH	22 h/80°C	<b>3.7</b>	NR	
13	Fluorene	<i>t</i> -BuOOH	22 h/rt	<b>3.7</b>	Fluorenone	100 2.3
14	Fluorene	<i>t</i> -BuOOH plus TEMPO	18 h/rt	<b>3.7</b>	Fluorenone	51 0.56
15	Diphenylmethane	<i>t</i> -BuOOH	22 h/rt	<b>3.7</b>	Benzophenone	64 1.45
16	Diphenylmethane	<i>t</i> -BuOOH	18 h/rt	Fe( <b>3.3</b> ) <sub>2</sub> Cl <sub>2</sub>	Benzophenone	38 0.86
17	Fluorene	<i>t</i> -BuOOH	22 h/rt	Fe( <b>3.3</b> ) <sub>2</sub> Cl <sub>2</sub>	Fluorenone	84 1.90
18	Fluorene	<i>t</i> -BuOOH	22 h/rt	Fe(OTf) <sub>2</sub>	Fluorenone	77 1.75

<sup>a</sup> Oxidants were used in a two-3.5 fold excess  
<sup>b</sup> 5 mol% **3.2**, 2mol % **3.7**, Fe(**3.3**)<sub>2</sub>Cl<sub>2</sub> and Fe(OTf)<sub>2</sub>  
<sup>c</sup> Determined by GC/MS  
<sup>d</sup> Number of moles (product) over number of moles (catalyst) times the reaction time. Determined from GC data  
<sup>e</sup> Identical conditions to entry 13, but in presence of 20 mol% TEMPO

3.3.3 *Additional experiments to better understand the nature of the mechanism of the oxidation reactions.*

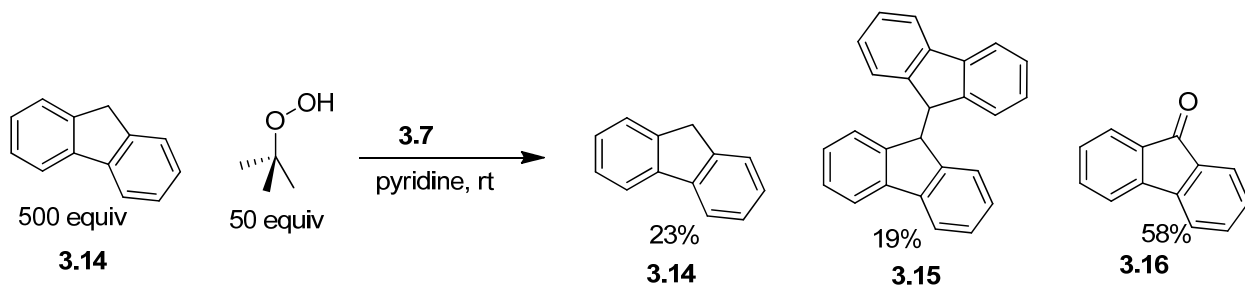
The realm of oxidation chemistry has been thoroughly explored, and it is well understood that the course of the reaction is strongly dependent on the reaction conditions such as solvents, stoichiometry and the choice of the oxidant.<sup>16</sup> I found it interesting that throughout all of the previously described experiments, an alcohol was never observed as an oxidation product, only the corresponding carbonyl compounds. This finding was consistent with a mechanism known as “oxygenated Fenton chemistry” that was first described by Sawyer *et al.* (Scheme 3.4).<sup>17</sup> It is suggested that the Fe(II) primarily forms an alkylperoxo species **A**, in which case species **A** then takes up oxygen to form **B**; species **B** converts methylene groups to ketones which may then be regenerated by reaction with R<sub>2</sub>CH<sub>2</sub> and oxygen. There are two possible sources that the oxygen may be supplied by, one of them being the atmosphere. Another potential source from which oxygen may be derived is through peroxide decomposition, as Fe(II) complexes have been known to disproportionate peroxides to give oxygen. Thus, the oxygen may not only come from the atmosphere, but as a result of the *t*-BuOOH decomposition. In view of that, I thought to study the effect that employing anaerobic reaction conditions had on catalytic activity. Consequently, when an oxidation reaction was performed under an inert atmosphere using same conditions as displayed in Table 3.2, substantial catalytic activity was still observed.



**Scheme 3.4.** Sawyer's proposed mechanism for "oxygenated Fenton chemistry".

I became interested in determining whether or not the proposed species **A** plays a part in my catalytic system. So, I next recorded UV-vis spectra of the most commonly employed catalyst, complex **3.7**. Complex **3.7** showed an extremely broad band around 350 nm and a distinguished peak at 247 nm. Interestingly, after the addition of  $t\text{-BuOOH}$ , a new broadened peak emerged at 420 nm and over time (24 h) this broadened peak at 420 nm became overlaid with a strong absorption appearing at 280 nm. Albeit, the new band at 420 nm may have been due to the formation of the Fe(II) alkylperoxo species **A**, time resolved UV-vis spectroscopy could not be used to follow the formation/decay of **A** due to the appearance of the strong absorption at 280 nm. Multiple researchers have described the formation of species **A** (Scheme 3.4) as yielding a LMCT band between 500-600 nm.<sup>18</sup> These reported values are at least in the same order of the new absorption at 420 nm that formed after addition of the  $t\text{-BuOOH}$ .

Alkylperoxy species **A** have been known to either undergo heterolysis or homolysis of the O-O bond to generate the seemingly elusive high valent iron oxo species  $[\text{Fe}=\text{O}]$ , which have been reported to be potential intermediates in iron catalyzed oxidation reactions.<sup>19</sup> Nevertheless, these high valent iron oxo species are reported to have been responsible for the formation of alcohols from alkanes and the formation of epoxides from olefins,<sup>20</sup> both of which were never observed as products in my investigations. Moreover, these high valent iron oxo species are said to generate UV-vis absorptions around 750 nm<sup>21</sup> which were also never observed, but this species is typically only observed at -40 °C. Another tactical approach used to determine the participation of a high valent iron oxo species was running a reaction with a large excess of the substrate over the oxidant. Accordingly, a large excess of the fluorene was used as a deliberate attempt to avoid overoxidation of a possible alcohol intermediate. Consequently, when a reaction with a molar ratio of 500:50:10 fluorene: *t*-BuOOH: **3.7**, was run and monitored by GC/MS, we only observed the presence of the unoxidized dihydrofluorene species **3.14**, the fluorene dimer **3.15** and the expected fluorenone **3.16** in a 1:1:3 ratio according to GCMS (Scheme 3.5). These products may have formed from radicals and no alcohols were observed which further discredited the involvement of a high valent iron oxo species.



**Scheme 3.5.** Investigation of possible radical involvement.



As mentioned before, a plausible explanation for the catalytic activity of complex **3.7** was the involvement of unselective radical species. Since the involvement of radicals could not be excluded, I next tested the effect of employing known radical scavengers. More specifically, I tested the effect of adding 20 mol% TEMPO (2,2,6,6-tetramethylpiperidine-1-oxyl, a scavenger for carbon-centered radicals) in the oxidation of fluorene (Table 3.2, entry 14). The presence of 20 mol% TEMPO appeared to have a negligible effect on the oxidation of fluorene as the reaction rate had only slightly decreased relative to the standard reaction without TEMPO. The use of 20 mol% of phenol was also investigated for the oxidation of fluorene. It, too, appeared to have only a negligible impact on the extent of oxidation relative to the standard reaction rate without phenol. Even though negligible differences in reaction rates suggested a mechanistic pathway that was inconsistent with radical participation, their involvement could still not yet be completely ruled out. Another probe for radical involvement is the oxidation of adamantane under standard conditions. This resulted in very little alcohol products; but small quantities of alcohol, ketone and pyridyl substituted adamantyl products were detected, implying a radical-like behavior. These observations strongly represent radical involvement in the oxidation reactions, but the absence of alcohols as products is more accurately represented by the mechanism depicted in Scheme 3.4.

### 3.4. Discussion - Kinetics

Finally, the reaction rates of the catalysts systems were studied. The substrate fluorene was used for the kinetic studies due to its availability, ease of oxidation and moderate TOF ( $\text{h}^{-1}$ ) value. The substrate consumption for the oxidation reaction of fluorene (entry 3, Table 3.1) was followed via GC over the course of five hours at room temperature. The complexes tested were **3.7**,

$[\text{Fe}(\mathbf{3.3})(\text{H}_2\text{O})_n][\text{OTf}]_2$  and  $\text{Fe}(\text{OTf})_2$ , and the decay of fluorene is shown in Figure 3.3. Figure 3.3 illustrates the linear trends for all three of the catalytic experiments in one graph.

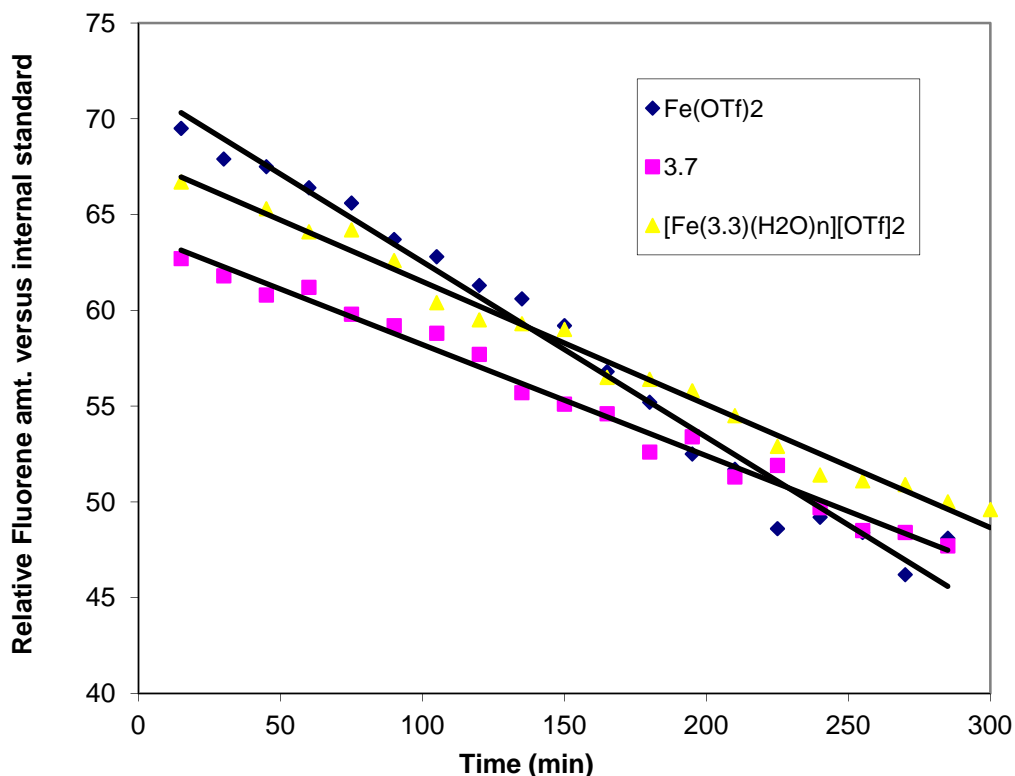


**Figure 3.3.** Decay of fluorene for the reaction in entry 3 (Table 3.1) over time for different catalysts.

After analysis of the kinetic data, the catalyzed reactions appear to be consistent with a pseudo-zero order rate law with respect to the substrate, which has been previously reported for other catalyzed reactions.<sup>22</sup> I was also able to derive observed rate constants for each catalyst from the slope of the lines in Figure 3.3. The observed rate constant for **3.7** was found to be  $0.059 \text{ min}^{-1}$ ,  $[\text{Fe}(\mathbf{3.3})(\text{H}_2\text{O})_n][\text{OTf}]_2$  was found to be  $0.064 \text{ min}^{-1}$  and  $\text{Fe}(\text{OTf})_2$  was  $0.092 \text{ min}^{-1}$ . The data shows that the catalytic ability of  $[\text{Fe}(\mathbf{3.3})(\text{H}_2\text{O})_n][\text{OTf}]_2$  with only one PHOX ligand in

its coordination sphere was similar to that of **3.7**, while the observed rate constant of  $\text{Fe}(\text{OTf})_2$  was slightly larger than that of complex **3.7**. The larger rate constant observed for  $\text{Fe}(\text{OTf})_2$  may be attributed to the fact that there is a need for open coordination sites on the iron center for catalytic activity. Unfortunately, there was no conclusive evidence allowing us to structurally elucidate a catalytically active species. However, the data in Figure 3.3 suggest that the catalytically active species is the same for both  $[\text{Fe}(\mathbf{3.3})(\text{H}_2\text{O})_n][\text{OTf}]_2$  and **3.7** in solution. In an attempt to further reveal the composition of the catalytically active species, I subjected complex **3.7** to conditions identical to those in Table 3.1, except no substrate was added. The residue was then spectroscopically analyzed by IR, MS and  $^1\text{H}$  NMR. Analysis of the IR spectra revealed three new IR bands at 1666, 1611 and  $1600\text{ cm}^{-1}$ . These new bands are consistent with  $\nu_{\text{C}=\text{N}}$  stretches and most likely due various forms of oxidized PHOX ligands. Analysis of the MS spectrum was not very informative, as only one peak could be assigned, which was consistent with a compound of the molecular formula  $[\text{Fe}(\mathbf{3.3})(\text{O})_2(\text{pyridine})(\text{OTf})]^+$ . This data presents the possibility that complex **3.7** may first have to lose the PHOX ligand in order to become catalytically active. On the contrary, there was never any sign of an induction period for complex **3.7**, which makes it unlikely that the species must first lose the chelating PHOX ligand before becoming catalytically active. As expected, the  $^1\text{H}$  NMR spectrum contributed no additional information, as all chemical shifts were severely broadened. Next, I was interested in determining the origin of the oxygen atom, observed in the MS spectrum for complex  $[\text{Fe}(\mathbf{3.3})(\text{O})_2(\text{pyridine})(\text{OTf})]^+$ . Thus, I carried out a similar reaction under conditions outlined in Table 3.1, but in the absence of *t*-BuOOH. Unfortunately, the MS spectrum also had a peak indicative of the formula  $[\text{Fe}(\mathbf{3.3})(\text{O})_2(\text{pyridine})(\text{OTf})]^+$  suggesting that the oxygen had come from an alternate source; such as the matrix or the atmosphere.

### 3.5 Summary and prospective

The study described in this chapter describes, for the first time, that iron PHOX complexes of the general formula  $[\text{Fe}(\text{PHOX})_2(\text{OTf})_2]$  are catalytically active in the oxidation of activated methylene groups to the corresponding ketones with isolated yields ranging from 38 to 93%. The catalysts general motif permits the oxidation of activated methylene groups to proceed at room temperature, as opposed to 90 °C, which was the temperature required for iron complexes of the general formula  $[\text{Fe}(\text{Cp})(\text{CO})(\text{PHOX})]^+[\text{I}]^-$ , to show catalytic activity. The absence of alcohols seen as products is consistent with “oxygenated Fenton chemistry”, which was described in Scheme 3.4. The UV-vis spectra of the reaction between complex **3.7** and an excess of *t*-BuOOH provide some evidence that is consistent with the formation of an iron alkylperoxo species  $[\text{Fe}-\text{OO}t\text{-Bu}]$ , which was also illustrated in “oxygenated Fenton chemistry”. Finally, kinetic measurements showed that the reaction was pseudo-zero order with respect to the substrate, and the mono-coordinated iron PHOX complex  $[\text{Fe}(\text{PHOX})(\text{OTf})_2]$  behaves similarly to the di-coordinated complex  $[\text{Fe}(\text{PHOX})_2(\text{OTf})_2]$ .

### 3.6 Experimental

Chemicals were treated as follows: acetonitrile was distilled from  $\text{CaH}_2$ . Other solvents,  $\text{CHCl}_3$ , pyridine,  $\text{CH}_2\text{Cl}_2$ , hexanes, the substrates for the catalytic experiments (Aldrich), and *t*-BuOOH (5.5 M in decane, Fluka) were used as received. Thoroughly dried  $\text{Fe}(\text{OTf})_2$  ( $\text{OTf}=\text{CF}_3\text{SO}_3^-$ ), iron complex **3.2** and the PHOX ligands **3.3-3.5** were synthesized according to the literature.<sup>5,6</sup> Metal complex syntheses were carried out under nitrogen employing standard schlenk techniques. Workup as well as the catalytic experiments was performed under aerobic conditions.

The NMR spectra were obtained at room temperature on either a Bruker Avance 300 MHz or a Varian Unity Plus 300 MHz instrument and referenced to a residual solvent signal. GC/MS spectra were recorded on a Hewlett Packard GC/MS system model 5988A. Exact masses were acquired on a JEOL MStation [JMS-700] mass spectrometer. IR spectra were recorded on a Thermo Nicolet 360 FT-IR spectrometer. Elemental analyses were performed by Atlantic Microlab Inc., Norcross, GA, USA. Magnetic moments were determined by the Evans method.<sup>11</sup>

$[\text{Fe}(\mathbf{3.3})_2]^{2+}[\text{OTf}]_2$  ( $[\mathbf{3.3}]^{2+}$ ): To a Schlenk flask containing  $\text{CH}_3\text{CN}$  (2 mL) and  $\text{Fe}(\text{OTf})_2$  (0.053 g, 0.15 mmol), phosphinoxazoline **3.3** (0.100g, 0.301 mmol) was added and the solids dissolved. The resulting deep red solution was allowed to stir at room temperature for 10 min. The solvent was removed under high vacuum, yielding a red-orange solid. Anal. calcd for  $\text{C}_{44}\text{H}_{36}\text{F}_6\text{FeN}_2\text{O}_8\text{S}_2\text{P}_2$ : C, 51.98; H, 3.57. Found: C, 52.08; H, 3.83.

NMR ( $\delta$ ,  $\text{CD}_3\text{CN}$ )  $^1\text{H}$  (full width at half maximum ca. 27 Hz) 8.12 (dd,  $J_{\text{HH}} = 27$  Hz,  $J_{\text{HH}} = 7$  Hz, 2H, Ph), 8.04–7.07 (m, 23H, Ph), 6.96 (d,  $J_{\text{HH}} = 7.5$  Hz, 2H, Ph), 6.68 (s, 1H), 4.76 (s, 2H,  $2\text{CH}'\text{H}$ ), 4.34 (s, 1H,  $\text{CH}'\text{H}$ ), 3.82 (s, 1H,  $2\text{CH}'\text{H}$ ), 3.66 (s, 1H,  $\text{CH}'\text{H}$ ), 3.19 (s, 2H,  $2\text{CH}'\text{H}$ ), 3.06 (s, 1H,  $\text{CH}'\text{H}$ );  $^{13}\text{C}\{^1\text{H}\}$  (partial) 170.8 (s,  $\text{C}=\text{N}$ ), 169.9 (s,  $\text{C}-\text{N}$ ), 69.1 (s,  $\text{CH}_2$ ), 68.4 (s,  $\text{CH}_2$ ), 59.7 (s,  $\text{CH}_2$ ), 55.2 (s,  $\text{CH}_2$ ).

HRMS calcd for  $\text{C}_{43}\text{H}_{36}\text{F}_3\text{FeN}_2\text{O}_5\text{SP}_2$  867.1120; found 867.1105 (corresponds to  $[\text{Fe}(\mathbf{3.3})_2(\text{OTf})]^+$ ). MS (FAB, NBA,  $m/z$ ): 867 ( $[\text{Fe}(\mathbf{3.3})_2(\text{OTf})]^+$ , 35%), 536 ( $[\text{Fe}(\mathbf{3.3})(\text{OTf})]^+$ , 60%), 332 ( $[\mathbf{3.3}]^+$ , 100%). IR ( $\text{cm}^{-1}$ , neat solid)  $\nu_{\text{C}=\text{N}}$  1627 (w), 1614 (w),  $\nu_{\text{SO}}$  1259 (s),  $\nu_{\text{CF}}$  1028 (s). Magnetic susceptibility (0.0108 M,  $\text{CD}_3\text{CN}$ ),  $\mu_{\text{eff}} = 2.26$  BM.

$[\text{Fe}(\mathbf{3.4})_2]^{2+}[\text{OTf}]_2$  ( $[\mathbf{3.4}]^{2+}$ ): To a Schlenk flask containing  $\text{CH}_3\text{CN}$  (2 mL) and  $\text{Fe}(\text{OTf})_2$  (0.043 g, 0.123 mmol), phosphinoxazoline **3.4** (0.100g, 0.246 mmol) was added and the solids dissolved. The

resulting deep red solution immediately transitioned into dark brown. The solvent was removed under high vacuum, yielding a red-brownish solid. Anal. calcd for  $C_{56}H_{44}F_6FeN_2O_8S_2P_2$ : C, 57.54; H, 3.79. Found: C, 54.63; H, 3.93.

HRMS calcd for  $C_{55}H_{44}F_3FeN_2O_6SP_2$  1035.1679; found 1035.1670 (corresponds to  $[Fe(\mathbf{3.4})_2(O)(OTf)]^+$ ). MS (FAB,3-NBA,  $m/z$  1051 ( $[Fe(\mathbf{3.4})_2(O)_2(OTf)]^+$ , 10%), 1035 ( $[Fe(\mathbf{3.4})_2(O)(OTf)]^+$ , 5%), 628 ( $[Fe(\mathbf{3.4})(O)(OTf)]^+$ , 30%), 612 ( $[Fe(\mathbf{3.4})(OTf)]^+$ , 25%), 408 ( $[\mathbf{3.8}]^+$ , 100%). IR ( $cm^{-1}$ , neat solid)  $\nu_{C=N}$  1604 (w),  $\nu_{S-O}$  1260 (s),  $\nu_{C-F}$  1028 (s). Magnetic susceptibility (0.0109 M,  $CD_3CN$ ),  $\mu_{eff} = 3.63$  BM.

$[Fe(\mathbf{3.3})(H_2O)_n]^{2+}[OTf]_2$ : To a Schlenk flask containing 2.0 mL of  $CH_3CN$  and  $Fe(OTf)_2$  (0.106 g, 0.3 mmol), phosphinooxazoline **3.3** (0.100 g, 0.3 mmol) was added and the solids dissolved. The resulting deep red solution was stirred at room temperature for 5 min. The solvent was then removed under vacuum.

MS (FAB, NBA,  $m/z$ ): 867 ( $[Fe(\mathbf{3.3})_2(OTf)]^+$ , 35%), 536 ( $[Fe(\mathbf{3.3})(OTf)]^+$ , 100%), 332 ( $[\mathbf{3.7}]^+$ , 80%). IR ( $cm^{-1}$ , neat solid)  $\nu_{O-H}$  3435 (br),  $\nu_{C=N}$  1657 (w), 1627 (w),  $\nu_{S-O}$  1223 (s),  $\nu_{C-F}$  1026 (m, s).

#### *Magnetic moment determination*

0.0108 M solutions of the iron complexes in  $CD_3CN$  were placed in a NMR tube, and as an internal standard, a capillary containing pure  $CD_3CN$  and TMS (1 mol%) was introduced into the tube. Proton NMR spectra were recorded, and the  $\Delta\nu$  value for the  $CD_3CN$  resonances determined. The magnetic moments were calculated according to the literature.<sup>11</sup>

#### *General procedure for the catalytic experiments*

The substrate fluorene (0.100g, 0.602 mmol) was dissolved in pyridine (2.0 mL) and the catalyst **3.7** (0.012 g, 0.012 mmol) was added. The oxidant *t*-BuOOH (1.07 mmol, 0.195 mL of a 5.5 M solution in decane) was added and the red solution stirred at room temperature for 12 h. The product was isolated as a yellow powder (0.099 g, 0.55 mmol, 91%) by column chromatography (basic alumina, eluent CHCl<sub>3</sub>/hexanes, 2:3). NMR ( $\delta$ , CDCl<sub>3</sub>) <sup>1</sup>H 7.72–7.66 (m, 2H, aromatic), 7.61–7.49 (m, 4H, aromatic), 7.36–7.29 (m, 2H, aromatic); <sup>13</sup>C{<sup>1</sup>H} 194.1 (s, C=O), 144.7 (s, aromatic), 135.0 (s, aromatic), 134.4 (s, aromatic), 129.4 (s, aromatic), 124.6 (s, aromatic), 120.6 (s, aromatic). IR (cm<sup>-1</sup>, neat solid)  $\nu_{\text{C=O}}$  1710 (s).

The substrate 9,10-dihydroanthracene (0.100 g, 0.50 mmol) was dissolved in pyridine (2.0 mL) and the catalyst **3.7** (0.011 g, 0.011 mmol) was added. The oxidant *t*-BuOOH (0.99 mmol, 0.180 mL of a 5.5 M solution in decane) was added and the red solution stirred at room temperature for 12 h. The product anthraquinone was isolated as a white-yellow powder (0.039 g, 0.187 mmol, 38%) by simple removing the solvent and washing the residue with dichloromethane. NMR ( $\delta$ , CDCl<sub>3</sub>) <sup>1</sup>H 8.36-8.33 (m, 4H, aromatic), 7.85-7.82 (m, 4H, aromatic). <sup>13</sup>C{<sup>1</sup>H} 183.4 (s, C=O), 134.4 (s, aromatic), 133.8 (s, aromatic), 127.5 (s, aromatic). IR (cm<sup>-1</sup>, neat)  $\nu_{\text{C=O}}$  1686 (s).

The substrate diphenylmethane (0.100 g, 0.50 mmol) was dissolved in pyridine (2.0 mL) and the catalyst **3.7** (0.013 g, 0.011 mmol) was added. The oxidant *t*-BuOOH (1.06 mmol, 0.193 mmol of a 5.5 M solution in decane) was added and the red solution was stirred at room temperature for 12 h. The product benzophenone was isolated as a white crystalline solid (0.039 g 0.214 mmol, 43%) by column chromatography (silica gel, CH<sub>2</sub>Cl<sub>2</sub>/hexanes, 1:4). NMR ( $\delta$ , CDCl<sub>3</sub>) <sup>1</sup>H 7.86-7.82 (m, 5H, aromatic), 7.65-7.48 (m, 9H, aromatic). <sup>13</sup>C{<sup>1</sup>H} 197.0 (s, C=O), 137.9 (s, aromatic), 132.6 (s, aromatic) 130.3 (s, aromatic), 128.5 (s, aromatic). IR (cm<sup>-1</sup>, neat)  $\nu_{\text{C=O}}$  1656 (s).

*UV-vis experiment in Fig. 4*

To the metal complex  $[3.7]^{2+}$  (0.002 g, 0.00196 mmol) pyridine (0.25 mL) was added, followed by *t*-BuOOH (0.25  $\mu$ L of a 5.5 M solution in decane, 0.138 mmol).  $\text{CH}_2\text{Cl}_2$  (1 mL) was immediately added and a UV-vis spectrum recorded. For comparison, an UV-vis spectrum under identical conditions without the *t*-BuOOH was recorded.

#### *2.1.4. Reaction kinetics monitored by GC (Figure 3.3)*

The substrate fluorene (0.05 g, 0.30 mmol) was dissolved in pyridine (2.0 mL) and the catalyst  $[3.7]^{2+}$  (0.0061 g, 0.006 mmol) was added. The oxidant *t*-BuOOH (0.53 mmol, 0.097 mL of a 5.5 M solution in decane) was added, and the solution stirred at room temperature. For analysis, aliquots were taken from the reaction mixture, filtered through a short pad of alumina (which was washed with 2 mL  $\text{CH}_2\text{Cl}_2$ ), and injected into the GC instrument. The substrate decay over time was determined by the ratio of its signal intensity to the signal intensity of decane, which was the solvent for the *t*-BuOOH and served as internal standard.

### 3.7 References

- <sup>1</sup> W.M. Czaplik, M. Mayer, A. Jacobi von Wangelin, *Angew. Chem. Int. Ed.* **2009**, *48*, 607.
- <sup>2</sup> (a) Wallenhorst, G. Kehr, H. Luftmann, R. Fröhlich, G. Erker, *Organometallics*. **2008**, *27*, 6547.; (b) S. McTavish, G.J.P. Britovsek, T.M. Smit, V.C. Gibson, A.J.P. White, D.J. Williams, *J. Mol. Catal. A: Chem.* **2007**, *261*, 293.
- <sup>3</sup> C.P. Casey, H. Guan, *J. Am. Chem. Soc.* **2009**, *131*, 2499.
- <sup>4</sup> Y. Feng, C. Ke, G. Xue, L. Que Jr., *Chem. Commun.* **2009**, 50;  
M.S. Chen, M.C. White, *Science* **2007**, *318*, 783.
- <sup>5</sup> S.L. Sedinkin, N.P. Rath, E.B. Bauer, *J. Organomet. Chem.* **2008**, *693*, 3081.



<sup>6</sup> (a) P. von Matt, A. Pfaltz, *Chem. Angew, Int. Ed. Engl.* **1993**, *32*, 566; (b) J. Sprinz, G. Helmchen, *Tetrahedron Lett.* **1993**, *34*, 1769; (c) G.J. Dawson, C.G. Frost, J.M. Williams, S.J. Coote, *Tetrahedron Lett.* **1993**, *34*, 3149.

<sup>7</sup> (a) G. Helmchen, A. Pfaltz, *Acc. Chem. Res.* **2000**, *33*, 336; (b) H.A. McManus, P.J. Guiry, *Chem. Rev.* **2004**, *104*, 4151.

<sup>8</sup> P. Braunstein, G. Clerc, X. Morise, *New J. Chem.* **2003**, *27*, 68.

<sup>9</sup> Sedinkin, S. L.; Rath, N. P.; Bauer, E. B. *J. Organomet. Chem.* **2008**, *693*, 3081.

<sup>10</sup> K.S. Hagen, *Inorg. Chem.* **2000**, *39*, 5867.

<sup>11</sup> S. Gosiewska, J.J.L.M. Cornelissen, M. Lutz, A.L. Spek, G. van Koten, R.J.M. Klein Gebbink, *Inorg. Chem.* **2006**, *45*, 4214.

<sup>12</sup> G.S. Girolami, T.B. Rauchfuss, R.J. Angelici, *Synthesis and Technique in Inorganic Chemistry*, third ed., University Science Books, Mill Valley, 1999.

<sup>13</sup> Bousseksou, G. Molnár, J.A. Real, K. Tanaka, *Coord. Chem. Rev.* **2007**, *251*, 1822; (b) M. Arai, W. Kosaka, T. Matsuda, S. Ohkoshi, *Angew. Chem. Int. Ed.* **2008**, *47*, 688.

<sup>14</sup> M. Nakanishi, C. Bolm, *Adv. Synth. Catal.* **2007**, *349*, 861.

<sup>15</sup> G.J.P. Britovsek, J. England, S.K. Spitzmesser, A.J.P. White, D.J. Williams, *Dalton Trans.* **2005**, 945.

<sup>16</sup> F. Gozzo, *J. Mol. Catal. A: Chem.* **2001**, *171*, 1.

<sup>17</sup> D.T. Sawyer, A. Sobkowiak, T. Matsushita, *Acc. Chem. Res.* **1996**, *29*, 409.

<sup>18</sup> (a) F.G. Gelalcha, G. Anilkumar, M.K. Tse, A. Brückner, M. Beller, *Chem. Eur. J.* **2008**, *14*, 7687. (b) F. Namuswe, G.D. Kasper, A.A. Narducci Sarjeant, T. Hayashi, C.M. Krest, M.T. Green, P. Moënne-Loccoz, D.P. Goldberg, *J. Am. Chem. Soc.* **2008**, *130*, 14189; (c) M.P. Jensen, A. Mairata i Payeras, A.T. Fiedler, M. Costas, J. Kaizer, A. Stubna, E. Münck, L. Que Jr., *Inorg. Chem.* **2007**, *46*, 2398; (d) M.R. Bukowski, H.L. Halfen, T.A. van den Berg, J.A. Halfen, L. Que Jr., *Angew. Chem. Int. Ed.* **2005**, *44*, 584; (e) M.P. Jensen, M. Costas, R.Y.N.

Ho, J. Kaizer, A. Mairata i Payeras, E. Münck, L. Que Jr., J.-U. Rohde, A. Stubna, *J. Am. Chem. Soc.* **2005**, *127*, 10512; (f) M.P. Jensen, S.J. Lange, M.P. Mehn, E.L. Que, L. Que Jr., *J. Am. Chem. Soc.* **2003**, *125*, 2113.

<sup>19</sup> (a) M. Sook Seo, T. Kamachi, T. Kouno, K. Murata, M. Joo Park, K. Yoshizawa, W. Nam, *Angew. Chem. Int. Ed.*, **2007**, *46*, 2291; (b) N.A. Stephenson, A.T. Bell, *Inorg. Chem.* **2007**, *46*, 2278;

<sup>20</sup> A. Agarwala, D. Bandyopadhyay, *Catal. Lett.* **2008**, *124*, 256.

<sup>21</sup> Y. Zhou, X. Shan, R. Mas-Ballesté, M.R. Bukowski, A. Stubna, M. Chakrabarti, L. Slominski, J.A. Halfen, E. Münck, L. Que Jr., *Angew. Chem. Int. Ed.* **2008**, *47*, 1896.

<sup>22</sup> R.V. Chaudhari, A. Seayad, S. Jayasree, *Catal. Today* , **2001**, *66*, 371.

**Chapter 4.**  *$\alpha$ -aminopyridine and N-, O- coordinating polydentate pyridyl ligands and the catalytic activity of their respective iron(II) complexes in oxidation reactions: A comparative study of activity and ligand decomposition*

### 4.1 Aim of the Chapter

The limited application and harsh conditions associated with the iron oxidation systems described in chapter 3 led to the search for an improved iron-based oxidation catalyst. Reported herein is the synthesis and characterization of new mono- and bis(2-picolyl)amine ligands, various multidentate N-, O- coordinating ligands, their respective iron(II) complexes as well as their corresponding catalytic activity. These complexes were then monitored for the efficacy of their catalytic ability in the oxidation of secondary alcohols and activated methylene groups utilizing peroxide oxidants. We compare the activities of these new complexes with those of the known complexes previously employed in the title reactions. Moreover, we also report studies aimed at mechanistic elucidation and ligand decomposition pathways and how such decay impairs the catalytic ability of the catalysts system.

### 4.2 Introduction

Iron based catalyst systems have gained much interest in recent years as a result of its abundance, low cost and non-toxicity. Iron based salts and complexes have become increasingly applied as catalysts in numerous organic transformations, such as in C-C,<sup>1</sup> C-N,<sup>2</sup> and C-P<sup>3</sup> bond forming reactions, heteroatom-heteroatom bond forming reactions,<sup>4</sup> reductions,<sup>5</sup> polymerizations<sup>6</sup> in addition to other functional group interconversions. Iron based systems have also been

extensively investigated as catalysts in oxidation reactions of organic substrates. Their role as catalysts in oxidation reactions, dates back over 100 years and is known as Fenton chemistry, that is the oxidative ability of iron salts in combination with peroxides to oxidatively functionalize alkanes.<sup>7</sup> Giff and GoAgg systems were well established amongst the community by the beginning of the 1980s by Barton, and these systems use somewhat similar conditions: the oxidative power associated with simple iron salts in combination with dioxygen or peroxide oxidants with acetic acid in pyridine.<sup>8</sup> Currently, the mechanism for these oxidation systems is the main focus of interest for many research groups,<sup>9</sup> and the original non-radical mechanism suggested by Barton<sup>10</sup> has since been challenged.<sup>11</sup> As a result of the potential involvement of unselective radicals in Fenton and Gif systems, their practicality for use in the synthesis of complex organic molecules is null. In fact, Fenton chemistry is so unselective that it is rarely used in industry for the synthesis of fine chemicals and typically limited to the treatment of wastewater, where it is believed to disinfect via oxidative decomposition of organic compounds.<sup>12</sup>

Ergo, it seems logical that current research endeavors have directed their efforts towards the development of iron complexes that can be employed as catalysts in synthetically useful oxidation reactions under milder conditions. An interest in the synthesis and study of non-heme iron oxidation catalysts was inspired by the natural ability of certain iron containing enzymes, such as the cytochrome P450 family<sup>13</sup>, methane monooxygenase<sup>14</sup> and Rieske dioxygenase<sup>15</sup> to catalyze stereoselective oxidation reactions.<sup>16</sup> There are two types of iron containing enzymes and they are heme and non-heme oxygenases. These well-defined enzymes bear nitrogen coordinating ligands in their coordination sphere and are capable of carrying out selective oxidation reactions under physiological conditions. Research efforts aimed at the preparation of iron containing complexes capable of mimicking the active sites of these enzymes<sup>17</sup> has become the main focus

of several research groups recently, and these efforts have yielded a number of catalyst systems that demonstrate excellent selectivities as well as high turnover numbers  $h^{-1}$  (TON).<sup>18</sup> The preparation of some of these complexes is performed in-situ,<sup>19</sup> and they have been successfully employed as efficient catalysts in a number of oxidation reactions including the oxidation of alkanes,<sup>20</sup> benzylic methylene groups,<sup>21</sup> alcohols,<sup>22</sup> in oxidative cleavage reactions,<sup>23</sup> and in the epoxidation of olefins.<sup>24</sup> Although, in-situ formation of complexes seems to offer the advantage of expedition, preformed well-defined non-heme iron complexes perform exceptionally well in oxidation reactions. One example is White's preformed complex **4.14**, which selectively oxidizes tertiary C-H units to the corresponding alcohols.<sup>25</sup>

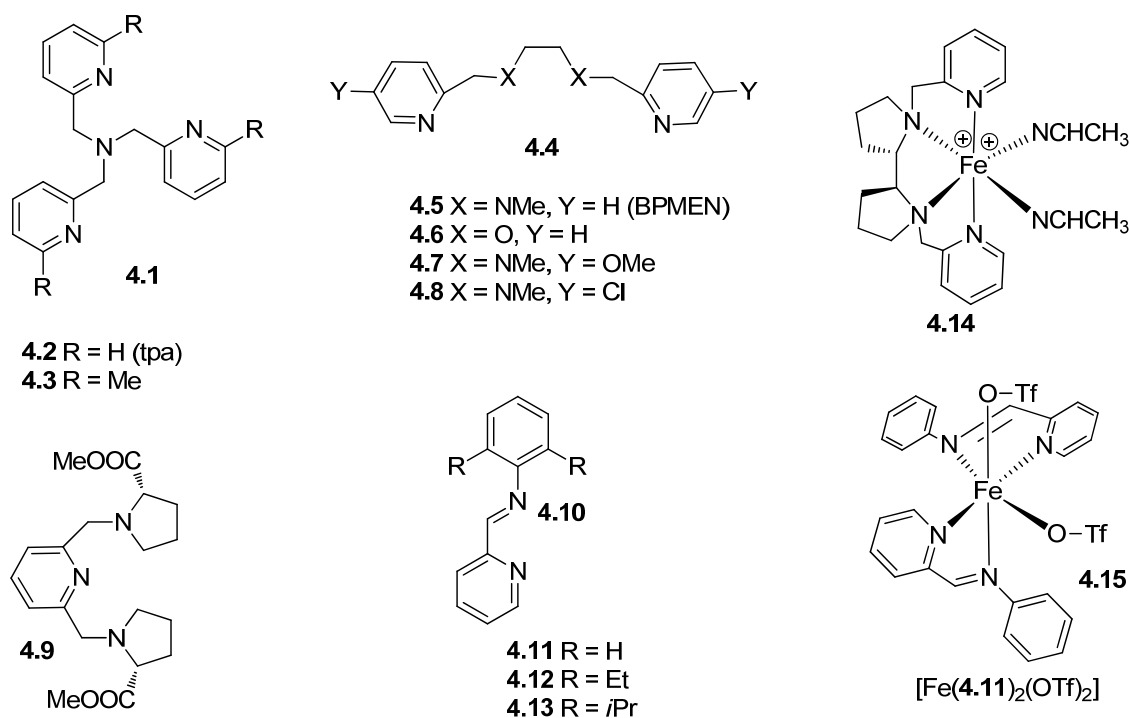


**Figure 4.1.** Known non-heme type ligands and their corresponding iron complexes.

Iron complexes featuring the tris(2-picolyl)amine (tpa) ligands **4.1** and BPMEN (**4.5**) were employed by Que and co-workers for alkane oxidations, which resulted in high alcohol/ketone

ratios.<sup>26</sup> Ligands **4.6-4.8**,<sup>27</sup> **4.9**<sup>28</sup> and bispidine<sup>29</sup> have also been utilized in the synthesis of catalytically active complexes, and their ability to rapidly increase structural complexity in organic molecules has gained considerable interest in recent past.<sup>30</sup> Despite the fact that many of the existing systems appear to be feasible options for an oxidation system, a majority of them suffer from drawbacks, such as poor turnover numbers and selectivities,<sup>31</sup> or require toxic and hazardous conditions for them to occur.<sup>32</sup> The low turnover numbers and selectivity issues have been attributed to the participation of an unselective radical species or to catalyst deactivation, via ligand decomposition pathways.<sup>33</sup> It has been demonstrated that the catalyst deactivation pathways may be avoided through the strategic design of a more robust ligand system, and the concentration of free radicals may be kept low through alteration of reaction conditions. However, the toxic/hazardous conditions required for many are unavoidable.

Thus, I have devoted considerable efforts aimed at the development of a more mild oxidation protocol that utilizes aqueous peroxide oxidants in combination with iron complexes that feature bi- and tridentate aminopyridine based ligands. Other members of our research group were also interested in the improvement and advancement of current oxidation reaction manifolds beyond what has been achieved through the use of strictly nitrogen coordinating ligands.<sup>34</sup> Thus, our group sought access to iron complexes that would feature multidentate ligands bearing both oxygen and nitrogen donor atoms that could also be used as catalysts in combination with the peroxide oxidants.

Investigations of iron catalyzed transformations with a special interest in how the ligand structure effects the catalytic activity of an iron complex<sup>35</sup> has been a large part of our overall research interests. In recent months, we have reported a series of iron complexes  $[\text{Fe}^{\text{II}}(\mathbf{4.10})_2(\text{OTf})_2]$  ( $\text{OTf} = \text{CF}_3\text{SO}_3^-$ ) featuring  $\alpha$ -iminopyridine ligands **4.10-4.13**, which were

subsequently utilized as catalysts in the oxidation of activated methylene groups and secondary alcohols, using *t*-BuOOH, to generate the corresponding carbonyl compounds (4 h, RT, 3 mol% catalyst load, 22-91% yield).<sup>33a</sup> This study showed that employing sterically and electronically modified ligands of **4.10** in complex synthesis only had a marginal impact on catalytic activity, as the differences in activity among the complexes were small. The idea that the ligand architectures could somehow influence the catalytic activity of their respective iron complexes led me to perform a study comparing the efficacy of these iron complexes, bearing the aforesaid bi- and tridentate ligand systems, as catalysts in iron based oxidation systems. I was especially interested in determining whether the denticity of the ligands has an impact on the catalytic activity of their respective iron complexes.

## 4.3 Results

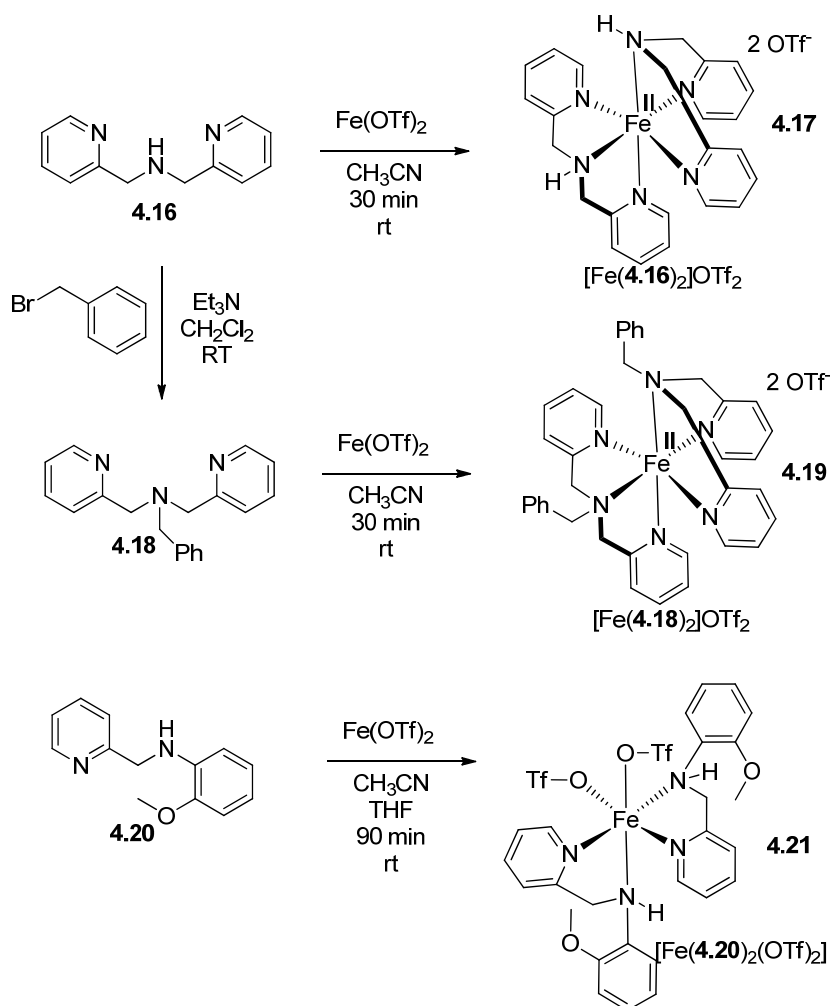
### 4.3.1 *Synthesis of new iron complexes*

I began by selecting a set of aminopyridyl ligands containing only nitrogen donor atoms, differed from one another in terms of their structural framework and denticity. These ligands were then converted to their respective iron complexes. In addition to the targeted ligands I also prepared the known tpa complex [Fe(**4.2**)(OTf)<sub>2</sub>], which was synthesized according to literature procedure<sup>36</sup> and will be consistently referred to as [Fe(**tpa**)(OTf)<sub>2</sub>], as was the case for [Fe(**4.11**)<sub>2</sub>(OTf)<sub>2</sub>], which was also synthesized and characterized in our laboratory.<sup>33a</sup>

To study the effect of different denticities, I used the commercially available, tridentate bis(2-pyridylmethyl)amine (bpa) ligand **4.16** (Scheme 1). Literature reports established that complexes of the general formula [Fe<sup>III</sup>(**4.16**)Cl<sub>3</sub>]<sup>37</sup> and [Fe<sup>II</sup>(**4.16**)<sub>2</sub>]X<sub>2</sub> (X = Cl<sup>-</sup>, Br<sup>-</sup>)<sup>38</sup> are catalytically active in oxidation reactions, and their continued employment is forthcoming.<sup>39</sup> Alt-

though the ease associated with the preparation of complexes  $[\text{Fe}^{\text{III}}(\mathbf{4.16})\text{Cl}_3]$  and  $[\text{Fe}^{\text{II}}(\mathbf{4.16})_2]\text{X}_2$  makes them attractive candidates for the present study, it is well known that  $\text{L}_n\text{Fe}^{\text{III}}$  complexes tend to form stabilized oxo-bridged dimers of iron having the formula  $[\text{L}_n\text{Fe}-\text{O}-\text{FeL}_n]$ .<sup>40</sup> In fact, complex  $[\text{Fe}^{\text{III}}(\mathbf{4.16})_2]\text{X}_2$  where  $\text{X} = \text{Cl}^-$ , is extremely sensitive and readily dimerizes and oxidizes in air to form a stable oxo-bridged  $\text{Fe}^{\text{III}}$  dimer.<sup>35b</sup> At first glance, it appears that dimers of this type would be unlikely to exhibit catalytic ability as they are coordinatively saturated and thermodynamically stable. Some oxo-bridged iron complexes do exhibit catalytic activity in alkane oxidation reactions,<sup>41</sup> but studies showed that their efficacy and TON's are low.<sup>42</sup> It is believed that the intrinsic stability of the oxo-bridged iron complexes may decrease or even inhibit catalytic cycles owing to the diminished activity and low TON's. Furthermore, not only do complexes of the type  $[\text{Fe}^{\text{II}}(\mathbf{4.16})_2]\text{X}_2$  ( $\text{X} = \text{Cl}^-$ ,  $\text{Br}^-$ ) form relatively stable dimers and oxo-bridged species, they also lack any potential open sites for substrate coordination, a prerequisite for catalytic activity. To this end, our laboratory demonstrated that  $[\text{Fe}^{\text{III}}(\mathbf{4.16})_2]\text{Cl}_2$  had very little activity in any oxidation reaction, while Chen and co-workers showed that  $[\text{Fe}(\mathbf{tpa})\text{Cl}_2]\text{ClO}_4$  exhibited no activity in the oxidation of cyclohexane using  $\text{H}_2\text{O}_2$ .<sup>25</sup> As a consequence, complexes of the type  $[\text{Fe}^{\text{III}}(\mathbf{4.16})_2]\text{X}_2$  ( $\text{X} = \text{Cl}^-$ ,  $\text{Br}^-$ ) will not be included for current or future investigations.





**Scheme 4.1.** Synthesis of iron complexes.

Referring to complexes described in chapter 3, it should be remembered that complexes of the general type  $[\text{Fe}(\text{L})_2]^{2+}[\text{X}^-]_2$  ( $\text{X} =$  weakly coordinated counterion) held the greatest promise for catalytic activity. Thus, I quickly proposed the preparation of iron complex  $[\text{Fe}^{\text{II}}(\mathbf{4.16})_2]\text{OTf}_2$  which promoted the use of OTf ( $= \text{CF}_3\text{SO}_3^-$ ), a weakly bound triflate anion. In the case of two weakly coordinated triflate anions, such complexes readily provide two open coordination sites, a requirement for catalytic activity. As seen in Scheme 4.1, complex **4.17** has all six coordination sites blocked by the two ligands which could hamper its catalytic activity, but the presence of two tridentate ligands **4.16** in the coordination sphere could also block decomposition pathways

as well as the formation of oxo-bridged dimers.<sup>43</sup> Complex **4.17** was easily prepared by reacting two equivalents of the commercially available ligand **4.16** with Fe(OTf)<sub>2</sub> in CH<sub>3</sub>CN. A slow diffusion crystallization at low temperature, using diethyl ether, generated the iron complex [Fe<sup>II</sup>(**4.16**)<sub>2</sub>]OTf<sub>2</sub> as needle-like red crystals in 96% isolated yield (Scheme 1).

After a general methodology for synthesis of iron complex **4.17** was established, I immediately wondered whether or not coordination of the N-H in **4.16** to the iron center would increase its acidity, and if so, how would this acidic proton effect its ability to efficiently catalyze an oxidation reaction? To determine the influence of the N-H unit on catalytic activity, I needed a structurally analogous complex that did not contain the N-H unit for comparison purposes. Thus, I pursued the synthesis of ligand **4.18** in which the hydrogen from ligand **4.16** was replaced by a benzyl group, affording the known<sup>44</sup> bis(2-pyridylmethyl)benzyl amine (bpba) ligand **4.18** (Scheme 1). The respective complex was prepared by reacting two equivalents of ligand **4.18** with Fe(OTf)<sub>2</sub> in acetonitrile. After washing with diethyl ether and crystallization from pentane, the iron complex [Fe<sup>II</sup>(**4.18**)<sub>2</sub>]OTf<sub>2</sub> was isolated as a red-tan powder in 90% yield. Previous studies using ligand **4.18** for complex synthesis report the synthesis and characterization of oxo-bridged diiron complexes of the general formula [Fe<sup>III</sup><sub>2</sub>(O)(OOR)(**4.18**)](ClO<sub>4</sub>)<sub>2</sub>.<sup>39</sup> Nevertheless, to the best of my knowledge, this is the first case in which synthesis of complex **4.19** has been reported.

Although, a complex that features two tridentate ligands in the coordination sphere may prevent bimolecular decomposition pathways, it may also slow down or inhibit catalytic cycles, as they occupy all six coordination sites, which impedes substrate coordination.<sup>45</sup> I was intrigued to see what effect a complex bearing two bidentate ligands versus a complex bearing two tridentate ligands would have on catalytic activity. There are two types of bidentate nitrogen based ligands

I was interested in using for the comparison; one being the imine based ligand **4.10** (Figure 4.1) and the  $\alpha$ -aminopyridyl based ligand **4.20** (Scheme 4.1). Because our laboratory has already synthesized and characterized a library of such imine ligands **4.11-4.13**, I only had to prepare the  $\alpha$ -aminopyridyl ligand. Ligand **4.20** was synthesized by reductive amination of 2-pyridine carboxaldehyde with 2-methoxyaniline following a literature procedure for the related tridentate ligand **4.16**.<sup>34a</sup> Respectively, ligand **4.20** was then converted to the corresponding iron complex  $[\text{Fe}^{\text{II}}(\mathbf{4.20})_2(\text{OTf})_2]$  as described above in Scheme 4.1. After slow diffusion crystallization using diethyl ether, complex **4.21** was isolated in 93% yield as a purple block like crystalline solid. Additional  $\alpha$ -aminopyridyl based ligands were synthesized, but difficulties associated with the work-up and isolation of their respective iron complexes made their catalytic application an impossible task.

The multidentate *N,O*- coordinating ligands were synthesized previously in our laboratory by simple alkylation of the commercially available (*S*)-amino alcohol, yielding the corresponding chiral tridentate (*N, O, N*) and tetradentate (*N, O, N, N*) based ligands **4.22**, **4.24** and **4.26** which are displayed in Figure 4.2.<sup>46</sup> The pentadentate (*N, N, N, O, N*) was synthesized by exhaustive alkylation of the commercially available ethanolamine and is depicted in Figure 4.2. Although ligands **4.22** and **4.24** are chiral, we had no intentions of attempting to find an enantioselective catalytic application of the ligands at this time, and as a result, the enantiopurity of the ligands and their intermediates was not determined during their syntheses. However, an optical rotation for ligand **4.22** was established (+67.4), proving that it was in fact optically active, and the chiral information from the starting (*S*)-amino alcohol was not completely lost during the synthesis. The three ligands **4.22**, **4.24** and **4.26** were then employed in the synthesis of their correspond-

ing iron complexes  $[\text{Fe}^{\text{II}}(\mathbf{4.22})_2]\text{OTf}_2$ ,  $[\text{Fe}^{\text{II}}(\mathbf{4.24})(\text{OTf})_2]$  and  $[\text{Fe}^{\text{II}}(\mathbf{4.26})\text{OTf}]\text{OTf}$ , respectively, using identical conditions to those used for the synthesis of **4.17**, **4.19** and **4.21** Scheme 4.1.<sup>46</sup>

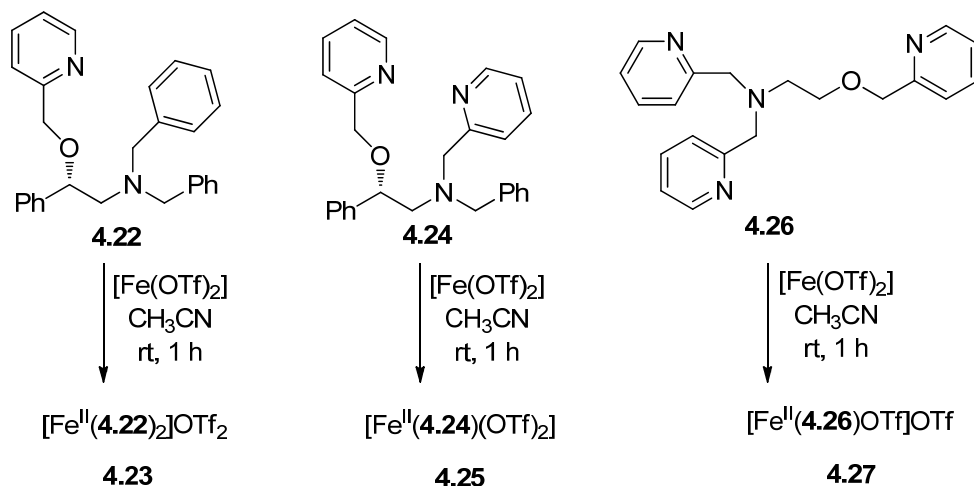


**Figure 4.2.** Selected multidentate *N*-, *O*- coordinating ligands and the synthesis of their respective iron complexes.

### 4.3.2 Characterization of the new iron complexes

The new complexes,  $[\text{Fe}^{\text{II}}(\mathbf{4.16})_2]\text{OTf}_2$ ,  $[\text{Fe}^{\text{II}}(\mathbf{4.18})_2]\text{OTf}_2$ ,  $[\text{Fe}^{\text{II}}(\mathbf{4.20})_2(\text{OTf})_2]$ ,  $[\text{Fe}^{\text{II}}(\mathbf{4.22})_2]\text{OTf}_2$ ,  $[\text{Fe}^{\text{II}}(\mathbf{4.24})(\text{OTf})_2]$  and  $[\text{Fe}^{\text{II}}(\mathbf{4.26})\text{OTf}]\text{OTf}$ , were all spectroscopically characterized utilizing MS (FAB), IR, UV/Visible,  $^1\text{H}$  and  $^{19}\text{F}$  NMR spectroscopy, magnetic measurements and elemental analyses. Moreover, complexes  $[\text{Fe}^{\text{II}}(\mathbf{4.16})_2]\text{OTf}_2$  and  $[\text{Fe}^{\text{II}}(\mathbf{4.20})_2(\text{OTf})_2]$  were structurally characterized (*vide infra*), while all efforts to acquire X-Ray structures of the remaining complexes have failed. Hence, their exact coordination geometry has not yet been confirmed. The data for IR, NMR spectroscopy and UV/Visible spectrophotometry associated with the complexes featuring aminopyridine ligands are compiled in Table 1.

**Table 4.1.** Selected physical data of the new iron complexes.

	IR, $\nu_{\text{NH}}$ ( $\text{cm}^{-1}$ )	UV/Visible <sup>a</sup>		Magnetic moments <sup>b</sup>	<sup>19</sup> F NMR	
	free ligand/complex	nm ( $\text{CH}_2\text{Cl}_2$ )	$E$ ( $\text{M}^{-1} \text{cm}^{-1}$ )	$\mu_{\text{eff}}$ (BM)	ppm	$\nu_{1/2}$ (Hz)
$[\text{Fe}(\mathbf{4.16})_2]^{2+}$	3316/3245	435	7450 (MLCT)	1.83	-78	38
$[\text{Fe}(\mathbf{4.18})_2]^{2+}$	-/-	= 550	<100 (d-d)	4.40	-79	36
$[\text{Fe}(\mathbf{4.20})_2(\text{OTf})_2$	3391/3248	= 550	<100 (d-d)	4.63	-64	5100

<sup>a</sup> In  $\text{CH}_3\text{CN}$ , with concentrations ranging from  $0.3 \times 10^{-3}$  to  $1.4 \times 10^{-3}$  M. <sup>b</sup> In the solid state at 298 K, determined with a magnetic susceptibility balance

As mentioned before, complex **4.17** has been previously synthesized but with bromide<sup>35a</sup> and iodide<sup>35b</sup> counterions. A magnetic moment of  $\mu_{\text{eff}} = 1.83$  BM was determined for complex **4.17** using a magnetic susceptibility balance. This complex also displays defined <sup>1</sup>H and <sup>13</sup>C{<sup>1</sup>H} NMR spectra within the diamagnetic region. Unfortunately, after analysis of the well resolved <sup>1</sup>H and <sup>13</sup>C{<sup>1</sup>H} NMR spectra, it was realized that the proposed structure was not in agreement with the structure established by X-Ray diffraction (illustrated in Scheme 4.1). Moreover, it seemed that the magnetic moment was not exactly zero as expected for a complex with low spin configuration.<sup>35</sup> Thus, the observed intermediate effective magnetic moment may be the result of spin crossover regime. The original <sup>1</sup>H NMR suggested a complex with *cis* configuration of pyridyl and N-H units while that of the X-ray confirmed a *trans* isomer. I hypothesized that the elucidated *trans* configuration may experience dynamic behavior so rapidly in solution at room temperature that the ligands are interpreted as equivalent. In order to corroborate this theory, a low temperature <sup>1</sup>H NMR was recorded at -50 °C. At such a low temperature, an entirely new set of signals emerged from the baseline, suggesting the presence of two non-equivalent ligands in the coordination sphere. Therefore, it appears feasible to assume **4.17** does exhibit dynamic behavior at room temperature. Interestingly, complexes  $[\text{Fe}^{\text{II}}(\mathbf{4.16})_2]\text{Br}_2$  and  $[\text{Fe}^{\text{II}}(\mathbf{4.16})_2]\text{Cl}_2$  also were also isolated as *trans* isomers.<sup>35</sup>

As expected, analysis of MS,  $^{19}\text{F}$  NMR and elemental analysis establishes that complex  $[\text{Fe}^{\text{II}}(\mathbf{4.18})_2]\text{OTf}_2$  also features two tridentate ligands **4.18** in the coordination sphere with two triflate anions existing as counterions. Interpretation of the  $^1\text{H}$  NMR spectrum revealed a large window of chemical shifts between  $\delta = -20$  and 120 ppm, which may be the result of paramagnetic behavior. Consequently, the effective magnetic moment of complex **4.19** was determined to be  $\mu_{\text{eff}} = 4.40$  BM supporting the idea of paramagnetism which is consistent with other related high-spin  $\text{Fe}^{\text{II}}$  systems previously reported in the literature.<sup>26a,32a</sup> Review of the spectroscopic data for the aminopyridyl complex  $[\text{Fe}^{\text{II}}(\mathbf{4.20})_2(\text{OTf})_2]$  confirmed the presence of two bidentate ligands and two triflate anions in the coordination sphere. Complex **4.21** had an effective magnetic moment of  $\mu_{\text{eff}} = 4.63$  BM indicating it also was paramagnetic. Additionally, paramagnetic shifts between  $\delta = 0$  and 120 were observed. As was the case with complex **4.17**, the structural framework for complex **4.21** was also unequivocally elucidated using X-Ray diffraction (vide infra), and the general formulation  $[\text{Fe}^{\text{II}}(\mathbf{4.20})_2(\text{OTf})_2]$  was confirmed by elemental analysis.

Another benefit of utilizing complexes bearing triflate anions was that their position could be easily established through analysis of  $^{19}\text{F}$  NMR spectra. Accordingly, the  $^{19}\text{F}$  NMR spectra of the three complexes were recorded in  $\text{CD}_3\text{CN}$  and subsequently analyzed. It is known that non-coordinated OTf counterions give solvent dependent resonances around  $\delta = -70$  ppm that drastically shift downfield between  $\delta = 60$  and 80 ppm upon coordination to an  $\text{Fe}^{\text{II}}$  center.<sup>47</sup> In complexes **4.17** and **4.19**, the  $^{19}\text{F}$  NMR resonances were  $\delta = -78$  and  $-79$  ppm (Table 4.1), which falls within the ideal range for a non-coordinated, free triflate counterion. Likewise, the widths at half height ( $\nu_{1/2}$ ) for the  $^{19}\text{F}$  NMR resonances, which may also be used to assess the OTf position in solution, are 38 and 36 Hz, respectively (Table 4.1). The  $\nu_{1/2}$  can be used to determine the presence or absence of dynamic processes in solution involving the OTf counterion. The absence of

any dynamic processes seems feasible as all six coordination sites are occupied by the two tridentate ligands. On the contrary, the aminopyridine complex **4.21** features two bidentate ligands and two weakly coordinated triflate anions within the coordination sphere, and its  $^{19}\text{F}$  NMR spectrum exhibited a broad resonance at  $\delta = -64$  ppm ( $\nu_{1/2} = 5100$  Hz). This broad resonance and large width at half height are indicative of a dynamic process involving rapid exchange of the OTf anion and  $\text{CD}_3\text{CN}$  solvent.<sup>26a</sup>

Next, investigations, of all three complexes having nitrogen only donor atoms, were performed using UV/Visible spectrophotometry. The UV/Visible spectra of these three complexes, **4.17**, **4.19** and **4.21** were recorded in  $\text{CH}_3\text{CN}$  and  $\text{CH}_2\text{Cl}_2$ . Surprisingly, only complex **4.17** displayed a metal-to-ligand charge transfer (MLCT) band ( $\lambda = 435$  nm) that could be easily identified (Figure 4.2, which shows traces recorded in  $\text{CH}_3\text{CN}$ ). Both the molar absorptivity ( $\epsilon$ ) of the MLCT, which was calculated to be  $7450 \text{ M}^{-1}\text{cm}^{-1}$ , and the wavelength are in accordance with structurally similar  $\text{Fe}^{\text{II}}$  complexes with nitrogen coordinating ligands.<sup>26a,32a,48</sup> Then, UV/Visible spectra were recorded in a non-coordinating solvent,  $\text{CH}_2\text{Cl}_2$ . To much surprise, the UV/Visible spectra were nearly identical implying that the structure of the three complexes are the same despite different solvents, and there is no displacement of ligand donors in the presence of coordinating solvents. UV/Visible spectra for the remaining two complexes **4.19** and **4.21** were recorded and only exhibited weak d-d transitions, and no MLCT bands were observed in either  $\text{CH}_2\text{Cl}_2$  or  $\text{CH}_3\text{CN}$ .<sup>49</sup>

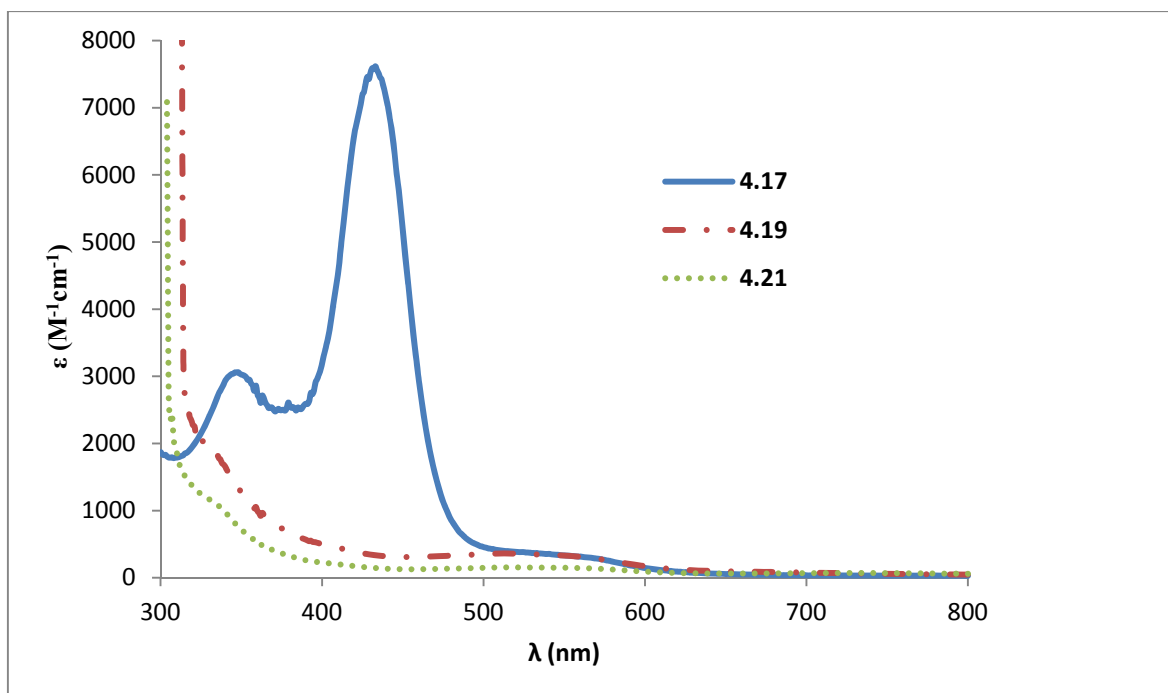


**Figure 4.3.** UV/Visible spectra of complexes **4.17**: $[\text{Fe}^{\text{II}}(\mathbf{4.16})_2]\text{OTf}_2$  (solid line), **4.19**: $[\text{Fe}^{\text{II}}(\mathbf{4.18})_2]\text{OTf}_2$  and **4.21**: $[\text{Fe}^{\text{II}}(\mathbf{4.20})_2(\text{OTf})_2]$  in  $\text{CH}_3\text{CN}$ .

As stated earlier, IR can be used to assess the position of the triflate anion. Thus, IR spectra for all three complexes **4.17**, **4.19** and **4.21** were acquired in which all three complexes displayed strong identifiable bands representing the OTf counteranion. The free triflate counteranion usually display its IR stretches at 1268, 1223, 1143 and 1030  $\text{cm}^{-1}$ . After comparison of the IR spectra for the three complexes in the solid state, it was obvious that many of them had similar stretches, yet some of the stretches contained shoulders for complex **4.21**, which indicated that the triflate is coordinated to the iron center.<sup>32c,50</sup> Upon coordination of ligands **4.16** and **4.20** to the iron center, a shift to a lower wavenumber was expected for the stretches representing the N-H functionalities. Consequently, complexes **4.17** and **4.21** contained N-H stretches at 3245 and 3248  $\text{cm}^{-1}$ , which were 100  $\text{cm}^{-1}$  lower than their respective free ligands. Recently in our laboratory, IR spectra for the *N*-, *O*- multidentate complexes **4.23**, **4.25** and **4.27** was recorded, which



proved to be not as informative as previous spectra due to the absence of any N-H or O-H units present on the ligands to monitor ligand coordination. However, the IR spectra were instrumental in suggesting the location of the OTf counter anion.

In order to unambiguously determine the molecular structures of the new iron complexes, X-ray structures were established of complexes **4.17** and **4.21** (Figure 4.3). Crystallographic parameters are given in Table 4.2 and key bond lengths and bond angles are given in Table 4.3. For complex **4.17**, the bond angles for the *N* in *cis* positions around the iron center range from 82.54(9) to 98.26(9) $^{\circ}$  and those *N* atoms in the *trans* positions range from 174.15(7) to 178.06(8) $^{\circ}$ .

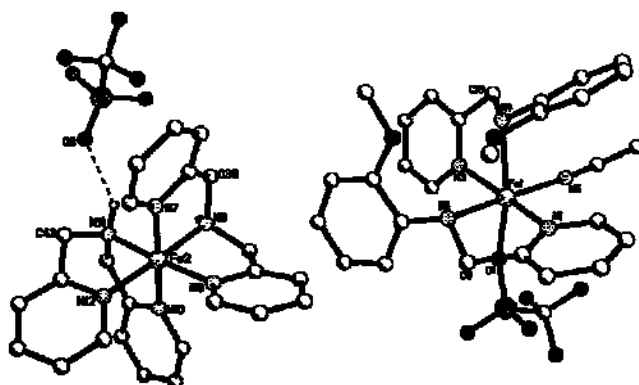


**Figure 4.3.** X-Ray structures of  $[\text{Fe}^{\text{II}}(\mathbf{4.16})_2]^{***}\text{OTf}$  (left) and  $[\text{Fe}^{\text{II}}(\mathbf{4.20})_2(\text{OTf})(\text{CH}_3\text{CN})]^+$  (right). Hydrogen atoms, solvent molecules, and one of the OTf counter ions have been omitted for clarity. Plots giving thermal ellipsoids are given in the supporting information.

Therefore, the structure is best described as distorted octahedral. The N-Fe-N bond angles within the ligand ranges from 82.54(9) to 85.78(9) $^{\circ}$ , whereas the angles between the ligands range from 91.04(9) to 101.9(2). Hence, the average “bite angle” for ligand **4.16** is around 84 $^{\circ}$ . This average “bite angle” may be the reason for the slight distortion from the ideal octahedral coordination geometry. The Fe-N bond lengths are between 1.984(2) and 2.011(2) Å; falling

within the range for standard Fe-N bond lengths of low-spin Fe<sup>II</sup> complexes. The solid-state X-Ray structure confirms that the two triflate anions are not coordinated to the iron center. However, there is a hydrogen bond between the S-O portion of the OTf anion and the N-H unit of the ligand (Figure 4.3, left structure), and the average bond length is between 2.0 and 2.3 Å, which is typical for structurally similar complexes featuring different counteranions such as Br<sup>-</sup> and Cl<sup>-</sup>. After comparison of the crystallographic parameters for structurally similar complexes [Fe<sup>II</sup>(**4.16**)<sub>2</sub>]OTf<sub>2</sub> and [Fe<sup>II</sup>(**4.16**)<sub>2</sub>]X<sub>2</sub> (X = Br<sup>-</sup>, Cl<sup>-</sup>), it became evident that many of the key bond lengths and bond angles were very similar, but the coordination geometries of **4.16** were different. The N-H units in complexes [Fe<sup>II</sup>(**4.16**)<sub>2</sub>]X<sub>2</sub> (X = Br<sup>-</sup>, Cl<sup>-</sup>) are *trans* to each other; whereas in complex [Fe<sup>II</sup>(**4.16**)<sub>2</sub>]OTf<sub>2</sub> the N-H units are *cis* to one another and *trans* to a pyridyl ring. complex **4.17** exhibits dynamic behavior in solution, as evidenced by broadened signals, representing the *cis* isomer, at room temperature and sharp signals, representing the *trans* isomer, at -50 °C. It is unknown whether or not complexes [Fe<sup>II</sup>(**4.16**)<sub>2</sub>]X<sub>2</sub> (X = Br<sup>-</sup>, Cl<sup>-</sup>) also exhibit dynamic behavior, but due to the disparity in counteranions, the other isomers may precipitate out of solution.

**Table 4.2.** Crystallographic parameters for complexes **4.17** and **4.21**.

	[Fe <sup>II</sup> ( <b>4.16</b> ) <sub>2</sub> ](OTf) <sub>2</sub>	[Fe <sup>II</sup> ( <b>4.20</b> ) <sub>2</sub> ](OTf) <sub>2</sub>
Empirical formula	C <sub>56</sub> H <sub>58</sub> F <sub>12</sub> Fe <sub>2</sub> N <sub>14</sub> O <sub>12</sub> S <sub>4</sub>	C <sub>29</sub> H <sub>31</sub> F <sub>3</sub> FeN <sub>5</sub> O <sub>5</sub> S
Formula weight	1587.10	864.62
Temperature, Wavelength	100(2) K, 0.71073 Å	100(2) K, 0.71073 Å
Crystal system, Space group	Monoclinic, P <sub>n</sub>	Triclinic, P1
Unit cell dimensions	a = 16.9936(10) Å b = 9.3511(6) Å c = 20.5805(12) Å alpha = gamma = 90°, beta = 102.006(3)°	a = 10.5308(6) Å b = 13.4426(8) Å c = 13.9190(9) Å alpha = 75.702(3), beta = 77.494(3) gamma = 79.812(3)
Volume, Z	3198.9(3) Å <sup>3</sup> , 2	1848.13(19) Å <sup>3</sup> , 2
Density (calculated)	1.648 Mg/m <sup>3</sup>	1.554 Mg/m <sup>3</sup>
Absorption coefficient	0.692 mm <sup>-1</sup>	0.609 mm <sup>-1</sup>
Crystal size (mm <sup>3</sup> )	0.28 x 0.27 x 0.20 mm <sup>3</sup>	0.22 x 0.10 x 0.09 mm <sup>3</sup>
Theta range for data collection	2.02 to 32.18°	2.95 to 32.60°
Reflections collected	139854	42411
Independent reflections	21639 [R(int) = 0.0636]	7510 [R(int) = 0.0521]
Completeness to theta = 25.00° (%)	100.0	98.6
Absorption correction	Semi-empirical from equivalents	Semi-empirical from equivalents
Max. and min. transmission	0.8717 and 0.8277	0.9461 and 0.8791
Data/ restraints/ parameters	21639/15/937	7510/51/516
Goodness-of-fit on F <sub>2</sub>	1.021	1.015
Final R indices [I>2sigma(I)]	R1 = 0.0468, wR2 = 0.1148	R1 = 0.0391, wR2 = 0.0822
R indices (all data)	R1 = 0.0579, wR2 = 0.1222	R1 = 0.0629, wR2 = 0.0921
Absolute structure parameter	0.669(9)	
Largest diff. peak and hole	1.381 and -0.761 e Å <sup>-3</sup>	0.696 and -0.483 e Å <sup>-3</sup>

**Table 4.3.** Key bond lengths (Å) and angles (°).

[Fe <sup>II</sup> ( <b>4.16</b> ) <sub>2</sub> ](OTf) <sub>2</sub>		[Fe <sup>II</sup> ( <b>4.20</b> ) <sub>2</sub> ](OTf) <sub>2</sub>	
Fe2-N7	1.964(2)	Fe1-N1	2.1463(19)
Fe2-N8	2.006(2)	Fe1-N2	2.257(2)
Fe2-N9	1.997(2)	Fe1-N3	2.1577(19)
Fe2-N10	1.986(2)	Fe1-N4	2.249(2)
Fe2-N11	2.011(2)	Fe1-N5	2.160(2)
Fe2-N12	1.990(2)	N1-Fe1-N2	76.37(7)
N8-Fe2-N9	82.51(10)	N2-Fe1-N3	94.71(7)
N9-Fe2-N10	97.02(9)	N1-Fe1-N5	94.08(8)
N7-Fe2-N11	94.33(10)	N1-Fe1-N3	169.42(7)
N7-Fe2-N10	178.06(8)	N2-Fe1-N5	169.47(7)
N8-Fe2-N12	175.45(10)	N2-Fe1-O1	92.56(7)

As far as complex **4.21** is concerned, the bond angles for the N atoms in *cis* positions around the iron center range from 76.37(7) to 94.71(7) $^{\circ}$  and the bond angles for N atoms in the *trans* position around 169.4 $^{\circ}$ . Again, the geometry may be best describes as slightly distorted octahedral. Also, the N-H units are *cis* to each other just like in complex **4.17**. The N-Fe-N bond angles within the ligands are 76.37(7) and 75.59(7) $^{\circ}$  respectively, and 94.71(7) and 98.32(7) $^{\circ}$  between ligands. Thus, the average “bite angle” for the  $\alpha$ -aminopyridyl ligand **4.20** is about 75 $^{\circ}$ , which also contributed to the less than ideal octahedral geometry. The Fe-N bond lengths are between 2.1463(19) and 2.257(2) Å; This which falls within the range for Fe-N bond lengths of standard high-spin Fe<sup>II</sup> complexes, which are typically 2.2 Å, and is around 0.2 Å longer than the corresponding low-spin Fe<sup>II</sup> complexes . Additional corroboration of the high spin configuration for complex **4.21** was obtained by magnetic measurements acquired through utilization of a magnetic susceptibility balance (Table 4.1). The X-Ray of complex **4.21** confirmed that one of the triflate ions and one solvent molecule of CH<sub>3</sub>CN were coordinated to the iron center, while the second triflate ion served as a counteranion. Oddly enough, the solvent molecule of CH<sub>3</sub>CN was not present in the original solid state spectral data, as evidenced by IR and elemental analysis. I attributed the presence of CH<sub>3</sub>CN to the protocol for obtaining X-Ray quality crystals of complex **4.21**, which employed CH<sub>3</sub>CN as a solvent.

The discussed protocol for complex synthesis yielded three well-defined and spectroscopically characterized iron complexes **4.17**, **4.19** and **4.21**, in addition to the previously synthesized complexes [Fe<sup>II</sup>(**4.2**)(OTf)<sub>2</sub>] and [Fe<sup>II</sup>(**4.11**)<sub>2</sub>(OTf)<sub>2</sub>], which were subsequently used for catalytic investigations.

### 4.3.3 *Catalysis and catalytic efficiency*

In 2007, Gebbink and coworkers reported the oxidation of cyclohexane as a standard test reaction; which may be used to aid in the prediction of the course of reaction. In this test reaction, a large excess of the cyclohexane over the peroxide oxidant is employed to mitigate overoxidation<sup>27</sup>. From the oxidation products, an alcohol-to-ketone (A/K) ratio is calculated, which provides information about the pathway of the reaction.<sup>10</sup> If the alcohol/ketone ratio is low ( $\leq 1.0$ ), then it most likely follows an unselective free-radical oxidation, and if it is high, then it most likely entails a metal-centered based oxidant. For that reason, we studied a plethora of cyclohexane/H<sub>2</sub>O<sub>2</sub> or cyclohexane/*t*-BuOOH ratios for all complexes, and the results are listed in Table 4.4.

**Table 4.4.** Alcohol/ketone ratios after cyclohexane oxidation

	Reaction time (min)	Peroxide/substrate ratio	Alcohol/ketone ratio
Cyclohexane oxidation with fast addition of H <sub>2</sub> O <sub>2</sub> <sup>b</sup>			
[Fe <sup>II</sup> ( <b>4.16</b> ) <sub>2</sub> ] <sup>2+</sup>	120	0.1	0.25
	240	0.1	0.25
[Fe <sup>II</sup> ( <b>4.18</b> ) <sub>2</sub> ] <sup>2+</sup>	120	0.1	0.25
[Fe <sup>II</sup> ( <b>4.20</b> ) <sub>2</sub> (OTf) <sub>2</sub> ]	120	0.1	0.33
Cyclohexane oxidation with slow addition of H <sub>2</sub> O <sub>2</sub> <sup>c</sup>			
[Fe <sup>II</sup> ( <b>4.16</b> ) <sub>2</sub> ] <sup>2+</sup>	25	0.01	6.6
[Fe <sup>II</sup> ( <b>4.18</b> ) <sub>2</sub> ] <sup>2+</sup>	25	0.01	1.1
[Fe <sup>II</sup> ( <b>4.20</b> ) <sub>2</sub> (OTf) <sub>2</sub> ]	25	0.01	1.5
" <b>19</b> "	25	0.01	3.0
Cyclohexane oxidation with slow addition of <i>t</i> -BuOOH <sup>c</sup>			
[Fe <sup>II</sup> ( <b>4.16</b> ) <sub>2</sub> ] <sup>2+</sup>	25	0.1	0.5
[Fe <sup>II</sup> ( <b>4.18</b> ) <sub>2</sub> ] <sup>2+</sup>	25	0.1	0.66
[Fe <sup>II</sup> ( <b>4.20</b> ) <sub>2</sub> (OTf) <sub>2</sub> ]	25	0.1	0.66
Cyclohexane oxidation with slow addition of H <sub>2</sub> O <sub>2</sub> <sup>c</sup>			
[Fe <sup>II</sup> ( <b>4.22</b> ) <sub>2</sub> ] <sup>2+</sup>	25	0.01	0.7
[Fe <sup>II</sup> ( <b>4.24</b> )(OTf) <sub>2</sub> ]	25	0.01	1.1
[Fe <sup>II</sup> ( <b>4.26</b> )OTf] <sup>+</sup>	25	0.01	0.6
Cyclohexane oxidation with fast addition of <i>t</i> -BuOOH <sup>b</sup>			
[Fe <sup>II</sup> ( <b>4.22</b> ) <sub>2</sub> ] <sup>2+</sup>	25	0.01	0.5
[Fe <sup>II</sup> ( <b>4.24</b> )(OTf) <sub>2</sub> ]	25	0.01	0.7
[Fe <sup>II</sup> ( <b>4.26</b> )OTf] <sup>+</sup>	25	0.01	0.3

<sup>a</sup>Peroxide/catalyst ratio = 10. Details are given in the Experimental Section. <sup>b</sup>Fast addition of H<sub>2</sub>O<sub>2</sub> or *t*-BuOOH to the reaction mixture. <sup>c</sup>Slow addition over 25 min of a 90 mM H<sub>2</sub>O<sub>2</sub> or *t*-BuOOH solution to the reaction mixture.

As far as the oxidation reactions employing H<sub>2</sub>O<sub>2</sub> are concerned, the A/K ratios appear to be significantly influenced by the rate at which the oxidant was added by the cyclohexane/H<sub>2</sub>O<sub>2</sub> ratio. For example, when the H<sub>2</sub>O<sub>2</sub> was added quickly to the substrate cyclohexane and catalyst, the A/K ratios were low and ranged from 0.25 and 0.33, where the A/K ratios were calculated via GC analysis of the reaction mixtures. Interestingly, the cyclohexane/oxidant ratio exerted no influence on the outcome of the A/K ratio when the oxidant was added rapidly. However, when the H<sub>2</sub>O<sub>2</sub> was added slowly over 25 minutes, as a 90 mM solution via syringe pump, to the reaction mixture at a 0.01 H<sub>2</sub>O<sub>2</sub>/cyclohexane ratio, the A/K ratio was much higher when complex **4.17**

was used as a catalyst. At the same H<sub>2</sub>O<sub>2</sub>/cyclohexane ratio the A/K ratio was typically >1.0 when complexes **4.19** and **4.21** were used as catalysts. As stated earlier, it is believed that low A/K ratios are the result of unselective free radical chain mechanisms, and these free radical species are present in high concentration only when the peroxide oxidant is added rapidly.<sup>51</sup> Although, when the oxidant is added slowly as a 90 mM solution using a syringe pump, the concentration of the unselective free radical species is attenuated, allowing for the peroxide to react with the Fe<sup>II</sup> complex, generating the high-valent metal based oxidant [Fe<sup>n</sup>=O].<sup>47</sup> This high-valent iron-oxo species is believed to be the terminal oxidant, whereby incorporating an oxygen into the C-H bond of cyclohexane resulting in cyclohexanol, which in turn is considered to be responsible for such a high A/K ratio. It is strongly believed that a high-valent iron-oxo species is involved when complex **4.17** is used as a catalysts, as evidenced from the high A/K ratio of 6.6, which is on the same order as reported for structurally similar iron complexes such as [Fe<sup>II</sup>(tpa)(OTf)<sub>2</sub>].<sup>25</sup>

Unfortunately, the A/K ratios for complexes **4.23**, **4.25** and **4.27** were consistently low (0.5-1.1) irrespective of the oxidant utilized and the rate of addition. Thus, it seems that the oxidation of hydrocarbons, using complexes bearing multidentate *N*-, *O*- ligands, proceeds via a pathway that involves an unselective free radical species. Be that as it may, the A/K ratio studies applying *t*-BuOOH as an oxidant displayed different results, where the A/K ratios were low (0.30-0.70) irrespective of the *t*-BuOOH/cyclohexane ratio or rate of oxidant addition. The literature reports that *t*-BuO<sup>•</sup> radicals are known for the induction of radical chain autooxidation pathways which may account for this difference in A/K ratios with *t*-BuOOH.<sup>12d</sup> Notably, the A/K ratios did not change, even when the experiments were performed under anaerobic conditions. Under anaerobic conditions, when the oxidant was added to the catalyst in the absence of substrate, a very dis-

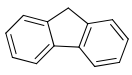
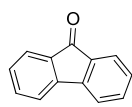
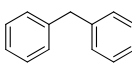
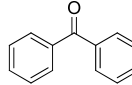
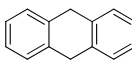
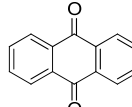
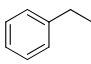
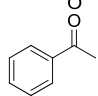
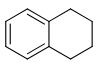
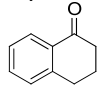
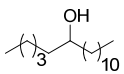
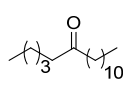
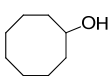
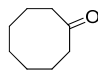
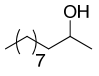
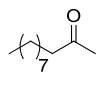
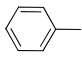
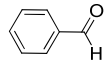
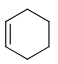
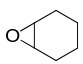
tinct evolution of bubbles and heat was observed, which very well could be evidence for peroxide decomposition to water and oxygen, otherwise known as catalase activity. Thus, the Fe<sup>II</sup> induced decomposition of peroxides, could provide its own source of oxygen even under inert conditions.

Another objective of the A/K ratio studies performed on the new Fe<sup>II</sup> complexes was to determine the scope of the reaction and identify complexes exhibiting superior activity. In addition to the A/K ratio investigations, preliminary screening efforts were performed in an attempt to establish which complexes exhibited optimum catalytic activity. From these studies it was determined that complex **4.17**, from the class of complexes featuring strictly nitrogen based ligands, and complex **4.25**, from the class of complexes featuring multidentate *N*-, *O*- ligands, showed the most promising results. Complexes **4.17** (Table 4.5) and **4.25** (Table 4.6) were employed as catalysts in the oxidation of secondary alcohols and activated methylene groups utilizing *t*-BuOOH or H<sub>2</sub>O<sub>2</sub> as the oxidant.<sup>32a</sup>

By analogy to complex **4.17**, I hypothesized that complex **4.15**, having two sites that are only temporarily occupied by a labile two electron donor anion, may exhibit higher reactivity towards the peroxide oxidant. Consequently, their efficacy was put to the test and both complexes were employed in oxidation reactions with the intention of comparing their isolated yields (Table 4.5).



**Table 4.5.** Oxidation reactions employing complexes  $[\text{Fe}^{\text{II}}(\mathbf{4.16})_2]^{2+}$  and  $[\text{Fe}^{\text{II}}(\mathbf{4.11})_2(\text{OTf})_2]$  as catalysts and *t*-BuOOH as the oxidant.

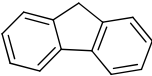
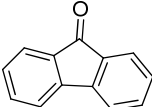
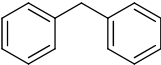
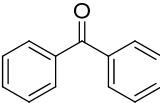
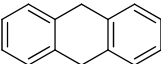
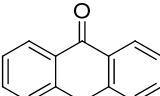
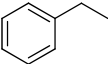
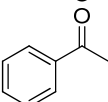
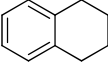
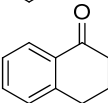
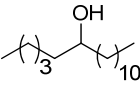
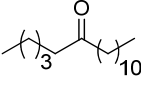
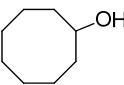
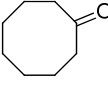
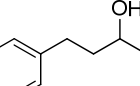
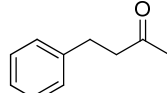
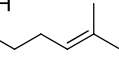
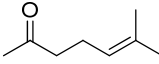
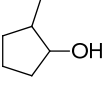
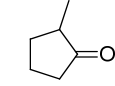
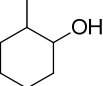
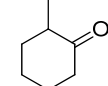
Entry	Substrate	Product <sup>a</sup>	Yield using $[\text{Fe}^{\text{II}}(\mathbf{4.16})_2]^{2+}$ (%) <sup>b</sup>	Yield using $[\text{Fe}^{\text{II}}(\mathbf{4.11})_2(\text{OTf})_2]$ (%) <sup>b</sup>
1			85	91
2			76	74
3			79	51
4			34	47
5			71	22
6			69	-
7			67	47
8			58	23
9			57	-
10			28	-

<sup>a</sup>Typical conditions: substrate (0.6 mmol), *t*-BuOOH (2.4 mmol) and catalyst (3 mol%), 4 h at room temperature in  $\text{CH}_3\text{CN}/\text{pyridine}$  (1:1, 2 mL). The products were isolated using column chromatography. <sup>b</sup>% yield after isolation of product.

Table 4.5 shows that a stoichiometric ratio of 4:1 for *t*-BuOOH:substrate, 3 mol% catalyst loading and 4-8 h reaction time at room temperature was chosen as the standard reaction conditions. With the application of these conditions, the expected ketones were isolated in 34 to 85% yield. Under identical conditions, toluene was oxidized to benzaldehyde in 57% yield and cyclohexene generated the expected epoxide in 28% yield. Peculiarly, the oxidation of primary alcohols to the corresponding aldehydes was never observed. The reason why the oxidation of prima-

ry alcohols was never seen is not entirely clear. An inherent interest in the catalytic activity of all new iron complexes prepared in our laboratory led to additional exploratory studies on complexes **4.19** and **4.21**, which immediately revealed that, despite their differences in denticity and size, their catalytic abilities were similar to that of complex **4.17**. The complex  $[\text{Fe}^{\text{II}}(\mathbf{4.11})_2(\text{OTf})_2]$ , which was previously prepared and characterized by our laboratory, behaved similarly in oxidation reactions, resulting in isolations ranging from 22 to 91% yield. Analysis of the isolated yields in Table 4.5 demonstrated that complex  $[\text{Fe}^{\text{II}}(\mathbf{4.11})_2(\text{OTf})_2]$  had similar activity when being compared to complex **4.17** in the oxidation of “doubly” activated methylene groups such as anthracene and fluorene. On the other hand, the activity of complex  $[\text{Fe}^{\text{II}}(\mathbf{4.11})_2(\text{OTf})_2]$  displayed poor activity when being compared to complex **4.17** in the oxidation of secondary alcohols. Moreover, complex  $[\text{Fe}^{\text{II}}(\mathbf{4.11})_2(\text{OTf})_2]$  exhibited no activity, when being compared to complex **4.17**, in the epoxidation of cyclohexene and oxidation of toluene.

**Table 4.6.** Oxidation reactions of activated methylene groups and secondary alcohols using complex[Fe<sup>II</sup>(**4.24**)(OTf)<sub>2</sub>] as catalyst

Entry	Substrate	Product	Yield using [Fe <sup>II</sup> ( <b>4.24</b> )(OTf) <sub>2</sub> ] <sup>2+</sup> (%)
1			90 <sup>a</sup> 65 <sup>b</sup>
2			80 <sup>a</sup> 64 <sup>b</sup>
3			46 <sup>b</sup>
4			78 <sup>a</sup>
5			63 <sup>a</sup>
6			36 <sup>b</sup>
7			39 <sup>b</sup>
8			70 <sup>c</sup>
9			69 <sup>a</sup>
10			70 <sup>a,d</sup>
11			68 <sup>a,d</sup>

<sup>a</sup> Substrate (0.6 mmol), H<sub>2</sub>O<sub>2</sub> (30% in H<sub>2</sub>O, 1.8 mmol), and the catalyst [Fe<sup>II</sup>(**4.24**)(OTf)<sub>2</sub>] (0.018 mmol) in CH<sub>2</sub>CN (1 mL) for 2 h at room temperature.  
<sup>b</sup> Substrate (0.6 mmol), *t*-BuOOH (2.4 mmol) and the catalyst [Fe<sup>II</sup>(**4.24**)(OTf)<sub>2</sub>] (0.018 mmol) in acetone (2 mL) for 8 h at room temperature.  
<sup>c</sup> With *t*-BuOOH in pyridine  
<sup>d</sup> In the NMR spectra a second set of signals indicated the presence of the enol tautomer.

Table 4.6 shows that complex **4.25** was successfully used as a catalyst in the oxidation of multiple substrates when H<sub>2</sub>O<sub>2</sub> was used as the oxidant. The conditions involved a three-fold excess of the peroxide oxidant over the substrate, a 3 mol% precatalyst loading and CH<sub>3</sub>CN as the solvent of choice. Under these conditions, the activated methylene groups were oxidized to the anticipated ketones in 46 to 90% isolated yields (entries 1,2,4 and 5 in Table 4.6). Secondary alcohols were oxidized to the expected ketones in 68 to 70% isolated yields (entries 9, 10 and 11 in Table 4.6). As follows, clearly, under the conditions outlined in Table 4.6, complex **4.25** displays higher activity in the oxidation of activated methylene groups than in the oxidation of secondary alcohols.

Although CH<sub>3</sub>CN yielded auspicious results, we also demonstrated that pyridine, also widely used in related oxidation systems,<sup>52</sup> can be used (entry 8 in Table 4.6). However, according to the principles of “Green Chemistry” and the fact that it is a known carcinogen, pyridine is referred to as “undesirable”. Conjointly, the same principles refer to CH<sub>3</sub>CN as being “usable” but not quite “preferred”.<sup>53</sup> In such a way, we immediately wondered if an alternative, more environmentally friendly solvent could be used in the title oxidation reaction. Thus, after consulting the principles of “Green Chemistry” as well as keeping in mind potential solubility issues, the choice to use acetone was made. Encouragingly, for our purposes, acetone is significantly less harmful, environmentally benign and referred to as “preferred”. Consequently, some oxidations were performed using acetone as solvent and *t*-BuOOH as the oxidant. Under these conditions, the overall yields ranged from 36 to 65%. The activated methylene groups were oxidized to the corresponding carbonyl compounds in 46 to 65% isolated yields (entries 1-3 in Table 4.6), and the secondary alcohols were oxidized to the desired ketones in 36 to 39% isolated yields (entries

6 and 7 in Table 4.6). Again, as evidenced by data associated with the use of acetone, it seemed that the activated methylene groups were oxidized more efficiently than that of the secondary alcohols.

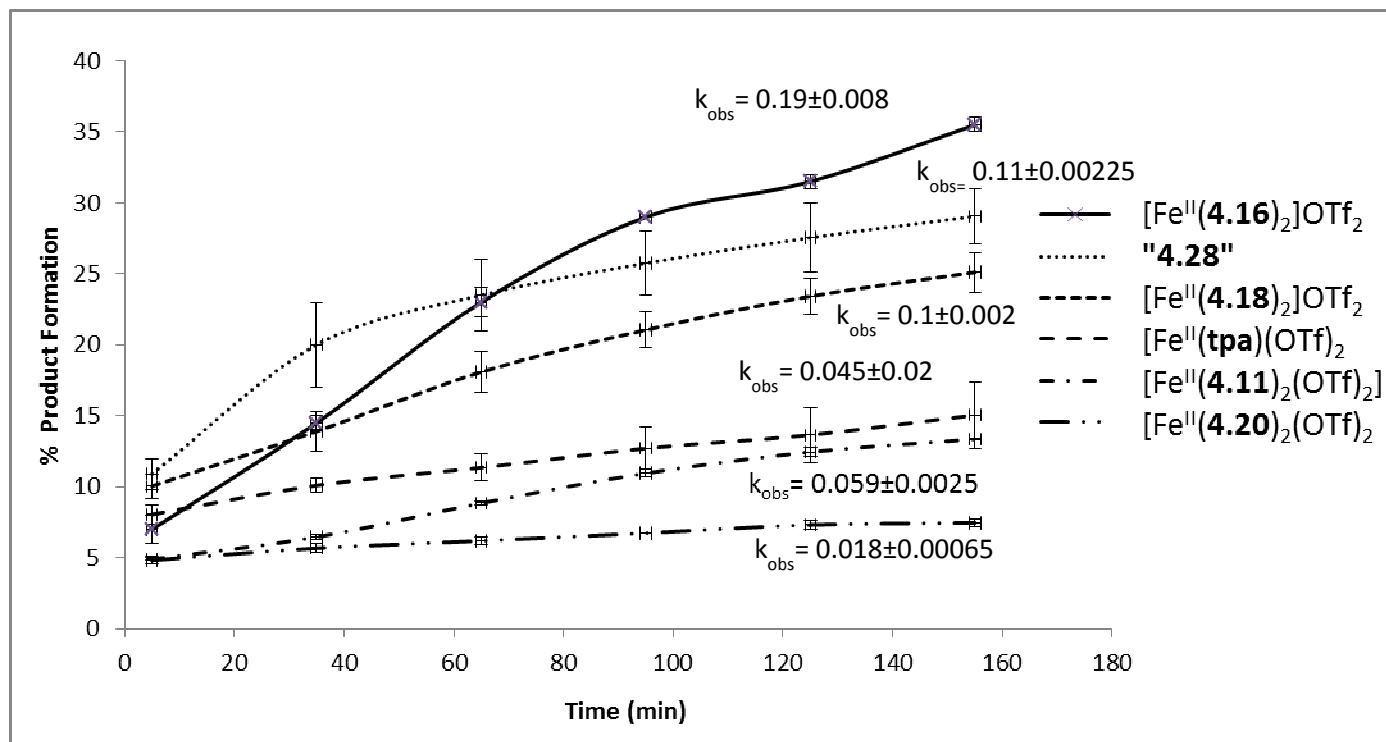


**Figure 4.4.** Activity comparison of different iron complexes featuring strictly *N*-donor ligands. The  $k_{\text{obs}}$  values were determined from the linear trends of the traces, which are not shown above.

In order to extrapolate kinetic information for each of the synthesized complexes bearing *N*-donor ligands, the oxidation of diphenylmethane with *t*-BuOOH, at a reduced catalyst loading of 0.3 mol%, was followed over the course of 3 hours for all of the iron complexes **4.17**, **4.19**, **4.21** as well as the previously prepared complexes  $[\text{Fe}^{\text{II}}(\mathbf{4.11})_2(\text{OTf})_2]$  and  $[\text{Fe}^{\text{II}}(\mathbf{tpa})(\text{OTf})_2]$  by GC. The catalyst loading was reduced in an attempt to slow down the reaction for a facile monitoring and comparison. Review of the traces illustrated in Figure 4.4 revealed that the all of the com-

plexes typically followed a pseudo-zero-order rate law and are accompanied by their respective observed rate constants  $k_{\text{obs}}$ . Additionally, a trace for compound “4.28” was included in Figure 4.4, which represented a compound that was formed after treating complex 4.17 with *t*-BuOOH. Comparison of the traces in Figure 4.4 suggests that the catalytic activity is similar for complexes 4.17 and 4.19 ( $k_{\text{obs}} = 0.19$  and  $0.10 \text{ min}^{-1}$ ). Complexes 4.21,  $[\text{Fe}^{\text{II}}(\mathbf{4.11})_2(\text{OTf})_2]$  and  $[\text{Fe}^{\text{II}}(\mathbf{tpa})(\text{OTf})_2]$  all demonstrated slightly lower catalytic activity ( $k_{\text{obs}} = 0.018$ ,  $0.059$  and  $0.045 \text{ min}^{-1}$ , respectively). Recalling Table 4.5, this data is consistent with the lower activity of  $[\text{Fe}^{\text{II}}(\mathbf{4.11})_2(\text{OTf})_2]$  compared to 4.17.

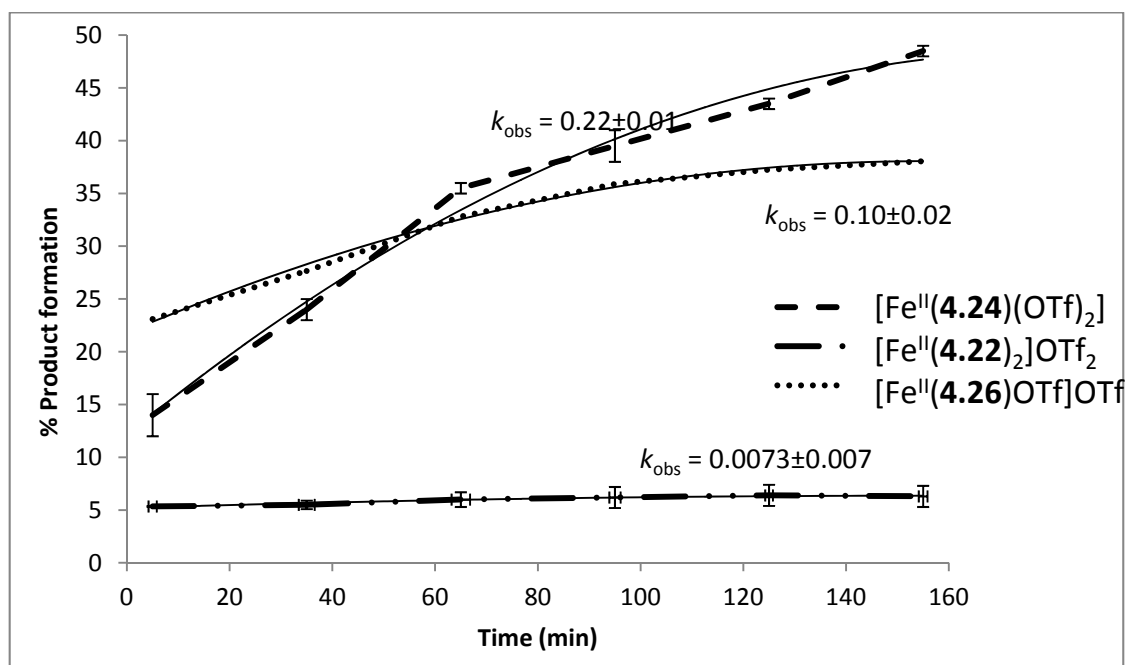


**Figure 4.5.** Activity comparison of different iron complexes featuring multidentate *N*-, *O*- donor ligands. The  $k_{\text{obs}}$  values were determined from the linear trends of the traces, which are not shown above.

As before, we were interested in determining any potential differences in catalytic activity for the complexes featuring multidentate *N*-, *O*- ligands. Hence, kinetic data on complexes 4.23, 4.25 and 4.27 were acquired in an identical manner (oxidation of diphenylmethane, with *t*-

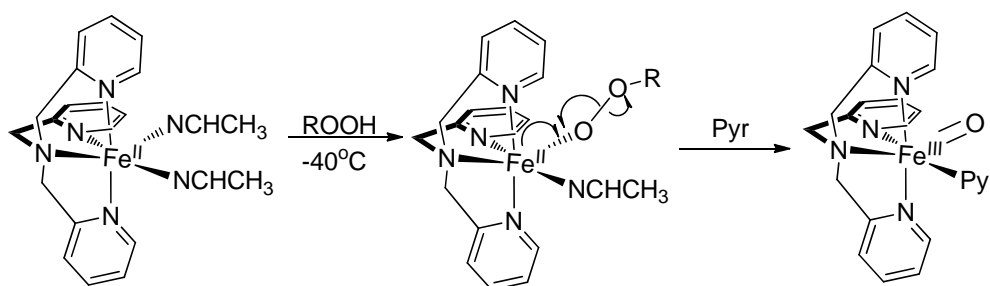
BuOOH, was followed over the course of 3 hours at a reduced catalyst loading of 0.3 mol% by GC). Once more, the activity of the complexes followed a pseudo-zero-order rate law and the observed rate constants ( $k_{\text{obs}}$ ) were derived (Figure 4.5) from the linear trends of the respective traces, which are not shown.

Interestingly, the differences in observed rate constants shown in both Figure 4.4 and Figure 4.5 suggest that an increase in the number of neutral two electron donor atoms is accompanied with an increase in catalytic activity, at least at a reduced catalyst loading. As mentioned before, when the initial screening of catalytic activity, using the standard 3 mol% catalyst loading, was performed to identify complexes with higher activity, no significant differences in yields were observed. Therefore, by slowing down the reaction, we were able to observe the influence that ligands with increasing denticity had on the catalyst activity for all of the iron(II) complexes being investigated.

#### 4.3.4 Experiments to better understand the course of the oxidation reaction

As is the case for most transformations, the reaction pathway for iron-catalyzed oxidation reactions utilizing peroxide oxidants is still up for debate and the main focus of current research. A plausible mechanistic understanding pertaining to the reaction pathway for iron-catalyzed oxidation reactions utilizing peroxide oxidants is depicted in Scheme 4.2.<sup>10a,47,54</sup> A general consensus has been reached regarding the first step in iron-catalyzed oxidation reaction, which appears to be the peroxide oxidant attacking the  $\text{Fe}^{\text{II}}$  center, further oxidizing it to the  $[\text{Fe}^{\text{III}}\text{-O-O-R}]$  (**4A**) iron-peroxo intermediate which is merely a prelude of the true oxidant.<sup>55</sup> The steps to follow heavily depend on the reaction conditions such as pH<sup>56</sup>, spin state of iron complex<sup>57</sup> and concentration and determine whether **4A** undergoes heterolysis or homolysis. Homolysis typically re-

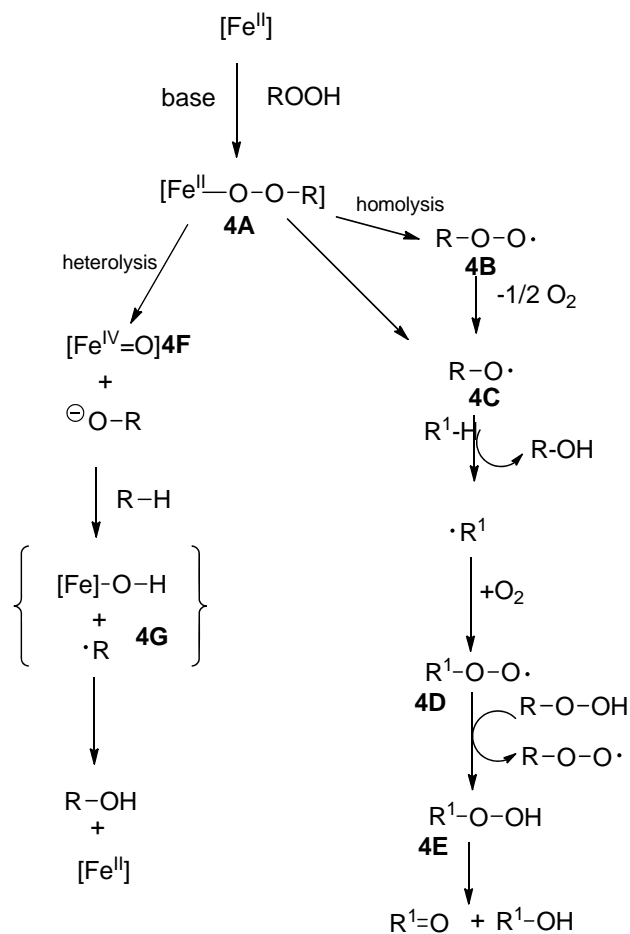
sults in the formation of R-O· and H-O· radicals which can subsequently remove hydrogen atoms from hydrocarbons, resulting in an unselective radical chain oxidation reaction similar to the Haber-Weis mechanism (Scheme 4.3, right-side).<sup>10a</sup> However, in some cases, direct spectroscopic evidence for the formation of the high-valent iron-oxo species,  $[\text{Fe}^{\text{IV}}(\text{O})(\text{tpa})]^{2+}$ , was observed from the homolysis of the transient low spin intermediate,  $[\text{Fe}^{\text{II}}(\text{tpa})(\text{OO}t\text{-Bu})]^{2+}$  (Scheme 4.2).<sup>58</sup> Moreover, the inclusion of lewis bases enhances the yield of this  $\text{Fe}^{\text{IV}}=\text{O}$  species via a “push” effect in the O-O bond homolysis of a non-heme iron-peroxo species.<sup>58</sup> As such, our systems conveniently included pyridine as a component of the solvent mixture, hence, increasing the chances of the formation of this  $\text{Fe}^{\text{IV}}=\text{O}$  metal based oxidant.



**Scheme 4.2.** Formation of  $[\text{Fe}^{\text{III}}(\text{O})(\text{tpa})]^{2+}$  by homolysis of  $[\text{Fe}^{\text{II}}(\text{tpa})(\text{OO}t\text{-Bu})]^{2+}$ .

The oxygen (Scheme 4.3, right side) is included throughout the entirety of the pathway and may come from the atmosphere or iron induced decomposition of the peroxides. Radical **4D** decomposes via a Russel type termination,<sup>59</sup> while peroxide **4E** undergoes an iron induced decomposition<sup>60</sup> and is responsible for the low A/K ratios frequently observed in alkane oxidations. Although radical species **4D** and peroxide **4E** in solution generally yield poor A/K ratios, the oxidation reaction may still occur via an iron-based oxidant as long as the concentrations of the aforesaid species are kept low by slow addition of the oxidant.<sup>10a,47</sup>



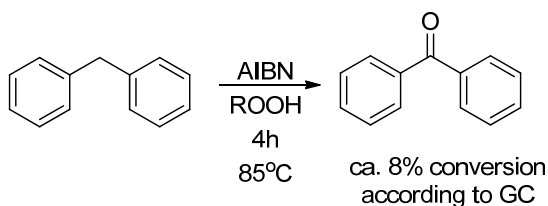


**Scheme 4.3.** Simplified reactivities of iron complexes with ROOH (R = H, *t*-Bu)

The heterolysis of iron-peroxo species **4A** results in a metal based oxidant  $[\text{Fe}^{\text{V}}=\text{O}]$  (**4F**).<sup>49,61</sup> The high valent iron-oxo species **4F** is well known in the field of biomimetic, nonheme iron oxidation chemistry, and it has been spectroscopically,<sup>62</sup> crystallographically<sup>63,64</sup> and computationally<sup>65</sup> characterized. The  $[\text{Fe}^{\text{V}}=\text{O}]$  species can be supported by the donor atoms in the surrounding coordination sphere, ultimately increasing its lifetime long enough to introduce an oxygen atom into the C-H bond proceeding through a “bound-rebound mechanism”<sup>10a</sup> involving intermediate **4G**, where radical intermediate R $\cdot$  presumably does not escape the solvent cage. This route reportedly generates alcohol products and the  $[\text{Fe}^{\text{II}}]$  is recycled back into another catalytic cycle of the oxidation reaction.

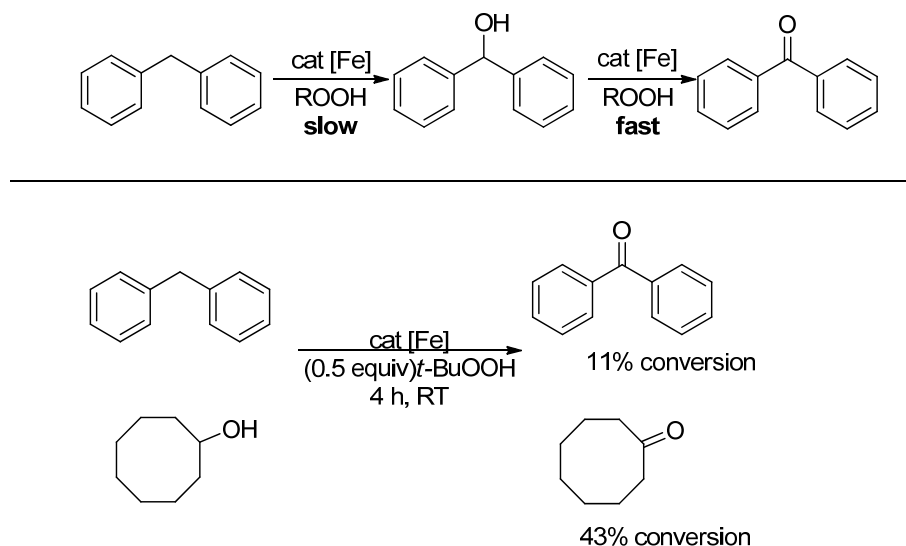
The results shown in Table 4.4 elude to the likelihood of strong radical participation during the catalytic oxidation of cyclohexane using *t*-BuOOH. The results presented in Table 4.4 are consistent with the belief that most iron catalyzed oxidations, applying *t*-BuOOH as the oxidant, follow radical pathways. Overall, the only complex that appeared to proceed through a high valent iron-oxo intermediate **4F** (Scheme 4.2, left side) was complex **4.17** which resulted in an A/K ratio of 6.6. The non-radical pathway associated with complex **4.17** may be due to the N-H feature, which increases in acidity upon coordination, and an iron-oxo intermediate's involvement could be enhanced by lower pH levels.<sup>51</sup> Additionally, the A/K ratio calculated from complex **4.17** does not change when performed in the presence of the well known radical scavenger, 2,4,6-tri-*tert*-butylphenol (TBPH).<sup>66</sup>

It has been postulated that catalytic oxidation reactions employing *t*-BuOOH as the oxidant largely follow a radical mechanism and these radical species are believed to be the result of homolytic cleavage of iron-peroxo intermediates. As such, I was interested to see how replacement of the catalyst with a known radical initiator, azobisisobutyronitrile (AIBN), would affect the outcome of the reaction. This resulted in only 8% of diphenylmethane being converted to benzophenone. The poor conversion may be explained by the absence of the iron catalyst, which may be required in order to form and donate a continual supply of *t*-BuO<sup>•</sup> radicals to ensure progression.



**Scheme 4.4.** Attempted oxidation utilizing a known radical initiator in placement of iron catalyst.

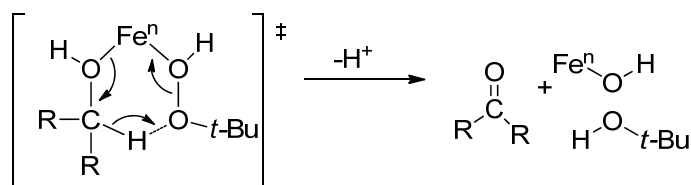
Curiously, the oxidation reactions involving the activated methylene groups (Table 4.5, entries 1 to 5) never yielded alcohols as products, even when an excess of substrate was used. The oxidation of benzylic alcohols, such as  $\alpha$ -methylbenzyl alcohol, proceeded to the ketones using peroxides even in the absence of catalyst.<sup>67</sup> Thus, it may be that the oxidation of activated methylene groups may progress extremely slowly to the alcohols, under the given conditions, which then spontaneously oxidize further to their respective carbonyl compounds (Scheme 4.5). For this reason, A/K ratios could not be calculated using substrates featuring activated methylene groups, making it impossible to expound a feasible mechanism. In order to substantiate the plausibility of alcohols oxidizing faster than hydrocarbons and activated methylene groups, a “competition experiment” where a 1:1 mixture of diphenylmethane:cyclooctanol were oxidized using 0.5 eq of *t*-BuOOH. After 2 hours, by GC analysis of the reaction mixture revealed that 43% of the cyclooctanol was oxidized to cyclooctanone and only 11% of the diphenylmethane was oxidized to benzophenone, providing additional corroboration that secondary alcohols oxidize more rapidly than activated methylene groups. This was true when both complex **4.17** and **4.25** were employed as catalysts (Scheme 4.5). However, the evidence suggesting secondary alcohols are oxidized significantly faster than activated methylene groups conflicts with data presented in Table 4.5 and 4.6, where the corresponding carbonyls from the activated methylene groups were consistently isolated in higher yields, regardless of the catalyst. Hence far, a mechanistic understanding of these oxidation reactions is, at best, unclear.



**Scheme 4.5.** Potential oxidation pathway (top) and a competition experiment between activated methylene group and a secondary alcohol.

After mechanistic investigations pertinent to activated methylene groups ceased, I immediately pontificated about rational mechanistic pathways in which secondary alcohols could be transformed into their expected ketones, as they most likely proceed through a different mechanism than that of the activated methylene groups. Undoubtedly, another noteworthy finding was that the oxidation of primary alcohols was rarely observed under the established reaction conditions and typically involved severely prolonged reaction times and high temperatures. In such context, it seems appropriate that the oxidation of secondary alcohols may include a radical pathway<sup>68</sup> or a six-membered cyclic transition state (Scheme 4.6).<sup>47</sup> Lawrence Que and coworkers reported that in such a transition state, both the peroxide oxidant and the alcohol would first coordinate to the iron center; followed by an intramolecular hydride abstraction from the alcohol by the peroxide (Scheme 4.6). This thermodynamically favored transition state would also account for the differences in reactivity observed during the oxidation of primary versus secondary alcohols, as the electron density at the oxygen of the secondary alcohol is expected to be greater

than that of the electron density at the oxygen of the primary alcohol, in-turn increasing the rate at which the oxygen of the secondary alcohol interacts with the iron center to eventually produce the anticipated ketone. Accordingly, when 5-heptadecanol and 1-hexadecanol were treated with 2.0 eq of *t*-BuOOH under the established reaction conditions, only 5-heptadecanone (61%) was observed after 1 hour.

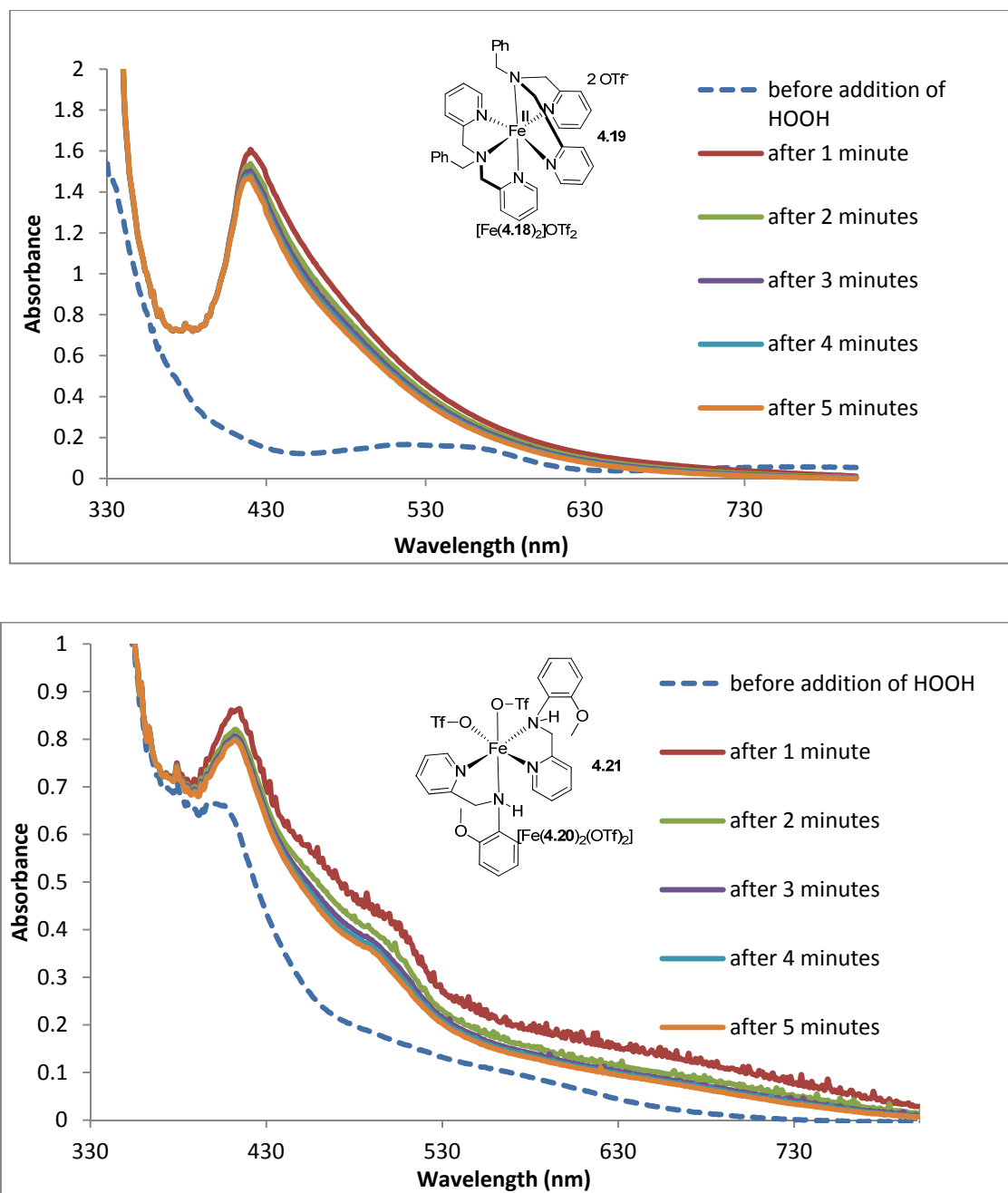


**Scheme 4.6.** Potential cyclic transition state for the oxidation of secondary alcohols.

On the other hand, the reaction may follow another route such as a radical pathway as shown in the homolysis of species **4A** (Scheme 4.3, right-hand side). The fact that only small differences in isolated yields, involving the typical 3 mol% catalyst loading, were observed between all of the different catalysts, regardless of their denticity, structural framework and electronic nature, which may be explained by the involvement of an unselective radical species. The fact that the individuals structural framework or electronic nature has a small impact on the catalytic activity, at the normal loading, implies that the various ligands may not exert any influence on the catalytic activity of their respective iron complexes. On that account, I prepared oxidation reactions, using the standard conditions, where the catalyst was replaced with  $\text{Fe}(\text{OTf})_2$ , the precursor used in metal complex syntheses. Indeed, almost no conversion from diphenylmethane to benzophenone was observed. Even in the case where several of the catalysts were formed *in situ*, by combination of the  $\text{Fe}(\text{OTf})_2$  and corresponding ligand, the result was severely diminished catalytic activity.

However, none of the oxidation reactions, employing any of the catalysts, were inhibited in the presence of a well known radical scavenger. Although, no reactions were shut down by radical scavengers, Vadivelu suggested that iron-catalyzed oxidation reactions proceed through numerous mechanistic pathways concurrently,<sup>28a,69</sup> and it could be possible that the applied radical scavenger only blocks one of them.

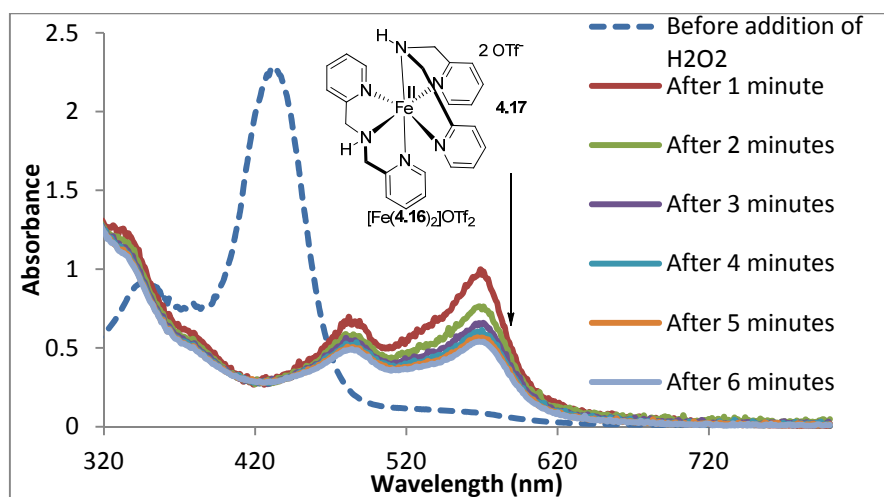
Despite the actual mechanistic pathway for iron-catalyzed oxidation reactions, one widely accepted aspect of these oxidation reactions is that the peroxide oxidant always attacks the iron center first, forming the iron hydroperoxide species  $[\text{Fe}^{\text{III}}\text{-O-O-R}]$  (**4A**). Species **4A** has been observed through the use of UV/Vis spectrophotometry and has been reported to have given a charge transfer band between  $\lambda = 550$  and  $630$  nm.<sup>27,49,55,70,71</sup> In light of my previous experience associated with UV/Vis spectrophotometry, it occurred to me that studying the kinetics for the formation and/or decay of the iron hydroperoxo species **4A** may provide additional insight into the corresponding catalytic activity. Consequently, I monitored the solutions of catalysts in  $\text{CH}_3\text{CN}$ , after treatment with the peroxide oxidant, over time using UV/Vis. Unavailingly, these efforts were unsuccessful as the formation and decay could not be accurately studied over time due to their short lifetime as well as limits associated with the software on the UV/Vis instrumentation. However, in subsequent attempts, when cyclohexane was added to the solutions of catalysts in  $\text{CH}_3\text{CN}$  followed by the addition of oxidant, the dissipation of the new bands was less rapid and as a result could be followed over time using UV/Vis. Henceforth, all subsequent UV/Vis studies involved the following over time of a solution of the complexes, in  $\text{CH}_3\text{CN}$ , that were treated with peroxide oxidant in the presence of cyclohexane.



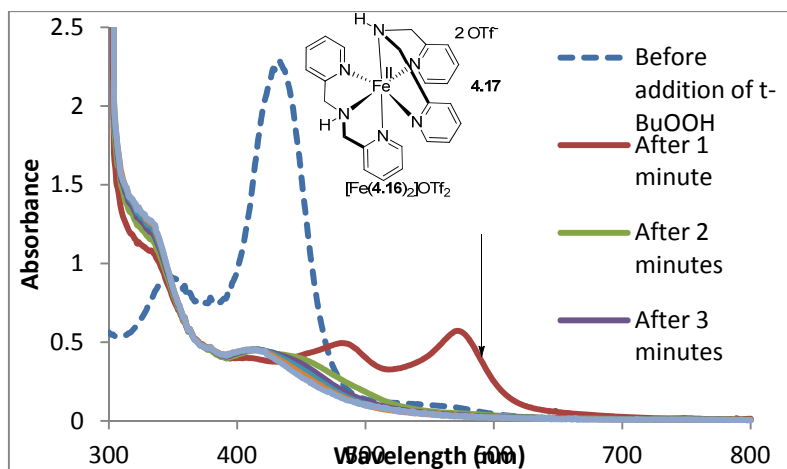
**Figure 4.5.** Time-resolved UV/Visible spectra of complex **4.19** (top) and complex **4.21** (bottom) in  $\text{CH}_3\text{CN}$  after addition of  $\text{H}_2\text{O}_2$  in presence of cyclohexane. Dotted line represents before oxidant addition.

Upon addition of  $\text{H}_2\text{O}_2$  to the benzylated complex **4.19** a new shoulder appeared around  $\lambda = 480$  nm which slowly disappeared over the course of 5 minutes. After the addition of  $\text{H}_2\text{O}_2$  to complex **4.21** a new band at  $\lambda = 424$  nm appeared, with a molar absorption around  $700 \text{ M}^{-1}\text{cm}^{-1}$ ,

which barely changed with time. The calculated values of the absorptivity coefficients of the new bands caused me to classify them as being charge-transfer. The UV/Vis results were nearly identical for complexes **4.19** and **4.21** when *t*-BuOOH was used as an oxidant. As the data suggests, the  $\lambda_{\max}$  of the new bands were lower than what is typically expected for iron-peroxo species, but reports show that complexes of similar type do display charge transfer bands around 450 nm.<sup>16b</sup> Although, the origin of the new bands was initially attributed to the formation of the iron-peroxo species, they could have also formed as a result of structural changes brought on by the oxidative decomposition of the ligands or oxidation of the metal center itself. In lieu of concrete evidence supporting the involvement of an iron-peroxo intermediate, it seems noteworthy that the rapid spectral changes observed instantaneously, after treatment with the oxidant, demonstrate a high degree of reactivity, for both complexes **4.19** and **4.21**, towards the peroxide oxidants.



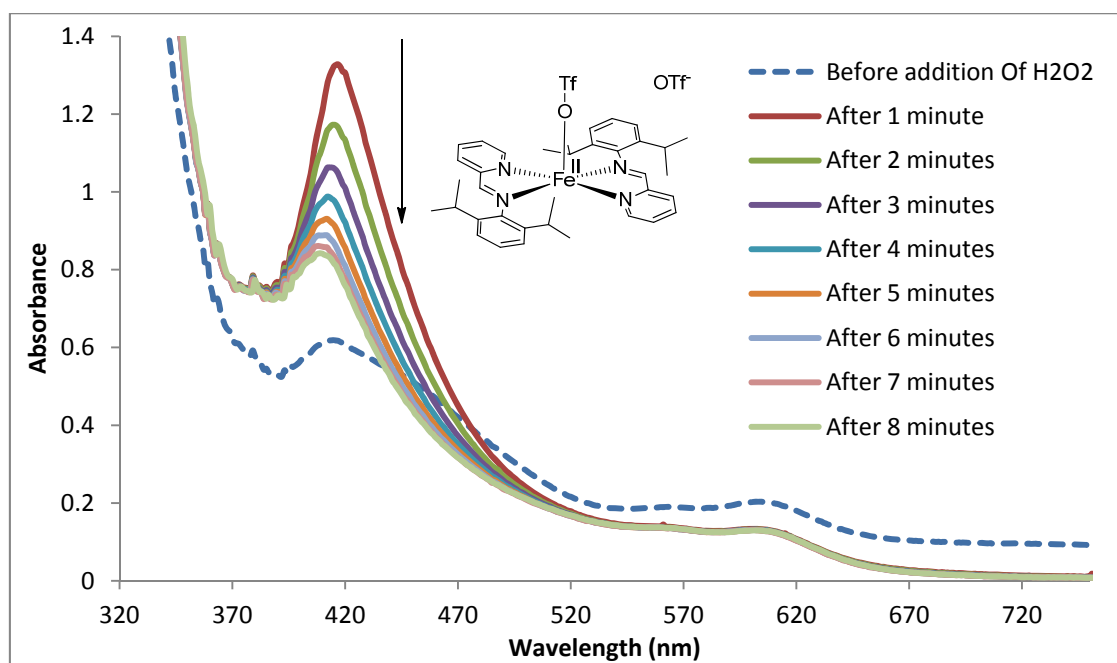




**Figure 4.6.** Time-resolved UV/Visible spectroscopy spectra of complex **4.16** in  $\text{CH}_3\text{CN}$  after addition of  $\text{H}_2\text{O}_2$  (top) and *t*-BuOOH (bottom) in presence of cyclohexane. Dotted lines represents before oxidant addition.

Encouragingly, when a solution of complex **4.16** was studied using UV/Vis, major spectroscopic changes were noticed following the treatment of the solution with  $\text{H}_2\text{O}_2$  and *t*-BuOOH. UV/Vis spectra were recorded before and after the addition of the oxidant in 1 minute intervals. Before the oxidant was added the solution of complex **4.16** appeared to generate an ideal UV/Vis spectrum that contained a picturesque metal-to-ligand charge transfer band (MLCT) at  $\lambda = 434$  nm. Promptly following the addition of the  $\text{H}_2\text{O}_2$  oxidant, the strong charge transfer band at 434 nm disappeared while two new bands at  $\lambda = 490$  and 572 nm appeared. The band at 572 nm falls into line with previous literature reports for the characteristic  $[\text{Fe}^{\text{II}}\text{-O-O-H}]$  iron-peroxo species as does the molar absorptivity value ( $\epsilon = 4000 \text{ M}^{-1} \text{ cm}^{-1}$ ) associated with this band.<sup>27,49,61</sup> Time-resolved UV/Vis spectra was recorded to monitor the decay of this band which showed that the band had consistently and slowly decayed over the period of six minutes and completely disappeared after 15 minutes. In any case, when a solution of complex **4.16** was treated with *t*-BuOOH, the original charge-transfer band did in fact disappear while two new bands at  $\lambda = 490$  and 579 nm appeared. The molar absorptivity coefficient ( $\epsilon$ ) calculated for this band was around

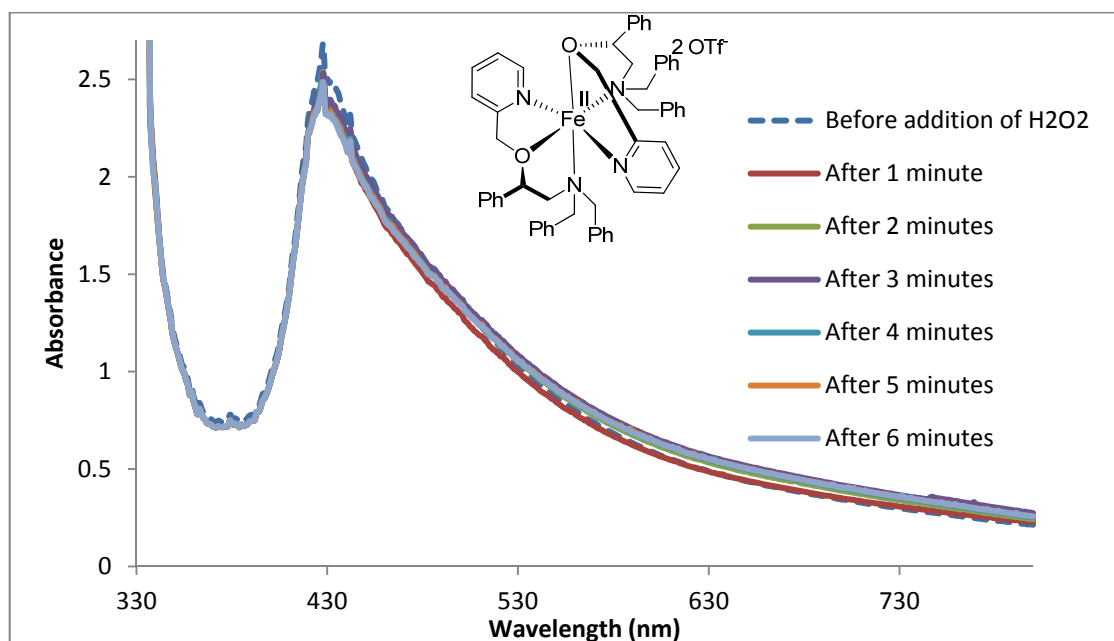
$700 \text{ M}^{-1} \text{ cm}^{-1}$ , which was an order of magnitude less than the value associated with the band formed from the addition of  $\text{H}_2\text{O}_2$ . Nonetheless, the decay of the new band at 579 nm could not be properly followed over time as it had completely depleted after only two minutes. Although, the evidence supports the involvement of an iron-peroxo species, the identities of the new bands around 600 nm could not be unequivocally established. As a result, the new bands around 600 nm could also be due to an evanescent species formed from complex decomposition.



**Figure 4.7.** Time-resolved UV/Visible spectroscopy spectra of complex  $[\text{Fe}^{\text{II}}(\mathbf{4.13})_2(\text{OTf})_2]$  in  $\text{CH}_3\text{CN}$  after addition of  $\text{H}_2\text{O}_2$  in presence of cyclohexane. Dotted lines represents before oxidant addition

I was intrigued by the fact that complex **4.21** behaved so differently from complex **4.17**, as it did not undergo any significant spectral changes (i.e. disappearance of charge transfer band and appearance of the two new bands around 600 nm) upon the addition of the peroxide oxidant. As such, I was interested in determining how the analogous imine complex  $[\text{Fe}^{\text{II}}(\mathbf{4.13})_2(\text{OTf})_2]$  behaved in the presence of the peroxide oxidant. In that event, complex  $[\text{Fe}^{\text{II}}(\mathbf{4.13})_2(\text{OTf})_2]$  was

treated with  $\text{H}_2\text{O}_2$  and followed over time. Directly after the addition of the oxidant, the existing charge-transfer band grew rapidly in intensity, which soon thereafter, slowly decayed over the course of ten minutes. Indubitably, the change in intensity of the charge-transfer band could be, in part, the result of the drastic increase in polarity from the addition of the aqueous peroxide solution. On the contrary, when complexes **4.17**, **4.19** and **4.21** were treated with the same polar aqueous peroxide solutions, no noticeable change in the intensity of the charge-transfer band was observed, let alone a drastic increase as seen with complex  $[\text{Fe}^{\text{II}}(\mathbf{4.13})_2(\text{OTf})_2]$ . More significantly, the charge transfer band for complex  $[\text{Fe}^{\text{II}}(\mathbf{4.13})_2(\text{OTf})_2]$  took 10 minutes to disappear, whereas the corresponding band in complex **4.17** seemed to disappear immediately after treatment with the oxidant. Albeit, these changes appear noteworthy, the slow decay of the charge-transfer band for complex  $[\text{Fe}^{\text{II}}(\mathbf{4.13})_2(\text{OTf})_2]$  may also be due to a slower complex decomposition, as the imine based ligand, **4.13**, is less susceptible to oxidative degradation than their amine based counterparts.



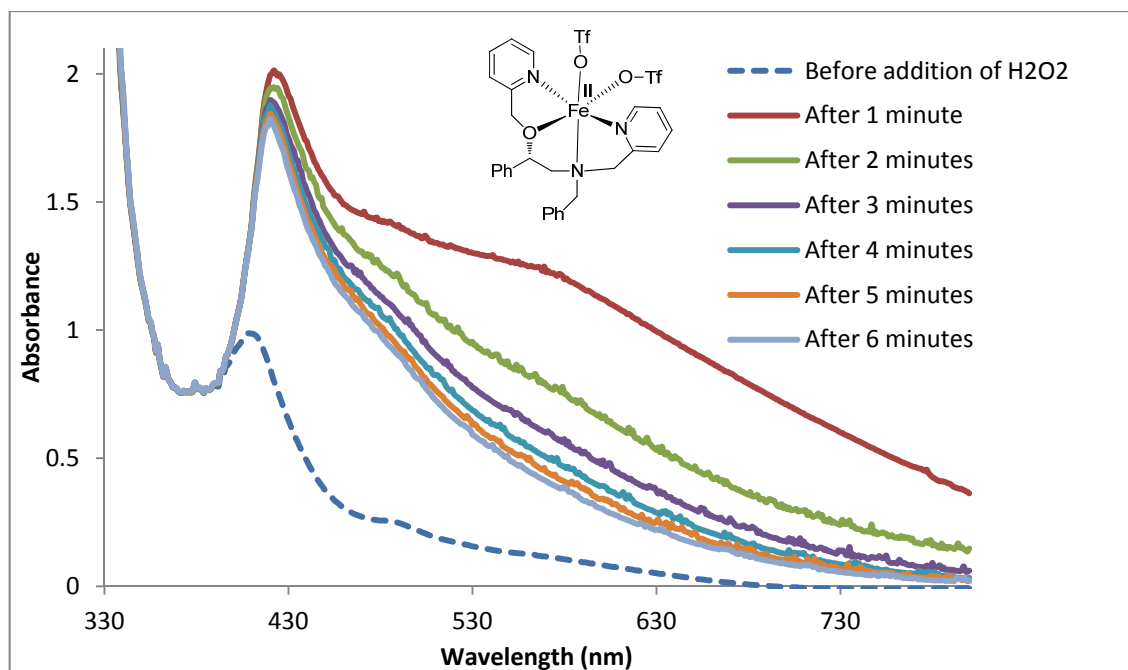


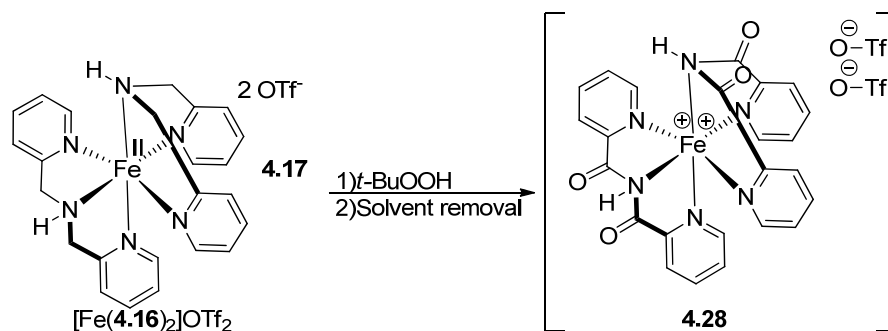
**Figure 4.8.** Time resolved UV-vis spectra of complexes **4.23** (top) and **4.25** (bottom) in  $\text{CH}_3\text{CN}$  after addition of  $\text{H}_2\text{O}_2$  in presence of cyclohexane. Dotted line represents before oxidant was added.

The top UV spectrum in Figure 4.8 illustrates that complex **4.23** reacts very little towards the peroxide oxidant and as a result, minimal spectroscopic changes in absorbance were observed. On the other hand, when complex **4.25** was treated with the oxidant, a new widened band appeared at 580 nm which subsequently disappeared over the course of several minutes. Thus, it appears that with complex **4.25**, a short lived species formed after addition of the oxidant, whereas complex **4.23** remained unchanged. The band at 580 nm could reflect the presence of an iron hydroperoxo species, but these species are usually only observed at lower temperatures, where the lifetimes are expected to be longer.<sup>58</sup> These data are consistent with the fact that complex **4.23** has no sites available for attack by peroxide, thus no iron hydroperoxo species is expected. And complex **4.25**, having two sites only loosely occupied by weakly coordinating triflate counterions, explains the rapid spectroscopic changes observed after addition of the oxidant. However, the two complexes show comparable activity as catalysts in oxidation reactions.

Hence, based on the activities and UV-vis spectra for both complexes, it cannot be determined whether or not they operate by the same mechanistic pathway.

#### 4.3.5 Ligand decomposition pathways and their impact on the catalytic activity

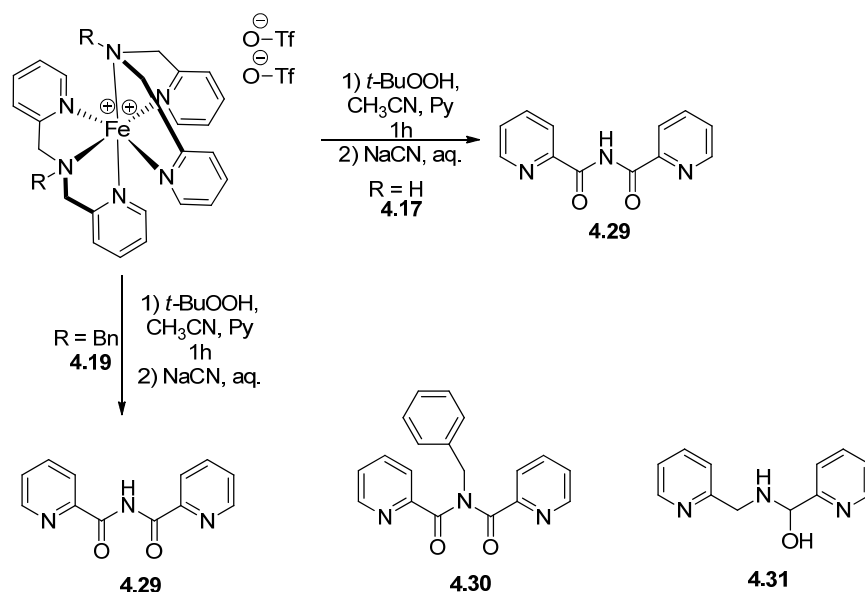
As revealed from previous investigations, our research laboratory has clearly demonstrated that at a reduced catalyst loading the structural framework of a ligand can have an influence on the catalytic performance of their respective metal complexes.<sup>57</sup> Another current topic of debate is the degree of impact that oxidative ligand degradation has on catalytic activity.<sup>57</sup> While some reports suggest that oxidative ligand decomposition under reaction conditions can impair the catalytic activity, others claim the exact opposite.<sup>72,73</sup> Thus, I was interested in establishing the extent to which oxidative ligand decomposition, under the established reaction conditions, occurred in my own ligand systems and the impact these changes had on their respective catalytic activity.



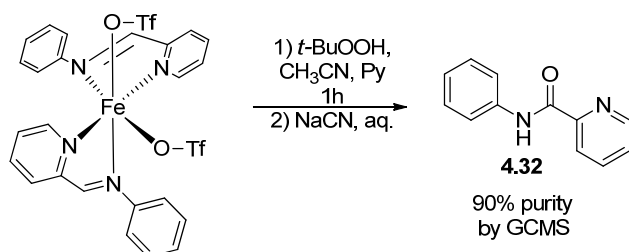
**Scheme 4.7.** Experiment to determine the effect of the catalytic, oxidative conditions on the catalyst composition.

Therefore, I treated a solution containing only complex **4.17** with *t*-BuOOH but without substrate using otherwise the established reaction conditions outlined in Table 4.5. The result of exposing **4.17** to the established oxidation conditions was a convoluted and inseparable mixture of

decomposition products that could not be spectroscopically identified [although a species bearing two oxidized ligands **4.16** was identified by MS], presumably owing to the complexity of the mixture (Scheme 4.7). Subsequently, this mixture will be referred to as **4.28**. I realized that the only way to identify the extent of oxidative damage of the ligands was to displace them from the metal center and spectroscopically analyze them. Therefore, a solution of complex **4.17** was treated with *t*-BuOOH in the absence of a substrate. Next, an aqueous solution of NaCN was added to the reaction mixture to displace the ligand or the oxidation decomposition products. These products were subsequently extracted and analyzed using GC/MS, NMR spectroscopy and IR. Complexes **4.15**, **4.19**, **4.2** and  $[\text{Fe}^{\text{II}}(\text{tpa})(\text{OTf})_2]$  were treated and extracted in a similar fashion and analyzed via GC/MS. The identified products are exhibited in Scheme 4.8 and the recovered mass for all ligand displacements was nearly 90%, hence, minimum amounts of the ligands were lost during the work-up.



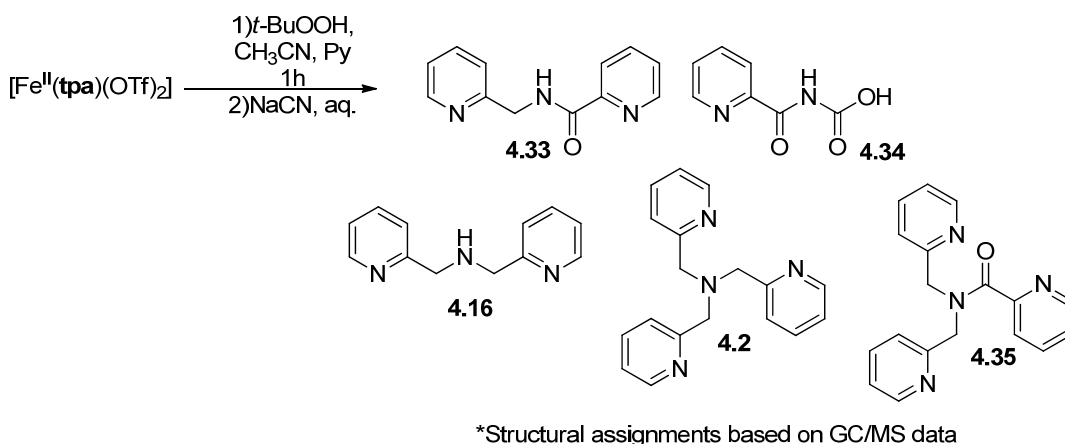
\*Additional decomposition products detected. Structural assignments are based on GC/MS



**Scheme 4.8.** Experiments to determine ligand-decomposition products under catalytic, oxidative conditions.

The ligands that were displaced from complex **4.17** provided spectroscopic evidence that both ligands were completely oxidized to only the corresponding diamide, **4.29**. The ligands displaced from the benzylated complex, **4.19**, were analyzed as being a complex mixture of oxidatively damaged ligands, where only three of the major products are shown in Scheme 4.8. Analysis of the complex mixture displaced from **4.19** suggested the presence of the diamide ligand **4.29** accompanied by **4.30** and **4.31**; the benzyl and picolyl units undergo oxidative cleavage, following the oxidation of the CH<sub>2</sub> units, which has been reported previously for copper complexes featuring structurally similar ligands.<sup>74</sup> Even after displacement of the ligands from com-

plex  $[\text{Fe}^{\text{II}}(\mathbf{4.11})_2(\text{OTf})_2]$ , it appeared that the imine ligand was oxidized to the corresponding amide, **4.32**. Displacement of the ligand from complex  $[\text{Fe}^{\text{II}}(\mathbf{tpa})(\text{OTf})_2]$  yielded another complex mixture of partially oxidized fragments, including the original and unscathed **tpa** ligand (Scheme 4.9).

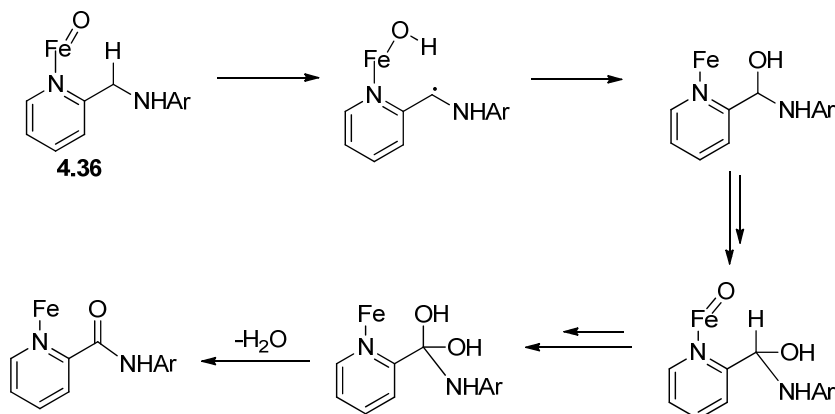


**Scheme 4.9.** Experiments to determine ligand-decomposition products under oxidative conditions.

A potential explanation for how the ligands are oxidized to the corresponding amides would be through an intramolecular oxygen transfer from an  $\text{Fe}=\text{O}$  species **4.36** (Scheme 4.9). This pathway was previously described using an intramolecular aryl hydroxylation reaction involving the iron complex  $[\text{Fe}^{\text{II}}(\mathbf{L})(\text{CH}_3\text{CN})_2](\text{ClO}_4)_2$  ( $\mathbf{L}$  = modified **tpa**).<sup>75</sup> Both iron<sup>76</sup> and copper<sup>77</sup> complexes bearing diamide ligands are known in which the diamide is coordinated to the metal center. Complexes of this type do still have the ability to catalytically activate  $\text{H}_2\text{O}_2$ ,<sup>78</sup> increasing the probability that the oxidized ligands were still coordinated to the iron center even after they had been oxidized to their respective amides. All evidence suggests that the ligands were in fact oxidized while tethered to the iron center. To further support this claim, complex **4.17** was treated identically to other ligand displacement conditions, except *t*-BuOOH was not added. Analysis of



the recovered reaction material after displacement revealed only unoxidized ligand **4.16**. Thus, it seems unlikely that the ligands were oxidized during the work-up process.



**Scheme 4.9.** Potential pathway for the oxidation of the NCH<sub>2</sub> units.

Once I had established the extent of oxidative damage of the ligands, I was interested in studying how the oxidation of the ligands effected the catalytic activity and selectivity. Consequently, I employed material **4.28** (Scheme 4.7) in the oxidation of diphenylmethane using identical conditions to those outlined in Table 4.5. Unexpectedly, the catalytic activity of **4.28** behaves similarly to that of the unoxidized **4.17**. ( $k_{\text{obs}} = 0.11$  and  $0.19$ , respectively). Unfortunately, no spectroscopic or structural information was acquired for material **4.28**, making a direct comparison of observed rate constants unreliable. Finally, the selectivity of **4.28** was studied through the oxidation of cyclohexane and subsequent determination of an A/K ratio. The A/K ratio decreased from 6.6 for unoxidized **4.17** to 3.0, indicating that some of the selectivity was lost after oxidation. However, a direct comparison could not be made as the exact composition for material **4.28** could not be established. Hence, it seems appropriate to suggest that the oxidative conditions do, in fact, diminish the selectivity of the complex but have no substantial impact on the catalytic activity.

## 4.4 Discussion

The investigations reported herein clearly demonstrate that iron complexes **4.17** and **4.19** featuring two tridentate  $\alpha$ -aminopyridine ligands should be considered another effective group of iron catalysts capable of oxidizing activated methylene groups and secondary alcohols, under mild conditions, to the anticipated carbonyl compounds. Although both of these complexes contain two tridentate ligands, they still exhibited increased catalytic activity and selectivity relative to all other complexes studied. The fact that complex **4.17** alone gave such promising results gave rise to an appealing future for additional studies and optimization efforts.

The fact that the two complexes which exhibited the highest catalytic activity feature two tridentate ligands in the coordination sphere appears to be counterintuitive, as one would expect complexes of this type to have reduced activity due to the lack of any open coordination sites. Typically, the biomimetic, nonheme iron catalysts known to date feature one tetradentate or pentadentate ligand bearing nitrogen or oxygen donor atoms. Surprisingly, complexes **4.17** and **4.19** display catalytic activity that is even slightly better than complex  $[\text{Fe}^{\text{II}}(\text{tpa})(\text{OTf})_2]$  in the oxidation of activated methylene groups (Figure 4.4). Assuming that **4.17** does proceed through an iron-peroxo intermediate  $[\text{Fe}^{\text{III}}\text{-OOR}]$ , this suggests that complex **4.17** must disassociate one of the donor atoms, pyridyl pendant arm, of the tridentate ligand in order to make an open coordination site available for initial peroxo formation. Another plausible pathway for electronically saturated complexes such as **4.17** is to proceed through an outer-sphere electron-transfer mechanism,<sup>79</sup> which would imply that the significant spectroscopic changes observed in the UV/Vis of Figure 4.6 is merely the result of oxidative decomposition of ligands over time or the oxidation from iron(II) to iron(III).

A comparison of observed rate constants after the kinetic studies presented the possibility that the catalyst's reactivity may be influenced by the denticity of the ligands, as suggested by the lower catalytic activities of complex **4.21**, bearing two bidentate  $\alpha$ -aminopyridine ligands, and complex **4.15**, bearing two bidentate imine ligands. In every instance, the complexes bearing tri- and tetradentate ligands consistently exhibited better catalytic performance than those with bidentate ligands.

Another noteworthy finding was the fact that the oxidized material **4.22** performed just as well in the kinetic studies, illustrated in Figure 4.4, as the other complexes. Moreover, the spectroscopic evidence obtained from the ligand decomposition and displacement studies revealed that the  $\text{NCH}_2$  units of the ligands become oxidized to the corresponding amides, as reported previously for similar complexes that have been structurally characterized.<sup>80</sup> Literature reports suggest that, even after the exposure to the oxidizing conditions, the resulting amides remain as their original denticity. Thus, they may also exist in their original coordination mode<sup>68,69</sup> which appears to be the main reason for their ability to preserve the catalytic activity. It has been previously established that manganese complexes bearing pyridyl based ligands always experience oxidation of their ligands to pyridyl-2-carboxylic acid derivatives before exhibiting any observable catalytic oxidation products.<sup>64</sup> As evidenced by the kinetics displayed in Figure 4.4, there is no induction period observed with our systems. Under the circumstances, I was unable to determine whether or not ligand oxidation was an essential requirement in order to initiate any sort of catalytic activity, but I was able to confirm that ligand oxidation does not inhibit catalytic activity.

## 4.5 Summary and prospective

Overall, I have synthesized and spectroscopically characterized a series of complexes of the general formula  $[\text{Fe}^{\text{II}}(\text{L}_n)]\text{OTf}_2$  ( $n = 2,3,4,5$ ) featuring bi- and tridentate  $\alpha$ -aminopyridine and tri-, tetra- and pentadentate *N*-, *O*- coordinating ligands  $\text{L}_n$  where  $n$  is the number of donor atoms. Two of these complexes were structurally characterized via single X-Ray diffraction. All of the new complexes exhibited catalytic activity in the oxidation of activated methylene groups and secondary alcohols to the corresponding carbonyl compounds (3 mol% catalyst, 3-4 equivalents ROOH, RT, 4-8 h, 28 to 90% isolated yield). Kinetic studies were performed on the complexes synthesized herein as well as previously synthesized complexes  $[\text{Fe}^{\text{II}}(\text{tpa})(\text{OTf})_2]$  and  $[\text{Fe}^{\text{II}}(\mathbf{4.11})_2(\text{OTf})_2]$  in order to determine and compare the relative catalytic activities.

It was determined that the denticity of the ligands does in fact influence the catalytic activity, as the complexes bearing tetra- and tridentate ligands displayed higher  $k_{\text{obs}}$  than the complexes bearing bidentate ligands. Under the given catalytic conditions, it was established that the ligands undergo oxidative decomposition. The decomposition products were identified as being the result of oxidizing the  $\text{NCH}_2$  unit to the corresponding amide  $\text{NC}=\text{O}$ . It is believed that the oxidative degradation of the ligands does not impact the original denticity and the ligand remains coordinated to the metal center. Even after complex **4.17** was subjected to oxidative, catalytic conditions, its catalytic activity closely resembled that of its unoxidized predecessor.

The results reported herein supplement the existing knowledge surrounding nonheme iron-catalyzed oxidation reactions utilizing peroxides as the terminal oxidant. The expansion on this knowledge is, at the very least, an attractive starting point for the development of an even more efficient and environmentally benign catalyst system, which is becoming more important in these times of heightened environmental awareness. More specifically, bearing the knowledge of pos-

sible oxidative decomposition pathways of the ligand as well as the denticity contribution, one could utilize this as a tool to aid in the future development of an entirely new series of amide based ligands that may be subsequently employed for the synthesis of catalytically active iron complexes.

## 4.6 Experimental

Chemicals were treated as follows: toluene and diethyl ether distilled from Na/benzophenone; CH<sub>2</sub>Cl<sub>2</sub>, MeOH, and CH<sub>3</sub>CN distilled from CaH<sub>2</sub>. CHCl<sub>3</sub>, silica, pyridine, tri(2-picolyl)amine (tpa, **4.2**), bis(2-picolyl)amine (**4.16**, all Aldrich), and other materials were used as received. Ligand **4.18** and [Fe(OTf)<sub>2</sub>]<sup>81</sup> were prepared according to the literature. Complexes **4.23**, **4.25** and **4.27** were all prepared previously in our laboratory according to modified literature procedures.<sup>82</sup> All reactions were carried out under nitrogen and by employing standard Schlenk techniques, and workups were carried out in the air.

NMR spectra were obtained at room temperature on a Bruker Avance 300 MHz or a Varian Unity Plus 300 MHz instrument at room temperature and were referenced to a residual solvent signal; all assignments are tentative. GC-MS spectra were recorded on a Hewlett Packard GC-MS System Model 5988A. UV/Visible spectra were recorded on Varian Cary 50 Bio spectrophotometer. Exact masses were obtained on a JEOL MStation [JMS-700] mass spectrometer. IR spectra were recorded on a Thermo Nicolet 360 FTIR spectrometer. Elemental analyses were performed by Atlantic Microlab Inc., Norcross, GA, USA. Magnetic moments, <sup>19</sup>F NMR spectra, and UV/Visible data are listed in Table 1.

Synthesis

Ligand **4.20** : 2-Pyridine carboxaldehyde (1.0 g, 9.34 mmol) was dissolved in methanol (10 mL), cooled with an ice bath, while 2-methoxyaniline (1.16 g, 9.43 mmol) in methanol (10 mL) was added dropwise. The ice bath was then removed, allowing the reaction to stir for 1 h at room temperature. Then NaBH<sub>4</sub> (0.741 g, 19.61 mmol) was added in 3 portions at 0 °C. The reaction mixture was then allowed to stir overnight at room temperature. After 12 h, aqueous HCl solution (5m) was added until a pH of 4 was reached. The reaction mixture was then allowed to stir at room temperature for an additional hour. Then aqueous NaOH (2m) solution was added until a pH of 12 was reached. Then CH<sub>2</sub>Cl<sub>2</sub> (30 mL) was added and the two layers were transferred to a separating funnel. The organic phase was collected and the product was extracted from the aqueous layer, using CH<sub>2</sub>Cl<sub>2</sub> (2x30 mL). The combined organic layers were dried over sodium sulfate and the solvent was removed under vacuum to yield a yellow oil that was subsequently purified by means of column chromatography (CH<sub>2</sub>Cl<sub>2</sub>/Et<sub>3</sub>N 90:10 as eluent) to give ligand **4.20** as a red oil (1.87 g, 8.73 mmol, 94%). <sup>1</sup>H NMR (300 MHz, CDCl<sub>3</sub>, 25°C, TMS): δ = 8.55 (d, J<sub>H,H</sub> = 2.9 Hz, 1H; pyrid-yl-H), 7.53 (t, J<sub>H,H</sub> = 6.7 Hz, 1H; pyridyl-H), 7.28 (d, J<sub>H,H</sub> = 7.2 Hz, 1H; pyridyl-H), 7.10 (d, J<sub>H,H</sub> = 7.2 Hz, 1H; pyridyl-H), 6.82–6.75 (m, 2H; Ar-H), 6.67–6.62 (m, 1H; Ar-H), 6.51 (d, J<sub>H,H</sub> = 7.6 Hz, 1H; Ar-H), 5.19 (s, 1H; NH), 4.45 (s, 2H; CH<sub>2</sub>), 3.82 ppm (s, 3H; OCH<sub>3</sub>); <sup>13</sup>C {<sup>1</sup>H} NMR (300 MHz, CDCl<sub>3</sub>, 25°C, TMS): b = 159.5 (s; aromatic), 149.6 (s; aromatic), 147.4 (s; aromatic), 138.2 (s; aromatic), 137.1 (aromatic), 122.4 (s; aromatic), 121.8 (s; aromatic), 117.2 (s; aromatic), 110.6 (s; aromatic). 109.9 (s; aromatic), 55.8 (s; NCH<sub>2</sub>), 49.6 ppm (s; OCH<sub>3</sub>); IR (neat oil): ν = 3391 cm<sup>-1</sup> (m, NH); MS (FAB): m/z (%): 214 (100) [**4.20**<sup>+</sup>].

[Fe(**4.16**)<sub>2</sub>]OTf<sub>2</sub>: CH<sub>3</sub>CN (3 mL) was added to a Schlenk flask containing [Fe(OTf)<sub>2</sub>] (0.211 g, 0.483 mmol). Ligand **4.16** (0.192 g, 0.967 mmol) was added to the resulting yellow transparent solution and the resulting red solution was allowed to stir for 30 min at room temperature.

This mixture was then concentrated to about 1 mL, cooled down to 0°C, layered with diethyl ether (10 mL), and stored at -18°C overnight to yield a red crystalline precipitate. The supernatant was decanted and the precipitate was dried under high vacuum to give [Fe(**4.16**)<sub>2</sub>]OTf<sub>2</sub> as red crystals (0.351 g, 0.466 mmol, 96%). <sup>1</sup>H NMR (300 MHz, CD<sub>3</sub>CN, 25°C, TMS): δ =9.12 (brs, 4H; pyridyl-H), 7.97 (brs, 2H; pyridyl-H), 7.82 (t, *J*<sub>HH</sub> =7.2 Hz, 8H; pyridyl-H), 7.64 (brs, 2H; pyridyl-H), 5.95 (s, 2H; NH), 5.36–5.25 ppm (m, 8H; 4CH<sub>2</sub>); <sup>1</sup>H NMR (300 MHz, D<sub>6</sub> acetone, -50°C, TMS): b=9.11 (d, <sup>2</sup>*J*<sub>H,H</sub> =5.0 Hz, 2H; NCH pyridyl), 8.29 (d, <sup>2</sup>*J*<sub>H,H</sub> =5.0 Hz, 2H; NCH, pyridyl), 7.93 (t, <sup>3</sup>*J*<sub>H,H</sub> =7.3 Hz, 2H; pyridyl), 7.79 (t, <sup>3</sup>*J*<sub>H,H</sub> =7.3 Hz, 2H; pyridyl), 7.71 (d, <sup>2</sup>*J*<sub>H,H</sub> =7.4 Hz, 4H; pyridyl), 7.29 (t, <sup>3</sup>*J*<sub>H,H</sub> =6.0 Hz, 2H; pyridyl), 6.05 (s, 2H; NH), 5.19 (dd, <sup>2</sup>*J*<sub>H,H</sub> =8.4 Hz, 2H; NCHH'), 4.44 (d, <sup>2</sup>*J*<sub>H,H</sub> =16.5 Hz, 2H; NCHH'), 4.35 (d, <sup>2</sup>*J*<sub>H,H</sub> =18.5 Hz, 2H; NCHH'), 4.27 ppm (d, <sup>2</sup>*J*<sub>H,H</sub> =11.5 Hz, 2H; NCHH'); <sup>13</sup>C {<sup>1</sup>H} NMR (75 MHz, D<sub>6</sub> acetone, 25°C, TMS): b=164.4 (pyridyl), 156.0 (pyridyl), 137.8 (pyridyl), 128.5 (pyridyl), 124.3 (pyridyl), 59.0 ppm (CH<sub>2</sub>); IR (neat solid): ν =3245 (m, N-H), 1254 (s, OTf), 1162 (sh, OTf), 1028 cm<sup>-1</sup> (sh, OTf); MS (FAB): m/z (%): 603 (30) [Fe(**4.16**)<sub>2</sub>OTf<sup>+</sup>], 404 (100) [Fe(**4.16**)OTf<sup>+</sup>], 255 (20) [Fe(**4.16**)<sup>+</sup>]; HRMS: m/z calcd for C<sub>25</sub>H<sub>26</sub>F<sub>3</sub><sup>56</sup>FeN<sub>6</sub>O<sub>3</sub>S: 603.10883; found: 603.1091 (corresponds to [Fe(**4.16**)<sub>2</sub>(OTf)<sup>+</sup>]); elemental analysis calcd (%) for C<sub>26</sub>H<sub>26</sub>F<sub>6</sub>FeN<sub>6</sub>O<sub>6</sub>S<sub>2</sub>: C: 41.50, H: 3.48, found: C: 41.64, H: 3.49.

[Fe(**4.18**)<sub>2</sub>]OTf<sub>2</sub>: CH<sub>3</sub>CN (2 mL) was added to a Schlenk flask containing benzylbis(2-picolyl)amine (**4.18**, 0.082 g, 0.283 mmol). Subsequently, [Fe(OTf)<sub>2</sub>] (0.062 g, 0.141 mmol) was added to the red-orange solution. The red-orange solution was then heated at 60°C for 1 h. The resulting solution was cooled down to 0°C and layered with diethyl ether (8 mL) and stored at -18°C overnight to yield a red-tan precipitate. The supernatant was decanted and the resulting solid was washed with cold diethyl ether (3x5 mL) and dried under high vacuum to give the product

[Fe(**4.18**)<sub>2</sub>](OTf)<sub>2</sub> as a red-tan solid (0.119 g, 0.128 mmol, 90%). <sup>1</sup>H NMR (300 MHz, CD<sub>3</sub>CN, 25°C, TMS): δ=111.6 (brs, 2H; pyridyl-H), 75.9 (brs, 2H; pyridyl-H), 64.6 (brs, 2H; pyridyl-H), 58.0 (brs, 2H; pyridyl-H), 44.5 (brs, 2H; pyridyl-H), 42.5 (brs, 2H; pyridyl-H), 41.3 (brs, 2H; pyridyl-H), 15.4 (s, 3H), 13.7 (s, 3H), 8.36 (brs, 2H), 7.36 (brs, 4H), 6.20 (brs, 2H), 4.81–4.17 (m, 4H), 3.39 (s, 1H), 1.99 (s, 1H), -10.2 (s, 1H; pyridyl-H), -16.4 (s, 1H; pyridyl-H), -19.0 ppm (s, 2H; pyridyl-H); IR (neat solid) ν =1251 (s, OTf), 1152 (m, OTf), 1028 cm<sup>-1</sup> (s-sh, OTf); MS (FAB): m/z (%): 783 (30) [Fe(**4.18**)<sub>2</sub>(OTf)]<sup>+</sup>, 494 (100) [Fe(**4.18**)(OTf)]<sup>+</sup>; HRMS: m/z calcd for C<sub>39</sub>H<sub>38</sub>F<sub>3</sub><sup>56</sup>FeN<sub>6</sub>O<sub>3</sub>S: 783.20270; found: 783.2018 (corresponds to [Fe(**4.18**)<sub>2</sub>(OTf)]<sup>+</sup>); elemental analysis calcd (%) for C<sub>40</sub>H<sub>38</sub>F<sub>6</sub>FeN<sub>6</sub>O<sub>6</sub>S<sub>2</sub>: C: 51.51, H: 4.11; found: C: 50.68, H: 4.07.

[Fe(**4.20**)<sub>2</sub>(OTf)<sub>2</sub>]: CH<sub>3</sub>CN (3 mL) was added to a Schlenk flask containing [Fe(OTf)<sub>2</sub>] (0.265 g, 0.607 mmol). Ligand **4.20** (0.260 g, 1.22 mmol) was added to the yellow transparent solution and the resulting red-purple solution was allowed to stir for 1.5 h at room temperature. This mixture was then concentrated to about 1.5 mL, cooled down to 0°C, layered with diethyl ether (10 mL), and stored at -18°C overnight to yield a purple crystalline precipitate. The supernatant was decanted and the precipitate was dried under high vacuum to give [Fe(**4.20**)<sub>2</sub>(OTf)<sub>2</sub>] as purple crystals (0.443 g, 0.566 mmol, 93%). <sup>1</sup>H NMR (300 MHz, CD<sub>3</sub>CN, 25°C, TMS): δ=53.9 (brs, 2H; pyridyl-H), 45.3 (brs, 2H; pyridyl-H), 11.9 (brs, 2H; pyridyl-H), 6.6–4.4 (brs, ca. 18H), -20.8 ppm (s, 2H; pyridyl-H); IR (neat solid): ν =3268 (w, N-H), 1239 (s, OTf), 1157 (m, OTf), 1024 cm<sup>-1</sup> (s, sh, OTf); MS (FAB): m/z (%): 633 (30) [Fe(**4.20**)<sub>2</sub>(OTf)]<sup>+</sup>, 419 (100) [Fe(**4.20**)(OTf)]<sup>+</sup>; HRMS: m/z calcd for C<sub>27</sub>H<sub>28</sub>F<sub>3</sub><sup>56</sup>FeN<sub>4</sub>O<sub>5</sub>S: 633.10809; found: 633.1081 (corresponds to [Fe(**4.20**)<sub>2</sub>(OTf)]<sup>+</sup>); elemental analysis calcd (%) for C<sub>28</sub>H<sub>28</sub>F<sub>6</sub>FeN<sub>4</sub>O<sub>8</sub>S<sub>2</sub>: C: 42.98, H: 3.61; found: C: 42.57, H: 3.74.

#### 4.6.1 Typical experiment to determine the alcohol / ketone ratios in Table 4.4.



To a vial containing  $[\text{Fe}(\mathbf{4.16})_2]\text{OTf}_2$  (0.004 g, 0.005 mmol),  $\text{CH}_3\text{CN}$  (4.0 mL) was added. The mixture was allowed to stir at room temperature for several minutes and subsequently cyclohexane (0.460 g, 5.47 mmol) was added and stirred until the reaction mixture became homogeneous. A syringe pump was filled with  $\text{CH}_3\text{CN}$  (0.6 mL) and aqueous hydrogen peroxide (0.006 g, 30 % wt in  $\text{H}_2\text{O}$ , 0.054 mmol). The hydrogen peroxide solution (90 mM) was added to the substrate/catalyst mixture dropwise over the course of 25 minutes at room temperature with constant stirring. After an additional 15 minutes of stirring at room temperature, approximately 0.5 mL of the reaction mixture was filtered through a short pad of silica gel, and GC chromatograms were recorded.

#### 4.6.2 Experimental Procedure to determine the activities in Figure 4.4.

Complex  $[\text{Fe}^{\text{II}}(\mathbf{4.16})_2]\text{OTf}_2$  (0.001g, 0.0013 mmol) and diphenylmethane (0.103 g, 0.61 mmol) were dissolved in 1:1  $\text{CH}_3\text{CN}$  : pyridine (2 mL), and *t*-BuOOH (0.304 g, 70 wt% in  $\text{H}_2\text{O}$ , 2.36 mmol) was added in one portion at room temperature. A sample (0.3mL) was taken first after 5 min., then in time intervals of 30 min. Samples were immediately quenched with  $\text{PPh}_3$  (0.15 g, 0.57 mmol), filtered through a short pad of silica gel, rinsed with  $\text{CH}_2\text{Cl}_2$  (3 mL), and analyzed by GC. The other complexes were analyzed under strictly identical conditions. Each experiment was performed at least twice and no significant differences were observed.

#### 4.6.3 Experimental procedure to determine activities in Figure 4.5

The substrate diphenylmethane (0.100 g, 0.601 mmol) and the catalyst **4.23** (0.035 g, 0.018 mmol) were dissolved in acetone (2.0 mL). The oxidant *t*-BuOOH (0.344 mL, 70 wt% in  $\text{H}_2\text{O}$ , 2.4 mmol) was added dropwise and the dark purple solution was stirred for 5 minutes. Then 0.1 mL of reaction mixture was removed, filtered through a pipette filter containing 0.5 cm silica and

a cotton plug, and flushed with  $\text{CH}_2\text{Cl}_2$  (1 mL). The sample was analyzed by GC and additional 0.1 mL fractions were analyzed similarly in 30 minute intervals. The two other complexes **4.25** and **4.27** were analyzed similarly.

*4.6.4 Experimental procedure to record time-resolved UV-vis spectra of the metal complexes after addition of the oxidant (Figures 4.5, 4.6, 4.7 and 4.8)*

A  $0.30 \text{ mmol L}^{-1}$  solution of complex  $[\text{Fe}^{\text{II}}(\mathbf{4.16})_2]\text{OTf}_2$  in  $\text{CH}_3\text{CN}$  was prepared. After addition of cyclohexane (0.0078 g, 0.926 mmol), a UV-vis spectrum was recorded. To this solution (containing  $0.115 \times 10^{-3} \text{ mmol } [\text{Fe}^{\text{II}}(\mathbf{4.16})_2]\text{OTf}_2$ ),  $\text{H}_2\text{O}_2$  (10  $\mu\text{L}$ , 30 wt%, aqueous solution, 0.09 mmol) was added and UV-vis spectra were recorded over time in 1 minute intervals at room temperature. Identical experiments were performed with the other complexes and also with *t*-BuOOH (20  $\mu\text{L}$ , 70 wt% in  $\text{H}_2\text{O}$ , 0.138 mmol).

*4.6.5 Representative experimental procedure to determine ligand decomposition pathways*

To a Schlenk flask containing  $[\text{Fe}^{\text{II}}(\mathbf{4.16})_2]\text{OTf}_2$  (0.151 g, 0.200 mmol),  $\text{CH}_3\text{CN}$  (2.0 mL) and pyridine (2.0 mL) were added. The resulting red solution was allowed to stir at room temperature while *t*-BuOOH (2.87 mL, 70 wt % in  $\text{H}_2\text{O}$ , 20.07 mmol) was added dropwise. The resulting purple solution was allowed to stir at room temperature for 4 hours yielding a yellow-red solution. The solvent was removed under reduced pressure at 60 °C to ensure all pyridine was evaporated, giving a black oil to which  $\text{CH}_2\text{Cl}_2$  (10 mL) was added. Then a saturated solution of NaCN (10.0 mL) was added and the solution was allowed to stir for one hour at room temperature. The organic and aqueous layer of the reaction mixture were separated. The green aqueous layer was washed with methylene chloride ( $2 \times 20 \text{ mL}$ ) and the combined organic fractions were washed with a saturated brine solution ( $3 \times 20 \text{ mL}$ ). The methylene chloride layer was dried with  $\text{Na}_2\text{SO}_4$

and the solvent was removed, yielding the bisamide **4.23** as a yellow oil (0.084 g, 0.369 mmol, 92%).

$^1\text{H}$  NMR ( $\text{CDCl}_3$ ):  $\delta$ = 12.97 (s, 1H, NH), 8.69 (d, 2H,  $J_{H,H}$ =4.4, pyridyl), 8.28 (d, 2H,  $J_{H,H}$ =7.8), 7.87 (d, 2H,  $J_{H,H}$ =7.5, pyridyl), 7.5 (t, 2H,  $J_{H,H}$ =4.9, pyridyl); MS (FAB):  $m/z$  (%): 227 (50) [**4.23** $^+$ ]; IR (neat solid)  $\nu$ =1677  $\text{cm}^{-1}$  (C=O, s).

#### 4.6.6 Experimental Section for the catalysis runs in Table 4.5.

General. The solvents (including pyridine) and the substrates utilized for catalysis (all Aldrich) were used as received. The oxidant *t*-BuOOH (70 wt% in  $\text{H}_2\text{O}$ , Aldrich) was used as received. NMR spectra were obtained at room temperature on a Bruker Avance 300 MHz or a Varian Unity Plus 300 MHz instrument and referenced to a residual solvent signal; all assignments are tentative. IR spectra were recorded on a Thermo Nicolet 360 FT-IR spectrometer and GC/MS spectra were recorded on a Hewlett Packard GC/MS System Model 5988A. Fluorenone. The substrate fluorene (0.100 g, 0.601 mmol) and the catalyst  $[\text{Fe}^{\text{II}}(\mathbf{4.16})_2]\text{OTf}_2$  (0.014 g, 0.018 mmol) were dissolved in pyridine (1.0 mL) and acetonitrile (1.0 mL). The oxidant *t*-BuOOH (0.344 mL, 70 wt % in  $\text{H}_2\text{O}$ , 2.4 mmol) was added dropwise and the tan solution was shaken for 5 hours at room temperature. The pyridine and  $\text{CH}_3\text{CN}$  solvents were removed under vacuum. The product fluorenone was isolated by column chromatography as an colorless oil (0.092 g, 0.510 mmol, 85 %) using silica gel and  $\text{CHCl}_3$  as eluent.  $^1\text{H}$  NMR (300 MHz,  $\text{CD}_3\text{CN}$ , 25 °C, TMS):  $\delta$ =7.46 (d, 2H,  $J_{H,H}$ =7.35, aromatic), 7.25 (d, 2H,  $J_{H,H}$ =7.53, aromatic), 7.15-7.07 (m, 4H, aromatic);  $^{13}\text{C}\{^1\text{H}\}$  NMR (75 MHz,  $\text{CDCl}_3$ , 25 °C, TMS):  $\delta$ =193.8 (s, C=O), 144.3 (s, aromatic), 134.1 (s, aromatic), 133.3 (s, aromatic), 129.0 (s, aromatic), 124.2 (s, aromatic), 120.3 (s, aromatic); IR (neat solid)  $\nu$ =1710s  $\text{cm}^{-1}$  (C=O).

Benzophenone. The substrate diphenylmethane (0.100 g, 0.588 mmol), utilizing the oxidant *t*-BuOOH (0.336 mL, 70 wt % in H<sub>2</sub>O, 2.35 mmol) and catalyst [Fe<sup>II</sup>(**4.16**)<sub>2</sub>]OTf<sub>2</sub> (0.013 g, 0.017 mmol), was converted to benzophenone as a white crystalline solid (0.081 g, 0.444 mmol, 76 %) as described above for fluorene, using CH<sub>2</sub>Cl<sub>2</sub> as eluent. <sup>1</sup>H NMR (300 MHz, CD<sub>3</sub>CN, 25 °C, TMS): δ=7.83-7.79 (m, 4H, aromatic), 7.61-7.56 (m, 2H, aromatic), 7.51-7.46 (m, 4H, aromatic); <sup>13</sup>C{<sup>1</sup>H} NMR (75 MHz, CDCl<sub>3</sub>, 25 °C, TMS): δ=196.7 (s, C=O), 137.6 (s, aromatic), 132.5 (s, aromatic), 130.1 (s, aromatic), 128.3 (s, aromatic); MS (EI): *m/z* (%): 182 (20) [M<sup>+</sup>], 105 (100) [M-Phenyl<sup>+</sup>].

Anthraquinone. The substrate anthracene (0.100 g, 0.554 mmol), utilizing the oxidant *t*-BuOOH (0.317 mL, 70 wt % in H<sub>2</sub>O, 2.22 mmol) and the catalyst [Fe<sup>II</sup>(**4.16**)<sub>2</sub>]OTf<sub>2</sub> (0.012 g, 0.014 mmol), was converted to anthraquinone as a yellow solid (0.092 g, 0.441 mmol, 79 %) as described above for fluorene, using CH<sub>2</sub>Cl<sub>2</sub>/hexanes 5/2 as eluent. <sup>1</sup>H NMR (300 MHz, CD<sub>3</sub>CN, 25 °C, TMS): δ = 8.35-8.26 (m, 4H, aromatic), 7.87-7.78 (m, 4H, aromatic); <sup>13</sup>C{<sup>1</sup>H} NMR (75 MHz, CDCl<sub>3</sub>, 25 °C, TMS): δ=183.9 (s, C=O), 134.9 (s, aromatic), 134.3 (s, aromatic), 128.1 (s, aromatic); IR (neat solid) ν=1674 cm<sup>-1</sup> (s, C=O).

Acetophenone. The substrate ethylbenzene (0.100 g, 0.941 mmol), utilizing *t*-BuOOH (0.538 mL, 70 wt % in H<sub>2</sub>O, 3.77 mmol) and catalyst [Fe<sup>II</sup>(**4.16**)<sub>2</sub>]OTf<sub>2</sub> (0.021 g, 0.028 mmol) was converted to acetophenone (0.038 g, 0.316, 34 %) as described above for fluorene, using ethyl acetate/toluene as eluent. <sup>1</sup>H NMR (300 MHz, CD<sub>3</sub>CN, 25 °C, TMS): δ = 7.82 (dd, 2H, *J*<sub>H,H</sub> = 1.2, aromatic), 7.45-7.40 (m, 1H, aromatic), 7.35-7.29 (m, 2H, aromatic), 2.46 (s, 3H, CH<sub>3</sub>); <sup>13</sup>C{<sup>1</sup>H} NMR (75 MHz, CDCl<sub>3</sub>, 25 °C, TMS): δ=198.1 (s, C=O), 137.1 (s, aromatic), 133.1 (s, aromatic), 128.6 (s, aromatic), 128.3 (s, aromatic), 26.6 (s, CH<sub>3</sub>); IR (neat solid) ν = 1688 cm<sup>-1</sup> (C=O, s).

3,4-dihydronaphthalene-1(2H)-one. The substrate 1,2,3,4-tetrahydronaphthalene (0.100 g, 0.756 mmol), utilizing *t*-BuOOH (0.432 mL, 70 wt % in H<sub>2</sub>O, 3.03 mmol) and catalyst [Fe<sup>II</sup>(**4.16**)<sub>2</sub>]OTf<sub>2</sub> (0.017 g, 0.023 mmol) was converted to 3,4-dihydronaphthalene-1(2H)-one (0.079 g, 0.540 mmol, 71%) as described above for fluorene, using ethyl acetate/hexanes as eluent. <sup>1</sup>H NMR (300 MHz, CD<sub>3</sub>CN, 25 °C, TMS): δ = 8.06-8.04 (m, 1H, aromatic), 7.58 (m, 1H, aromatic), 7.48 (t, 1H, *J*<sub>H,H</sub>=7.4, aromatic), 7.32-7.25 (m, 1 H, aromatic), 2.99 (t, 2H, *J*<sub>H,H</sub>=5.9, CH<sub>2</sub>), 2.68 (t, 2H, CH<sub>2</sub>), 2.20-2.12 (m, 2H,

CH<sub>2</sub>); <sup>13</sup>C{<sup>1</sup>H} NMR (75 MHz, CDCl<sub>3</sub>, 25 °C, TMS): δ=198.6 (C=O), 144.7, 133.6, 132.9, 129.0, 127.4, 126.9, 39.4, 30.0, 23.6.

6-Heptadecanone. The substrate 6-heptadecanol (0.100 g, 0.389 mmol), utilizing *t*-BuOOH (0.223 mL, 70 wt. % in H<sub>2</sub>O, 1.56 mmol) and catalyst [Fe<sup>II</sup>(**4.16**)<sub>2</sub>]OTf<sub>2</sub> (0.008 g, 0.011 mmol) was converted to heptadecanone (0.068 g, 0.267 mmol, 69 %) as described above for fluorene, using CH<sub>2</sub>Cl<sub>2</sub>/hexanes as eluent. <sup>1</sup>H NMR (300 MHz, CD<sub>3</sub>CN, 25 °C, TMS): δ = 2.38 (t, 4H, *J*(H,H)=7.4, 2CH<sub>2</sub>C=O), 1.56 (m, 4H, CH<sub>2</sub>), 1.25 (m, 20H, 12CH<sub>2</sub>), 0.87 (m, 6H, 2CH<sub>3</sub>); <sup>13</sup>C{<sup>1</sup>H} NMR (75 MHz, CDCl<sub>3</sub>, 25 °C, TMS): δ=212.2 (s, C=O), 43.2 (s, CH<sub>2</sub>), 43.1 (s, CH<sub>2</sub>), 32.3 (s, CH<sub>2</sub>), 31.8 (s, CH<sub>2</sub>), 30.0 (s, CH<sub>2</sub>), 29.9 (s, CH<sub>2</sub>), 29.8 (s, CH<sub>2</sub>), 29.7 (s, CH<sub>2</sub>), 29.6 (s, CH<sub>2</sub>), 24.3 (s, CH<sub>2</sub>), 23.9 (s, CH<sub>2</sub>), 23.1 (s, CH<sub>2</sub>), 22.9 (s, CH<sub>2</sub>), 14.5 (s, CH<sub>3</sub>), 14.3 (s, CH<sub>3</sub>); IR (neat solid) ν = 1714 cm<sup>-1</sup> (C=O, s).

2-Undecanone. The substrate 2-undecanol (0.05 g, 0.290 mmol), utilizing the oxidant *t*-BuOOH (0.166 mL, 70 wt %, in H<sub>2</sub>O, 1.16 mmol) and catalyst [Fe<sup>II</sup>(**4.16**)<sub>2</sub>]OTf<sub>2</sub> (0.007 g, 0.008 mmol) was converted to 2-undecanone (0.033 g, 0.193 mmol, 67 %), as described above for fluorene, using CH<sub>2</sub>Cl<sub>2</sub>/ hexanes as eluent. <sup>1</sup>H NMR (300 MHz, CD<sub>3</sub>CN, 25 °C, TMS): δ = 2.41 (t,

2H,  $J_{H,H}=7.3$  Hz,  $\text{CH}_2\text{C}=\text{O}$ ), 2.15 (s, 3H,  $\text{CH}_3\text{C}=\text{O}$ ), 1.56 (t, 2H,  $J_{H,H}=7$  Hz,  $\text{CH}_2$ ), 1.27 (m, 12H,  $6\text{CH}_2$ ), 0.88 (t, 3H,  $J_{H,H}=7.3$  Hz,  $\text{CH}_3$ );  $^{13}\text{C}\{^1\text{H}\}$  NMR (75 MHz,  $\text{CDCl}_3$ , 25 °C, TMS):  $\delta=209.8$  (s,  $\text{C}=\text{O}$ ), 44.2 (s), 32.3 (s), 30.2 (s), 29.8 (s), 29.6 (s), 29.5 (s), 24.3 (s), 23.1 (s), 14.5 (s); IR (neat solid)  $\nu=1717\text{ cm}^{-1}$  ( $\text{C}=\text{O}$ , s).

Cyclooctanone. The substrate cyclooctanol (0.100 g, 0.779 mmol), utilizing *t*-BuOOH (0.446 mL, 70 wt % in  $\text{H}_2\text{O}$ , 3.12 mmol), and catalyst  $[\text{Fe}^{\text{II}}(\mathbf{4.16})_2]\text{OTf}_2$  (0.017 g, 0.023 mmol) was converted to cyclooctanone (0.057 g, 0.451 mmol, 58 %), as described above for fluorene, using ethyl acetate/hexanes as eluent.  $^1\text{H}$  NMR (300 MHz,  $\text{CD}_3\text{CN}$ , 25 °C, TMS):  $\delta=2.13$ - $2.09$  (m, 4H,  $2(\text{CH}_2)\text{C}=\text{O}$ ), 1.60-1.34 (m, 4H,  $2\text{CH}_2$ ), 1.27-1.21 (m, 4H,  $2\text{CH}_2$ ), 1.08-1.07 (m, 2H,  $2\text{CH}_2$ );  $^{13}\text{C}\{^1\text{H}\}$  NMR (75 MHz,  $\text{CDCl}_3$ , 25 °C, TMS):  $\delta=218.9$  (s,  $\text{C}=\text{O}$ ), 41.9 (s,  $\text{CH}_2$ ), 27.2 (s,  $\text{CH}_2$ ), 25.6 (s,  $\text{CH}_2$ ), 24.7 (s,  $\text{CH}_2$ ); MS (EI):  $m/z$  (%): 126 (20) [ $M^+$ ], 98 (100) [ $M-\text{C}=\text{O}^+$ ].

Benzaldehyde. The substrate toluene (0.101 g, 1.10 mmol), utilizing *t*-BuOOH (0.627 mL, 70 wt % in  $\text{H}_2\text{O}$ , 4.38 mmol), and catalyst  $[\text{Fe}^{\text{II}}(\mathbf{4.16})_2]\text{OTf}_2$  (0.024 g, 0.032 mmol) was converted to benzaldehyde (0.066 g, 0.621 mmol, 57 %), as described above for fluorene, using ethyl acetate/toluene as eluent.  $^1\text{H}$  NMR (300 MHz,  $\text{CD}_3\text{CN}$ , 25 °C, TMS):  $\delta=9.84$  (s, 1H,  $\text{CHO}$ ), 7.73-7.69 (m, 2H, aromatic), 7.48-7.42 (m, 1H, aromatic), 7.37-7.32 (m, 2H, aromatic);  $^{13}\text{C}\{^1\text{H}\}$  NMR (75 MHz,  $\text{CDCl}_3$ , 25 °C, TMS):  $\delta=192.3$  (s,  $\text{C}=\text{O}$ ), 136.4 (s, aromatic), 134.4 (s, aromatic), 129.7 (s, aromatic), 128.9 (s, aromatic); IR (neat solid)  $\nu=1702\text{ s cm}^{-1}$  ( $\text{C}=\text{O}$ ).

Cyclohexene oxide. The substrate cyclohexene (0.100 g, 1.22 mmol), utilizing *t*-BuOOH (0.696 mL, 70 wt % in  $\text{H}_2\text{O}$ , 4.87 mmol) and catalyst  $[\text{Fe}^{\text{II}}(\mathbf{4.16})_2]\text{OTf}_2$  (0.027 g, 0.036 mmol) was converted to cyclohexene oxide (0.033 g, 0.336 mmol, 28 %) as described above for fluorene, using  $\text{CH}_2\text{Cl}_2$ /hexanes as eluent.  $^1\text{H}$  NMR (300 MHz,  $\text{CD}_3\text{CN}$ , 25 °C, TMS):  $\delta=3.04$  (s, 2H,

2CHO), 1.91-1.69 (m, 4H, 2CH<sub>2</sub>), 1.38-1.14 (m, 4H, 2CH<sub>2</sub>); <sup>13</sup>C{<sup>1</sup>H} NMR (75 MHz, CDCl<sub>3</sub>, 25 °C, TMS): δ=52.2 (s, C-O), 24.3 (s, CH<sub>2</sub>), 19.3 (s, CH<sub>2</sub>).

#### 4.6.7 Experimental section for the catalysis runs in Table 4.6

The substrate fluorene (0.100 g, 0.601 mmol) and the catalyst **4.25** (0.013 g, 0.018 mmol) were dissolved in acetone (2.0 mL). The oxidant *t*-BuOOH (0.344 mL, 70 wt % in H<sub>2</sub>O, 2.4 mmol) was added dropwise and the dark solution was shaken for 8 hours at room temperature. The pyridine and CH<sub>3</sub>CN solvents were removed under vacuum. The product fluorenone was isolated by column chromatography as a colorless oil (0.071 g, 0.394 mmol, 65 %) using silica gel and CHCl<sub>3</sub> as eluent. <sup>1</sup>H-NMR δ<sub>H</sub> (300.13 MHz; CDCl<sub>3</sub>; Me<sub>4</sub>Si) 7.46 (2H, d, *J*<sub>HH</sub> = 7.35, aromatic), 7.27 (2H, d, *J*<sub>HH</sub> = 7.53, aromatic), 7.12-7.07 (4H, m, aromatic). <sup>13</sup>C-NMR δ<sub>C</sub> (75.5 MHz; CDCl<sub>3</sub>; Me<sub>4</sub>Si) 193.8 (s, C=O), 144.4 (s, aromatic), 134.6 (s, aromatic), 134.1 (s, aromatic), 129.0 (s, aromatic), 124.2 (s, aromatic), 120.3 (s, aromatic). IR (neat) ν<sub>max</sub>/cm<sup>-1</sup> 1711s (C=O).

**Benzophenone.** The substrate diphenylmethane (0.100 g, 0.594 mmol), utilizing the oxidant *t*-BuOOH (0.340 mL, 70 wt % in H<sub>2</sub>O, 2.38 mmol) and catalyst **4.25** (0.013 g, 0.017 mmol), was converted to benzophenone as a white crystalline solid (0.069 g, 0.378 mmol, 64 %) as described above for fluorene, using CH<sub>2</sub>Cl<sub>2</sub> as eluent. <sup>1</sup>H-NMR δ<sub>H</sub> (300.13 MHz; CDCl<sub>3</sub>; Me<sub>4</sub>Si) 7.79 (4H, d, *J*<sub>HH</sub> = 7.2, aromatic), 7.61-7.55 (2H, m, aromatic), 7.50-7.45 (4H, m, aromatic). <sup>13</sup>C-NMR δ<sub>C</sub> (75.5 MHz; CDCl<sub>3</sub>; Me<sub>4</sub>Si) 196.7 (s, C=O), 137.6 (s, aromatic), 132.5 (s, aromatic), 130.1 (s, aromatic), 128.3 (s, aromatic). MS (EI): *m/z* 182 (MI, 20%), 105 (MI-Phenyl).

**Anthraquinone.** The substrate anthracene (0.100 g, 0.554 mmol), utilizing the oxidant *t*-BuOOH (0.317 mL, 70 wt % in H<sub>2</sub>O, 2.22 mmol) and catalyst **4.25** (0.013 g, 0.016 mmol), was

converted to anthraquinone as a yellow solid ( 0.053 g, 0.254 mmol, 46 %) as described above for fluorene, using  $\text{CH}_2\text{Cl}_2$ / hexanes 5/2 as eluent.  $^1\text{H-NMR}$   $\delta_{\text{H}}$  (300.13 MHz;  $\text{CDCl}_3$ ;  $\text{Me}_4\text{Si}$ ) 8.35-8.26 (4H, m, aromatic), 7.87-7.78 (4H, m, aromatic).  $^{13}\text{C-NMR}$   $\delta_{\text{C}}$  (75.5 MHz;  $\text{CDCl}_3$ ;  $\text{Me}_4\text{Si}$ ) 184.0 (s, C=O), 134.9 (s, aromatic), 134.3 (s, aromatic), 128.1 (s, aromatic). IR (neat)  $\nu_{\text{max}}/\text{cm}^{-1}$  1673s (C=O).

Cyclooctanone. The substrate cyclooctanol (0.100 g, 0.779 mmol), utilizing *t*-BuOOH (0.446 mL, 70 wt % in  $\text{H}_2\text{O}$ , 3.12 mmol), and catalyst **4.25** (0.017 g, 0.023 mmol) was converted to cyclooctanone (0.038 g, 0.301 mmol, 39 %), as described above for fluorene, using ethyl acetate/hexanes as eluent.  $^1\text{H-NMR}$   $\delta_{\text{H}}$  (300.13 MHz;  $\text{CDCl}_3$ ;  $\text{Me}_4\text{Si}$ ) 2.36-2.32 (m, 4H,  $(\text{CH}_2)_2$  C=O), 1.85-1.76 (m, 4H,  $\text{CH}_2$ ), 1.52-1.43 (m, 4H,  $\text{CH}_2$ ), 1.34-1.30 (m, 2H,  $\text{CH}_2$ ).  $^{13}\text{C-NMR}$   $\delta_{\text{C}}$  (75.5 MHz;  $\text{CDCl}_3$ ;  $\text{Me}_4\text{Si}$ ) 218.4 (s, C=O), 41.9 (s,  $\text{CH}_2$ ), 27.2 (s,  $\text{CH}_2$ ), 26.3 (s,  $\text{CH}_2$ ), 25.7 (s,  $\text{CH}_2$ ), 24.7 (s,  $\text{CH}_2$ ). MS (EI): *m/z* 126 (MI, 20%), 98 (MI-C=O, 100%).

6-Heptadecanone. The substrate 6-heptadecanol (0.100 g, 0.389 mmol), utilizing *t*BuOOH (0.223 mL, 70 wt. % in  $\text{H}_2\text{O}$ , 1.56 mmol) and catalyst **4.25** (0.009 g, 0.011 mmol) was converted to heptadecanone (0.036 g, 0.141 mmol, 36 %) as described above for fluorene, using  $\text{CH}_2\text{Cl}_2$ /hexanes as eluent.  $^1\text{H-NMR}$   $\delta_{\text{H}}$  (300.13 MHz;  $\text{CDCl}_3$ ;  $\text{Me}_4\text{Si}$ ) 2.38 (t, 4H,  $J_{\text{HH}} = 7.4$ ,  $(\text{CH}_2)_2$  C=O), 1.59-1.54 (m, 4H,  $\text{CH}_2$ ), 1.32-1.24 (m, 24H,  $\text{CH}_2\text{CH}_3$ ), 0.91-0.86 (m, 6H,  $\text{CH}_3$ ).  $^{13}\text{C-NMR}$   $\delta_{\text{C}}$  (75.5 MHz;  $\text{CDCl}_3$ ;  $\text{Me}_4\text{Si}$ ) 212.2 (s, C=O), 43.2 (s,  $\text{CH}_2$ ), 43.1 (s,  $\text{CH}_2$ ), 32.3 (s,  $\text{CH}_2$ ), 31.9 (s,  $\text{CH}_2$ ), 30.0 (s,  $\text{CH}_2$ ), 29.9 (s,  $\text{CH}_2$ ), 29.8 (s,  $\text{CH}_2$ ), 29.7 (s,  $\text{CH}_2$ ), 29.6 (s,  $\text{CH}_2$ ), 24.3 (s,  $\text{CH}_2$ ), 23.9 (s,  $\text{CH}_2$ ), 23.1 (s,  $\text{CH}_2$ ), 22.9 (s,  $\text{CH}_2$ ), 14.5 (s,  $\text{CH}_3$ ), 14.3 (s,  $\text{CH}_3$ ). IR (neat)  $\nu_{\text{max}}/\text{cm}^{-1}$  1714s (C=O).

#### 4.6.8 Experimental section for the catalysis runs in Table 4.6



Fluorenone. The substrate fluorene (0.098 g, 0.589 mmol) and the catalyst **4.25** (0.013 g, 0.017 mmol) were dissolved in CH<sub>3</sub>CN (2.0 mL). The oxidant H<sub>2</sub>O<sub>2</sub> (0.182 mL, 30 wt % in H<sub>2</sub>O, 1.77 mmol) was added dropwise and the dark solution was shaken for 2 hours at room temperature. The CH<sub>3</sub>CN solvent was removed under vacuum. The product fluorenone was isolated by column chromatography as yellow solid (0.096 g, 0.532 mmol, 90 %) using silica gel and CHCl<sub>3</sub> as eluent. <sup>1</sup>H-NMR δ<sub>H</sub> (300.13 MHz; CDCl<sub>3</sub>; Me<sub>4</sub>Si) 7.46 (2H, d, *J*<sub>HH</sub> = 7.35, aromatic), 7.27 (2H, d, *J*<sub>HH</sub> = 7.53, aromatic), 7.12-7.07 (4H, m, aromatic). <sup>13</sup>C-NMR δ<sub>C</sub> (75.5 MHz; CDCl<sub>3</sub>; Me<sub>4</sub>Si) 193.8 (s, C=O), 144.4 (s, aromatic), 134.6 (s, aromatic), 134.1 (s, aromatic), 129.0 (s, aromatic), 124.2 (s, aromatic), 120.3 (s, aromatic). IR (neat) ν<sub>max</sub>/cm<sup>-1</sup> 1711s (C=O).

Benzophenone. The substrate diphenylmethane (0.107 g, 0.636 mmol), utilizing the oxidant H<sub>2</sub>O<sub>2</sub> (0.196 mL, 30 wt % in H<sub>2</sub>O, 1.91 mmol) and catalyst **4.25** (0.015 g, 0.019 mmol), was converted to benzophenone as a white crystalline solid (0.092 g, 0.505 mmol, 79 %) as described above for fluorene, using CH<sub>2</sub>Cl<sub>2</sub> as eluent. <sup>1</sup>H-NMR δ<sub>H</sub> (300.13 MHz; CDCl<sub>3</sub>; Me<sub>4</sub>Si) 7.79 (4H, d, *J*<sub>HH</sub> = 7.2, aromatic), 7.61-7.55 (2H, m, aromatic), 7.50-7.45 (4H, m, aromatic). <sup>13</sup>C-NMR δ<sub>C</sub> (75.5 MHz; CDCl<sub>3</sub>; Me<sub>4</sub>Si) 196.7 (s, C=O), 137.6 (s, aromatic), 132.5 (s, aromatic), 130.1 (s, aromatic), 128.3 (s, aromatic). MS (EI): *m/z* 182 (MI, 20%), 105 (MI-Phenyl).

Acetophenone. The substrate ethylbenzene (0.099 g, 0.932 mmol), utilizing the oxidant H<sub>2</sub>O<sub>2</sub> (0.288 mL, 30 wt % in H<sub>2</sub>O, 2.80 mmol) and catalyst **4.25** (0.021 g, 0.027 mmol), was converted to acetophenone as a colorless oil (0.087 g, 0.724 mmol, 77 %) as described above for fluorene, using CHCl<sub>3</sub> as eluent. <sup>1</sup>H-NMR δ<sub>H</sub> (300.13 MHz; CDCl<sub>3</sub>; Me<sub>4</sub>Si) 7.91 (2H, d, *J*<sub>HH</sub> = 5.9, aromatic), 7.49 (1H, t, *J*<sub>HH</sub> = 6.1, aromatic), 7.41 (2H, t, *J*<sub>HH</sub> = 6.3 aromatic). <sup>13</sup>C-NMR δ<sub>C</sub> (75.5 MHz; CDCl<sub>3</sub>; Me<sub>4</sub>Si) 197.9 (s, C=O), 137.0 (s, aromatic), 133.1 (s, aromatic), 128.5 (s, aromatic), 128.2 (s, aromatic), 26.5 (s, CH<sub>3</sub>).

2-methylcyclopentanone. The substrate 2-methylcyclopentanol (0.112 g, 1.12 mmol), utilizing the oxidant  $\text{H}_2\text{O}_2$  (0.345 mL, 30 wt % in  $\text{H}_2\text{O}$ , 3.35 mmol) and catalyst **4.25** (0.026 g, 0.033 mmol), was converted to 2-methylcyclopentanone as a colorless oil (0.076 g, 0.774 mmol, 69 %) as described above for fluorene, using  $\text{CH}_2\text{Cl}_2$  as eluent.

2-methylcyclohexanone. The substrate 2-methylcyclohexanol (0.108 g, 0.945 mmol), utilizing the oxidant  $\text{H}_2\text{O}_2$  (0.292 mL, 30 wt % in  $\text{H}_2\text{O}$ , 2.84 mmol) and catalyst **4.25** (0.021 g, 0.028 mmol), was converted to 2-methylcyclohexanone as a colorless oil (0.072 g, 0.642 mmol, 68 %) as described above for fluorene, using  $\text{CH}_2\text{Cl}_2$  as eluent.  $^1\text{H-NMR}$   $\delta_{\text{H}}$  (300.13 MHz;  $\text{CDCl}_3$ ;  $\text{Me}_4\text{Si}$ ) 2.32 (2H, m,  $\text{CH}_2\text{C}=\text{O}$ ), 2.10 (1H, m,  $\text{CHC}=\text{O}$ ), 1.98-1.85 (4H, m,  $\text{CH}_2$ ), 1.68 (2H, m,  $\text{CH}_2$ ), 1.03 (3H, d,  $^3J_{\text{HH}} = 1.5$ ,  $\text{CH}_3$ ).  $^{13}\text{C-NMR}$   $\delta_{\text{C}}$  (75.5 MHz;  $\text{CDCl}_3$ ;  $\text{Me}_4\text{Si}$ ) 212.8 (s,  $\text{C}=\text{O}$ ), 45.2 (s,  $\text{CH}_2$ ), 41.7 (s,  $\text{CHCH}_3$ ), 36.1 (s,  $\text{CH}_2$ ), 27.4 (s,  $\text{CH}_2$ ), 25.0 (s,  $\text{CH}_2$ ), 14.7 (s,  $\text{CH}_3$ ).

6-methyl-5-heptene-2-one. The substrate 6-methyl-5-heptene-2-ol (0.101 g, 0.787 mmol), utilizing the oxidant  $\text{H}_2\text{O}_2$  (0.244 mL, 30 wt % in  $\text{H}_2\text{O}$ , 2.36 mmol) and **4.25** (0.018 g, 0.024 mmol), was converted to 6-methyl-5-heptene-2-one as a colorless oil (0.069 g, 0.538 mmol, 68 %) as described above for fluorene, using  $\text{CH}_2\text{Cl}_2$  as eluent.  $^1\text{H-NMR}$   $\delta_{\text{H}}$  (300.13 MHz;  $\text{CDCl}_3$ ;  $\text{Me}_4\text{Si}$ ) 5.06 (1H, t,  $J_{\text{HH}} = 7.14$ ,  $\text{C}=\text{CHCH}_2$ ), 2.45 (2H, t,  $J_{\text{HH}} = 7.2$ ,  $\text{C}=\text{OCH}_2$ ), 2.24 (2H, q,  $J_{\text{HH}} = 7.3$ ,  $\text{CH}_2\text{CH}_2\text{CH}$ ), 2.13 (s, 3H,  $\text{CH}_3\text{C}=\text{O}$ ).  $^{13}\text{C-NMR}$   $\delta_{\text{C}}$  (75.5 MHz;  $\text{CDCl}_3$ ;  $\text{Me}_4\text{Si}$ ) 208.7 (s,  $\text{C}=\text{O}$ ), 132.6 (s,  $(\text{CH}_3)_2\text{C}=\text{CHCH}_2$ ), 122.6 (s,  $(\text{CH}_3)_2\text{C}=\text{CHCH}_2$ ), 43.6 (s,  $\text{CH}_3\text{C}=\text{O}$ ), 29.8 (s,  $\text{C}=\text{OCH}_2\text{CH}_2$ ), 25.3 (s,  $\text{C}=\text{OCH}_2\text{CH}_2$ ), 22.5 (s,  $\text{CH}_3\text{C}=\text{CH}$ ), 17.5 (s,  $\text{CH}_3\text{C}=\text{CH}$ ).

3,4-dihydronaphthalene-1(2H)-one. The substrate 3,4-dihydronaphthalene-1(2H)-ol (0.101 g, 0.764 mmol), utilizing the oxidant  $\text{H}_2\text{O}_2$  (0.236 mL, 30 wt % in  $\text{H}_2\text{O}$ , 2.29 mmol) and catalyst **4.25** (0.017 g, 0.023 mmol), was converted to 3,4-dihydronaphthalene-1(2H)-one as a colorless

oil (0.067 g, 0.458 mmol, 60 %) as described above for fluorene, using  $\text{CH}_2\text{Cl}_2$  as eluent.  $^1\text{H}$ -NMR  $\delta_{\text{H}}$  (300.13 MHz;  $\text{CDCl}_3$ ;  $\text{Me}_4\text{Si}$ ) 7.68 (1H, d,  $J_{\text{HH}} = 3.4$ , aromatic), 7.38 (1H, t,  $J_{\text{HH}} = 6$ , aromatic), 7.22 (1H, t,  $J_{\text{HH}} = 7.3$ , aromatic), 7.17 (1H, d,  $J_{\text{HH}} = 7.7$ , aromatic), 2.89 (2H, t,  $J_{\text{HH}} = 6.19$ ,  $\text{C}=\text{OCH}_2$ ), 2.58 (2H, t,  $J_{\text{HH}} = 6.3$ ,  $\text{CH}_2$ ), 2.10-2.02 (2H, m,  $\text{CH}_2$ ).  $^{13}\text{C}$ -NMR  $\delta_{\text{C}}$  (75.5 MHz;  $\text{CDCl}_3$ ;  $\text{Me}_4\text{Si}$ ) 198.0 (s,  $\text{C}=\text{O}$ ), 144.4 (s, aromatic), 133.2 (s, aromatic), 132.6 (s, aromatic), 128.7 (s, aromatic), 127.0 (s, aromatic), 126.4 (s, aromatic), 39.0 (s,  $\text{CH}_2$ ), 29.6 (s,  $\text{CH}_2$ ), 23.2 (s,  $\text{CH}_2$ ).

2-hexadecanone. The 2-hexadecanol (0.093 g, 0.383 mmol), utilizing the oxidant  $\text{H}_2\text{O}_2$  (0.118 mL, 30 wt % in  $\text{H}_2\text{O}$ , 21.15 mmol) and catalyst **4.25** (0.009 g, 0.011 mmol), was converted to 2-hexadecanone as a colorless oil (0.086 g, 0.357 mmol, 93 %) as described above for fluorene, using  $\text{CH}_2\text{Cl}_2$  as eluent.  $^1\text{H}$ -NMR  $\delta_{\text{H}}$  (300.13 MHz;  $\text{CDCl}_3$ ;  $\text{Me}_4\text{Si}$ ) 2.38 (2H, t,  $J_{\text{HH}} = 17$ ,  $\text{CH}_2\text{C}=\text{O}$ ), 2.10 (3H, s,  $\text{CH}_3\text{C}=\text{O}$ ), 1.33-1.20 (26H, m,  $\text{CH}_2$ ), 0.87 (3H, t,  $^3J_{\text{HH}} = 3.2$ ,  $\text{CH}_3$ );  $^{13}\text{C}$ -NMR  $\delta_{\text{C}}$  (75.5 MHz;  $\text{CDCl}_3$ ;  $\text{Me}_4\text{Si}$ ) 209.9 (s,  $\text{C}=\text{O}$ ), 43.9 (s,  $\text{CH}_2$ ), 32.0 (s,  $\text{CH}_2$ ), 29.7 (s,  $\text{CH}_2$ ), 29.6 (s,  $\text{CH}_2$ ), 29.58 (s,  $\text{CH}_2$ ), 29.53 (s,  $\text{CH}_2$ ), 29.5 (s,  $\text{CH}_2$ ), 29.4 (s,  $\text{CH}_2$ ), 29.3 (s,  $\text{CH}_2$ ), 23.9 (s,  $\text{CH}_2$ ), 22.7 (s,  $\text{CH}_2$ ), 14.3 (s,  $\text{CH}_3$ ).

#### 4.6.9 UV-Vis spectra of complex $[\text{Fe}^{\text{II}}(\mathbf{4.16})_2]\text{OTf}_2$ in $\text{CH}_2\text{Cl}_2$ and $\text{CH}_3\text{CN}$ .

UV vis spectra of the complexes  $[\text{Fe}^{\text{II}}(\mathbf{4.16})_2]\text{OTf}_2$  (solid line),  $[\text{Fe}^{\text{II}}(\mathbf{4.18})_2]\text{OTf}_2$  and  $[\text{Fe}^{\text{II}}(\mathbf{4.20})_2(\text{OTf})_2]$  in  $\text{CH}_3\text{CN}$  (top) and  $\text{CH}_2\text{Cl}_2$  (bottom). There are barely differences in the spectra irrespective of the solvent used, demonstrating that the coordinating solvent  $\text{CH}_3\text{CN}$  does not displace the ligands.

## 4.7 References

<sup>1</sup> M. Lin, X.-l. Chen, T. Wang, P. Yan, S.-x. Xu, Z. Zhan, *Chem. Lett.* **2011**, *40*, 111 – 113 ; G. C. Midya, S. Paladhi, K. Dhara, J. Dash, *Chem. Commun.* **2011**, *47*, 6698 ; M. Mayer, W. M. Czaplik, A. Jacobi von Wangelin, *Adv. Synth. Catal.* **2010**, *352*, 2147 ; T. Hata, S. Iwata, S. Seto, H. Urabe, *Adv. Synth. Catal.* **2012**, *354*, 1885 ; S. Gulak, A. Jacobi von Wangelin, *Angew. Chem.* **2012**, *124*, 1386; *Angew. Chem. Int. Ed.* **2012**, *51*, 1357 .

<sup>2</sup> J. Bonnamour, C. Bolm, *Org. Lett.* **2011**, *13*, 2012.

<sup>3</sup> W. Han, P. Mayer, A. R. Ofial, *Adv. Synth. Catal.* **2010**, *352*, 1667.

<sup>4</sup> O. G. Mancheno, J. Dallimore, A. Plant, C. Bolm, *Org. Lett.* **2009**, *11*, 2429.

<sup>5</sup> A. Berkessel, S. Reichau, A. von der Hçh, N. Leconte, J.-M. Neudçrfl, *Organometallics* **2011**, *30*, 3880; J. Yang, T. D. Tilley, *Angew. Chem.* **2010**, *122*, 10384 ; *Angew. Chem. Int. Ed.* **2010**, *49*, 10186 ;M. Fluckiger, A. Togni, *Eur. J. Org. Chem.* **2011**, 4353 ; J. M. S. Cardoso, B. Royo, *Chem. Commun.* **2012**, *48*, 4944.

<sup>6</sup> A. M. Tondreau, C. Milsmann, A. D. Patrick, H. M. Hoyt, E. Lobkovsky, K. Wieghardt, P. J. Chirik, *J. Am. Chem. Soc.* **2010**, *132*, 15046.

<sup>7</sup> H. J. H. Fenton, *J. Chem. Soc. Trans.* **1894**, *65*, 899.

<sup>8</sup> a) D. H. R. Barton, *Tetrahedron* **1998**, *54*, 5805 – 5817; b) D. H. R. Barton, *Tetrahedron* **1994**, *50*, 1011 ; c) D. H. R. Barton, D. Doller, *Pure Appl. Chem.* **1991**, *63*, 1567 ; d) D. H. R. Barton, E. Csuhai, D. Doller, N. Ozbalik, G. Balavoine, *Proc. Natl. Acad. Sci. USA* **1990**, *87*, 3401

<sup>9</sup> a) F. Gozzo, *J. Mol. Catal. A* **2001**, *171*, 1; b) B. Singh, J. R. Long, F. Fabrizia de Biani, D. Gatteschi, P. Stavropoulos, *J. Am. Chem. Soc.* **1997**, *119*, 7030.

<sup>10</sup> D. H. R. Barton, *Chem. Soc. Rev.* **1996**, *25*, 237.

- <sup>11</sup> a) P. Stavropoulos, R. C. Elenigil-C, etin, A. E. Tapper, *Acc. Chem. Res.* **2001**, *34*, 745 ;  
b) D. W. Snelgrove, P. A. McFaul, K. U. Ingold, D. D. M. Wayner, *Tetrahedron Lett.* **1996**, *37*,  
823; c) M. J. Perkins, *Chem. Soc. Rev.* **1996**, *25*, 229 ; d) F. Minisci, F. Fontana, S. Araneo, F.  
Recupero, S. Banfi, S. Quici, *J. Am. Chem. Soc.* **1995**, *117*, 226.
- <sup>12</sup> E. Neyens, J. Baeyens, *J. Hazard. Mater.* **2003**, *98*, 33.
- <sup>13</sup> P. R. Ortiz de Montellano, *Chem. Rev.* **2010**, *110*, 932.
- <sup>14</sup> a) E. P. Talsi, K. P. Bryliakov, *Coord. Chem. Rev.* **2012**, *256*, 1418 ; b) P. C. A.  
Bruijninx, G. van Koten, R. J. M. Klein Gebbink, *Chem. Soc. Rev.* **2008**, *37*, 2716.
- <sup>15</sup> T. Buggl, S. Ramaswamy, *Current Opinion in Chemical Biology*, **2008**, *12*, 134. b) K.  
Chen, L. Que, *Angew. Chem. Int. Ed.* **1999**, *38*.
- <sup>16</sup> Diaddario, L.L.; Robinson, W. R.; Margerum D. *Inorg. Chem.* **1983**, *22*, 1021.
- <sup>17</sup> a) L. Que, Jr. , W. B. Tolman, *Nature*, **2008**, *455*, 333; b) M. Costas, M. P. Mehn, M. P.  
Jensen, L. Que, Jr. , *Chem. Rev.* **2004**, *104*, 939.
- <sup>18</sup> a) A. Beck, B. Weibert, N. Burzlaff, *Eur. J. Inorg. Chem.* **2001**, *521*; b) M. Costas, K.  
Chen, L. Que, Jr. , *Coord. Chem. Rev.* **2000**, *200*, 517 ; c) J. T. Groves, *J. Inorg. Biochem.*  
**2006**, *100*, 434 ; d) P. D. Oldenburg, L. Que, Jr. , *Catal. Today*, **2006**, *117*, 15; e) N. Burzlaff,  
*Angew. Chem.* **2009**, *121*, 5688; *Angew. Chem. Int. Ed.* **2009**, *48*, 5580.
- <sup>19</sup> B. Join, K. Mçller, C. Ziebart, K. Schrçder, D. Gçrdes, K. Thurow, A. Span-  
nenberg, K. Junge, M. Beller, *Adv. Synth. Catal.* **2011**, *353*, 3023.
- <sup>20</sup> a) A. Company, L. Gomez, X. Fontrodona, X. Ribas, M. Costas, *Chem. Eur. J.* **2008**, *14*,  
5727; b) J. Tang, P. Gamez, J. Reedijk, *Dalton Trans.* **2007**, 4644 ; c) F. Li, M. Wang, C. Ma, A.  
Gao, H. Chen, L. Sun, *Dalton Trans.* **2006**, 2427.

<sup>21</sup> a) A. Company, L. Gomez, X. Fontrodona, X. Ribas, M. Costas, *Chem. Eur. J.* **2008**, *14*, 5727; b) J. Tang, P. Gamez, J. Reedijk, *Dalton Trans.* **2007**, 4644; c) F. Li, M. Wang, C. Ma, A. Gao, H. Chen, L. Sun, *Dalton Trans.* **2006**, 2427.

<sup>22</sup> a) R. R. Fernandes, J. Lasri, M. F. C. Guedes da Silva, J. A. L. da Silva, J. J. R. Frausto da Silva, A. J. L. Pombeiro, *J. Mol. Catal. A*, **2011**, *351*, 100; b) S. A. Moyer, T. W. Funk, *Tetrahedron Lett.* **2010**, *51*, 5430 ; c) E. Balogh-Hergovich, G. Speier, *J. Mol. Catal. A* **2005**, *230*, 9; d) H. Hosseini-Monfared, C. Nather, H. Winkler, C. Janiak, *Inorg. Chim. Acta*, **2012**, *391*, 75.

<sup>23</sup> a) P. Comba, H. Wadepl, S. Wunderlich, *Eur. J. Inorg. Chem.* **2011**, 5242 ; b) T. M. Shaikha, F.-E. Hong, *Adv. Synth. Catal.* **2011**, *353*, 1491.

<sup>24</sup> a) M. Wu, C.-X. Miao, S. Wang, X. Hu, C. Xia, F. E. Kuhn, W. Sun, *Adv. Synth. Catal.* **2011**, *353*, 3014 ; b) K. Schröder, B. Join, A. Jose Amali, K. Junge, X. Ribas, M. Costas, M. Beller, *Angew. Chem.* **2011**, *123*, 1461 ; *Angew. Chem. Int. Ed.* **2011**, *50*, 1425 ; c) F. G. Gelalcha, G. Anilkumar, M. K. Tse, A. Bruckner, M. Beller, *Chem. Eur. J.* **2008**, *14*, 7687 ; d) P. C. A. Bruijninx, I. L. C. Buurmans, S. Gosiewska, M. A. H. Moelands, M. Lutz, A. L. Spek, G. van Koten, R. J. M. Klein Gebbink, *Chem. Eur. J.* **2008**, *14*, 1228; e) F. Oddon, E. Girgenti, C. Lebrun, C. Marchi-Delapierre, J. Pecaut, S. Menage, *Eur. J. Inorg. Chem.* **2012**, 85.

<sup>25</sup> a) M. S. Chen, M. C. White, *Science*, **2007**, *318*, 783; b) M. S. Chen, M. C. White, *Science*, **2010**, *327*, 566.

<sup>26</sup> K. Chen, M. Costas, L. Que, Jr., *J. Chem. Soc. Dalton Trans.* **2002**, 672.

<sup>27</sup> a) J. England, R. Gondhia, L. Bigorra-Lopez, A. R. Petersen, A. J. P. White, G. J. P. Britovsek, *Dalton Trans.* **2009**, 5319; b) J. England, C. R. Davies, M. Banaru, A. J. P. White, G. J. P. Britovsek, *Adv. Synth. Catal.* **2008**, *350*, 883; c) G. J. P. Britovsek, J. England, A. J. P. White, *Dalton Trans.* **2006**, 1399 ; d) G. J. P. Britovsek, J. England, A. J. P. White, *Inorg.*

*Chem.* **2005**, *44*, 8125 ; e) G. J. P. Britovsek, J. England, S. K. Spitzmesser, A. J. P. White, D. J. Williams, *Dalton Trans.* **2005**, 945.

<sup>28</sup> S. Gosiewska, H. P. Permentier, A. P. Bruins, G. van Koten, R. J. M. Klein Gebbink, *Dalton Trans.* **2007**, 3365.

<sup>29</sup> a) P. Comba, M. Maurer, P. Vadivelu, *Inorg. Chem.* **2009**, *48*, 10389 ; b) M. R. Bukowski, P. Comba, A. Lienke, C. Limberg, C. Lopez de Laorden, R. Mas-Balleste, M. Merz, L. Que, Jr. , *Angew. Chem.* **2006**, *118*, 3524 ; *Angew. Chem. Int. Ed.* **2006**, *45*, 3446.

<sup>30</sup> M. Christmann, *Angew. Chem.* **2008**, *120*, 2780; *Angew. Chem. Int. Ed.* **2008**, *47*, 2740.

<sup>31</sup> A. N. Biswas, A. Pariyar, S. Bose, P. Das, P. Bandyopadhyay, *Catal. Commun.* **2010**, *11*, 1008.

<sup>32</sup> (a)“Green chemistry Articles of Interest to the Pharmaceutical industry”, *Org. Process Res. Dev.* **2010**, *14*, 19.; (b)R. Cirminna, M. Pagliaro, “Industrial Oxidations with Organocatalyst TEMPO and its derivatives” *Org. Process Res. Dev.* **2010**, *14*, 245.

<sup>33</sup> T. J. Collins, *Acc. Chem. Res.* **1994**, *27*, 279 ; b) A. Marques, M. Marin, M.-F. Ruasse, *J. Org. Chem.* **2001**, *66*, 7588.

<sup>34</sup> S. Sedinkin, “Rational Ligand Design for Potential Application in Transition Metal Catalysis”, *Thesis, University of Missouri-St. Louis*, **2011**.

<sup>35</sup> a) P. Shejwalkar, N. P. Rath, E. B. Bauer, *Dalton Trans.* **2011**, *40*, 7617 ; b) P. Shejwalkar, N. P. Rath, E. B. Bauer, *Molecules.* **2010**, *15*, 2631; c) M. Lenze, S. L. Sedinkin, N. P. Rath, E. B. Bauer, *Tetrahedron Lett.* **2010**, *51*, 2855 – 2858 ; d) M. Lenze, E. B. Bauer, *J. Mol. Catal. A.* **2009**, *309*, 117..

<sup>36</sup> A. Diebold, K. S. Hagen, *Inorg. Chem.* **1998**, *37*, 215.

<sup>37</sup> a) N. M. F. Carvalho, A. Horn, Jr., A. J. Bortoluzzi, V. Drago, O. A. C. Antunes, *Inorg. Chim. Acta.* **2006**, 359, 90 ; b) D. Mandon, A. Nopper, T. Litrol, S. Goetz, *Inorg. Chem.* **2001**, 40, 4803.

<sup>38</sup> a) A. Malassa, H. Gçrls, A. Buchholz, W. Plass, M. Westerhausen, *Z. Anorg. Allg. Chem.* **2006**, 632, 2355 ; b) C. J. Davies, G. A. Solan J. Fawcett, *Polyhedron.* **2004**, 23, 310.

<sup>39</sup> a) N. M. F. Carvalho, O. A. C. Antunes, A. Horn, Jr., *Dalton Trans.* **2007**, 1023; b) K. Visvaganesan, R. Mayilmurugan, E. Suresh, M. Palaniandavar, *Inorg. Chem.* **2007**, 46, 10294.

<sup>40</sup> ] J. Cui, M. S. Mashuta, R. M. Buchanan, C. A. Grapperhaus, *Inorg. Chem.* **2010**, 49, 10427.

<sup>41</sup> E. Balogh-Hergovich, G. Speier, M. Reglier, M. Giorgi, E. Kuzmann, Attila Vertes, *Eur. J. Inorg. Chem.* **2003**, 1735.

<sup>42</sup> K. Visvaganesan, E. Suresh, M. Palaniandavar, *Dalton Trans.* **2009**, 3814 .

<sup>43</sup> ] A. Thibon, J.-F. Bartoli, S. Bourcier, F. Banse, *Dalton Trans.*, **2009**, 9587.

<sup>44</sup> H. R. Lucas, L. Li, A. A. Narducci Sarjeant, M. A. Vance, E. I. Solomon, K. D. Karlin, *J. Am. Chem. Soc.* **2009**, 131, 3230.

<sup>45</sup> A. C. Mayer, C. Bolm in *Iron Catalysis in Organic Chemistry*, 1st ed. (Ed. : B. Plietker), Wiley-VCH, Weinheim, 2008, Chapter 3, pp. 73 – 123.

<sup>46</sup> M. Lenze, S. Sedinkin, E. Bauer, *J. Mol. Cat.: A*, **2013**, 41, 2109.

<sup>47</sup> D. W. Blakesley, S. C. Payne, K. S. Hagen, *Inorg. Chem.*, **2000**, 39, 1979.

<sup>48</sup> V. Balland, F. Banse, E. Anxolabehere-Mallart, M. Nierlich, J.-J. Girerd, *Eur. J. Inorg. Chem.*, **2003**, 2529.



- <sup>49</sup> T. Buchen, P. Gutlich, *Inorg. Chim. Acta.*, **1995**, *231*, 221.
- <sup>50</sup> S. Gosiewska, J. J. L. M. Cornelissen, M. Lutz, A. L. Spek, G. van Koten, R. J. M. Klein Gebbink, *Inorg. Chem.*, **2006**, *45*, 4214.
- <sup>51</sup> J. Kim, R. G. Harrison, C. Kim, L. Que, Jr., *J. Am. Chem. Soc.*, **1996**, *118*, 4373.
- <sup>52</sup> a) M. N. Kopylovich, T. C. MacLeod, M. Haukka, G. I. Amanullayeva, K. T. Mahmudov, A. J. Pombeiro, *J. Inorg. Biochem.*, **2012**, *115*, 72.; b) M. S. Chen, M. C. White, *Science*, **2010**, *327*, 566.; c) C. Pavan, J. Legros, C. Bolm, *Adv. Synth. Catal.* **2007**, *347*, 703.
- <sup>53</sup> K. Alfonsi, J. Colberg, P. J. Dunn, T. Fevig, S. Jennings, T. A. Johnson, H. P. Kleine, C. Knight, M. A. Nagy, D. A. Perry, M. Stefaniak, *Green Chem.* **2010**, *10*, 31.
- <sup>54</sup> a) M. P. Jensen, A. Mairata i Payeras, A. T. Fiedler, M. Costas, J. Kaizer, A. Stubna, E. Munck, L. Que, Jr., *Inorg. Chem.* **2007**, *46*, 2398; b) C. Nguyen, R. J. Guajardo, P. K. Mascharak, *Inorg. Chem.*, **1996**, *35*, 6273.
- <sup>55</sup> M. S. Seo, T. Kamachi, T. Kouno, K. Murata, M. J. Park, K. Yoshizawa, W. Nam, *Angew. Chem.* **2007**, *119*, 2341; *Angew. Chem. Int. Ed.*, **2007**, *46*, 2291.
- <sup>56</sup> F. Shi, M. K. Tse, Z. Li, M. Beller, *Chem. Eur. J.*, **2008**, *14*, 8793.
- <sup>57</sup> M. R. Bukowski, H. L. Halfen, T. A. van den Berg, J. A. Halfen, L. Que, Jr., *Angew. Chem.* **2005**, *117*, 590; *Angew. Chem. Int. Ed.*, **2005**, *44*, 584.
- <sup>58</sup> J. Kaizer, M. Costas, L. Que, *Angew. Chem. Int. Ed.* **2003**, *42*, 3671.
- <sup>59</sup> G. A. Russell, *J. Am. Chem. Soc.*, **1957**, *79*, 3871.
- <sup>60</sup> A. Breheret, C. Lambeaux, S. Menage, M. Fontecave, F. Dallemer, E. Fache, J.-L. Pierre, P. Chautemps, M.-T. Averbusch-Pouchot, C. R. *Acad. Sci. Chemistry.*, **2001**, *4*, 27.
- <sup>61</sup> C. Krebs, D. G. Fujimori, C. T. Walsh, J. M. Bollinger, Jr. *Acc. Chem. Res.*, **2007**, *40*, 484.

- <sup>62</sup> M. P. Jensen, M. Costas, R. Y. N. Ho, J. Kaizer, A. Mairata i Payeras, E. Munck, L. Que, Jr., J.-U. Rohde, A. Stubna, *J. Am. Chem. Soc.*, **2005**, *127*, 10512.
- <sup>63</sup> J.-U. Rohde, J. H. In, M. H. Lim, W. W. Brennessel, M. R. Bukowski, A. Stubna, E. Munck, W. Nam, L. Que, Jr., *Science.*, **2003**, *299*, 1037.
- <sup>64</sup> J. Kaizer, M. Costas, L. Que, *Angew. Chem. Int. Ed.* **2003**, *42*, 3671.
- <sup>65</sup> A. Decker, J.-U. Rohde, E. J. Klinker, S. D. Wong, L. Que, Jr., E. I. Solomon, *J. Am. Chem. Soc.*, **2007**, *129*, 15983.
- <sup>66</sup> D. H. R. Barton, V. N. Le Gloahec, H. Patin, F. Launay, *New J. Chem.* **1998**, *22*, 559.
- <sup>67</sup> M. Lenze, E. Martin, N. Rath, E. Bauer, *ChemPlusChem*, **2013**, *78*, 101.
- <sup>68</sup> a) X. Baucherel, L. Gonsalvi, I. W. C. E. Arends, S. Ellwood, R. A. Sheldon, *Adv. Synth. Catal.* **2004**, *346*, 286; b) F. Minisci, F. Recupero, A. Cecchetto, C. Gambarotti, C. Punta, R. Faletti, R. Paganelli, G. Franco Pedulli, *Eur. J. Org. Chem.* **2004**, 109.
- <sup>69</sup> G. Roelfes, M. Lubben, R. Hage, L. Que, Jr., *Chem. Eur. J.* **2000**, *6*, 2152.
- <sup>70</sup> a) J. Kaizer, M. Costas, L. Que, Jr., *Angew. Chem.* **2003**, *115*, 3799 – 3801; *Angew. Chem. Int. Ed.* **2003**, *42*, 3671; b) A. Mairata i Payeras, R.Y. N. Ho, M. Fujita, L. Que, Jr., *Chem. Eur. J.* **2004**, *10*, 4944; c) Y. He, J. D. Gordon, C. R. Goldsmith, *Inorg. Chem.* **2011**, *50*, 12651.
- <sup>71</sup> F. Namuswe, G. D. Kasper, A. A. Narducci Sarjeant, T. Hayashi, C. M. Krest, M. T. Green, P. Moenne-Loccoz, D. P. Goldberg, *J. Am. Chem. Soc.* **2008**, *130*, 14189.
- <sup>72</sup> D. M. Pearson, N. R. Conley, R. M. Waymouth, *Organometallics.*, **2011**, *30*, 1445.
- <sup>73</sup> D. Pijper, P. Saisaha, J. W. de Boer, R. Hoen, C. Smit, A. Meetsma, R. Hage, R. P. van Summeren, P. L. Alsters, B. L. Feringa, W. R. Browne, *Dalton Trans.* **2010**, *39*, 10375.

- <sup>74</sup> a) M. C. Br̄hmer, S. Mundinger, S. Brase, W. Bannwarth, *Angew. Chem.* **2011**, *123*, 6299; *Angew. Chem. Int. Ed.* **2011**, *50*, 6175; b) S. S. Massoud, F. R. Louka, M. Mikuriya, H. Ishida, F. A. Mautner, *Inorg. Chem. Commun.*, **2009**, *12*, 420.
- <sup>75</sup> S. J. Lange, H. Miyake, L. Que, Jr., *J. Am. Chem. Soc.* **1999**, *121*, 6330.
- <sup>76</sup> a) D. Wu, *Acta Crystallogr. Sect. E* **2009**, *65*, m1340; b) T. Kajiwara, R. Sensui, T. Noguchi, A. Kamiyama, T. Ito, *Inorg. Chim. Acta.*, **2002**, *337*, 299.
- <sup>77</sup> H. Chowdhury, S. H. Rahaman, R. Ghosh, S. Kumar Sarkar, H.-K. Fun, B. Kumar Ghosh, *J. Mol. Struct.* **2007**, *826*, 170.
- <sup>78</sup> C. Panda, M. Ghosh, T. Panda, R. Banerjee, S. S. Gupta, *Chem. Commun.* **2011**, *47*, 8016.
- <sup>79</sup> K. Barbusinski, *Ecol. Chem. Eng. S* **2009**, *76*, 347.
- <sup>80</sup> J. M. Rowland, M. M. Olmstead, P. K. Mascharak, *Inorg. Chem.*, **2002**, *41*, 2754.
- <sup>81</sup> K. S. Hagen, *Inorg. Chem.* **2000**, *39*, 5867.
- <sup>82</sup> M. Lenze, S. Sedinkin, E. B. Bauer, *J. Mol. Catal.* (submitted)

## **Chapter 5.** *Chemoselective, Iron(II)-catalyzed oxidation of secondary alcohols over primary alcohols utilizing H<sub>2</sub>O<sub>2</sub> as the oxidant.*

### **5.1 Aim of the Chapter**

This chapter describes herein the implementation of a spectroscopically and structurally characterized iron(II) complex, possessing two tridentate  $\alpha$ -aminopyridine ligands, that exhibited unprecedented reactivity and selectivity in oxidation reactions utilizing aqueous H<sub>2</sub>O<sub>2</sub>. This environmentally benign, iron-based catalyst system is capable of selectively oxidizing secondary alcohols to the corresponding hydroxyl ketones in the presence of primary alcohols.

### **5.2 Introduction**

Oxidation reactions are extremely useful and powerful tools for the functionalization and derivitization of organic molecules. For this reason, they are frequently employed in the synthesis of complex targets such as the development and production of active pharmaceutical ingredients (API).<sup>1</sup> For the oxidation of alcohols several protocols are available<sup>2</sup> that have been known for decades. Albeit the oxidation of alcohols is well established, many of the protocols suffer from major drawbacks, thus, hampering their application on large scales.

Our group has taken a non-toxic, ecologically-friendly approach to rectifying the issues associated with the existing conditions for the oxidation of alcohols. This approach has resulted in a promising alternative to established conditions and involves a nonheme iron(II) based catalyst system that applies peroxide oxidants such as hydrogen peroxide (H<sub>2</sub>O<sub>2</sub>) or *t*-BuOOH.<sup>3</sup> The advantages of such a system are the non-toxicity, cheapness and abundance of iron and the fact that peroxides are cheap, commercially available and their only reduced products are alcohols and

water. The application of such a catalyst system, involving iron complexes and peroxides, may be regarded as a drastic improvement and follows the general principles of Green Chemistry. Such conditions for oxidation reactions no longer require extreme care or rigorous precautions, hence, may be performed on larger scales of pharmaceutical manufacturing and industrial production.<sup>3</sup> A majority of the oxidations described in literature focus on the oxidation of either primary alcohols or the oxidation of secondary alcohols.<sup>4</sup> The oxidation of primary alcohols can either be stopped at the aldehyde stage or undergo further oxidation to their corresponding carboxylic acids. Usually the archetype substrate for investigation was benzyl alcohol, and a mixture of aldehydes and carboxylic acids has been obtained on occasion.<sup>5</sup> The oxidation of secondary alcohols at room temperature has been reported previously to be catalyzed by multiple iron catalysts.<sup>6</sup>

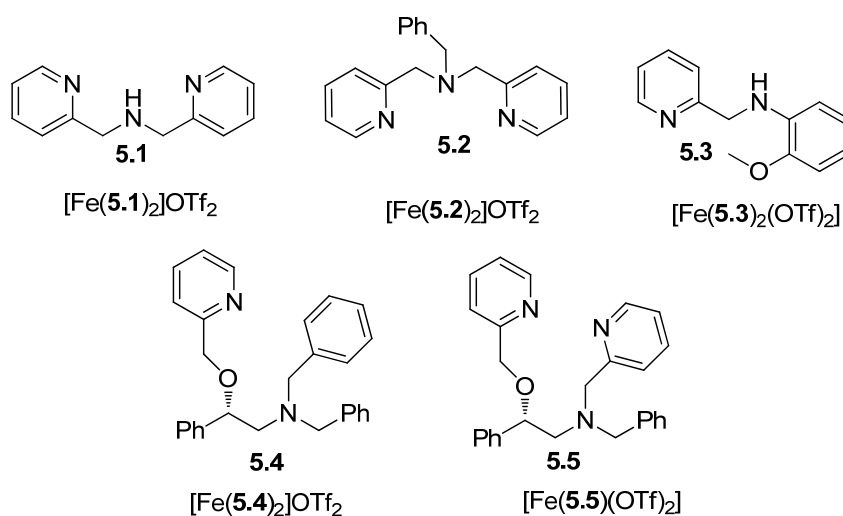


**Figure 5.1.** Previously prepared iron complexes to be tested in the study.

It is well known that a number of iron catalysts exist that are capable of rapidly oxidizing primary or secondary alcohol functionalities. However, when a primary alcohol and a secondary alcohol are present in the same molecule, both units are capable of being oxidized, and a selec-

tive catalyst system is needed. The selective oxidation of secondary alcohols, in the presence of primary alcohols, utilizing aqueous H<sub>2</sub>O<sub>2</sub> is lagging relative to the investigation of oxidations involving purely monofunctional alcohols.<sup>7</sup> The few examples of investigations that do study intramolecular selectivity typically only investigate using one 1,2-diol and in these examples the reaction mixtures required elevated temperatures for several hours to generate the product.<sup>6,7</sup> Reported herein is an iron(II)-based catalyst system for the rapid, selective oxidation of secondary alcohols in a variety of diols at room temperature utilizing aqueous H<sub>2</sub>O<sub>2</sub> as the oxidant.

As mentioned in Chapter 4, the previously synthesized iron complexes featuring bi- and tridentate  $\alpha$ -aminopyridine, bidentate  $\alpha$ -iminopyridine and *N*-, *O*-coordinating polydentate pyridyl ligands are all catalytically active in the oxidation of activated methylene groups and secondary alcohols to the corresponding ketones employing peroxides as oxidants.<sup>8</sup> At any rate, none of these iron complexes exhibited catalytic activity in the oxidation of aliphatic or aromatic primary alcohols. Hence, I decided to see if I could exploit this unique reactivity to promote a selective oxidation of the secondary alcohol in preference to the oxidation of the primary alcohol within the structural confinement of the same molecule. According to the A/K ratio studies performed in Chapter 4, complex [Fe(**5.1**)<sub>2</sub>]<sup>2+</sup>OTf<sub>2</sub> displayed the most promising results, as far as selectivity was concerned, and thus, will be the complex of choice for future studies.<sup>8</sup>

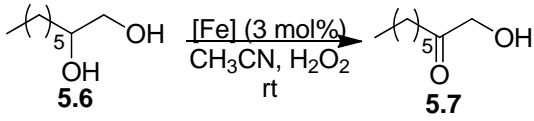
## 5.3 Results

### 5.3.1 Catalytic efficacy and selectivity screening

Preliminary screening efforts, designed to probe the catalytic efficacy of various iron complexes displayed in Figure 5.1, involved the use of octane-1,2-diol (**5.6**) with H<sub>2</sub>O<sub>2</sub> (30 wt% in H<sub>2</sub>O) as the oxidant (Table 5.1). In this particular screening, only [Fe(**5.1**)<sub>2</sub>]<sup>2+</sup>OTf<sub>2</sub> showed cata-

lytic activity (OTf = CF<sub>3</sub>SO<sub>3</sub><sup>-</sup>).<sup>8</sup> Several solvent screening experiments demonstrated that CH<sub>3</sub>CN was the best choice when using complex [Fe(**5.1**)<sub>2</sub>]<sup>2+</sup>OTf<sub>2</sub> as other solvents such as pyridine, CH<sub>2</sub>Cl<sub>2</sub>, THF and acetone were tested but all resulted in diminished yields relative to those obtained while using CH<sub>3</sub>CN. Using these conditions, the secondary alcohol unit in **5.6** was nearly completely oxidized to the respective  $\alpha$ -hydroxy ketone product (**5.7**), within 15 minutes at room temperature, having 95% selectivity according to GC. Surprisingly, only the diol starting material **5.6** or trace amounts of various oxidation products were observed when all other complexes were applied as catalysts, regardless of the reaction time or solvent used (Table 5.1). Absolutely no oxidation product was observed in the absence of catalyst or when a catalytic amount of Fe(OTf)<sub>2</sub>, the iron source used in the synthesis of the complexes, was employed.

Table 5.1. Catalyst screening.

		
Complex <sup>a</sup>	Time	Conversion (selectivity) <sup>b</sup>
[Fe( <b>5.1</b> ) <sub>2</sub> ] <sup>2+</sup> OTf <sub>2</sub>	15 minutes <sup>c</sup>	95% (95%)
[Fe( <b>5.2</b> ) <sub>2</sub> ] <sup>2+</sup> OTf <sub>2</sub>	15 minutes <sup>c</sup>	< 1%
[Fe( <b>5.3</b> ) <sub>2</sub> ](OTf) <sub>2</sub>	15 minutes <sup>c</sup>	< 1%
[Fe( <b>5.4</b> ) <sub>2</sub> ] <sup>2+</sup> OTf <sub>2</sub>	15 minutes <sup>c</sup>	< 5%
[Fe( <b>5.5</b> )(OTf) <sub>2</sub> ]	15 minutes	< 1%
no catalyst	15 minutes	< 1%
Fe(OTf) <sub>2</sub>	15 minutes	< 5%
[Fe( <b>5.1</b> ) <sub>2</sub> ] <sup>2+</sup> OTf <sub>2</sub> <sup>d</sup>	15 minutes	90% (95%)

<sup>a</sup> The substrate (**5.6**, 0.34 mmol) and the catalyst (0.01 mmol) were dissolved in CH<sub>3</sub>CN (1 mL). H<sub>2</sub>O<sub>2</sub> (30 wt% in H<sub>2</sub>O, 0.85 mmol) was added dropwise at room temperature with stirring within 5 minutes.

<sup>b</sup> Determined by GC; selectivity reported for product **5.7**.

<sup>c</sup> After 24 h, 90% starting material and a random mixture of oxidation products was observed.

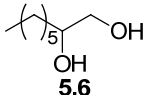
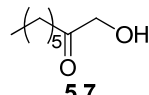
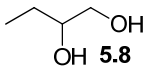
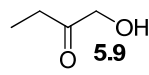
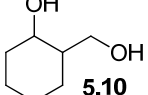
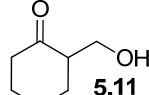
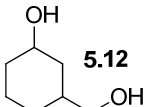
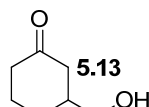
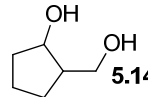
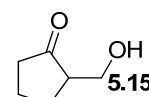
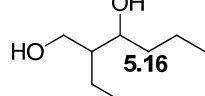
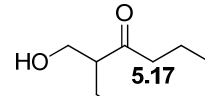
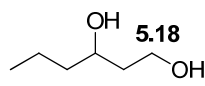
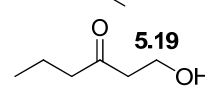
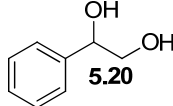
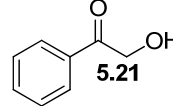
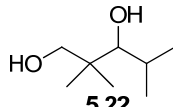
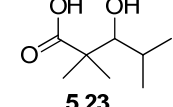
<sup>d</sup> Same conditions as in <sup>a</sup>, but the complex was generated *in situ* by combining the iron source Fe(OTf)<sub>2</sub> and the ligand **5.1** in the solvent prior to the addition of the substrate and the H<sub>2</sub>O<sub>2</sub>.

Review of Table 5.1 clearly shows that complex [Fe(**5.1**)<sub>2</sub>]<sup>2+</sup>OTf<sub>2</sub> exhibits superior reactivity, compared to all other catalysts being considered, in the title reaction. This complex was previously synthesized in our laboratory by combining Fe(OTf)<sub>2</sub> and bis(picoly)amine ligand **5.1**.<sup>7</sup>

<sup>8</sup> The application of complex [Fe(**5.1**)<sub>2</sub>]<sup>2+</sup>OTf<sub>2</sub>, is extremely practical, as both the iron source, Fe(OTf)<sub>2</sub>, and the bis(picoly)amine ligand **5.1** are commercially available, and the complex formation is quantitative, straightforward and fast. Moreover, it is possible to accomplish an *in situ* formation of complex [Fe(**5.1**)<sub>2</sub>]<sup>2+</sup>OTf<sub>2</sub>, where the catalytic activity and selectivity of the *in situ* one is nearly as high as the preformed complex [Fe(**5.1**)<sub>2</sub>]<sup>2+</sup>OTf<sub>2</sub> (Table 5.1, last entry).



Table 5.2. Selective oxidation of diols.

Entry	Substrate	Product	Isolated Yield <sup>a</sup>
1	 5.6	 5.7	82%
2	 5.8	 5.9	84%
3	 5.10	 5.11	63%
4	 5.12	 5.13	71%
5	 5.14	 5.15	58%
6	 5.16	 5.17	83%
7	 5.18	 5.19	54%
8	 5.20	 5.21	53%
9	 5.22	 5.23	<sup>b</sup>

<sup>a</sup> The substrate (1 mmol) and the catalyst [Fe(5.1)<sub>2</sub>]<sup>2+</sup>OTf<sub>2</sub> (0.03 mmol 3 mol%) were dissolved in CH<sub>3</sub>CN (2 mL). The oxidant H<sub>2</sub>O<sub>2</sub> (30 wt% in H<sub>2</sub>O, 2.6 mmol) was added dropwise at room temperature with stirring within 10 minutes. After an additional 5 minutes of stirring, the product was immediately isolated by column chromatography.

<sup>b</sup> An inseparable mixture of three products was observed by NMR, GC and GCMS, which were the carboxylic acid 5.23, the corresponding aldehyde and the hydroxy ketone.

The optimized conditions, derived from the screening efforts in Table 5.1, were used to oxidized a plethora of diols to the corresponding hydroxy ketones, and the results are present in Ta-

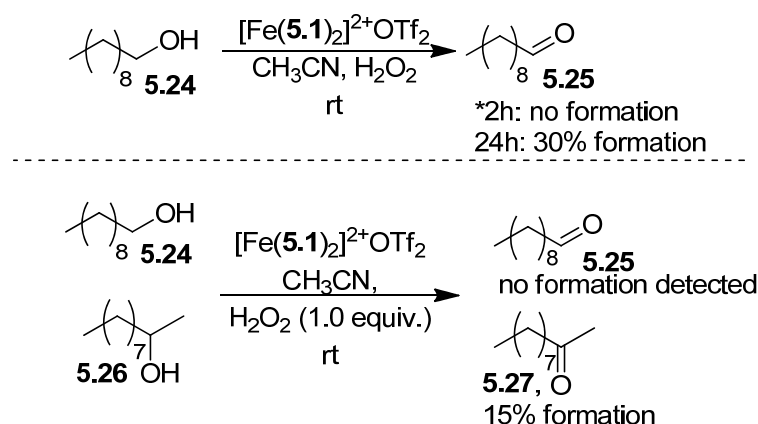
ble 5.2. It was quickly determined that 1,2- and 1,3-diols could be selectively oxidized to the respective hydroxyl ketones within 15 minutes at room temperature. Albeit the oxidation of secondary alcohols was observed within 15 minutes at room temperature, a slow oxidation of the primary alcohols was observed in solution over the course of several hours, thus, the reactions were worked up after 15 minutes of reaction time. In none of the 1,2-diol oxidations was a C-C bond fission observed, as was the case for other, related oxidation protocols.<sup>2,6,7</sup> The substrate **5.22** demonstrated a limitation of the catalyst system. It was unexpectedly oxidized to an inseparable mixture of products that contained the expected hydroxyl ketone as well as various oxidation products from the primary alcohol functionality. Studies to determine the influence that branching exerts on the outcome of the reaction are currently underway.

### 5.3.2 Experiments to better understand the selectivity

In an attempt to gain a better understanding of the selectivity of the reaction, additional experiments were carried out. As has already been established, the primary alcohol functionality is not oxidized at all, at least within the 15 minute time frame it takes for the secondary alcohol functionality to be oxidized. To determine the extent of which the oxidation of the primary alcohol unit takes place, I subjected 1-decanol (**5.24**) to oxidation under the identical conditions to those used in Table 5.2 (Scheme 5.1, top left). After 2 h had passed, only unoxidized starting material was detected and after 24 h, 30% conversion to the corresponding aldehyde was observed. To such a degree, it is obvious that primary alcohols do oxidize, but they oxidize orders of magnitude more slowly than secondary alcohols. In this fashion, it is presumed that the selectivities displayed in Table 5.2 are merely the result of kinetic resolution. In order to corroborate such a presumption, I designed an experiment in which the intermolecular kinetics of oxidation could be monitored (Scheme 5.1, bottom right). In this experiment, 1-decanol (**5.24**), 2-decanol (**5.26**) and

aqueous  $\text{H}_2\text{O}_2$  were employed in a 1:1:1 stoichiometric ratio under the conditions otherwise identical to those in Table 5.2. As expected, the oxidation of the primary alcohol was not observed after 15 minutes at room temperature, as determined by GC. The partial oxidation of the secondary alcohol to the hydroxyl ketone **5.27** was observed, but in the presence of the primary alcohol, the formation was lower than what was typically observed when only secondary alcohols were exposed to oxidation. I hypothesize that the primary alcohol could potentially coordinate to the metal center, thereby deactivating or impairing any subsequent catalytic activity.

In order to gain additional information about potential mechanistic pathways, I first investigated if the reaction proceeded through a free radical mechanism. Accordingly, the oxidation of octane-1,2-diol (**5.6**) was performed in the presence of 2,4,6-tri-*tert*-butylphenol (TTBP), a bulky well known radical scavenger.<sup>9</sup> Neither a catalytic nor substoichiometric amount of TTBP abolished or slowed down the rate of oxidation. However, when a stoichiometric amount of TTBP was used, the reaction was slowed down; but it is known that TTBP has a large oxidation potential, and once it is oxidized, it loses its radical scavenger ability. When only a catalytic amount of phenol was applied, no oxidation took place, which could very well be due to the fact that phenol deactivates or impairs catalytic activity in a similar fashion to primary alcohols.



**Scheme 5.1.** Investigations to better understand the selectivity of the reaction.

Several literature reports exist that suggest several possible mechanistic pathways for the oxidations of alcohols utilizing peroxides. In hydride transfer (HT)<sup>10</sup> or hydrogen atom transfer (HAT)<sup>11</sup> mechanisms, hydrides or hydrogen atoms are transferred to the iron complex. The involvement of a high-valent  $\text{Fe}^n=\text{O}$  species in oxidation reactions in HAT mechanisms has been widely investigated. Unfortunately, based on the experiments described herein, a mechanism for the reaction could not be established. In complex  $[\text{Fe}(\mathbf{5.1})_2]\text{OTf}_2$  all of the coordination sites are

occupied by ligands, thus, a site must first be opened in order to initially form the iron-peroxo or high-valent iron oxo ( $\text{Fe}^n=\text{O}$ ) species.

## 5.4 Summary and prospective

Reported herein, was the fact that the easily accessible complex  $[\text{Fe}(\mathbf{5.1})_2]\text{OTf}_2$  could be used as a catalyst; that is capable of rapidly and selectively oxidizing secondary alcohols, in the presence of primary alcohols, to the corresponding hydroxy ketones (15 minutes, 3 mol% catalyst loading, aqueous  $\text{H}_2\text{O}_2$  oxidant, room temperature,  $\text{CH}_3\text{CN}$  solvent, 53 to 84% isolated yields). The mild conditions, moderate yields and short reaction times make this system an attractive starting point for additional optimization efforts.

## 5.5 Experimental

### Preparation of Diols:

#### **2-hydroxycyclohexane-1-methanol.**

To a 100 mL schlenk flask, lithium aluminum hydride (1.67 g, 44.1 mmol) was added followed by diethyl ether (30 mL). The Slurry was stirred for 5 min at room temperature and the flask was then lowered into an ice bath. Then ethyl-2-cyclohexanonecarboxylate (2.50 g, 14.7 mmol), suspended in diethyl ether (20 mL), was added dropwise. After addition was complete the flask was removed from ice bath and allowed to warm to room temperature. The reaction mixture was stirred for 12 hours at room temperature. Next, ethyl acetate (30 mL) was added to reaction mixture to quench the unreacted lithium aluminum hydride and allowed to stir for one hour. Finally, saturated solution of aqueous sodium sulfate (40 mL) was added to precipitate aluminum. The white slurry was then filtered through a coarse fritted glass funnel containing 2 inch of celite. The filtrate was then transferred to a separatory funnel and both layers were

kept separate. Ethyl acetate was then used 3 X 20 mL to extract the product from the aqueous layer. All organic extracts were combined, dried using sodium sulfate and evaporated to dryness yielding a light yellow clear oil. The crude oil was then purified via column chromatography using ethyl acetate as eluent and 2-hydroxycyclohexane-1-methanol (0.993 g, 7.63 mmol, 52 %) was isolated as a colorless oil.

**D1:**  $^1\text{H-NMR}$   $\delta_{\text{H}}$  (300.13 MHz;  $\text{CDCl}_3$ ;  $\text{Me}_4\text{Si}$ ) 4.35-3.89 (2H, m, 2OH), 3.64-3.45 (3H,  $\text{CHOHCHCH}_2\text{OH}$ ), 2.00-1.03 (8H, m, 4 $\text{CH}_2$ ), 0.93-0.81 (1H, m,  $\text{CHCH}_2\text{OH}$ ).  $^{13}\text{C-NMR}$   $\delta_{\text{C}}$  (75.5 MHz;  $\text{CDCl}_3$ ;  $\text{Me}_4\text{Si}$ ) 75.9 (s,  $\text{CHOH}$ ), 69.1 (s,  $\text{CHCH}_2\text{OH}$ ), 45.9 (s,  $\text{CHCH}_2\text{OH}$ ), 35.1 (s,  $\text{CH}_2\text{CHOH}$ ), 27.2 (s,  $\text{CH}_2\text{CH}_2\text{CH}_2$ ), 24.9 (s,  $\text{CH}_2\text{CH}_2\text{CH}_2$ ), 23.5 (s,  $\text{CH}_2\text{CHCH}_2$ ).

**D2:**  $^1\text{H-NMR}$   $\delta_{\text{H}}$  (300.13 MHz;  $\text{CDCl}_3$ ;  $\text{Me}_4\text{Si}$ ) 4.35-3.89 (2H, m, 2OH), 3.64-3.45 (3H,  $\text{CHOHCHCH}_2\text{OH}$ ), 2.00-1.03 (8H, m, 4 $\text{CH}_2$ ), 0.93-0.81 (1H, m,  $\text{CHCH}_2\text{OH}$ ).  $^{13}\text{C-NMR}$   $\delta_{\text{C}}$  (75.5 MHz;  $\text{CDCl}_3$ ;  $\text{Me}_4\text{Si}$ ) 68.2 (s,  $\text{CHOH}$ ), 65.5 (s,  $\text{CHCH}_2\text{OH}$ ), 42.4 (s,  $\text{CHCH}_2\text{OH}$ ), 32.7 (s,  $\text{CH}_2\text{CHOH}$ ), 25.1 (s,  $\text{CH}_2\text{CH}_2\text{CH}_2$ ), 24.4 (s,  $\text{CH}_2\text{CH}_2\text{CH}_2$ ), 20.5 (s,  $\text{CH}_2\text{CHCH}_2$ ).

### **2-hydroxycyclopentane-1-methanol.**

To a 100 mL schlenk flask, lithium aluminum hydride (1.46 g, 38.4 mmol) was added followed by diethyl ether (30 mL). The slurry was stirred for 5 min at room temperature and the flask was then lowered into an ice bath. Then ethyl-2-cyclopentanonecarboxylate (2.00 g, 12.8 mmol), suspended in diethyl ether (20 mL), was added dropwise. After addition was complete the flask was removed from ice bath and allowed to warm to room temperature. The reaction mixture was stirred for 12 hours at room temperature. Next, ethyl acetate (30 mL) was added to reaction mixture to quench the unreacted lithium aluminum hydride and allowed to stir for one hour. Finally, saturated solution of aqueous sodium sulfate (40 mL) was added to precipitate

aluminum. The white slurry was then filtered through a coarse fritted glass funnel containing 2 inch of celite. The filtrate was then transferred to a separatory funnel and both layers were kept separate. Ethyl acetate was then used 3 X 20 mL to extract the product from the aqueous layer. All organic extracts were combined, dried using sodium sulfate and evaporated to dryness yielding a light yellow clear oil. The crude oil was then purified via column chromatography using ethyl acetate as eluent and 2-hydroxycyclopentane-1-methanol (1.07 g, 9.21 mmol, 72 %) was isolated as a colorless oil.

**D1:**  $^1\text{H-NMR}$   $\delta_{\text{H}}$  (300.13 MHz;  $\text{CDCl}_3$ ;  $\text{Me}_4\text{Si}$ ) 4.00 (1H, q,  $J_{\text{HH}} = 6.2$  Hz,  $\text{CHOH}$ ), 3.83 (2H, s,  $2\text{OH}$ ), 3.67 (1H, dd,  $J = 5.3$  Hz,  $\text{CHCHHOH}$ ), 3.49 (1H, t,  $J = 8.5/10.4$  Hz,  $\text{CHCHHOH}$ ), 2.00-1.53 (6H, m,  $3\text{CH}_2$ ), 1.21-1.14 (1H, m,  $\text{CHCH}_2\text{OH}$ ).  $^{13}\text{C-NMR}$   $\delta_{\text{C}}$  (75.5 MHz;  $\text{CDCl}_3$ ;  $\text{Me}_4\text{Si}$ ) 65.5 (s,  $\text{CHOH}$ ), 60.5 (s,  $\text{CHCH}_2\text{OH}$ ), 49.6 (s,  $\text{CHCH}_2\text{OH}$ ), 34.4 (s,  $\text{CH}_2\text{CHOH}$ ), 26.5 (s,  $\text{CH}_2\text{CH}_2\text{CH}_2$ ), 21.9 (s,  $\text{CH}_2\text{CH}_2\text{CH}$ ).

### 3-hydroxycyclohexane-1-methanol.

To a 100 mL schlenk flask, lithium aluminum hydride (1.32 g, 34.8 mmol) was added followed by diethyl ether (30 mL). The Slurry was stirred for 5 min at room temperature and the flask was then lowered into an ice bath. Then ethyl-3-hydroxycyclohexanecarboxylate (2.00 g, 11.6 mmol), suspended in diethyl ether (20 mL), was added dropwise. After addition was complete the flask was removed from ice bath and allowed to warm to room temperature. The reaction mixture was stirred for 12 hours at room temperature. Next, ethyl acetate (30 mL) was added to reaction mixture to quench the unreacted lithium aluminum hydride and allowed to stir for one hour. Finally, saturated solution of aqueous sodium sulfate (40 mL) was added to precipitate aluminum. The white slurry was then filtered through a coarse fritted glass funnel containing 2

inch of celite. The filtrate was then transferred to a separatory funnel and both layers were kept separate. Ethyl acetate was then used 3 X 20 mL to extract the product from the aqueous layer. All organic extracts were combined, dried using sodium sulfate and evaporated to dryness yielding a light yellow clear oil. The crude oil was then purified via column chromatography using ethyl acetate as eluent and 3-hydroxycyclohexane-1-methanol (0.818 g, 6.28 mmol, 54 %) was isolated as a colorless oil.

**D1:**  $^1\text{H-NMR}$   $\delta_{\text{H}}$  (300.13 MHz;  $\text{CDCl}_3$ ;  $\text{Me}_4\text{Si}$ ) 3.61-3.54 (1H, m,  $\text{CHOH}$ ), 3.51-3.37 (2H, m,  $\text{CHCH}_2\text{OH}$ ), 3.26 (2H, s, 2OH), 2.04-1.47 (5H, m,  $\text{CH}_2\text{CHOHCH}_2\text{CHCH}_2\text{OH}$ ), 1.30-1.13 (2H, m,  $\text{CH}_2$ ), 0.98-0.81 (2H, m  $\text{CH}_2$ ).  $^{13}\text{C-NMR}$   $\delta_{\text{C}}$  (75.5 MHz;  $\text{CDCl}_3$ ;  $\text{Me}_4\text{Si}$ ) 70.3 (s, COH), 67.6 (s,  $\text{CHCH}_2\text{OH}$ ), 39.2 (s,  $\text{CHCH}_2\text{OH}$ ), 35.5 (s,  $\text{CHOHCH}_2\text{CH}$ ), 34.4 (s,  $\text{CH}_2\text{CHOH}$ ), 28.3 (s,  $\text{CH}_2\text{CHCH}_2\text{OH}$ ), 23.7 (s,  $\text{CH}_2\text{CH}_2\text{CH}_2$ ).

**D2:**  $^1\text{H-NMR}$   $\delta_{\text{H}}$  (300.13 MHz;  $\text{CDCl}_3$ ;  $\text{Me}_4\text{Si}$ ) 3.61-3.54 (1H, m,  $\text{CHOH}$ ), 3.51-3.37 (2H, m,  $\text{CHCH}_2\text{OH}$ ), 3.26 (2H, s, 2OH), 2.04-1.47 (5H, m,  $\text{CH}_2\text{CHOHCH}_2\text{CHCH}_2\text{OH}$ ), 1.30-1.13 (2H, m,  $\text{CH}_2$ ), 0.98-0.81 (2H, m  $\text{CH}_2$ ).  $^{13}\text{C-NMR}$   $\delta_{\text{C}}$  (75.5 MHz;  $\text{CDCl}_3$ ;  $\text{Me}_4\text{Si}$ ) 67.6 (s, COH), 66.1 (s,  $\text{CHCH}_2\text{OH}$ ), 38.7 (s,  $\text{CHCH}_2\text{OH}$ ), 35.9 (s,  $\text{CHOHCH}_2\text{CH}$ ), 32.9 (s,  $\text{CH}_2\text{CHOH}$ ), 28.7 (s,  $\text{CH}_2\text{CHCH}_2\text{OH}$ ), 19.7 (s,  $\text{CH}_2\text{CH}_2\text{CH}_2$ ).

### Isolated Yields

#### **2-cyclohexanone-1-methanol.**

The substrate 2-hydroxycyclohexane-1-methanol (0.136 g, 1.04 mmol) and the catalyst  $[\text{Fe}(\mathbf{5.1})_2]^{2+}(\text{OTf})_2$  (0.024 g, 0.031 mmol) were dissolved in  $\text{CH}_3\text{CN}$  (2 mL). The oxidant  $\text{H}_2\text{O}_2$  (0.269 mL, 30 wt % in  $\text{H}_2\text{O}$ , 2.61 mmol) was added dropwise (0.027 mL/min) at room temperature until addition was complete. The reaction was stirred for additional 5 minutes at room tem-



perature. The CH<sub>3</sub>CN was removed under vacuum and DCM (10.0 mL) was added. The reaction mixture was dried with sodium sulfate and subsequently filtered through short pad of silica (1 in). The product 2-cyclohexanone-1-methanol was isolated by column chromatography as colorless oil (0.078 g, 0.608 mmol, 58 %) using silica gel and EtOAc as eluent. <sup>1</sup>H-NMR δ<sub>H</sub> (300.13 MHz; CDCl<sub>3</sub>; Me<sub>4</sub>Si) 3.68 (2H, qd J= not sure how to report coupling, CHCH<sub>2</sub>OH), 3.41 (1H, bs, OH), 2.55-1.25 (9H, m, 4CH<sub>2</sub>CHCH<sub>2</sub>). <sup>13</sup>C-NMR δ<sub>C</sub> (75.5 MHz; CDCl<sub>3</sub>; Me<sub>4</sub>Si) 214.9 (s, C=O), 62.8 (s, CH<sub>2</sub>OH), 52.2 (s, CH<sub>2</sub>C=O), 42.2 (s, CHCH<sub>2</sub>OH), 30.0 (s, CH<sub>2</sub>CHCH<sub>2</sub>OH), 27.5 (s, CH<sub>2</sub>CH<sub>2</sub>CH<sub>2</sub>), 24.7 (s, CH<sub>2</sub>CH<sub>2</sub>CH<sub>2</sub>).

### 3-cyclohexanone-1-methanol.

The substrate 3-hydroxycyclohexane-1-methanol (0.081 g, 0.622 mmol), utilizing the oxidant H<sub>2</sub>O<sub>2</sub> (0.160 mL, 30 wt % in H<sub>2</sub>O, 1.56 mmol) and catalyst [Fe(**5.1**)<sub>2</sub>]<sup>2+</sup>(OTf)<sub>2</sub> (0.014 g, 0.018 mmol), was converted to 3-cyclohexanone-1-methanol as a colorless oil (0.043 g, 0.335 mmol, 54 %) as described above for 2-hydroxycyclohexane-1-methanol, using EtOAc as eluent. <sup>1</sup>H-NMR δ<sub>H</sub> (300.13 MHz; CDCl<sub>3</sub>; Me<sub>4</sub>Si) 3.52 (2H, d, J= ?, C=OCH<sub>2</sub>CH), 2.40-1.38 (8H, 3CH<sub>2</sub>CHCH<sub>2</sub>OH). <sup>13</sup>C-NMR δ<sub>C</sub> (75.5 MHz; CDCl<sub>3</sub>; Me<sub>4</sub>Si) 211.7 (s, C=O), 66.9 (s, CH<sub>2</sub>OH), 44.4 (s, CHCH<sub>2</sub>OH), 41.5 (s, CH<sub>2</sub>C=O), 41.4 (s, C=OCH<sub>2</sub>), 27.7 (s, CH<sub>2</sub>), 25.0 (s, CH<sub>2</sub>).

### 2-cyclopentanone-1-methanol.

The substrate 2-hydroxycyclopentane-1-methanol (0.060 g, 0.516 mmol), utilizing the oxidant H<sub>2</sub>O<sub>2</sub> (0.133 mL, 30 wt % in H<sub>2</sub>O, 1.29 mmol) and catalyst [Fe(**5.1**)<sub>2</sub>]<sup>2+</sup>(OTf)<sub>2</sub> (0.012 g, 0.015 mmol), was converted to 2-cyclopentanone-1-methanol as a colorless oil (0.037 g, 0.324 mmol, 63 %) as described above for 2-hydroxycyclohexane-1-methanol, using EtOAc as eluent. <sup>1</sup>H-NMR δ<sub>H</sub> (300.13 MHz; CDCl<sub>3</sub>; Me<sub>4</sub>Si) 3.77 (2H, qd, \*not sure how to report coupling con-

stant,  $\text{CHCH}_2\text{OH}$ ), 2.41-1.65 (7H, m,  $3\text{CH}_2\text{CHOH}$ ).  $^{13}\text{C}$ -NMR  $\delta_{\text{C}}$  (75.5 MHz;  $\text{CDCl}_3$ ;  $\text{Me}_4\text{Si}$ ) 222.5 (s,  $\text{C}=\text{O}$ ), 62.0 (s,  $\text{CH}_2\text{OH}$ ), 50.6 (s,  $\text{CH}_2\text{C}=\text{O}$ ), 38.5 (s,  $\text{CHCH}_2\text{OH}$ ), 26.1 (s,  $\text{CH}_2\text{CHCH}_2\text{OH}$ ), 20.8 (s,  $\text{CH}_2\text{CH}_2\text{CH}_2$ ).

### 3-hexanone-1-ol.

The substrate 1,3-hexanediol (0.094 g, 0.795 mmol), utilizing the oxidant  $\text{H}_2\text{O}_2$  (0.204 mL, 30 wt % in  $\text{H}_2\text{O}$ , 1.99 mmol) and catalyst  $[\text{Fe}(\mathbf{5.1})_2]^{2+}(\text{OTf})_2$  (0.018 g, 0.023 mmol), was converted to 3-hexanone-1-ol as a colorless oil (0.066 g, 0.588 mmol, 71 %) as described above for 2-hydroxycyclohexane-1-methanol, using EtOAc as eluent.  $^1\text{H}$ -NMR  $\delta_{\text{H}}$  (300.13 MHz;  $\text{CDCl}_3$ ;  $\text{Me}_4\text{Si}$ ) 3.84 (2H, t,  $J = 5.6$ ,  $\text{CH}_2\text{OH}$ ), 2.66 (2H, t,  $J = 5.4$ ,  $\text{C}=\text{OCH}_2$ ), 2.42 (2H, t,  $J = 7.2$  Hz,  $\text{CH}_2\text{C}=\text{O}$ ), 1.61 (2H, s,  $J = 7.2$  Hz,  $\text{CH}_3\text{CH}_2\text{CH}_2$ ), 0.91 (3H, t,  $J = 7.5$  Hz,  $\text{CH}_3\text{CH}_2$ ).  $^{13}\text{C}$ -NMR  $\delta_{\text{C}}$  (75.5 MHz;  $\text{CDCl}_3$ ;  $\text{Me}_4\text{Si}$ ) 212.0 (s,  $\text{C}=\text{O}$ ), 58.1 (s,  $\text{CH}_2\text{OH}$ ), 45.5 (s,  $\text{C}=\text{OCH}_2$ ), 44.6 (s,  $\text{CH}_2\text{C}=\text{O}$ ), 17.3 (s,  $\text{CH}_3\text{CH}_2$ ), 13.8 (s,  $\text{CH}_3\text{CH}_2$ ).

### 2-butanone-1-ol.

The substrate 1,2-butanediol (0.120 g, 1.33 mmol), utilizing the oxidant  $\text{H}_2\text{O}_2$  (0.343 mL, 30 wt % in  $\text{H}_2\text{O}$ , 3.33 mmol) and catalyst  $[\text{Fe}(\mathbf{5.1})_2]^{2+}(\text{OTf})_2$  (0.031 g, 0.039 mmol), was converted to 2-butanone-1-ol as a colorless oil (0.099 g, 1.12 mmol, 84 %) as described above for 2-hydroxycyclohexane-1-methanol, using EtOAc as eluent.  $^1\text{H}$ -NMR  $\delta_{\text{H}}$  (300.13 MHz;  $\text{CDCl}_3$ ;  $\text{Me}_4\text{Si}$ ) 4.27 (2H, s,  $\text{C}=\text{OCH}_2\text{OH}$ ), 3.35 (1H, bs,  $\text{OH}$ ), 2.45 (2H, q,  $J = 7.4$ ,  $\text{CH}_3\text{CH}_2$ ), 1.14 (3H, t,  $J = 7.4$ ,  $\text{CH}_3\text{CH}_2$ ).  $^{13}\text{C}$ -NMR  $\delta_{\text{C}}$  (75.5 MHz;  $\text{CDCl}_3$ ;  $\text{Me}_4\text{Si}$ ) 210.4 (s,  $\text{C}=\text{O}$ ), 68.0 (s,  $\text{CH}_2\text{OH}$ ), 31.6 (s,  $\text{CH}_2\text{C}=\text{O}$ ), 7.45 (s,  $\text{CH}_3$ ).

### 2-octanone-1-ol.

The substrate 1,2-octanediol (0.062 g, 0.424 mmol), utilizing the oxidant H<sub>2</sub>O<sub>2</sub> (0.109 mL, 30 wt % in H<sub>2</sub>O, 1.06 mmol) and catalyst [Fe(**5.1**)<sub>2</sub>]<sup>2+</sup>(OTf)<sub>2</sub> (0.010 g, 0.012 mmol), was converted to 2-octanone-1-ol as a colorless oil (0.046 g, 0.318 mmol, 75 %) as described above for 2-hydroxycyclohexane-1-methanol, using EtOAc as eluent. <sup>1</sup>H-NMR δ<sub>H</sub> (300.13 MHz; CDCl<sub>3</sub>; Me<sub>4</sub>Si) 4.18 (2H, s, C=OCH<sub>2</sub>OH), 3.09 (1H, bs, OH), 2.34 (3H, t, J = 7.4 Hz, CH<sub>3</sub>CH<sub>2</sub>C=O), 1.56 (3H, t, J = 6.8 Hz, CH<sub>3</sub>CH<sub>2</sub>), 1.22-1.18 (8H, m, 4CH<sub>2</sub>). <sup>13</sup>C-NMR δ<sub>C</sub> (75.5 MHz; CDCl<sub>3</sub>; Me<sub>4</sub>Si) 209.9 (s, C=O), 68.1 (s, CH<sub>2</sub>OH), 38.4 (s, CH<sub>2</sub>C=O), 31.5 (s, CH<sub>2</sub>CH<sub>2</sub>C=O), 28.9 (s, CH<sub>2</sub>), 23.7 (s, CH<sub>2</sub>), 22.4 (s, CH<sub>2</sub>), 14.0 (s, CH<sub>3</sub>).

**2-hydroxy-1-phenylethanone.** The substrate 1-phenyl-1,2-ethanediol (0.116 g, 0.839 mmol), utilizing the oxidant H<sub>2</sub>O<sub>2</sub> (0.216 mL, 30 wt % in H<sub>2</sub>O, 2.10 mmol) and catalyst [Fe(**5.1**)<sub>2</sub>]<sup>2+</sup>(OTf)<sub>2</sub> (0.019 g, 0.025 mmol), was converted to 2-hydroxy-1-phenylethanone as a colorless oil (0.061 g, 0.448 mmol, 53 %) as described above for 2-hydroxycyclohexane-1-methanol, using EtOAc as eluent.

**2-ethyl-3-hexanone-1-ol.** The substrate 2-ethyl-1,3-hexanediol (0.200 g, 1.37 mmol), utilizing the oxidant H<sub>2</sub>O<sub>2</sub> (0.352 mL, 30 wt % in H<sub>2</sub>O, 3.42 mmol) and catalyst [Fe(**5.1**)<sub>2</sub>]<sup>2+</sup>(OTf)<sub>2</sub> (0.030 g, 0.041 mmol), was converted to 2-ethyl-3-hexanone-1-ol as a colorless oil (0.164 g, 1.14 mmol, 83 %) as described above for 2-hydroxycyclohexane-1-methanol, using EtOAc:CH<sub>2</sub>Cl<sub>2</sub> (1:1) as eluent. <sup>1</sup>H-NMR δ<sub>H</sub> (300.13 MHz; CDCl<sub>3</sub>; Me<sub>4</sub>Si) 3.83-3.67 (2H, qd, J = 7.3 Hz, HOCH<sub>2</sub>CHCH<sub>2</sub>CH<sub>3</sub>), 2.67-2.59 (1H, m, HOCH<sub>2</sub>CHCH<sub>2</sub>CH<sub>3</sub>), 2.48 (2H, t, J = 7.0 Hz, C=OCH<sub>2</sub>CH<sub>2</sub>), 1.71-1.46 (4H, m, 2CH<sub>2</sub>CH<sub>3</sub>), 0.95 (6H, m, 2CH<sub>2</sub>CH<sub>3</sub>). <sup>13</sup>C-NMR δ<sub>C</sub> (75.5 MHz; CDCl<sub>3</sub>; Me<sub>4</sub>Si) 215.2 (s, C=O), 62.4 (s, CH<sub>2</sub>OH), 54.8 (s, CH<sub>2</sub>CH(CH<sub>2</sub>CH<sub>3</sub>)C=O), 44.8 (s, C=OCH<sub>2</sub>CH<sub>2</sub>), 21.3 (s, CHCH<sub>2</sub>CH<sub>3</sub>C=O), 16.9 (s, CH<sub>2</sub>CH<sub>2</sub>CH<sub>3</sub>), 13.8 (s, CHCH<sub>2</sub>CH<sub>3</sub>C=O), 11.9 (s, CH<sub>2</sub>CH<sub>2</sub>CH<sub>3</sub>).

### Additional Experiments

**Intermolecular competition.** The substrates n-decanol (0.050 g, 0.315 mmol) and 2-decanol (0.050 g, 0.315 mmol) were placed into 7 mL vial with screw cap and CH<sub>3</sub>CN (1.0 mL) was added. Then H<sub>2</sub>O<sub>2</sub> (0.033 mL, 30 wt % in H<sub>2</sub>O, 0.315 mmol) was added dropwise (0.027 mL/min) at room temperature until addition was complete. The reaction was stirred for additional 5 minutes at room temperature. The CH<sub>3</sub>CN was removed under vacuum and DCM (5.0 mL) was added. The reaction mixture was dried with sodium sulfate and subsequently filtered through short pad of silica (1 in). The reaction mixture was analyzed using Gas Chromatography (FID). **Results:** After a total of 7 minutes reaction time, The GC chromatogram showed that only 2-decanol had been oxidized to 2-decananone (15 %). The only other two peaks were identified as the starting material.

**Radical Scavenger Investigation (Phenol).** The substrate 1,2-octanediol (0.050 g, 0.341 mmol), the radical scavenger phenol (0.016 g, 0.170 mmol) and catalyst [Fe(DPA)<sub>2</sub>]<sup>2+</sup>(OTf)<sub>2</sub> (0.007 g, 0.010 mmol) was placed into 7 mL vial with screw cap and CH<sub>3</sub>CN (1.0 mL) was added. Then H<sub>2</sub>O<sub>2</sub> (0.088 mL, 30 wt % in H<sub>2</sub>O, 0.854 mmol) was added dropwise (0.027 mL/min) at room temperature until addition was complete. The reaction was stirred for additional 5 minutes at room temperature. The CH<sub>3</sub>CN was removed under vacuum and DCM (5.0 mL) was added. The reaction mixture was dried with sodium sulfate and subsequently filtered through short pad of silica (1 in). The reaction mixture was analyzed using Gas Chromatography (FID). **Results:** After a total of 9 minute reaction time, The GC chromatogram showed that only very small amount of 2-octanone-1-ol (<5 %) had been produced and a remainder was unoxidized 1,2-octanediol (95 %).

**Radical Scavenger Investigation (2,4,6-tritertbutylphenol) A.** The substrate 1,2-octanediol (0.050 g, 0.341 mmol), the radical scavenger 2,4,6-tritertbutylphenol (0.005 g, 0.020 mmol) and catalyst  $[\text{Fe}(\text{DPA})_2]^{2+}(\text{OTf})_2$  (0.007 g, 0.010 mmol) were placed into 7 mL vial with screw cap and  $\text{CH}_3\text{CN}$  (1.0 mL) was added. Then  $\text{H}_2\text{O}_2$  (0.088 mL, 30 wt % in  $\text{H}_2\text{O}$ , 0.854 mmol) was added dropwise (0.027 mL/min) at room temperature until addition was complete. The reaction was stirred for additional 5 minutes at room temperature. The  $\text{CH}_3\text{CN}$  was removed under vacuum and DCM (5.0 mL) was added. The reaction mixture was dried with sodium sulfate and subsequently filtered through short pad of silica (1 in). The reaction mixture was analyzed using Gas Chromatography (FID). **Results:** After a total of 9 minute reaction time, The GC chromatogram showed that all of the 1,2-octanediol had been oxidized to 2-octanone-1-ol and the remaining peaks were identified as various oxidized forms of 2,4,6-tritertbutylphenol.

**Radical Scavenger Investigation (2,4,6-tritertbutylphenol) B.** The substrate 1,2-octanediol (0.050 g, 0.341 mmol), the radical scavenger 2,4,6-tritertbutylphenol (0.045 g, 0.170 mmol) and catalyst  $[\text{Fe}(\text{DPA})_2]^{2+}(\text{OTf})_2$  (0.007 g, 0.010 mmol) were placed into 7 mL vial with screw cap and  $\text{CH}_3\text{CN}$  (1.0 mL) was added. Then  $\text{H}_2\text{O}_2$  (0.088 mL, 30 wt % in  $\text{H}_2\text{O}$ , 0.854 mmol) was added dropwise (0.027 mL/min) at room temperature until addition was complete. The reaction was stirred for additional 5 minutes at room temperature. The  $\text{CH}_3\text{CN}$  was removed under vacuum and DCM (5.0 mL) was added. The reaction mixture was dried with sodium sulfate and subsequently filtered through short pad of silica (1 in). The reaction mixture was analyzed using Gas Chromatography (FID). **Results:** After a total of 9 minute reaction time, The GC chromatogram showed that most of the 1,2-octanediol had been oxidized to 2-octanone-1-ol and the remaining peaks were identified as various oxidized forms of 2,4,6-tritertbutylphenol.

**Radical Scavenger Investigation (2,4,6-tritertbutylphenol) C.** The substrate 1,2-octanediol (0.050 g, 0.341 mmol), the radical scavenger 2,4,6-tritertbutylphenol (0.089 g, 0.341 mmol) and catalyst  $[\text{Fe}(\text{DPA})_2]^{2+}(\text{OTf})_2$  (0.007 g, 0.010 mmol) were placed into 7 mL vial with screw cap and  $\text{CH}_3\text{CN}$  (1.0 mL) was added. Then  $\text{H}_2\text{O}_2$  (0.088 mL, 30 wt % in  $\text{H}_2\text{O}$ , 0.854 mmol) was added dropwise (0.027 mL/min) at room temperature until addition was complete. The reaction was stirred for additional 5 minutes at room temperature. The  $\text{CH}_3\text{CN}$  was removed under vacuum and DCM (5.0 mL) was added. The reaction mixture was dried with sodium sulfate and subsequently filtered through short pad of silica (1 in). The reaction mixture was analyzed using Gas Chromatography (FID). **Results:** After a total of 9 minute reaction time, The GC chromatogram showed that only half of the 1,2-octanediol had been oxidized to 2-octanone-1-ol while other half remained 1,2-octanediol and the remaining peaks were identified as various oxidized forms of 2,4,6-tritertbutylphenol.

**STANDARD for Radical Scavenger Investigation (without 2,4,6-tritertbutylphenol)**

. The substrate 1,2-octanediol (0.050 g, 0.341 mmol) and catalyst  $[\text{Fe}(\text{DPA})_2]^{2+}(\text{OTf})_2$  (0.007 g, 0.010 mmol) were placed into 7 mL vial with screw cap and  $\text{CH}_3\text{CN}$  (1.0 mL) was added. Then  $\text{H}_2\text{O}_2$  (0.088 mL, 30 wt % in  $\text{H}_2\text{O}$ , 0.854 mmol) was added dropwise (0.027 mL/min) at room temperature until addition was complete. The reaction was stirred for additional 5 minutes at room temperature. The  $\text{CH}_3\text{CN}$  was removed under vacuum and DCM (5.0 mL) was added. The reaction mixture was dried with sodium sulfate and subsequently filtered through short pad of silica (1 in). The reaction mixture was analyzed using Gas Chromatography (FID). **Results:** After a total of 9 minute reaction time, The GC chromatogram showed that almost all of the 1,2-octanediol had been oxidized to 2-octanone-1-ol while roughly 5 % remained 1,2-octanediol but

over oxidation occurred also where both OH's were oxidized constituting 5 %. So 90 % was 2-octanone-1-ol, 5 % 1,2-octanediol and 5 % 2-octanone-1-al.

**Catalyst comparison (5 catalysts were tested for chemoselectivity under similar conditions).** The substrate 1,2-octanediol (0.050 g, 0.341 mmol) and catalyst Blank was placed in a 7 mL vial with screw cap and CH<sub>3</sub>CN was added (1.0 mL). Then H<sub>2</sub>O<sub>2</sub> (0.088 mL, 30 wt % in H<sub>2</sub>O, 0.854 mmol) was added dropwise (0.027 mL/min) at room temperature until addition was complete. The reaction was stirred for additional 5 minutes at room temperature. The CH<sub>3</sub>CN was removed under vacuum and DCM (5.0 mL) was added. The reaction mixture was dried with sodium sulfate and subsequently filtered through short pad of silica (1 in). The reaction mixture was analyzed using Gas Chromatography (FID). **Results:** 0.150 mL fractions of the reaction mixture were taken at 2 different time intervals. First one after 10 minutes and the second after 24 hours. In all cases with each catalyst tested, after 10 minutes there was no product and after 24 hours only a mixture of oxidation products was observed (no selectivity) and there was still 90% of the 1,2-octanediol remaining.

## 5.6 References

<sup>1</sup> S. Caron, R. Dugger, S. Ruggeri, J. Ragan, D. Brown Rippin, *Chem. Rev.* **2007**, *106*, 2943.; R. Dugger, J. Ragan, D. Brown Ripin, *Org Process Res. Dev.*, **2005**, *9*, 253.

<sup>2</sup> F. Carey, R. Sundberg, *Advanced Organic Chemistry, Part B*, New York 5<sup>th</sup> ed, 2007.; H. Tohma, and Y Kita *Adv. Synth and Catal.* **2004**, *346*, 11.

<sup>3</sup> F. Gozzo, *J. Mol. Catal. A* **2001**, *171*, 1; b) B. Singh, J. R. Long, F. Fabrizia de Biani, D. Gatteschi, P. Stavropoulos, *J. Am. Chem. Soc.* **1997**, *119*, 7030.

<sup>4</sup> a) P. Stavropoulos, R. C. Elenigil-C, etin, A. E. Tapper, *Acc. Chem. Res.* **2001**, *34*, 745 ; b) D. W. Snelgrove, P. A. McFaul, K. U. Ingold, D. D. M. Wayner, *Tetrahedron Lett.* **1996**, *37*, 823; c) M. J. Perkins, *Chem. Soc. Rev.* **1996**, *25*, 229 ; d) F. Minisci, F. Fontana, S. Araneo, F. Recupero, S. Banfi, S. Quici, *J. Am. Chem. Soc.* **1995**, *117*, 226.

<sup>5</sup> a) E. P. Talsi, K. P. Bryliakov, *Coord. Chem. Rev.* **2012**, *256*, 1418 ; b) P. C. A. Bruijninx, G. van Koten, R. J. M. Klein Gebbink, *Chem. Soc. Rev.* **2008**, *37*, 2716.

<sup>6</sup> a) A. Beck, B. Weibert, N. Burzlaff, *Eur. J. Inorg. Chem.* **2001**, *521*; b) M. Costas, K. Chen, L. Que, Jr. , *Coord. Chem. Rev.* **2000**, *200*, 517 ; c) J. T. Groves, *J. Inorg. Biochem.* **2006**, *100*, 434 ; d) P. D. Oldenburg, L. Que, Jr. , *Catal. Today*, **2006**, *117*, 15; e) N. Burzlaff, *Angew. Chem.* **2009**, *121*, 5688; *Angew. Chem. Int. Ed.* **2009**, *48*, 5580.

<sup>7</sup> a) R. R. Fernandes, J. Lasri, M. F. C. Guedes da Silva, J. A. L. da Silva, J. J. R. Frausto da Silva, A. J. L. Pombeiro, *J. Mol. Catal. A*, **2011**, *351*, 100; b) S. A. Moyer, T. W. Funk, *Tetrahedron Lett.* **2010**, *51*, 5430 ; c) E. Balogh-Hergovich, G. Speier, *J. Mol. Catal. A* **2005**, *230*, 9; d) H. Hosseini-Monfared, C. Nather, H. Winkler, C. Janiak, *Inorg. Chim. Acta*, **2012**, *391*, 75.

<sup>8</sup> M. Wu, C.-X. Miao, S. Wang, X. Hu, C. Xia, F. E. Kuhn, W. Sun, *Adv. Synth. Catal.* **2011**, *353*, 3014 ; b) K. Schröder, B. Join, A. Jose Ama- li, K. Junge, X. Ribas, M. Costas, M. Beller, *Angew. Chem.* **2011**, *123*, 1461 ; *Angew. Chem. Int. Ed.* **2011**, *50*, 1425 ; c) F. G. Gelalcha, G. Anilkumar, M. K. Tse, A. Bruckner, M. Beller, *Chem. Eur. J.* **2008**, *14*, 7687 ; d) P. C. A. Bruijninx, I. L. C. Buurmans, S. Gosiewska, M. A. H. Moelands, M. Lutz, A. L. Spek, G.



van Koten, R. J. M. Klein Geb- bink, *Chem. Eur. J.* **2008**, *14*, 1228; e) F. Oddo, E. Girgenti, C. Lebrun, C. Marchi-Delapierre, J. Pecaut, S. Menage, *Eur. J. Inorg. Chem.* **2012**, 85.

<sup>9</sup> a) P. Comba, M. Maurer, P. Vadivelu, *Inorg. Chem.* **2009**, *48*, 10389 ; b) M. R. Bukowski, P. Comba, A. Lienke, C. Limberg, C. Lopez de Laorden, R. Mas-Balleste, M. Merz, L. Que, Jr. , *Angew. Chem.* **2006**, *118*, 3524 ; *Angew. Chem. Int. Ed.* **2006**, *45*, 3446.

<sup>10</sup> a) M. N. Kopylovich, T. C. Mac Leod, M. Haukka, G. I. Amanullayeva, K. T. Mahmudov, A. J. Pombeiro, *J. Inorg. Biochem.*, **2012**, *115*, 72.; b) M. S. Chen, M. C. White, *Science*, **2010**, *327*, 566.; c) C. Pavan, J. Legros, C. Bolm, *Adv. Synth. Catal.* **2007**, *347*, 703.

<sup>11</sup> M. S. Seo, T. Kamachi, T. Kouno, K. Murata, M. J. Park, K. Yoshizawa, W. Nam, *Angew. Chem.* **2007**, *119*, 2341; *Angew. Chem. Int. Ed.*, **2007**, *46*, 2291.

